Defense Threat Reduction Agency
8725 John J. Kingman Road, MS 6201
Fort Belvoir, VA 22060-6201

DTRA-TR-05-21

TECHNICAL REPORT

Collaborative Research: Calibration for IMS Stations in Eastern Asia

Approved for public release; distribution is unlimited.

July 2007

DTRA 01-00-C-0031

Paul Richards, et al.

Prepared by:
Lamont –Doherty Earth Observatory
Columbia University
661 Route 9 W
Palisades, New York 10964

DESTRUCTION NOTICE

FOR CLASSIFIED documents, follow the procedures in DoD 5550.22-M, National Industrial Security Program Operating Manual, Chapter 5, Section 7 (NISPOM) or DoD 5200.1-R, Information Security Program Regulation, Chapter 1X.

FOR UNCLASSIFIED limited documents, destroyed by any method that will prevent disclosure of contents or reconstruction of the document.

Retention of this document by DoD contractors is authorized in accordance with DoD 5220.22-M, Industrial Security Manual.

PLEASE NOTIFY THE DEFENSE THREAT REDUCTION AGENCY, ATTN: CST, 8725 JOHN J. KINGMAN ROAD, STOP-6201, FT BELVOIR, VA 22060-6201, IF YOUR ADDRESS IS INCORRECT, IF YOU WISH IT DELETED FROM THE DISTRIBUTION LIST, OR IF THE ADDRESSEE IS NO LONGER EMPLOYED BY YOUR ORGANIZATION.

DISTRIBUTION LIST UPDATE

This mailer is provided to enable DTRA to maintain current distribution lists for reports. (We would appreciate you providing the requested information.)

- ☐ Add the individual listed to your distribution list.
- ☐ Delete the cited organization/individual.
- ☐ Change of address.

Note:
Please return the mailing label from the document so that any additions, changes, corrections or deletions can be made easily. For distribution cancellation or more information call DTRA/CST (703) 767-4725.

NAME: _____

ORGANIZATION: _____

OLD ADDRESS	NEW ADDRESS
_____	_____
_____	_____
_____	_____

TELEPHONE NUMBER: ( ) _____

DTRA PUBLICATION NUMBER/TITLE	CHANGES/DELETIONS/ADDITONS, etc. *(Attach Sheet if more Space is Required)*
_____	_____
_____	_____
_____	_____

DTRA or other GOVERNMENT CONTRACT NUMBER: _____

CERTIFICATION of NEED-TO-KNOW BY GOVERNMENT SPONSOR (if other than DTRA):

SPONSORING ORGANIZATION: _____

CONTRACTING OFFICER or REPRESENTATIVE: _____

SIGNATURE: _____

REPORT DOCUMENTATION PAGE

Form Approved
OMB No. 0704-0188

Public reporting burden for this collection of information is estimated to average 1 hour per response, including the time for reviewing instructions, searching existing data sources, gathering and maintaining the data needed, and completing and reviewing the collection of information. Send comments regarding this burden, estimate or any other aspect of this collection of information, including suggestions for reducing this burden, to Washington Headquarters Services, Directorate for Information Operations and Reports, 1215 Jefferson Davis Highway, Suite 1204, Arlington, VA 22202-4302, and to the Office of Management and Budget, Paperwork Reduction Project (0704-0188), Washington, DC 20503.

1. AGENCY USE ONLY (*Leave blank*)	2. REPORT DATE	3. REPORT TYPE AND DATES COVERED
	041106	Technical 000322 - 030930

4. TITLE AND SUBTITLE

Collaborative Research Calibration for IMS Stations in Eastern Asia

5. FUNDING NUMBERS

C – DTRA 01-00-C-0031
DTRA 01-00-C-0029
DTRA 01-00-C-0033
PE – 463D
PR – CD
TA – CD
WU – DH01852, DH01853, DH01854

6. AUTHOR(S)

Paul Richards, John Armbruster, Vitaly L. Khalturin, Won-Young Kim, David Schaff, Felix Waldhauser, Michael West (Lamont-Doherty Earth Observatory)

7. PERFORMING ORGANIZATION NAME(S) AND ADDRESS(ES)

Lamont-Doherty Earth Observatory
Columbia University
61 Route 9 W
Palisades, NY 10964

8. PERFORMING ORGANIZATION REPORT

9. SPONSORING/MONITORING AGENCY NAME(S) AND ADDRESS(ES)

Defense Threat Reduction Agency
8725 John J. Kingman Road, MS 6201
Fort Belvoir, VA 22060-6201

NTD/ A. Taylor

10. SPONSORING/MONITORING AGENCY REPORT NUMBER

DTRA-TR-05-21

11. SUPPLEMENTARY NOTES

This work was sponsored by the Defense Threat Reduction Agency under RDT&E RMC code B 463D D K540 CD CD 01854 25904D

12a. DISTRIBUTION/AVAILABILITY STATEMENT

Approved for public release; distribution is unlimited.

12B. DISTRIBUTION CODE

13. ABSTRACT (Maximum 200 words)

We have compelted a three-year consortium effort led by Lamont to improve the capabiolity to locate seismic events based on data acquired by 30 International Monitoring System (IMS) stations in East Asia. We have developed and tested Source Specific Station Corrections (SSSCs) for Pn and Sn travel times at these 30 IMS stations (or suitable surrogates), and for 127 other stations used for validation testing. First we developed SSSCs via a 3-D model of the P-wave velocity for East Asia, and then we refined them empirically by applying a kriging algorithm to travel-time residuals for 525 Ground-Truth (GT) events whose epicenters in East Asia we showed are known to within 5 km. Using a leave-one-out approach, we relocated these 525 events recorded by various combinations of 140 regional stations. Miclocations were reduced for 66% of the events using the model-based SSSCs and for 85% of the events using kringed SSSCs. Meridian miclocation improved from 16.9 km to 11.4 km and 6.5 km respectively. Median error ellipse area was reduced from 2616 sq. km to 1633 sl.km, respectively. Error ellipse coverage was maintained at close to 90%.

14. SUBJECT TERMS

Explosion Monitoring
Source Specific Station Corrections (SSSCs)
International Monitoring System (IMS) stations
P-wave velocity

15. NUMBER OF PAGES

SECURITY CLASSIFICATION OF REPORT	SECURITY CLASSIFICATION OF THIS PAGE	SECURITY CLASSIFICATION OF ABSTRACT	20. LIMITATION OF ABSTRACT
UNCLASSIFIED	UNCLASSIFIED	UNCLASSIFIED	SAR

NSN 7540-01-280-5500

Standard Form 298 (Rev. 2-89)
Prescribed by ANSI Sta. 239-18, 298-102

CLASSIFIED BY:

N/A since Unclassified

DECLASSIFY ON:

N/A since Unclassified

6. AUTHOR(S) (Continued)

Valeriu Burlacu, Mark Fisk (Mission Research Corporation) Igor Morozov, Elena Morozova (University of Wyoming) Anastasia Stroujkova (University of Connecticut) Chandan Saikia (URS Group)

7. PERFORMING ORGANIZATION NAME(S) AND ADDRESS(ES) (Continued)

Mission Research Corporation
5001 Indian School Rd. NE
Albuquerque, NM 87110-3946

University of Wyoming
Department of Geology and Geophysics
Laramie, WY 82071-3006

URS Group
600 Montgomery Street
26th Floor
San Francisco, CA 94111-2728

University of Connecticut
Geoscience
Storrs, CT 06269

CONVERSION TABLE

Conversion Factors for U.S. Customary to metric (SI) units of measurement.

MULTIPLY →	BY →	TO GET
TO GET ←	BY ←	DIVIDE

angstrom	1.000 000 x E -10	meters (m)
atmosphere (normal)	1.013 25 x E +2	kilo pascal (kPa)
bar	1.000 000 x E +2	kilo pascal (kPa)
barn	1.000 000 x E -28	meter^2 (m^2)
British thermal unit (thermochemical)	1.054 350 x E +3	joule (J)
calorie (thermochemical)	4.184 000	joule (J)
cal (thermochemical/cm^2)	4.184 000 x E -2	mega joule/m^2 (MJ/m^2)
curie	3.700 000 x E +1	*giga bacquerel (GBq)
degree (angle)	1.745 329 x E -2	radian (rad)
degree Fahrenheit	$t_k = (t°f + 459.67)/1.8$	degree kelvin (K)
electron volt	1.602 19 x E -19	joule (J)
erg	1.000 000 x E -7	joule (J)
erg/second	1.000 000 x E -7	watt (W)
foot	3.048 000 x E -1	meter (m)
foot-pound-force	1.355 818	joule (J)
gallon (U.S. liquid)	3.785 412 x E -3	meter^3 (m^3)
inch	2.540 000 x E -2	meter (m)
jerk	1.000 000 x E +9	joule (J)
joule/kilogram (J/kg) radiation dose absorbed	1.000 000	Gray (Gy)
kilotons	4.183	terajoules
kip (1000 lbf)	4.448 222 x E +3	newton (N)
kip/inch^2 (ksi)	6.894 757 x E +3	kilo pascal (kPa)
ktap	1.000 000 x E +2	newton-second/m^2 (N-s/m^2)
micron	1.000 000 x E -6	meter (m)
mil	2.540 000 x E -5	meter (m)
mile (international)	1.609 344 x E +3	meter (m)
ounce	2.834 952 x E -2	kilogram (kg)
pound-force (lbs avoirdupois)	4.448 222	newton (N)
pound-force inch	1.129 848 x E -1	newton-meter (N-m)
pound-force/inch	1.751 268 x E +2	newton/meter (N/m)
pound-force/foot^2	4.788 026 x E -2	kilo pascal (kPa)
pound-force/inch^2 (psi)	6.894 757	kilo pascal (kPa)
pound-mass (lbm avoirdupois)	4.535 924 x E -1	kilogram (kg)
pound-mass-foot^2 (moment of inertia)	4.214 011 x E -2	kilogram-meter^2 (kg-m^2)
pound-mass/foot^3	1.601 846 x E +1	kilogram-meter^3 (kg/m^3)
rad (radiation dose absorbed)	1.000 000 x E -2	**Gray (Gy)
roentgen	2.579 760 x E -4	coulomb/kilogram (C/kg)
shake	1.000 000 x E -8	second (s)
slug	1.459 390 x E +1	kilogram (kg)
torr (mm Hg, 0^0 C)	1.333 22 x E -1	kilo pascal (kPa)

*The bacquerel (Bq) is the SI unit of radioactivity; 1 Bq = 1 event/s.
**The Gray (GY) is the SI unit of absorbed radiation.

TABLE OF CONTENTS

1. Executive Summary 1

1.1. Documentation 2

2. Introduction 8

2.1. Identification 8

2.2. Scope and Audience 9

2.3. Overview 9

3. Regionalization and travel-time Curves for East Asia 11

3.1. Subregion Boundaries 22

3.2. Regional Phases in the IASP91 Model, Compared with General Observation of these Phases in East Asia 23

3.3. Published Information on Regional Travel Times 25

3.3.1. The Former Soviet Union and Surrounding Areas 25

3.3.2. China and Surrounding Areas 30

3.4. Our Initial Set of Regional Travel Times in Subregions of Russia and Surrounding Areas 31

3.4.1. Scandinavian Shield (Region #1) 31

3.4.2. East European Platform (Region #2) 34

3.4.3. Cenozoic Folded Regions (Region #3) 36

3.4.4. Ural Fold Zone (Region #4) 37

3.4.5. West Siberian Platform (Region #5b) 38

3.4.6. Kazakh Massif (Region #5c) 40

3.4.7. Turan Plateau (Region #5d) 43

3.4.8. Altay-Sayan Folded Region (Region #6) 46

3.4.9. Tian Shan Orogenic Zone (Region #7) 48

3.4.10. Baykal-Mongolian Fold Zone (Region #12) 52

3.4.11. East Siberian Platform (Region #15) 56

3.4.12. Northeast Territory and Chukot Peninsula (Region #16) 57

3.5. Our Regionalization of China and Surrounding Areas 58

3.5.1. Tarim and North Chinese Platforms (Regions #8 and #11) 58
3.5.2. Tibetan Plateau (Region #10) 61
3.5.3. Sikkam, Sichuan-Yunan Region (Region #20a) 63
3.5.4. Our Revision of Travel Times and Velocity Models for China 65
3.6. Our Regionalization of the Indian Subcontinent 68
3.6.1. Pamir, Hindu Kush and Himalaya (Region #9) 68
3.6.2. Our Revision of Velocity Models for the Indian Subcontinent 69
3.7. The Continent/Ocean Boundary 74
4. Data Sets 76
4.1. Kitov Data Set of Soviet-Era Underground Nuclear Explosions 76
4.2. Additional Explosion Reference Events, used in our May 2002 CCB Proposal and for the Present Study 78
4.3. Data from Field Stations Used to Record 19 Soviet-Era PNEs 79
4.4. The Annual Bulletin of Chinese Earthquakes 84
4.5. Additional Information on GT Events Used in this Study 85
5. Model Revision and Computation of SSSCs 86
5.1. The Bondár Method of SSSC Computation 86
5.2. Our Method of 3D Ray-Tracing in Heterogeneous Structures 88
5.3. Final Development of Model-Based SSSCs 93
5.4. Model Errors and Model-Based SSSCs 98
5.5. Kriging 104
6. Validation testing and Performance Metrics 119
6.1. Introduction 119
6.2. Model Validation 120
6.2.1. Mislocation 121
6.2.2. Error Ellipse Area and Coverage 123
6.2.3. Standard Error of Observations 124
6.2.4. Discussion 125
6.3. Evaluation of Kriged SSSCs 125

6.3.1. Mislocation 126
6.3.2. Error Ellipse Area and Coverage 130
6.3.3. Standard Error of Observations 132
6.3.4. Discussion 133
6.4. Results for Pn only 134
6.5. Variability of Location Quality 135
7. Conclusions and Recommendations 140
8. References 142
Appendix A Compilation of Seismic Reference Events in Asia A-1
Appendix B Seismic Reference Events B-1
Appendix C Phase Data from Peaceful Nuclear Explosions in Northern Eurasia C-1
Appendix D The Latitude/Longitude Points which Determine our Region Boundaries D-1
Appendix E Pn and Sn SSSCs and Modeling Errors E-1
Appendix F RDSS Validation Test Report F-1
Distribution List. DL-1

FIGURES

1 Map showing the location of 30 IMS stations (11 primary, 19 auxiliary) which we have calibrated in this project. The markers for primary stations are inverted green triangles while those for auxiliary stations are green triangles. 13

2 Maps of topography and regionalization boundaries (upper) and the numbering convention used for the various subregions (lower) defined in our CCB proposal of May 2002. In our final 3D model we make significant revisions for the continent/ocean transition, and for India and China (as discussed in Sections 3.5 - 3.7), but the changes we have made for the Former Soviet Union are relatively minor (see Section 5). 21

3 Major Deep Seismic Sounding profiles of Kazakhstan and nearby regions. 28

4 Pn velocities (km/s) from DSS profiles based on chemical explosions in and near Kazakhstan. 30

5 Travel-time residual (in seconds) for the West Siberian Platform (Region #5b - IASP91), for first arriving P waves out to 2200 km. Initial travel time model. 40

6 Travel-time residual (in seconds) for the Kazakh Massif (Region #5c - IASP91), for first arriving P waves out to 2200 km. Initial travel time model. 43

7 Travel-time residual (in seconds) for the Turan Plateau (Region #5d - IASP91), for first arriving P waves out to 2200 km. Initial travel time model. 46

8 Travel-time residual (in seconds) for the Altay-Sayan (Region #6 - IASP91), for first arriving P waves out to 2200 km. Initial travel time model. 48

9 Travel-time residual (in seconds) for the Tian Shan Orogenic Zone (Region #7 - IASP91), for first arriving P waves out to 2200 km. Initial travel time model. Unusually for the territory of Russia and Central Asia, this region has travel times for Pn that are significantly greater than those of the IASP91 travel time model. 52

10 Travel-time residual (in seconds) for the Tarim Platform and the North Chinese Platform (Region #8 or 11 - IASP91), for first arriving P waves out to 2200 km. Initial travel time model. 61

11 Boundaries of 1D velocity models for China and surrounding areas. 66

12 The boundaries shown in Figure 11 are superimposed on province boundaries (a), tectonic units (b), Moho topography (contoured at 2 km depth intervals) (c), and seismicity (d). 67

13 Region names and numbers, for the 1D structures used in our model of the Indian sub-continent. 74

14 Here are shown the seaward extent of regions, previously defined as continental, which characterize shallow seas to the east and south of East Asia. 75

15 Map showing locations of GT explosions (red stars) and recording seismographic stations (blue triangles) used for validation tests in support of our May 2002 CCB proposal. Also shown are great circle paths between events and stations. 79

16 Seven "Deep Seismic Sounding" (DSS) profiles in Northern Eurasia. 19 PNEs (stars) were used to acquire these data. The many small dots (appearing as dark lines along the profiles) give the location of more than 3000 temporary seismographic stations for the DSS experiments carried out in the former Soviet Union from 1977 to 1988. 81

17 Reduced travel time curves are shown for 22 of the regions depicted in Figure 2. The dashed line ("observed regional") in each case represents the Pn travel-time relationship for the region, as given above in Section 3. The gray line is the IASP91 standard Pn travel time. The dark line ("modeled regional") is the travel time in a 1D structure comprised of a series of layers, in each of which the P-wave velocity increases linearly with depth. The rms misfit is smaller than 0.25 s in all cases. This figure indicates very significant departures from the IASP91 travel times for Pn propagation in different parts of East Asia. 89

18 On the upper right, is shown the system of grid points that allows layer numbers to be identified for a laterally-varying Earth model. Each grid point, or node, is specified by its cartesian coordinates. Lower left, shows a tetrahedron within which the velocity has a linear gradient, so that the ray path follows the arc of a circle. 91

19 a) Geometry of a ray near the surface in the spherical Earth approximated by tetrahedra. Angles d and g are much smaller than shown, in practice. b) Difference between computed travel times and IASP91 travel times, for a 1° x 1° grid. Blue line shows the difference between the actual computed time (ray traced in tetrahedra) and the IASP91 travel time. Red line shows predicted error due to surface approximation (see text). Black line is the

difference between actual and predicted error (blue - red). c) Same as b), except node spacing is reduced to 0.5°. This error is negligible beyond 2°. 92

20 The region boundaries and numbering system used for 36 1D regions in East Asia and surrounding areas, which together make up the 3D velocity model in which 3D ray tracing was used to give our model-based SSSCs. Appendix D provides the lat/long values which specify these boundaries. 94

21 Residuals (observed arrival times minus times expected on the basis of GT information and travel times computed for the model shown in Figure 20), for the field station data associated with six PNEs in Russia for which our observed arrival times and GT information are believed to be of highest quality (see Table 8). 97

22 Pn modeling errors as functions of epicentral distance (total path length from event to station) for IASP91 (red curve) and our regionalized model (magenta curve). Also shown are travel-time misfits to the model-based SSSCs, binned by distance, for Pn phase arrivals (green markers). 98

23 Sn modeling errors as functions of epicentral distance.Markers are defined as in Figure 22. 99

24 Model-based Pn SSSC for station BRVK. The markers (plus signs) indicate the locations of the calibration events. Black and red markers represent positive and negative residuals, respectively, with marker size proportional to the travel-time residual relative to the predicted travel times by 3D ray tracing. 100

25 Modeling errors associated with the Pn SSSC computed using 3D ray tracing for station BRVK. Markers are defined as in Figure 24. 101

26 Model-based Sn SSSC for station BRVK. Markers are defined as in Figure 24. 102

27 Modeling errors associated with the Sn SSSC computed using 3D ray tracing for station BRVK. Markers are defined as in Figure 24. 103

28 Model-based and kriged Pn SSSC for station BRVK. Markers are defined as in Figure 24. 106

29 Grid of kriged modeling errors associated with the Pn SSSC computed for station BRVK. Markers are defined as in Figure 24. 107

30 Model-based and kriged Sn SSSC for station BRVK. Markers are defined as in Figure 24. 108

31 Grid of kriged modeling errors associated with the Sn SSSC computed for station BRVK. Markers are defined as in Figure 24. 109

32 Pn travel-time residuals for station BRVK, before applying model-based Pn SSSCs (IASP91).Black and red markers represent positive and negative residuals, respectively, with marker size proportional to the travel-time residual relative to the predicted travel times. 112

33n travel-time residuals for station BRVK, after applying model-based Pn SSSCs. Markers are defined as in Figure 32. 113

34 Pn travel-time residuals for station BRVK, after applying model-based plus kriged Pn SSSCs. Markers are defined as in Figure 32. 114

35 Mean Pn travel time residuals for all the stations that recorded at least 3 GT events. Blue markers and curve represent the residuals by station without SSSCs (IASP91), green markers and curve represent the residuals by station when model-based SSSCs were applied, and magenta markers and curve represent the residuals by station when model-based SSSCs and kriging were applied. 115

36 Standard deviation of the Pn travel times for all the stations that recorded at least 3 GT events. Markers are defined as in Figure 35. 116

37 Mean Sn travel time residuals for all the stations that recorded at least 3 GT events. Markers are defined as in Figure 35. 117

38 Standard deviation of the Sn travel times for all the stations that recorded at least 3 GT events. Markers are defined as in Figure 35. 118

39 Map of events (red stars) and recording seismic stations (blue triangles) of the data set used for model validation.The green triangles represent the 30 IMS stations that our consortium was tasked to calibrate. Also shown are great circle Pn paths between events and station. 120

40 Map of events (red stars) and recording seismic stations (blue triangles), IMS stations (green triangles) and great circle Sn paths. Markers are defined as in Figure 39. 121

41 Mislocation distances with and without using model-based SSSCs with respect to corresponding GT locations. The green symbols show the events for which the mislocation error is smaller using SSSCs than without.

Red symbols show the events for which the mislocation errors are smaller without using SSSCs. The bisecting line corresponds to equivalent mislocation errors for the two solutions (with and without SSSCs). 122

42 Map showing the distribution of the mislocation results for IASP91 and model-based SSSCs. The green circles show the events for which the mislocation error is smaller using SSSCs than without while the red squares represent the events for which the mislocation errors are smaller without using SSSCs. 123

43 Scatter plot of error ellipse areas computed with (x-axis) and without (y-axis) using model-based SSSCs. Green symbols represent error ellipse areas that are smaller when using the SSSCs than without. 124

44 Relocation results, with and without using SSSCs, for a PNE (Meridian-2) in the Former Soviet Union on 19 September 1973. Mislocation errors relative to the ground-truth location are 20.8 km without using SSSCs, 8.5 km using model-based SSSCs, and 6.6 km using kriged SSSCs. The error ellipse areas are 710 km2 without using SSSCs, 425 km2 using model-based SSSCs, and 357 km2 using kriged SSSCs. 127

45 Relocation results, with and without using SSSCs, for a PNE (Azgir-10) in the Former Soviet Union on 24 October 1979. Mislocation errors relative to the ground-truth location are 19.6 km without using SSSCs, 6.8 km using model-based SSSCs, and 1.0 km using kriged SSSCs. Magenta square markers represent calibration points. The error ellipse areas are 455 km^2 without using SSSCs, 264 km^2 using model-based SSSCs, and 79 km^2 using kriged SSSCs. 128

46 Mislocation distances with and without using kriged SSSCs with respect to corresponding GT locations. Markers and the line are defined as in Figure 41. 129

47 Map showing the distribution of the mislocation results for IASP91 and model-based SSSCs and kriging. Markers are defined as in Figure 42. 130

48 Scatter plot of error ellipse areas computed with (x-axis) and without (y-axis) using kriged SSSCs. Markers are defined as in Figure 43. 131

49 Cumulative probability distribution of the coverage parameter without SSSCs (red), with model-based SSSCs (green), with model-based SSSCs and kriging (magenta, and the theoretical 90 percentile c2 distribution with two degrees of freedom (black). 132

50 Scatter plot of the standard error of observations with (x-axis) and without (y-axis) using kriged SSSCs. The green symbols represent solutions with smaller standard errors using SSSCs, while the red symbols show the solutions with smaller standard errors without using SSSCs. 133

51 Area of the 90% confidence ellipses, as a function of azimuthal gap, for events that have fewer than 10 defining phases. 136

52 Area of the 90% confidence ellipses, as a function of azimuthal gap, for events that have between 5 and 15 defining phases. 136

53 Area of the 90% confidence ellipses, as a function of azimuthal gap, for events that have between 15 and 25 defining phases. 137

54 Area of the 90% confidence ellipses, as a function of azimuthal gap, for events that have between 30 and 40 defining phases. 137

55 Area of the 90% confidence ellipses, as a function of the number of defining phases, for events that have an azimuthal gap lying between 65° and 75°. 138

56 Area of the 90% confidence ellipses, as a function of the number of defining phases, for events that have an azimuthal gap lying between 95° and 105°. 138

57 Area of the 90% confidence ellipses, as a function of the number of defining phases, for events that have an azimuthal gap lying between 120° and 130°. 139

58 Area of the 90% confidence ellipses, as a function of the number of defining phases, for events that have an azimuthal gap greater than 200°. These events thus have a poor station distribution. 139

TABLES

1 Information on the thirty IMS stations of Group 1, for which we have obtained model-based and kriged SSSCs for Pn and Sn, and have evaluated the resulting location improvements. These stations are shown on a map of East Asia in Figure 1. 11

2 Information on the set of 128 stations in East Asia, additional to the 30 IMS stations of Table 1, which we have also analyzed in order to evaluate and validate our claims of location improvements using SSSCs. 14

3 List of DSS Profiles, using chemical explosions, conducted in or near Kazakhstan. 26

4 Empirical travel times reported for seven DSS profiles in and near Kazakhstan. 28

5 Apparent Pn velocity measured from seven DSS profiles in and near Kazakhstan. 29

6 Refined P-velocity models for sub-regions of China. 67

7 Our layered velocity models for subregions of the Indian subcontinent 71

8 The list of 19 PNEs for which we have acquired empirical phase picks. The penultimate column indicates the quality of available information on absolute timing and absolute source and station location for these profiles. 83

9 Mean travel time residuals and velocity corrections for each region 95

10 Comparison of Pn and Sn travel-time residuals for station BRVK. 110

11 RMS of mean and standard deviation of Pn and Sn travel-time residuals for all the stations that recorded at least 3 GT events. 111

12 Location performance metrics for Pn and Sn. 134

13 Location performance metrics for Pn alone. 134

Section 1 Executive Summary

This technical report documents the results of a consortium led by the Lamont-Doherty Earth Observatory of Columbia University, which worked for three years with four other organizations to improve the capability to locate seismic events based on data acquired by 30 stations of the International Monitoring System (IMS) in East Asia.

We developed source-specific travel times for the regional phases Pn and Sn, for each of these 30 IMS stations. These travel times are reported as corrections to the standard (IASP91) model of travel times. We also developed such Source Specific Station Corrections (SSSCs) for an additional 128 stations in East Asia, used for validation testing. Our SSSCs were computed by 3D ray tracing in a velocity model of East Asia which we developed using 36 different regions, in each of which we obtained velocity as a function of depth. Our model-based SSSCs were re ned empirically by applying a kriging algorithm to travel-time residuals for ground-truth (GT) events. Off-line validation tests were performed by evaluating travel-time residuals and by relocating GT events, with and without using SSSCs. To test the validity of the model directly, relocation tests were first performed using model-based SSSCs without kriging. Tests were then performed to evaluate the kriged SSSCs, using a leave-one-out approach so that events were not simultaneously used both to compute and to test the SSSCs.

Nuclear explosions dominated our ground-truth datasets in the first two years of this project. In particular we used source parameters for Soviet-era Peaceful Nuclear Explosions (PNEs). But this approach, while quite satisfactory for calibrating stations in much of Russia and Central Asia (which made up approximately half the IMS stations we studied) could not be extended to the remaining stations, for which it was necessary to develop GT information on signi cant numbers of earthquakes. By use of the double-difference method for locating many seismic events at the same time, and detailed fault maps, we obtained 64 GT earthquakes (with absolute epicenter errors less than 5 km with high confidence) by re-analyzing the Annual Bulletin of Chinese Earthquakes (ABCE) for a 15-year period (1985 to 1999). This bulletin contains phase picks for approximately 1000 earthquakes in and near China, each year.

Using Pn and Sn arrival times for our GT data sets, we relocated 525 events recorded by various combinations of 140 regional stations in East Asia. Mislocations were reduced for 66% of the

events using the model-based SSSCs, and for 85% of the events using model-based SSSCs re ned by kriging. Median mislocation improved from 16.9 km to 11.4 km and 6.5 km, respectively. Median error ellipse area was reduced from 2,616 km^2 to 1,633 km^2 and 722 km^2, respectively. Error ellipse coverage (percentage of GT locations within 90% error ellipses) was 89% without using SSSCs, 91% using model-based SSSCs, and 92% using kriged SSSCs. These results were obtained for source locations, stations, and paths, that sample very extensive and diverse geological provinces throughout much of Asia. Though we used both Pn and Sn phase picks, in practice the addition of Sn data provided only marginal improvement over the use of Pn alone.

These results were confirmed in May 2003 by an integration test conducted by the Research and Development Support System for the group then known as the Center for Monitoring Research.

In all cases, our results demonstrate that the regionalization and travel-times curves, developed by the Lamont Consortium for Group 1 stations, along with the computational methods of 3D ray tracing and kriging, have produced Pn and Sn SSSCs, and modeling errors, that significantly improve the location performance and uncertainty estimates in East Asia. We expect that these SSSCs will perform, on average, as well as indicated by the validation test results for the model-based SSSCs; and substantially better for regions surrounding the Lop Nor, Semipalatinsk, Indian and Pakistan nuclear test sites, where high-quality calibration data have been utilized.

The underlying reason why our SSSCs provide very signi cant reductions in mislocation and in the size of confidence ellipses, is that the standard IASP91 travel times give a poor representation of regional travel times for much of East Asia. Finally, we note that our overall method (of first obtaining model travel times and then kriging with empirical data) is well suited to calibration of any stations in East Asia that have a significant archive of reliably measured arrival times.

1.1. Documentation

Our results described in this report are supported by a CD containing details of our 3D model, our GT events (including phase picks in a standard format) and our model-based and kriged SSSCs together with an estimate of their errors. Our work is additionally documented by the papers and reports listed below.

Papers in reviewed journals:

Fisk, Mark D. Accurate locations of nuclear explosions at the Lop Nor Test Site using alignment of seismograms and IKONOS satellite imagery, Bull. Seism. Soc. Amer., 92, 2911 -- 2925, 2002.

Waldhauser, Felix, and Paul G. Richards. Reference events and empirical Source Specific Station Corrections for regional phases at IMS stations in China, Bulletin of the Seismological Society of America, submitted for publication, June 9, 2003.

Schaff, David P., and Paul G. Richards. Lg-wave cross correlation and double-difference location: application to the 1999 Xiuyan, China, sequence, Bulletin of the Seismological Society of America, submitted for publication, June 25, 2003.

Yang, Zhi-xian, Felix Waldhauser, Yun-tai Chen, and Paul G. Richards. Relocation of earthquakes in central-western China using the double-difference earthquake location algorithm, ms. submitted for publication, Journal of Seismology, May 2003.

Schaff, David P., and Paul G. Richards. High precision location of seismic activity across China, draft ms, for submission to SCIENCE, August 2003.

Waldhauser, Felix, David P. Schaff. Location of underground nuclear explosions at the Lop Nor Test Site, 1969 to 1996, draft ms, for submission to Bull. Seism. Soc. Amer., August 2003.

Richards, Paul G., Mark D. Fisk, Valeriu Burlacu, Vitaly I. Khalturin, Won-Young Kim, David P. Schaff, Anastasia Stroujkova, Felix Waldhauser, John Armbruster, Michael West, Igor Morozov, Elena Morozova, Vernon Cormier, and Chandan Saikia. Development and Validation Testing of a Regionalized Travel-Time Model, and Source-Specific Station Corrections for Thirty IMS Stations and Other Stations in East Asia, in preparation for submission to Bull. Seism. Soc. Amer., September 2003.

Papers in proceedings volumes of annual Seismic Research Review meetings:

Richards, Paul G., Won-Young Kim, Vitaly I. Khalturin. A Plan for Seismic Location Calibration of 30 IMS stations in Eastern Asia, in Proceedings of the 22nd Seismic Research Review, New Orleans, LA, 2000.

Conrad, Clint, Mark Fisk, Vitaly I. Khalturin, Won-Young Kim, Igor Morozov, Elena Morozova, Paul G. Richards, David Schaff, and Felix Waldhauser. Seismic Location Calibration for 30 International Monitoring System stations in Eastern Asia, in Proceedings of the 23rd Seismic Research Review, Jackson Hole, WY, 2001.

Armbruster, John, Valeriu Burlacu, Mark Fisk, Vitaly I Khalturin, Won-Young Kim, Igor Morozov, Elena Morozova, Paul G. Richards, David Schaff, and Felix Waldhauser. Seismic Location Calibration for 30 IMS stations in Eastern Asia, in Proceedings of the 24th Seismic Research Review, Ponte Vedra, FL, 2002.

Richards, Paul G., John Armbruster, Valeriu Burlacu, Vernon Cormier, Mark Fisk, Vitaly I Khalturin, Won-Young Kim, Igor Morozov, Elena Morozova, Chandan Saikia, David Schaff, Anastasia Stroujkova, and Felix Waldhauser. Seismic Location Calibration for 30 IMS stations in Eastern Asia: Final Results, in Proceedings of the 25th Seismic Research Review, Tucson, AZ, 2003.

Papers given at Oslo workshops, organized by NORSAR:

Emanov, A. F., A.G. Filena, V.I. Khalturin, W.-Y. Kim, and P.G. Richards. Earthquakes and Large Mining Blasts in Southwestern Siberia, Russia, in Proceedings of a Workshop on IMS location capability, Oslo, Norway, 1999.

Richards, Paul G. Accurate estimates of the absolute location of underground nuclear tests at the northern Novaya Zemlya Test Site, in Proceedings of a Workshop on IMS location capability, Oslo, Norway, 2000.

Richards, Paul G. A plan for seismic location calibration of 30 IMS stations in Eastern Asia, in Proceedings of a Workshop on IMS location capability, Oslo, Norway, 2000.

Fisk, Mark, Steven Bottone, Valeriu Burlacu, and Clinton Conrad. Preliminary Source Specific Station Corrections for Regional Phases at IMS Seismic Stations in Central Asia, in Proceedings of a Workshop on IMS location capability, Oslo, Norway, 2001.

Conrad, Clint, Mark Fisk, Vitaly I Khalturin, Won-Young Kim, Igor Morozov, Elena Morozova, Paul G. Richards, David Schaff, and Felix Waldhauser. Seismic Location Calibration for 30 IMS stations in Eastern Asia, in Proceedings of a Workshop on IMS location capability, Oslo, Norway, 2001.

Fisk, Mark, and Valeriu Burlacu. Source Specific Station Corrections for IMS Stations in Asia: Validation Test Results, in Proceedings of a Workshop on IMS location capability, Oslo, Norway, 2002.

Waldhauser, Felix, Paul G. Richards, David Schaff, Won-Young Kim. IMS Station Calibration and Earthquake Relocation in China, in Proceedings of a Workshop on IMS location capability, Oslo, Norway, 2002.

Richards, Paul G., Vitaly I. Khalturin, W.-Y. Kim, J. Armbruster, Mark Fisk, Valeriu Burlacu, Chandan Saikia, Gene Ichinose, Igor Morozov, Elena Morozova, Vernon Cormier, and Anastasia Stroujkova. Progress in Location Calibration for 30 IMS Stations in East Asia, in Proceedings of a Workshop on IMS location capability, Oslo, Norway, 2002.

Richards, Paul G. Calibration of 30 IMS stations in East Asia by the Lamont Consortium: Introduction and overview, in Proceedings of a Workshop on IMS location capability, Oslo, Norway, 2003.

Waldhauser, F., P.G. Richards, W.-Y. Kim, D. Schaff, J. Armbruster. GT Event Sets, and associated Datasets, in Proceedings of a Workshop on IMS location capability, Oslo, Norway, 2003.

Burlacu, Valeriu, and Mark Fisk. Source Specific Station Corrections for IMS Stations in Asia: Quantification of Location Performance, in Proceedings of a Workshop on IMS location capability, Oslo, Norway, 2003.

Other presentations:

Richards, Paul G. A Plan for Seismic Location Calibration of 30 IMS Stations in Eastern Asia, Spring meeting of the American Geophysical Union, 2000.

Richards, P.G, V.I. Khalturin, and W.-Y. Kim. Seismic Event Location in Eastern Asia: Current Problems and Future Solutions, meeting of the International Association of Seismology and Physics of the Earth's Interior, Hanoi, Vietnam, 2001.

Richards, P.G, V.I. Khalturin, and W.-Y. Kim. Seismic Event Location: Current Problems and Future Solutions, Annual Meeting of the Seismological Society of America, 2001.

Khalturin, V.I, and P.G. Richards. An Analysis of Announced Yields and Reported Magnitudes for Underground Nuclear Explosions at Novaya Zemlya, Annual Meeting of the Seismological Society of America, 2001.

Fisk, M., V. Burlacu, J. Armbruster, V.I. Khalturin, W.-Y. Kim, P.G. Richards, C. Saikia, G. Ichinose, E. Morozova, I. Morozov, V. Cormier. Progress in Wide-Area Seismic Event Location on the Regional Scale, Annual Meeting of the Seismological Society of America, 2002.

Richards, P.G., F. Waldhauser, D. Schaff, V.I. Khalturin, W.-Y. Kim, J. Armbruster, M. Fisk, R. Burlacu, C. Saikia, G. Ichinose, A. Stroujkova, and V. Cormier. Progress in Wide-Area Seismic Event Location on the Regional Scale, Annual Meeting of the Seismological Society of America, 2003.

Richards, P.G., and W.-Y. Kim. On Seismic Sources Characterized by Volume Changes, Annual Meeting of the Seismological Society of America, 2003.

Richards, P.G., F. Waldhauser, D. Schaff, V.I. Khalturin, W.-Y. Kim, M. Fisk, R. Burlacu, C. Saikia, I. Morozov, A. Stroujkova, and V. Cormier. Progress in Wide-Area Seismic Event Location on the Regional Scale, meeting of the International Association of Seismology and Physics of the Earth's Interior, Sapporo, Japan, 2003.

Rodi, W., E.R. Engdahl, E.A. Bergman, F. Waldhauser, G.L. Pavlis, H. Israelsson, and J.E. Dewey. A Comparison of Multiple-Event Location Methods, meeting of the International Association of Seismology and Physics of the Earth's Interior, Sapporo, Japan, 2003.

Section 2 Introduction

2.1 Identification

This document describes the development and validation testing of Source Specific Station Corrections (SSSCs) for the Group 1 set of IMS stations, carried out by the Lamont Consortium, for Pn and Sn regional travel times at seismic stations in East Asia.

These SSSCs were computed initially by 3D ray tracing through a structural model, derived from combining regionalized 1D travel-time curves for Asia based on published studies. The model-based SSSCs were then modified by applying a kriging algorithm (e.g., Bottone et al., 2002) to empirical travel-time observations from events with ground-truth (GT) locations. The resulting SSSCs are in the form of grid files (in a standard format for operational use) with one-degree resolution, extending out to 20 degrees from a given station. They represent travel-time corrections relative to the IASP91 travel-time tables (Kennett, 1991).

Off-line validation testing was performed by relocating GT events using the program *EvLoc* (e.g., IDC7.1.5, 2001), with and without the use of SSSCs.

All events used in this analysis have published locations that are considered accurate to within 10 km. The majority of events in Russia and Central Asia have GT locations accurate to within 1 km. In China, most events have GT locations accurate to within 5 km. (For definitions of GT location categories, see Yang and Romney, 1999.)

A leave-one-out approach was used at the stage of validation, so that events were not simultaneously used to both compute and test the SSSCs. Performance metrics are provided in terms of statistics of travel-time residuals, mislocation errors, the size of location error ellipses, and their coverage.

2.2. Scope and Audience

The goal of this effort is to provide SSSCs for operational use that improve the accuracy of location estimates of seismic events, and that reduce the uncertainty of these estimates, on the basis of the interpretation of the arrival times of regional seismic waves observed at thirty stations of the International Monitoring System (IMS) located in East Asia (see Table 1 and Figure 1).

This document describes our regionalization of Asia and travel-time curves for these regions, the underlying data sets, the calculation of SSSCs using 3D ray tracing and kriging, and the validation testing and performance metrics.

The intended audience for most of the time this three-year project has been carried out, has been the Center for Monitoring Research and Development Support System (RDSS) staff — who have performed integration testing of SSSCs (and other system enhancements) — together with other interested members of the scientific community. Our work has demonstrated that regional P-wave travel times in East Asia can range up to several seconds less than or greater than the standard IASP91 travel times, so we anticipate that any users of regional signals recorded by the Group 1 stations, who desire good estimates of event location, can benefit from application of our SSSCs.

2.3. Overview

Following this introduction, the present report is divided into five main Sections, namely: Regionalization and Travel-Time Curves for East Asia (Section 3), Data Sets (Section 4), Model Revision and Computation of SSSCs (Section 5), Validation Testing and Evaluation (Section 6), and Conclusions and Recommendations (Section 7).

Section 3 provides a comprehensive description of our procedure for breaking the vast East Asia region into subregions, accompanied by a review of data concerning the propagation of regional seismic waves and the estimation of travel times, in each subregion, as a function of distance for regional seismic phases Pg, Pn, Sn, and Lg. This Section 3 is presented chronologically in a way that reflects the initial approach and subsequent approaches actually adopted by the Lamont Consortium over the three year period from April 2000 to March 2003, during which most of our research was carried out.

Section 4 describes the ground truth (GT) data sets used for kriging empirical observations and for the off-line validation test. Appendices A and B provide further information on our GT events, and Appendix C describes arrival-time datasets associated with the Soviet-era Peaceful Nuclear Explosion (PNE) program. Section 5 presents the methods (3D ray-tracing and kriging) used to generate our SSSCs. Appendix D gives details of our final model (the boundaries of 36 sub-regions, and velocity as a function of depth within each sub-region). Section 6 describes the validation test and a quantitative assessment of our results, using standard evaluation metrics. These results demonstrate significant improvements in location performance due to the SSSCs. In Section 7 we provide conclusions regarding the results of the validation test and recommendations for use of these SSSCs in an operational system. Appendix E provides plots of the explicit SSSCs and modeling errors for thirty seismographic stations in East Asia. Off-line testing was also performed independently by RDSS staff. Appendix F provides the detailed results of the RDSS Validation Test Report.

It should be noted that our preferred approach to IMS station calibration emphasizes the acquisition and use of empirical travel times where possible, rather than relying upon a modeling approach. Our main concern is obtaining accurate travel times, and for this purpose the use of tomographic procedures, while of interest, often represents a circuitous way to obtain travel times. We prefer to obtain travel times directly where possible, acknowledging that such data can also, if desired, be used in tomography to improve structural models.

Section 3 Regionalization and Travel-Time Curves for East Asia

Here we document and justify our approach to obtaining travel times by a process of regionalization of East Asia. During 2000 and 2001 in our initial research we focused on a limited number of IMS stations in Central Asia and part of Russia, and made them the subject of a CCB proposal in May 2002 (Richards et al., 2002). For the present analysis of all thirty IMS stations in Group 1, our initial 3D model of travel times for East Asia was subsequently revised in four ways:

(1) by special studies of China;

(2) by special studies of India;

(3) by accommodating a separation of oceanic and continental regions that recognizes shallow oceans are typically underlain by continental crust; and

(4) by minor revisions of our initial travel time model for Russia and Central Asia.

In this Section we describe our initial work and the rst three of the revisions listed above. The fourth revision, is described below in Section 5.

Table 1 lists the thirty IMS stations of Group 1, for which we have obtained model-based and kriged SSSCs. The same stations are shown on a map of East Asia in Figure 1.

Table 1. Information on the thirty IMS stations of Group 1, for which we have obtained model-based and kriged SSSCs for Pn and Sn, and have evaluated the resulting location improvements. These stations are shown on a map of East Asia in Figure 1.

IMS Code	Country	Station Name	Lat (°N)	Long (°E)
PS12	China	Hailar	49.2670	119.7420
PS13	China	Lanzhou	36.0867	103.8444
PS23	Kazakhstan	Makanchi	46.8077	81.9769
PS25	Mongolia	Javhlant	47.8652	107.0528
PS29	Pakistan	Pari	33.6500	73.2517
PS31	Republic of Korea	Wonju	37.4421	127.8844
PS33	Russian Federation	Zalesovo	53.9367	84.7981
PS34	Russian Federation	Norilsk	69.4300	88.0830
PS35	Russian Federation	Peleduy	59.6553	112.4408

Table 1. Information on the thirty IMS stations of Group 1, for which we have obtained model-based and kriged SSSCs for Pn and Sn, and have evaluated the resulting location improvements. These stations are shown on a map of East Asia in Figure 1. (Continued)

IMS Code	Country	Station Name	Lat (°N)	Long (°E)
PS37	Russian Federation	Ussuriysk	44.2800	132.0800
PS41	Thailand	Chiang Mai	18.4575	98.9429
AS7	Bangladesh	Chittagong	22.3500	91.8167
AS20	China	Baijiatuan	40.0403	116.1750
AS21	China	Kunming	25.1233	102.7400
AS22	China	Sheshan	31.0956	121.1867
AS23	China	Xi'an	34.0394	108.9214
AS57	Kazakhstan	Borovoye	53.0581	70.2828
AS58	Kazakhstan	Kurchatov	50.7149	78.6208
AS59	Kazakhstan	Aktyubinsk	50.4348	58.0167
AS60	Kyrgyzstan	Ala-Archa	42.6333	74.4944
AS68	Nepal	Everest	27.9600	86.8200
AS86	Russian Federation	Seymchan	62.9330	152.3730
AS87	Russian Federation	Talaya	51.6807	103.6438
AS88	Russian Federation	Yakutsk	62.0308	129.6812
AS89	Russian Federation	Urgal	51.0986	132.3639
AS90	Russian Federation	Bilibino	68.0580	166.4490
AS91	Russian Federation	Tiksi	71.6300	128.8630
AS92	Russian Federation	Yuzhno-Sakhalinsk	46.9583	142.7610
AS93	Russian Federation	Magadan	59.5540	150.8050
AS100	Sri Lanka	Colombo	6.9000	79.8667

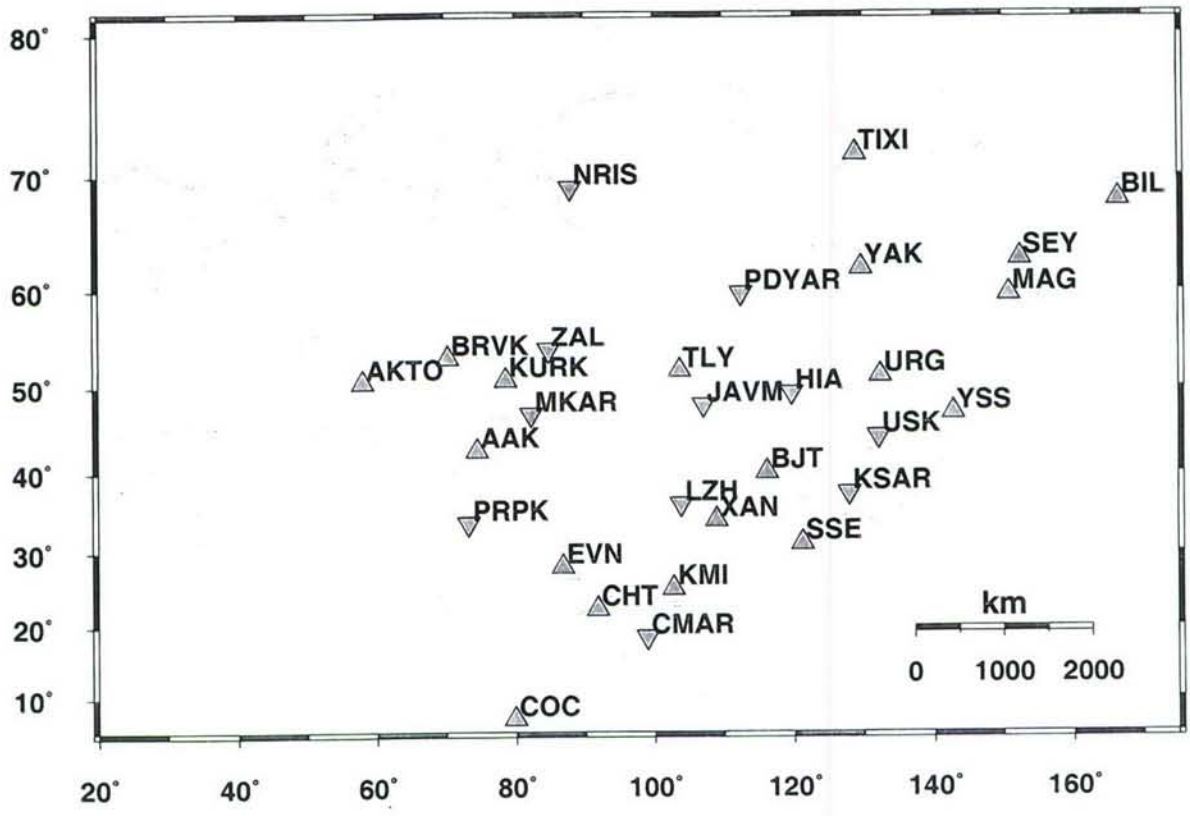


Figure 1. Map showing the location of 30 IMS stations (11 primary, 19 auxiliary) which we have calibrated in this project. The markers for primary stations are inverted green triangles while those for auxiliary stations are green triangles.

We note that at present not all of the stations in Figure 1 and Table 1 are operating and contributing data routinely to the IDC in Vienna. In some cases where stations have been operating and contributing only in recent years, we have based our SSSCs on data derived from a nearby station with a longer history of operation. For example, an array at Makanchi is now operating and contributing data to Vienna. Previous to this operation, we have had access to high-quality broadband three-component data from instrumentation installed in 1994 approximately ten km north of the current array. Similarly, Borovoye, Kurchatov, Makanchi and Ala-Archa are sites at which a variety of broadband instrumentation has been operated for several years, enabling significant empirical databases to be accumulated for calibration of IMS stations installed recently at slightly different locations with the same name. Aktyubinsk has been operated for several years

by Russian seismologists, and intermittently since 1994 by Kazakhstan. NIL (Nilore, Pakistan) is a station very close to the planned IMS primary station at Pari (PS29).

In addition to the stations listed in Table 1, we have derived SSSCs at 128 stations listed in Table 2. Some of these are useful surrogates for specific MS stations, not yet operating, that we are attempting to calibrate in Asia. Others are stations with significant archives of regional signals, and for which we can acquire data that enable relocations using the same general approach that we have applied to IMS stations in East Asia.

Table 2. Information on the set of 128 stations in East Asia, additional to the 30 IMS stations of Table 1, which we have also analyzed in order to evaluate and validate our claims of location improvements using SSSCs.

Station Code	Country	Station Name	Lat (°N)	Long (°E)
AAA	Kazakhstan	Alma-Ata	43.2069	76.9189
AAB	Kazakhstan	Talgar	43.2487	77.2237
ABKT	Turkmenistan	Alibek	37.9304	58.1189
ABS	Russian Federation	Abastumani	41.7500	42.8160
AKH	Russian Federation	Akhalkalaki	41.4170	43.4830
ALU	Ukraine	Alushta	44.6820	34.4030
ANN	Russian Federation	Anapa	44.8000	37.4330
ANR	Uzbekistan	Andizhan	40.7500	72.3700
APA	Russian Federation	Apatity	67.5690	33.4050
ARU	Russian Federation	Arti	56.4302	58.5625
ASH	Turkmenistan	Ashkhabad	37.9500	58.3500
BAK	Azerbaijan	Baku	40.3833	49.9000
BEY	Russian Federation	Becho	44.0500	42.6000
BILL	Russian Federation	Bilibino	68.0389	166.2711
BJT	China	Baijiatuan	40.0183	116.1679
BKR	Russian Federation	Bakuriani	41.7333	43.5167
BOD	Russian Federation	Bodaibo	57.8190	114.0040

Table 2. Information on the set of 128 stations in East Asia, additional to the 30 IMS stations of Table 1, which we have also analyzed in order to evaluate and validate our claims of location improvements using SSSCs. (Continued)

Station Code	Country	Station Name	Lat (°N)	Long (°E)
CD2	China	Chengdu	30.9100	103.7578
CHCP	Pakistan	Chirah-Chowk	33.6583	73.2638
CHM	Kazakhstan	Chimkent	42.3190	69.6030
CHTO	Thailand	Chiang Mai	18.7900	98.9769
CIF	China	Chifeng	42.2990	118.9750
CLI	China	Changli	39.7580	119.0930
CN2	China	Changchun	43.8014	125.4483
CQI	China	Chongqing	29.4220	106.5740
CRA	Ukraine	Chernovtsy	48.2833	25.9333
CUR	Russian Federation	Chagan-Uzun	50.1000	88.3500
DL2	China	Dalian	38.9061	121.6283
DSH	Tadzhikistan	Dushanbe	38.5583	68.7750
DUS	Russian Federation	Dusheti	42.0830	44.7000
ELT	Russian Federation	Yeltsovka	53.2620	86.2406
ENS	China	Enshi	30.2820	109.4980
ERE	Armenia	Yerevan	40.1733	44.4700
FAB	Kazakhstan	Fabrichnaya	43.1470	76.4470
FEO	Ukraine	Feodosiya	45.0190	35.3900
FRG	Uzbekistan	Fergana	40.3740	71.7850
FRU	Kyrgyzstan	Bishkek	42.8408	74.6136
GAR	Tajikistan	Garm	39.0300	70.3167
GBA	India	Gauribidanur Array	13.6042	77.4361
GEG	Russian Federation	Gegechkori	42.4170	42.3830
GOR	Russian Federation	Gori	41.9830	44.1330
GRO	Russian Federation	Groznyy	43.3200	45.7000
GRS	Armenia	Goris	39.5000	46.3333

Table 2. Information on the set of 128 stations in East Asia, additional to the 30 IMS stations of Table 1, which we have also analyzed in order to evaluate and validate our claims of location improvements using SSSCs. (Continued)

Station Code	Country	Station Name	Lat (°N)	Long (°E)
GYA	China	Guiyang	26.4586	106.6639
HHC	China	Hu-ho-hao-te	40.8494	111.5636
HIA	China	Hailar	49.2667	119.7417
ILI	Kazakhstan	Ili	43.8600	77.0320
IRK	Russian Federation	Irkutsk	52.2430	104.2710
JHJ	Japan	Hachijojima	33.1200	139.8200
KAB	Russian Federation	Kabansk	52.0500	106.6540
KAT	Turkmenistan	Kizyl-Arvat	39.0280	56.2700
KDS	Kyrgyzstan	Kadzhi-Say	42.1230	77.1880
KHE	Russian Federation	Kheis	80.6167	58.0500
KHO	Tajikistan	Khorog	37.4833	71.5333
KIS	Moldova	Kishinev	46.9980	28.8180
KKJ	Japan	Kaminokuni	41.7800	140.1800
KLD	Russian Federation	Kuldur	49.2300	131.7500
KPC	Russian Federation	Khapcheranga	49.7040	112.3790
KRM	Kazakhstan	Kurmenty	42.9870	78.2750
KRS	Kazakhstan	Krasnogorka	43.2500	75.1667
KRV	Azerbaijan	Kirovabad	40.6470	46.3190
KSV	Ukraine	Kosov	48.3150	25.0667
KUL	Tajikistan	Kulyab	37.9050	69.7880
KUR	Russian Federation	Kuril'sk	45.2333	147.8667
KYA	Russian Federation	Kyakhta	50.3667	106.4500
LEN	Armenia	Leninakan	40.7800	43.8000
LNK	Azerbaijan	Lenkoran	38.7580	48.8520
LSA	China	Lhasa	29.7000	91.1500
LVV	Ukraine	L'vov	49.8190	24.0310

Table 2. Information on the set of 128 stations in East Asia, additional to the 30 IMS stations of Table 1, which we have also analyzed in order to evaluate and validate our claims of location improvements using SSSCs. (Continued)

Station Code	Country	Station Name	Lat (°N)	Long (°E)
MA1	Russian Federation	Magadan 1	60.0460	150.7300
MAK	Russian Federation	Makhachkala	42.9610	47.5060
MEZ	Ukraine	Mezhgor'ye	48.5140	23.5140
MGD	Russian Federation	Magadan	60.0460	150.7300
MIK	Russian Federation	Mikhnevo	54.9500	37.7670
MJAR	Japan	Matsushiro Array	36.5427	138.2070
MKAR	Kazakhstan	Makanchi Seismic Array	46.7937	82.2904
MNK	Belarus	Minsk	54.5000	27.8340
MOS	Russian Federation	Moscow	55.7383	37.6250
MOY	Russian Federation	Mondy	51.6670	100.9930
MUR	Tajikistan	Murgab	38.3667	73.9333
NAK	Azerbaijan	Nakhichevan	39.2110	45.4120
NAM	Uzbekistan	Namangan	40.9910	71.6590
NRIL	Russian Federation	Norilsk	69.5049	88.4414
NRIS	Russian Federation	Norilsk	69.0061	87.9964
NRN	Kyrgyzstan	Naryn	41.4200	75.9780
NVS	Russian Federation	Novosibirsk	54.8404	83.2346
OBN	Russian Federation	Obninsk	55.1138	36.5687
PDY	Russian Federation	Peleduy	59.6333	112.7003
PRLS	Azerbaijan	Pirkuli	40.7840	48.6000
PRZ	Kyrgyzstan	Przheval'sk	42.4720	78.4060
PUL	Russian Federation	Pulkovo	59.7730	30.3240
PYA	Russian Federation	Pyatigorsk	44.0420	43.0660
PZH	China	Pankang	26.5040	101.7430
RAH	Ukraine	Rakhov	48.0550	24.1980

Table 2. Information on the set of 128 stations in East Asia, additional to the 30 IMS stations of Table 1, which we have also analyzed in order to evaluate and validate our claims of location improvements using SSSCs. (Continued)

Station Code	Country	Station Name	Lat (°N)	Long (°E)
RYB	Kyrgyzstan	Rybach'ye	42.4500	76.0833
SAM	Uzbekistan	Samarkand	39.6610	66.9530
SEM	Kazakhstan	Semipalatinsk	50.4083	80.2500
SHE	Azerbaijan	Shemakha	40.6460	48.6420
SHK	Japan	Shiraki	34.5300	132.6800
SHKS	Azerbaijan	Sheki	41.2030	47.1810
SIM	Ukraine	Simferopol	44.9490	34.1167
SNY	China	Shenyang	41.8278	123.5781
SOC	Russian Federation	Sochi	43.5700	39.7630
STE	Armenia	Stepanavan	41.0000	44.3733
SVE	Russian Federation	Sverdlovsk	56.8270	60.6367
TAS	Uzbekistan	Tashkent	41.3290	69.2960
TI2	Russian Federation	Tbilisi 2	41.7303	44.7414
TIA	China	Taian	36.2114	117.1240
TIXI	Russian Federation	Tiksi	71.6490	128.8665
TKM2	Kyrgyzstan	Tokmak	42.9208	75.5966
TLG	Kazakhstan	Talgar	43.2487	77.2237
TSK	Japan	Tsukuba	36.2108	140.1097
TUP	Russian Federation	Tupik	54.4250	119.9540
UER	Russian Federation	Ust'-Elegest	51.5630	94.0870
USK	Russian Federation	Ust'-Kan	50.9370	84.7730
UZH	Ukraine	Uzhgorod	48.6310	22.2930
VAN	Turkmenistan	Vannovskaya	37.9480	58.1080
WJH	China	Wujiahe	41.2890	108.1220
WMQ	China	Urumqi	43.8211	87.6950
WUS	China	Wushi	41.1990	79.2180

Table 2. Information on the set of 128 stations in East Asia, additional to the 30 IMS stations of Table 1, which we have also analyzed in order to evaluate and validate our claims of location improvements using SSSCs. (Continued)

Station Code	Country	Station Name	Lat (°N)	Long (°E)
XLT	China	Xilinhaote	43.8930	116.0740
YAL	Ukraine	Yalta	44.4875	34.1547
YCH	China	Yinchuan	38.6090	105.9330
YNT	China	Yantai	37.5250	121.3880
ZAK	Russian Federation	Zakamensk	50.3820	103.2810
ZEI	Georgia	Tsey	42.7700	43.8980
ZOT	China	Zhaotong	27.2840	103.7170
ZUG	Russian Federation	Zaimshi	42.4000	41.8000

The work of acquiring travel times of seismic waves in East Asia, for purposes of calibrating IMS stations, can conveniently be split into three steps. The first step is to identify the boundaries of subregions, within which travel times show little evidence of lateral variability. Our consortium began with this step in February 2001 at an Experts Group Review Meeting held at Lamont, during which consortium members worked together with two outside advisors (Dr. Charles Langston, of the University of Memphis; and Dr. E. Robert Engdahl, of the University of Colorado) and made a preliminary choice of subregion boundaries. We worked initially with 22 sub-regions. The second step is to review a wide variety of data and previous technical reports and publications, concerning the propagation of regional seismic waves in each subregion, and to obtain best estimates of the travel time as a function of distance, within each subregion, for each major observed seismic phase (notably, Pg, Pn, Sn, and Lg). The third step is to fit the travel times in each subregion with a 1D structural model, and to carry out ray tracing in the aggregated 3D model obtained from all the different 1D subregions, taking account of the need to smooth lateral transitions from one subregion to another.

In our initial research, which was made the basis of a successful CCB proposal in May 2002 (Richards et al., 2002), we needed to carry out only the first two steps, of the three steps outlined above. This was because our initial research used the procedure described by Bondár (1999),

which directly emphasizes acquisition of travel-time information (and forming averages of subregion travel times to predict total travel times for paths that cross regional boundaries), rather than using velocity models of crust and upper mantle and computing the travel times in that Earth model.

Subsequent to February 2001, the predictions of our preliminary regionalization have been compared with a variety of empirical travel times and revised if necessary. Thus, our regionalization has been modified both as to the regional boundaries in some instances, and as to the travel times within some subregions, in order to conform better with gross features of empirical data such as the travel times from Soviet-era Peaceful Nuclear Explosions recorded in East Asia, and the arrival times reported at stations in China for numerous earthquakes. The principal changes between our model of May 2002, and that obtained at the conclusion of our project (and described in this document) concern our regionalization of China and our use of numerous GT earthquakes in and near China. Our present model of East Asia is based on 36 sub-regions.

In Sections 3.1 to 3.7 we describe our approach to the regionalization of East Asia, using a chronological approach in which we first describe our initial model of travel times and the basis for it, then describe how and why it has been revised. Thus, Figure 2 shows two maps of the boundaries of the different subregions, as we defined them for our CCB proposal of May 2002 (Richards et al., 2002). The upper map shows boundaries together with topography. The lower map shows boundaries together with our initial numbering scheme for the different subregions.

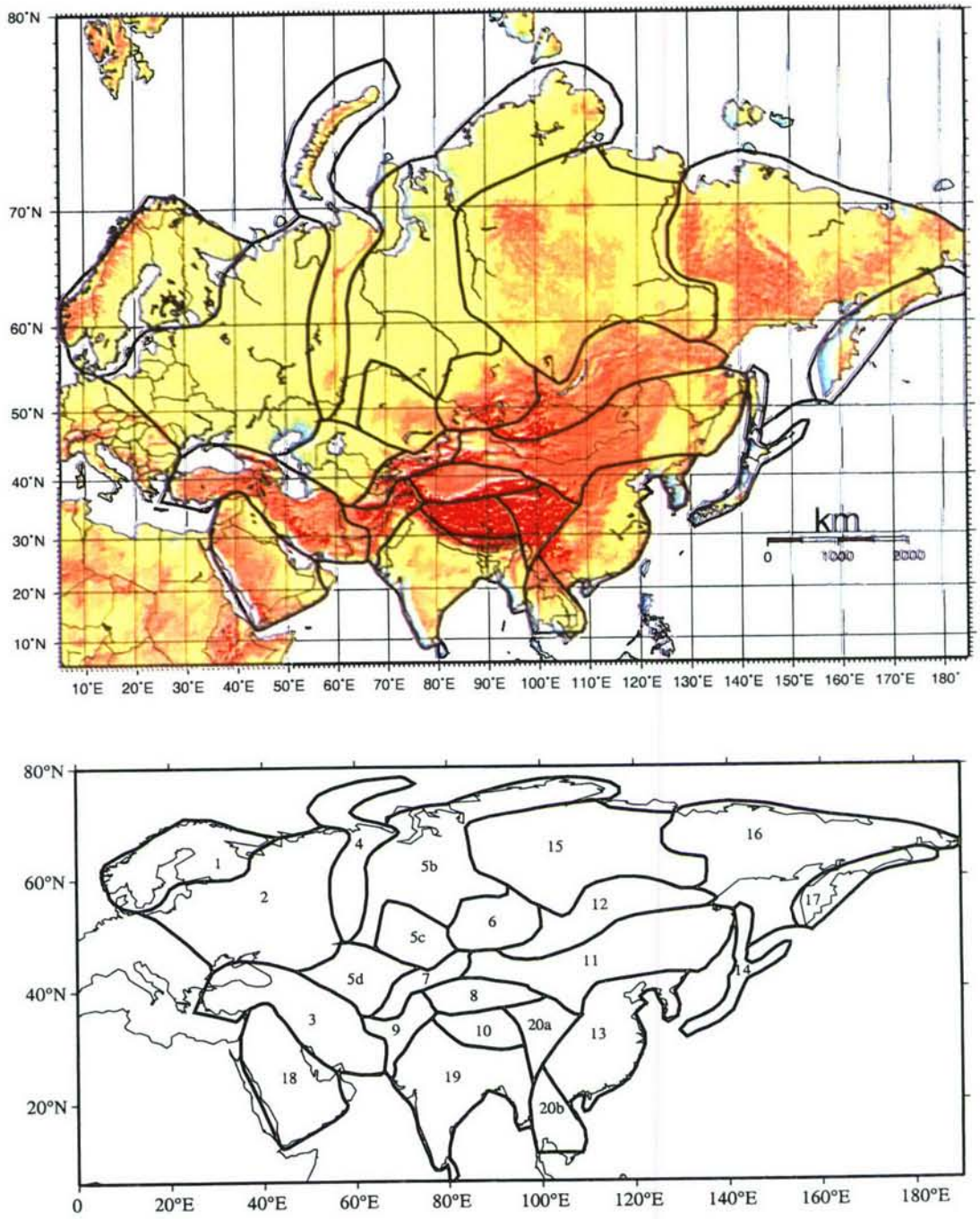


Figure 2. Maps of topography and regionalization boundaries (upper) and the numbering convention used for the various subregions (lower) defined in our CCB proposal of May 2002. In our final 3D model we make significant revisions for the continent/ocean transition, and for India and China (as discussed in Sections 3.5 - 3.7), but the changes we have made for the Former Soviet Union are relatively minor (see Section 5).

3.1. Subregion Boundaries

Our choice of subregion boundaries has been based on expert interpretation of maps of tectonic provinces. It also has taken into account published velocity structures of the crust and upper mantle (including lithospheric thickness), seismic activity, heat flow, and gravity. The tectonic approach is based on structural types such as shields, ancient and young platforms, and fold belts. While information on geophysical parameters has mostly been acquired in recent decades, the basic identification of different geologic provinces was made much earlier in most cases. Useful sources used for identifying subregions were

- The Tectonic map of Eurasia, compiled by the Geological Institute of the Soviet Academy of Science, 1:5,000,000, Moscow, 1966 (in Russian), and
- Seismotectonic map of Asia and Europe, 1:8,000,000, published by the Geological Institute of the Chinese Academy of Sciences, Beijing, 1981 (in Chinese).

The more important sources of information on the velocity structure of the crust and upper mantle, used to assign subregion boundaries for territory of the former Soviet Union, were Beloussov et al. (1991), Beloussov et al. (1992), Egorkin (1980), Karus (1984), Kirichenko and Kraev (2000), Kosminskaya (1980), Nersesov (1987), Pavlenkova (1996), Volvovsky (1991). It may be noted that our regionalization of the territory of the former USSR including Central Asia is based on major efforts made (a) in association with the program of activities known as Deep Seismic Sounding (DSS), and (b) in detailed geological mapping and geophysical surveys carried out during the Soviet era. The DSS profiles associated with nuclear explosions are well known from extensive publications in western journals. Less well known but also very useful in our research, have been the numerous earlier DSS profiles which were carried out with chemical explosions.

Our final regionalization of China is discussed further in Section 3.5. It is based on information in Xiu et al. (1989), Jih (1998), and references therein, together with advice from Chinese scientists (Chen Yun-tai, Yang Zhi-xian) with whom we have worked to interpret the seismicity of Sichuan and Yunnan provinces (Yang et al., 2003). In Section 3.6 we give our final regionalization of the Indian subcontinent, and in Section 3.7 our choice of boundary between oceanic and continental structures. These Sections 3.5 to 3.7 represent revisions to the initial regionalization depicted in Figure 2.

We next describe regional phases associated with the IASP91 model, contrasted with features generally observed in East Asia that differ from this standard travel time model; then we give our main sources of general information on travel times, followed by more detailed comments on subregion travel times and how these differ from IASP91.

3.2. Regional Phases in the IASP91 Model, Compared with General Observation of these Phases in East Asia

Regional phases are seismic waves which propagate in the crust, lithosphere and upper mantle, down to the region in which velocity increases rapidly with depth, at a depth of around 410 km. The Pg, Lg and Rg waves propagate within the continental crust with near constant velocity along the path and having only small regional variations. In most regions, the Pg apparent velocity is 6.10 - 6.25 km/s, Lg velocities are 3.50 - 3.60 km/s, and Rg velocity is in the range 2.7 - 3.0 km/s depending upon the dominant period of the wave train.

According to the IASP91 travel-time table there are two groups of Pn waves: Pn1 and Pn2. The Pn1 wave is the first arrival in the range interval 200 - 1700 km. It has near constant apparent velocity, increasing slightly from 8.08 km/s to 8.14 km/s (+1.2%).

The Pn2 wave of IASP91 appears as a first arrival at a range of around 1700 km, with velocity 8.5 km/s (+4.4%) in the range interval 1700 - 1800 km and velocity 8.9 km/s (+4.7%) in the range 1900 - 2000 km.

In the IASP91 table, the apparent velocity of P waves increases sharply at a range around 2000 km, from 8.9 km/s up to 9.5 km/s in the range 2000 - 2100 km, and increases further to 10.0 km/s in the range 2100 - 2200 km. (These are effects of two travel-time triplications, discussed further, below, in Section 3.4.) Hence this reference table has velocity increases totaling 11.2% over a short interval (2000 - 2200 km). The P waves with velocities of 9.5 km/s and greater propagate beneath the 410 km discontinuity and are usually called "teleseismic" P waves, although they are observed at distances where the regional phase Pn can also be seen. These teleseismic waves can be divided into two types, P1 and P2, for distances up to 2700 - 3000 km. The P1 waves propagate beneath the 410 km boundary and above the 660 km boundary. They are observed as a first arrival at distances between 2000 and 2600 km, with velocity slightly increasing from 10.0 km/s at 2200 km

up to 10.6 km/s (+6%) at 2600 km. The P2 wave appears as a first arrival in the 2600 - 2700 km distance range, where the P wave velocity increases from 10.6 km/s to 12.2 km/s (+15%). Beyond 2700 km the P2 velocity increases only 0.5% per 100 km.

In contrast to these travel times for IASP91, we find evidence in general for significant regional variation of P-wave velocities in East Asia out to distances of 2200 km, and less significant out to 2700 km. Of particular importance is the fact that for some regions of East Asia, Pn is observed as the first arrival out to distances of 2100 - 2200 km.

For Pn waves we use the designations Pn1, Pn2, and in some regions Pn3, in cases where the apparent velocity changes slightly with distance but does not exceed 9.5 km/s.

Sn waves experience significant regional variations in amplitude. They have travel-time variations that are 3 to 5 times larger than the regional variation of Pn travel times. (Unlike Pn, Sn-arrivals must typically be picked within a coda consisting of scattered waves, hence it is not surprising that they have a stronger variation.)

It is known that strong Sn waves are observed in areas south of the Alpine belt, but that very often this phase cannot be detected on records of the events located north of this belt. (The "Alpine belt" includes mountains extending far to the east of the European Alps, through the Caucasus, the Kopet-Dag Mountains, the Tian Shan, and Altay Sayan to Lake Baykal, all of which broadly are associated with the same major event, namely the closing of the Tethys Ocean.)

In Northern Eurasia, Sn waves are observed with apparent velocities 4.5 - 4.7 km/s in the distance range 1400 - 1700 km. Teleseismic S waves can be observed from 1500 - 1700 km and at greater distances, with apparent velocities 5.6 - 5.8 km/s. A time gap of about 20 - 30 s can be observed between regional Sn and teleseismic S waves on the same record, at distances 1400 - 1600 km. If only one S phase is observed in this distance range, uncertainty as to its identification (whether Sn or S) can result in significant scatter in empirical data, and significant travel-time residuals, to the extent that the wrong phase is identified and used for interpretation.

3.3. Published Information on Regional Travel Times

The extensive literature of Russian and Chinese publications on regional seismic travel times proved very helpful to our work. Here we summarize the principal publications. The literature on regional travel times in Indian is much less extensive.

3.3.1. The Former Soviet Union and Surrounding Areas

Although hundreds of papers (based mostly on DSS results) are devoted to the velocity structure of the crust and upper mantle of different regions of the former USSR and surrounding areas, only a few of them quote the primary travel-time data on which these studies are based. Again we stress that our approach to IMS station calibration has emphasized the acquisition and direct use of empirical travel times where possible, rather than relying upon models of Earth structure. References to specific publications that are important for particular subregions are given below. Here, we note that more general data on travel times from DSS data can be found in Karus (1984), Ryaboy (1989), Ryaboy (1991), Volvovsky (1991), and Zunnunov (1985).

It was easier to obtain travel-time information for seismically active zones, for which regional seismologists have collected many observational results, but unfortunately most of them were limited to distance ranges up to only 800 - 1000 km. Travel-time data for greater distances have been published only in a few papers. The most important of them is Nersesov and Rautian (1964). This main paper covered a very wide region, extending from Central Asia to the north and east as far as the Lena River (north of Lake Baykal). Subregional versions of data in the main paper were described in three reports and one paper: Khalturin (1974), Khalturin at al. (1978), Khalturin et al. (1994), Khalturin et al. (2001).

Other significant seismological publications containing travel-time information for more than one of our subregions are: Atabaev and Butovskaya (1986), Gorbunova (1990), Kirichenko and Kraev (2000), Lukk and Nersesov (1967), and Nersesov (1960).

Table 3 lists 27 Deep Seismic Sounding pro les in Central Asia carried out with chemical explosions. This table is assembled from information in Antonenko (1984), Shatsilov (1993), Zunnunov (1985) and the book "Seismic Models of the Lithosphere of the main Geostructures in territory of the USSR" published in 1980. Figure 3 shows the location of these 27 profiles, some

of which consisted of more than one segment. Table 4 gives the empirical travel time of Pn arrivals picked from seven DSS profiles using chemical explosions in and near Kazakhstan (information from Zunnunov, 1985). Table 5 gives a simple (straight line) travel time as a function of distance, for the Pn wave on these seven profiles, and also the distance over which this time vs. distance relation applies. Figure 4 shows seven values for the average Pn velocity obtained from the data associated with Table 4 and Table 5. All of this information was used in our regionalization of Central Asia and surrounding areas.

Section 3.4 gives more detailed comments on regional travel times within specific subregions of the former Soviet Union, together with figures showing the residual against the IASP91 travel times for some subregions within and near Central Asia.

Table 3. List of DSS Profiles, using chemical explosions, conducted in or near Kazakhstan.

N	Name or position	Profile end points	Length, km
1.	Turkestanski	42.5N 65.0E to 44.7N 75.0E 46.3N 81.0E to 49.0N 83.4E	1,550
2.	Charsky - Sinyuha	49.3N 80.8E to 50.4N 83.2E	220
3.	Sayakski, first line second line	43.1N 74.9E to 46.5N 76.8E 46.6N 77.3E to 51.1N 82.1E	600
4.	Aktogaysky	44.7N 78.6E to 47.5N 80.5E	350
5.	Kentierlausskiy	47.1N 72.9E to 47.5N 80.5E	570
6.	Zhalanash - Taldi-Kurgan	43.0N 78.5E to 45.0N 78.5E	220
7.	Issikski	43.3N 77.7E to 46.2N 77.3E	315
8.	Central Kazakhstansky	47.4N 70.7E to 49.0N 77.7E	540
9.	Issik-Kul - Balkhash	43.3N 77.0E to 46.0N 75.0E	430
10.	Slavgorodsky	46.2N 73.8E to 51.4N 77.5E	520
11.	Shchuchinsk - Severnoe	53.4N 71.6E to 56.3N 76.3E	700
12.	Karkaralinsky	48.8N 75.2E to 50.6N 69.2E	780
13a.	Temirtay-Petropavlovsk	50.3N 72.9E to 54.8N 69.4E	600
13b.	Balkhash-Temirtau	46.9N 75.0E to 50.3N 72.9E	500
14.	Uvanassky	43.6N 74.0E to 46.1N 65.2E	740

Table 3. List of DSS Profiles, using chemical explosions, conducted in or near Kazakhstan. (Continued)

N	Name or position	Profile end points	Length, km
15.	Aris'- Balkhash	42.5N 68.7E to 45.7N 73.4E	510
16.	Temirtau - Kuybishev	50.3N 72.9E to 52.2N 54.0E	1,360
17.	Peschaniy	43.9N 68.8E to 47.0N 72.6E	460
18.	Karatau - Tengiz Lake	43.2N 70.5E to 50.2N 69.0E	900
19.	Kzil-Orda - Dzheti-Konur	44.8N 65.6E to 47.7N 68.8E	400
20.	Meridian	42.8N 67.4E to 49.5N 68.3E	740
21.	1-T-70	47.4N 65.8E to 48.6N 58.6E	550
22.	Aktyubinsky	50.0N 62.1E to 50.2N 57.5E	300
23.	Kopet-Dag - Aral Sea	40.0N 58.0E to 43.8N 61.3E	650
24.	Kandagachsky	49.0N 59.5E to 50.8N 52.0E	540
25.	Chelkar - Volgograd	48.5N 58.0E to 49.0N 54.OE	930
26.	OP-1 and 11	41.2N 54.5E to 52.3N 53.7E	1,680
27.	Farab - Tamdi-Bulak	40.0N 63.5E to 43.0N 65.0E	430

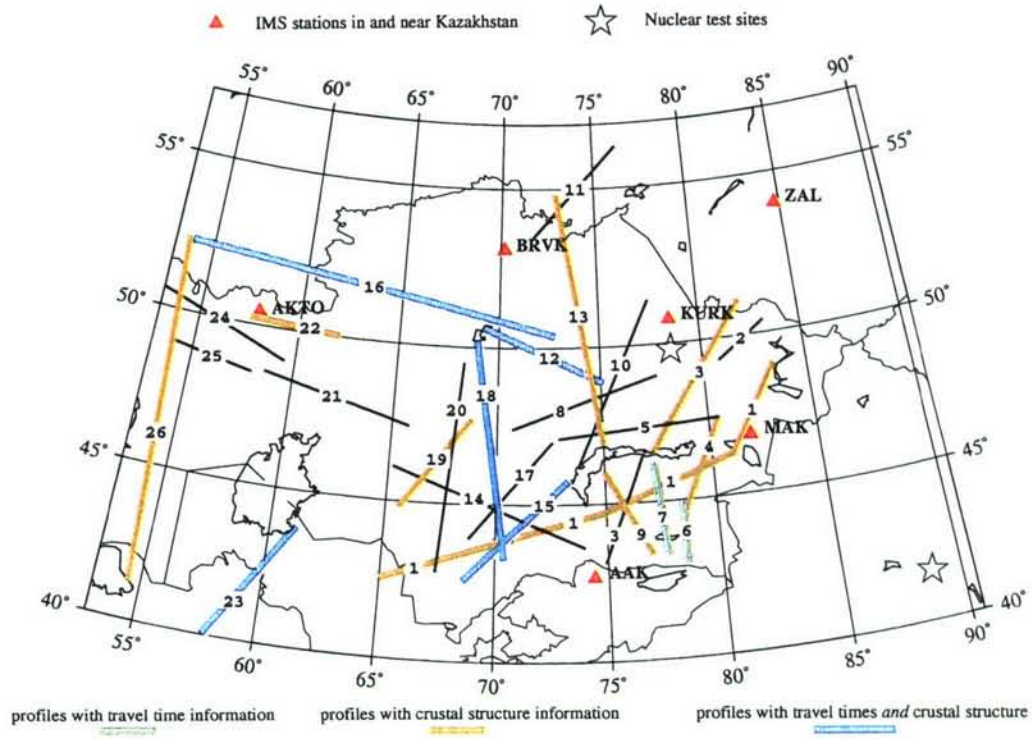


Figure 3. Major Deep Seismic Sounding profiles of Kazakhstan and nearby regions.

Table 4. Empirical travel times reported for seven DSS profiles in and near Kazakhstan.

	Profiles numbers on the map (Figure 3)							
R, km	**6**	**7**	**15**	**16**	**18**	**23**	**27**	IASP91
160	-	-	-	27.5	-	27.5	28.1	-
200	35.8	-	34.4	32.6	33.0	33.0	33.4	32.3
240	40.9	40.9	38.4	37.7	38.3	38.2	38.0	37.2
280	45.5	45.6	43.3	43.2	43.1	43.0	42.9	42.2
320	50.4	50.6	47.9	47.8	47.8	47.7	-	47.1
360	55.1	55.4	52.9	52.6	52.6	52.8	-	52.1

Table 4. Empirical travel times reported for seven DSS profiles in and near Kazakhstan.

	Profiles numbers on the map (Figure 3)							
R, km	6	7	15	16	18	23	27	IASP91
400	60.7	60.9	58.2	57.5	57.5	57.2	-	57.0
440	-	-	64.0	-	62.5	62.3	-	62.0
480	-	-	69.5	-	66.8	67.3	-	66.9
520	-	-	74.2	-	71.4	72.7	-	71.9
560	-	-	-	-	76.2	77.6	-	76.8
600	-	-	-	-	81.1	82.5	-	81.7
640	-	-	-	-	86.0	-	-	86.7
680	-	-	-	-	91.1	-	-	91.6
720	-	-	-	-	96.2	-	-	96.6
760	-	-	-	-	101.4	-	-	101.5
800	-	-	-	-	105.5	-	-	106.5
840	-	-	-	-	110.4	-	-	111.4
880	-	-	-	-	115.3	-	-	116.4

The numbering of profiles here is the same as in Table 3 and Figures 3 and 4. Thus,

#6 - Zhalanash - Taldy-Kurgan. From N. Tian-Shan to North.

#7 - Issik. From N. Tian-Shan to Balkhash Lake.

#15 - From Aris' (42.4N; 69.0E) to NE to Balkhash Lake, across South Kazakhstan.

#16 - From Temirtau (50N; 73E) to WNW direction to South Ural.

#18 - From Karatay (43.2N; 70.5E), S. Kazakhstan, across the Central Kazakhstan to Tengiz Lake.

#23 - From West Turkmenia to eastern part of Aral Lake.

#27 - Farab - Tamdibulak. West Uzbekistan, between Amu-Darya and Syr-Darya rivers.

Table 5. Apparent Pn velocity measured from seven DSS profiles in and near Kazakhstan.

#	Profile	Distance Range (km)	Apparent Velocity (km/s)	Travel-Time equation
6	Zhalanash-Taldykurgan	200 - 400	8.03	t = R/8.03 + 10.9
7	Issiksky	240 - 400	8.00	t = R/8.00 + 10.9
15	Aris'- Balkhash	200 - 520	8.04	t = R/8.04 + 9.3
16	Temir-Tau - Kuybishev	160 - 400	8.03	t = R/8.03 + 7.8

Table 5. Apparent Pn velocity measured from seven DSS profiles in and near Kazakhstan.

#	Profile	Distance Range (km)	Apparent Velocity (km/s)	Travel-Time equation
18	Karatay - Tengiz Lake	200 - 760 760 - 880	8.23 8.63	t = R/8.23 + 8.5 t = R/8.63 + 13.3
23	Kopet-Dag - Aral Sea	180 - 600	8.08	t = R/8.08 + 8.3
27	Farab - Tamdi-Bulak	200 - 360	8.11	t = R/8.11 + 8.5
-	IASP91	200 - 900	8.11	t = R/8.11 + 7.6

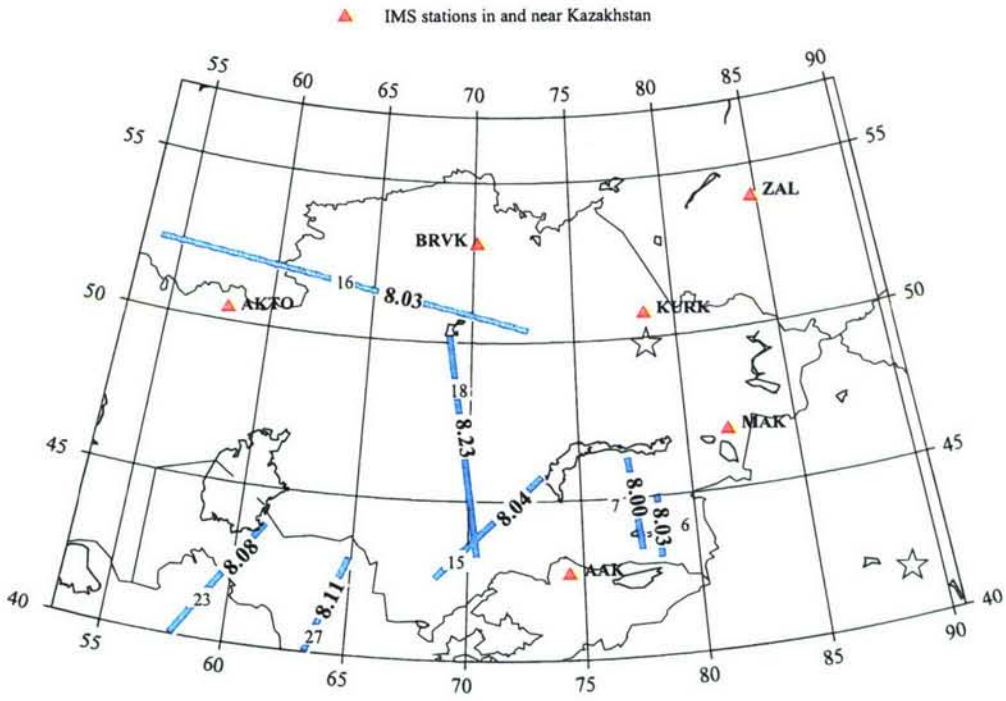


Figure 4. Pn velocities (km/s) from DSS profiles based on chemical explosions in and near Kazakhstan.

3.3.2. China and Surrounding Areas

In the late 1980s, the State Seismological Bureau (now the China Seismological Bureau) requested that each provincial seismological bureau in China compile seismic travel-time tables for earthquake location improvement. These tables, and associated crustal/upper mantle models, were

eventually published (in Chinese) as a book of 178 pages (Xiu et al., 1989). Several examples of these travel time relations were noted by Xu (2000) in his report to a NORSAR workshop on IMS location calibration. He compared the locations provided by use of these regionalized travel times against the locations provided by the Jeffreys-Bullen (J-B) tables, which are still widely used in China. In particular, Table 1 of Xu (2000), albeit not the text of his paper, showed that the locations using regionalized tables are signi cantly better than those based on J-B, for five chemical explosions of known location in different parts of China.

Jih (1998) reviewed location calibration efforts in China, and he too noted the results contained in the major summary given by Xiu et al. (1989). Jih pointed out that "With the exception of southeast and eastern China, the rst P arrivals from surface blasts in ... China are typically slower than those predicted with global models such as J-B or IASP91." This conclusion, supported by numerous studies, is in contrast to the broad results obtained for northern Eurasia. Thus, for the major shield regions of Russia we nd regional travel times are significantly *faster* than the IASP91 travel-time model. But for the major regions of extensional tectonics in China, we find regional travel times are significantly *slower* than the IASP91 travel-time model (Waldhauser and Richards, 2003).

3.4. Our Initial Set of Regional Travel Times in Subregions of Russia and Surrounding Areas

To provide the necessary background to the travel-time model that we finally developed in this three-year project, we here describe our initial efforts in obtaining regional travel-time relations, for Russia and surrounding areas, as used in our CCB proposal of May 2002 (Richards et al., 2002). It may be noted that only for the Kamchatka region (Region #17), did we originally use the IASP91 travel times for Russia and Central Asia. Later (in Section 5) we describe the changes we have made from our initial models, and their rationale.

3.4.1. Scandinavian Shield (Region #1)

This region consists of Scandinavia (Norway and Sweden), Finland, Karelia, and the Kola Peninsula of Russia. In this region there is little sedimentary cover, and granites are widely apparent at the surface. The eastern part (Kola and Karelia) is the region of the oldest (pre-

Riphean) folding of an earlier platform. In the western part (Finland and Sweden) are younger (pre-Carelian) structures. Part of the western section (Norway) includes the early Caledonian fold belt. This is the only region in Europe where 1.5 - 2.0 billion year old rocks appear at the surface. Seismic activity and heat flow are low. All tectonic and geophysical factors indicate a high-velocity structure for the crust and upper mantle in this region. The border between the Scandinavian Shield and the East European platform is clearly identifiable. It passes from the White Sea, to Onega and Ladoga Lake, then along the central part of Baltic Sea, and north from Denmark.

Careful seismological observations were first made in this region by Markus Båth. He was also among the first researchers to study Lg waves, which are clearly seen and which propagate efficiently in this region. His travel-time relations for regional phases Pg, Lg, Rg and Sn (Båth, 1977) are still used by local seismologists and can be recommended for location of seismic events:

H = 0 km	
t(Pg) = R/6.22 + 0	0 - 1500 km
t(Sn) = R/4.65 + 13.0	200 - 1500 km
t(Lg) = R/3.58 + 0	0 - 1500 km
t(Rg) = R/3.02 + 0	0 - 1000 km

For Pn waves, reliable data based on DSS were described by Bondár and Ryaboy (1997):

t(Pn1) = R/7.94 + 6.8	195 - 300 km
t(Pn2) = R/8.17 + 7.9	300 - 370 km
t(Pn3) = R/8.32 + 8.7	370 - 800 km

For distances more than 800 km, Pn travel-time data obtained for the East European Platform (Ryaboy, 1989) can be used. These are based on recent DSS studies of the structure and velocity-cross section (beneath 100 - 150 km) of the upper mantle of both regions, which are nearly similar for depths below 100 - 150 km. The following travel-time relations for Pn and P waves are therefore appropriate for distances greater than 800 km:

t(Pn3) = R/8.32 + 8.7	800 - 1200 km
t(Pn4) = R/8.61 + 13.5	1200 - 2200 km

t(P) = R/10.14 + 52.0	2200 - 2700 km

The main peculiarities of the P wave travel-time data for Scandinavia are:

(a) The low velocity Pn (7.94 km/s) in the distance range 200 - 300 km;

(b) The near constant and relatively high Pn velocity (8.32 km/s) for a wide range of epicentral distances, 400 - 1200 km, indicating that the P-wave speed for the top 200 km of the upper mantle is approximately constant. An increase in apparent velocity of Pn at about 1200 km distance corresponds to a discontinuous increase in P-wave speed at a depth of about 250 km, which has been detected in several regions;

(c) The apparent velocity of 8.61 km/s is observed out to a distance of 2200 km without significant change;

(d) At the so-called "20 degree discontinuity," the apparent velocity increases sharply by 12% to 10.14 km/s without an intermediate velocity of around 9.5 km/s (as in many other regions, and in the IASP91 travel times).

In summary of this region, we initially used the following travel times:

Region #1. SCANDINAVIAN SHIELD

P waves, first arrivals:

Time equations	Distance
t(Pg) = R/6.22 + 0	0 - 195 km
t(Pn1) = R/7.94 + 6.8	195 - 300 km
t(Pn2) = R/8.17 + 7.9	300 - 370 km
t(Pn3) = R/8.32 + 8.7	370 - 1200 km
t(Pn4) = R/8.61 + 13.5	1200 - 2200 km
t(P) = R/10.14 + 52.0	2200 - 2700 km

Other regional phases:

Time equations	Distance

t(Pg) = R/6.22 + 0	0 - 1500 km
t(Sn) = R/4.65 + 13.0	200 - 1500 km
t(Lg) = R/3.58 + 0	0 - 1500 km
t(Rg) = R/3.02 + 0	0 - 1000 km

3.4.2. East European Platform (Region #2)

The East European Platform (craton) occupies a huge area of the former USSR. It is bounded to the south by the Caspian Sea, the Caucasus, and Crimea; and to the west by a linear system of troughs from the East Carpathian region to the southern part of Scandinavia. To the east, the East European Platform is bordered by foothills of the Ural mountains.

The East European Platform is covered by sediments with average depth from 500 to 4000 m. Precambrian rocks are exposed at the surface only on the Ukrainian Shield. Under most parts of the East European Platform the Moho surface is flat, and average crustal thickness is within a narrow interval (38-44 km). Average P wave speed in the consolidated part of the crust is 6.5-6.6 km/s. Within this region, several subareas with slightly different structures have been identified:

(a) The Scythian Plate is a younger part of the East European Platform, adjacent to the Caucasus and Crimea, with slightly lower velocities in the crust and upper mantle, and having low seismicity;

(b) The PreCaspian Depression is a submerged part of the East European Platform, with a subcontinental type of crust in the northern part, covered by sediments having a thickness of more than 10 km. The thickness of the "non-consolidated" part of the crust in this subregion (with velocities less 5.8 km/s) has values as large as 22 km. The average crustal thickness is lower — about 40 km — and even reaches 32 - 34 km in the northern part of the Depression. This is compensated for by higher-than-average velocities in the consolidated part of the crust (6.7 - 6.8 km/s);

(c) Precambrian rocks are the surface only in the Ukrainian Shield, where Moho depth reaches 48 km and average velocities in the consolidated crust also are higher than average (6.7 - 6.8 km/s);

(d) The Timano-Pechora Province occupies the extreme northeast corner of the East European Platform. Here there are Baykal age granites lying beneath the thick sediments.

Travel-time data for the East European Platform were mostly obtained by Deep Seismic Sounding. Principal results were described by Ryaboy (1989) and Krasnopevtseva (1984), and summarized by Kirichenko and Kraev (2000) and by Starovoit et al. (2000).

The travel-time data for the East European Platform are similar to those for Scandinavia. The main difference is that for the East European Platform the low apparent velocities 7.94 km/s and 8.17 km/s (which are observed in Scandinavia in the distance range 200 - 370 km) are absent. So in the East European Platform, velocities beneath the Moho immediately start from 8.32 km/s.

Observations can be summarized by the following travel-time relations, which we used initially:

Region #2. EAST EUROPEAN PLATFORM

P waves, first arrivals:

Time equations	Distance
t(Pg) = R/6.23 + 0.6	0 - 200 km
t(Pn) = R/8.32 + 8.7	200 - 1200 km
t(Pn) = R/8.61 + 13.5	1200 - 2200 km
t(P1) = R/10.14 + 52.0	2200 - 2700 km
t(P2) = R/12.35 + 99.7	2700 - 3000km

Other regional phases:

Time equations	Distance
t(Pg) = R/6.23 + 0.6	0 - 400 km
t(Lg) = R/3.53 + 1.0	250 - 2500 km
t(Sn) = R/4.75 + 16.0	250 - 2500 km

3.4.3. Cenozoic Folded Regions (Region #3)

This region consists of a large area of the Alpine Belt from Turkey to Pakistan. It includes the Black Sea, Crimea, Turkey, and the Caucasus with the southern part of the Caspian Sea, all of the territory of Iran, and the western part of Pakistan. To the north it borders the southern part of the East European Platform (Scythian plate). To the east it is bounded along the Kopet-Dag fault zone by the Turan plate. Also to the east is Suleyman Ridge and to the south lies the Arabian plate.

The Cenozoic Folded Regions comprise an area with a high level of tectonic movement and seismic activity. For this region, high attenuation of seismic waves is typical. There is partial or full blockage of Lg and Rg waves and a high temperature gradient in the crust that leads to partial melting even in the lower crust, and a thick and shallow asthenosphere (beneath thin lithosphere). Over this large area we note several subareas with different tectonic styles and crust/upper-mantle structures:

(a) the Black Sea region with thin suboceanic crust, which blocks Lg and Rg propagation;

(b) the Caucasus region (further subdivided into the Greater and Lesser Caucasus). Here, as in Eastern Turkey and Western Iran, there has been recent volcanic activity and Lg - Rg waves are partially blocked;

(c) the southern deep-water basin of the Caspian Sea, also characterized by suboceanic crust. This part of the Caspian Sea completely blocks the propagation of Lg and Rg waves;

(d) the Iranian Plateau located northeast of the Zagros Mountains and southwest of the Kopet-Dag fault zone. Here there is high attenuation of seismic waves associated with shallow depths of the asthenosphere, and a partially melted zone within the upper mantle. Geothermal observations indicate a high temperature (about 900^{o} C), at depths in the range 30 - 40 km;

(e) the southwestern part of Iran along the Zagros area. This too is an area with low-efficiency of propagation of Lg waves.

We initially used the same travel-time relations for this region, as recommended by Kirichenko and Kraev (2000):

Time equations	Distance
t(Pg) = R/6.21 + 0.9	250 - 1200 km
t(Pn) = R/8.22 + 8.8	200 - 1800 km
t(Sn) = R/4.58 + 12.1	250 - 2000 km
t(Lg) = R/3.56 + 0.9	200 - 2200 km

3.4.4. Ural Fold Zone (Region #4)

The Ural mountains form a natural border between Europe and Asia, between the East European Platform and the West Siberian Plate. This region is a folded structure of Hercynian age, composed of Precambrian rocks. The Urals are an extremely long anticlinorium reaching more than 4000 km in length, and only 250 - 300 km wide. Tectonically this region includes the Taymyr Peninsula (the northeastern part of the West Siberian Plate), Novaya Zemlya, and the Ural Mountains, including their southern part which subsides beneath sediments of the PreCaspian Depression. The average crustal thickness along the central part of the Ural Fold Zone is 50 - 53 km. High velocities of P waves (6.0 km/s and more) begin immediately at the surface. Average crustal velocity is 6.7 km/s.

Travel-time data of regional phases from local events were studied by Lomakin et al. (1978). The epicentral distances of their data ranged from a few km out to 430 km. Very intensive PmP and SmS waves are traced from 130 km out to 300 km. The amplitude of PmP and SmS waves in the distance interval 140 - 280 km are 3-5 times larger than amplitudes of Pg or Pn and Lg or Sn waves. Their travel-time relations correspond to a Moho depth of 46 km and average velocity in the crust being 6.5 km/s for P and 3.8 km/s for S waves. DSS profile data for the Ural zone were summarized by Kirichenko and Kraev (2000). We initially used the following travel time relations:

Region #4. URAL FOLD ZONE

P waves, first arrivals:

Time equations	Distance
t(Pg) = R/6.25 + 0.2	0 - 220 km
t(Pn) = R/8.08 + 8.2	220 - 400 km

t(Pn) = R/8.32 + 9.6	400 - 1600 km
t(Pn) = R/8.60 + 15.9	1600 - 2000 km

Other regional phases:

Time equations	Distance
t(Pg) = R/6.25 + 0.2	50 - 1000 km
t(Sn) = R/4.69 + 14.5	220 - 1600 km
t(Lg) = R/3.59 + 0	50 - 2000 km

3.4.5. West Siberian Platform (Region #5b)

The West Siberian Platform is located between the Ural Fold Belt in the west and the East Siberian Platform (craton) in the east. To the north it is bordered by older structures of the Taymyr Peninsula, and to the south by the Kazakh Massif and the Altay-Sayan fold system. The West Siberian Plate is a young platform, of late Hercynian age. Geographically it is lowland with swamp prevailing on most of the land. It is covered by sediments with thickness reaching 3500 m in some places. The crust of the West Siberian Platform, with thickness in the range 33 - 39 km, is thinner than all surrounding areas. Average P-wave velocity in the crust is 6.5 - 6.6 km/s. The consolidated crust (i.e., the layers with P-wave speed greater than 5.8 km/s) begins at a depth of around 4 - 6 km.

The travel-time data for this region are obtained from long-distance DSS profiles. There are many publications giving detailed descriptions of the principal waves observed, but only in two of them were we able to find information directly on the travel time of P waves. Thus, the papers of Ryaboy (1985) and Barikhin et al. (1987) describe the results of several long DSS profiles, crossing the West Siberian Platform. We have also taken into account the data from ultra-long DSS profiles (based on PNE sources) summarized by Kirichenko and Kraev (2000). The main peculiarities of West Siberian Platform travel times are:

(a) high Pn velocities (8.35 km/s) observed at distances as short as 200 km. So, directly beneath the Moho the Pn velocity jumps up to 8.35 km/s, which differs from observations in Scandinavia or in the East European Platform;

(b) in the distance range 2000 - 2200 km the apparent P velocity is 9.62 km/s, which corresponds to a turning point in the upper mantle just beneath the 410 km discontinuity, and hence is a teleseismic arrival.

The travel-time relations summarizing all these observations and used in our initial work are as follows:

Region #5b. WEST SIBERIAN PLATFORM

P waves, first arrivals:

Time equations	Distance
t(Pg) = R/6.25 + 1.3	0 - 200 km
t(Pn1) = R/8.35 + 9.3	200 - 900 km
t(Pn2) = R/8.50 + 11.1	900 - 1700 km
t(Pn3) = R/8.65 + 14.6	1700 - 2000 km
t(P1) = R/9.62 + 37.9	2000 - 2200 km

Other regional phases:

Time equations	Distance
t(Pg) = R/6.25 + 1.3	50 - 1000 km
t(Sn) = R/4.75 + 15.4	250 - 2000 km
t(Lg) = R/3.56 + 0.6	50 - 2500 km

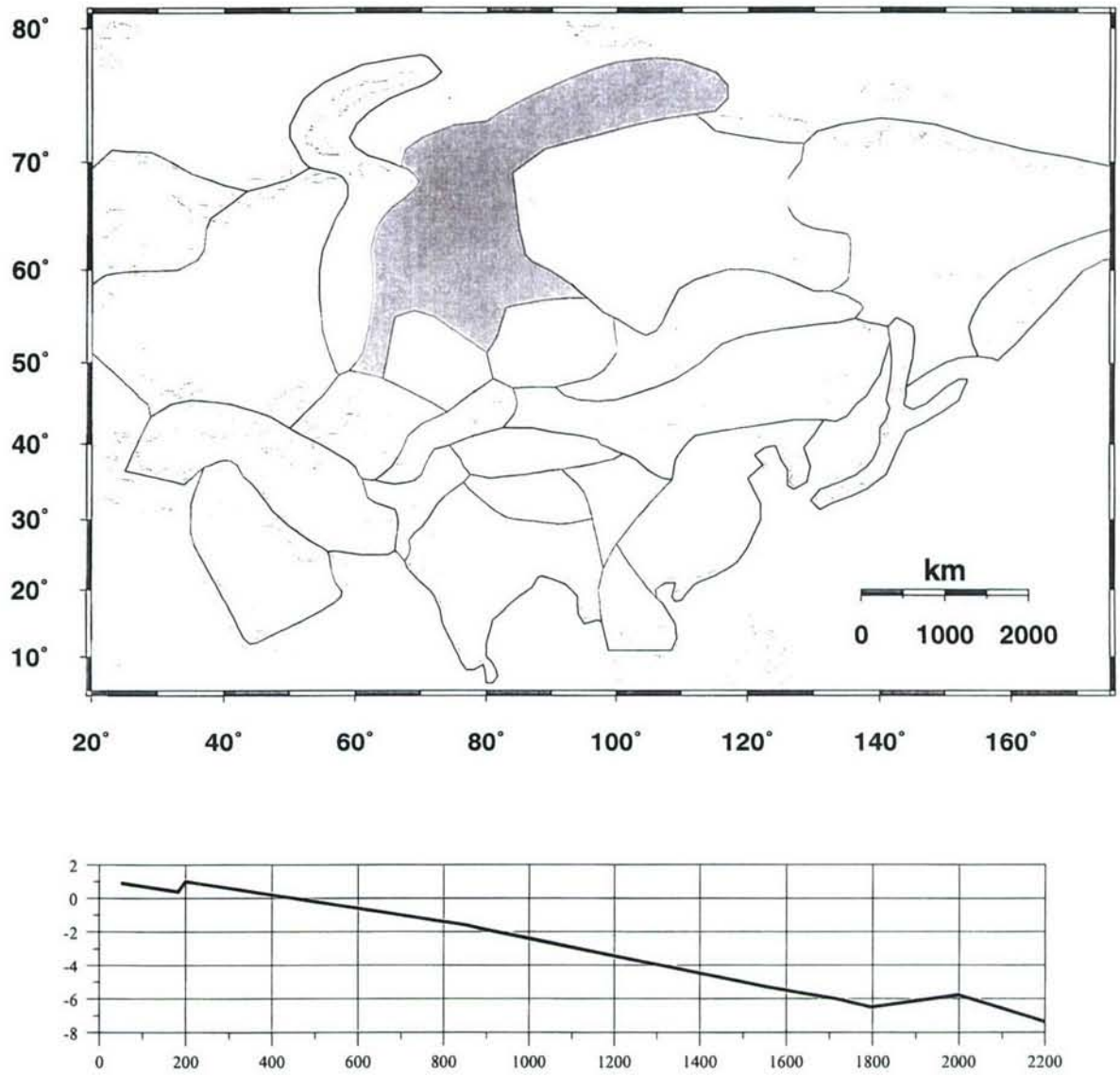


Figure 5. Travel-time residual (in seconds) for the West Siberian Platform (Region #5b - IASP91), for first arriving P waves out to 2200 km. Initial travel time model.

3.4.6. Kazakh Massif (Region #5c)

The Kazakh Massif is an old folded region of Caledonian and Hercynian ages. The folding process ended in the late Hercynian. This region is now dominated by at upland with average elevation 500 - 600 m. Due to constant uplifting, erosion has revealed rocks even of Baykal age, such as the

Kokchetav Mountains and Degelen Mountain. The Kazakh Massif is bounded on the north by the West Siberian Plateau, on the southwest by the Turan Plateau, on the southeast by the Tian Shan Mountain system, and on the east by the Altay-Sayan zone.

This is a stable and almost aseismic area, with activity occurring only in the eastern part of the Massif, where a very low level of seismicity is observed. The heat flow is moderate — about 50 to 70 mW/m^2. The geology and velocity structure of the region have been studied in detail by Russian geologists and geophysicists (Antonenko, 1984; Shatsilov, 1994; and many others.). Many DSS profiles crossed the area, as indicated in Figure 3 and Figure 4. The Moho surface is flat for the northern part of the Massif. Average Moho depth there is 42 - 44 km. Moho relief becomes more complicated to the south (south of about 46.0^{o} N) and depth there is 44 - 48 km.

The average P-wave speed in the crust is 6.6 - 6.7 km/s. Average velocity just below the Moho surface is about 7.95 - 8.05 km/s in the south subregion and 8.10 - 8.15 km/s in the north subregion. The velocity within the crust increases slowly with depth without low velocity zones. The same is typical for upper mantle cross-sections of the region.

Section 3.3 lists several publications containing travel-time data (obtained both by DSS and seismological methods) for the Kazakh Massif. See also Table 2, Table 3, and Table 4 and Figure 3 and Figure 4. DSS data were mostly obtained from Karus (1984), Zunnunov (1985), and Volvovsky (1991). Seismological observations giving travel-time data are mostly from Nersesov and Rautian (1964) and from Khalturin et al. (1974, 1987, 1994, 2001). Information on regional travel times for this region was also extracted from Antonenko (1984), Shatsilov (1993). For this region we initially used the following travel times:

Region #5c. KAZAKH MASSIF

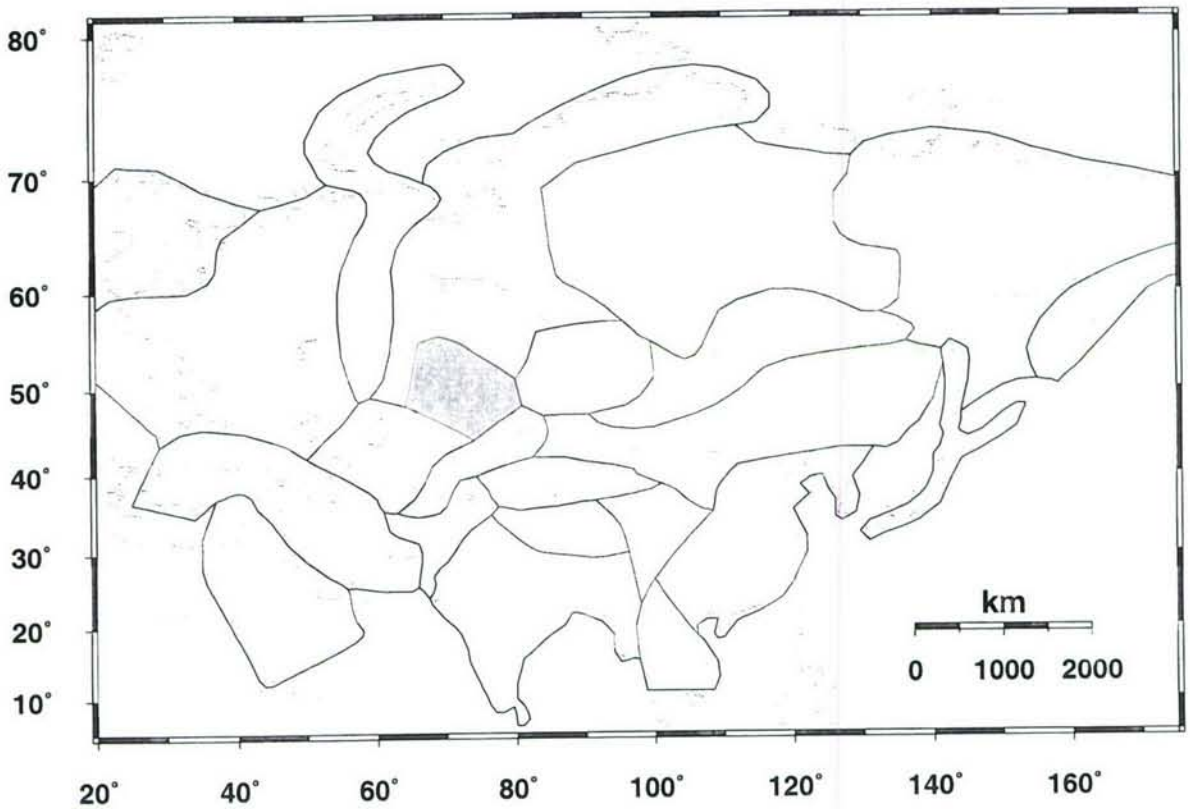
P waves, first arrivals:

Time equations	Distance
t(Pg) = R/6.21 + 0.8	0 - 200 km
t(Pn1) = R/8.13 + 8.4	200 - 900 km
t(Pn2) = R/8.36 + 11.4	900 - 1600 km

t(Pn3) = R/8.73 + 19.5	1600 - 2000km
t(P1) = R/9.57 + 39.6	2000 - 2200 km
t(P2) = R/10.10 + 51.7	2200 - 2400km
t(P3) = R/10.95 + 70.1	2400 - 2700 km
t(P) = R/12.00 + 91.5	2700 - 3400 km

Other regional phases:

Time equations	Distance
t(Pg) = R/6.21 + 0.8	50 - 1200 km
t(Sn) = R/4.68 + 13.8	200 - 1300 km
t(S) = R/5.58 + 94.7	1200 - 2000 km
t(Lg1) = R/3.57 + 0.5	200 - 1100 km
t(Lg2) = R/3.61 + 4.0	1100 - 2500 km
t(Rg) = R/3.0 + 2.0 (T=6-12 s)	400 - 2000 km



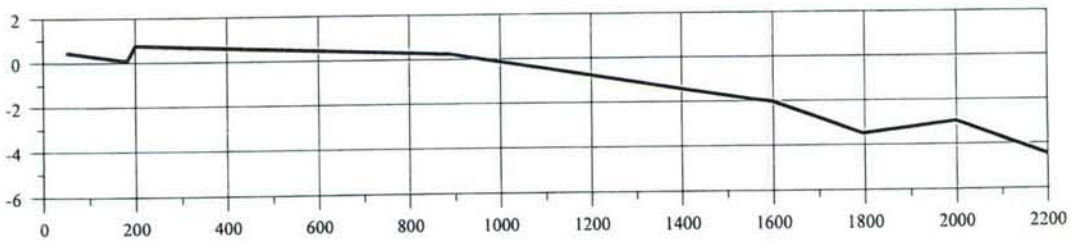


Figure 6. Travel-time residual (in seconds) for the Kazakh Massif (Region #5c - IASP91), for first arriving P waves out to 2200 km. Initial travel time model.

3.4.7. Turan Plateau (Region #5d)

The Turan plate is young and is a continuation of the West Siberian Platform. It is an area of Paleozoic age, folded, with a cover of thick sediments. Its tectonic relationship to neighboring

regions is similar to that of the Scythian plate on the southern part of East European Platform. Both are intermediate zones between a stable platform and active Cenozoic folding areas. The Turan plate has borders with the Ural Fold Zone, the West Siberian plate, and the Kazakh Massif in the north, and with the Caucasus-Iran folded zone to the south.

The northern part of the Turan Plateau is aseismic. Scattered seismicity increases to the southwest and southeast. Recent examples of earthquakes in this region are the Gazli events, which occurred during an eight year period (1976 - 1984) and which were dominated by three earthquakes (thought to be induced) with $M > 7.0$ in the vicinity of (41^{o} N, 63^{o} E). This activity occurred in what previously was believed to be an aseismic zone. Heat flow increases from north to south, with the temperature at the depth 100 km increasing (also north to south) from 900^{o} C to 1300^{o} C. The Moho surface is flat, with average depth around 40 - 44 km in the northern part and 38 - 40 km in the southern part. The average P-wave speed in the crust is 6.45 - 6.55 km/s. The average velocity just below the Moho decreases slightly from 8.0 - 8.1 km/s in the north to 7.8 - 7.9 km/s in the south.

Travel-time data for the region are available from earthquake observations (Yakovleva, 1971; S.A.Fedorov, 1984) and several DSS profiles observations (Zunnunov, 1985; Volvovsky, 1991). Information from Yakovleva (1971) and Fedorov (1984) was also used to derive travel times for this region. The average P-wave velocity in the first several hundred kilometers is nearly the same for both these types of empirical data, namely about 8.15 km/s. For this regions we initially used the following travel-time relations:

Region #5d. TURAN PLATEAU

P waves, first arrivals:

Time equations	Distance
$t(Pg) = R/6.25 + 1.0$	20 - 190 km
$t(Pn1) = R/8.15 + 8.2$	190 - 800 km
$t(Pn2) = R/8.36 + 10.7$	800 - 1600 km
$t(Pn3) = R/8.80 + 20.3$	1600 - 2000 km
$t(P1) = R/9.57 + 38.6$	2000 - 2200 km

t(P2) = R/10.10 + 50.8	2200 - 2400 km

Other regional phases:

Time equations	Distance
t(Pg) = R/6.25 + 1.0	50 - 600 km
t(Sn) = R/4.70 + 13.7	190 - 600 km
t(Lg) = R/3.56 + 0.8	100 - 1000 km

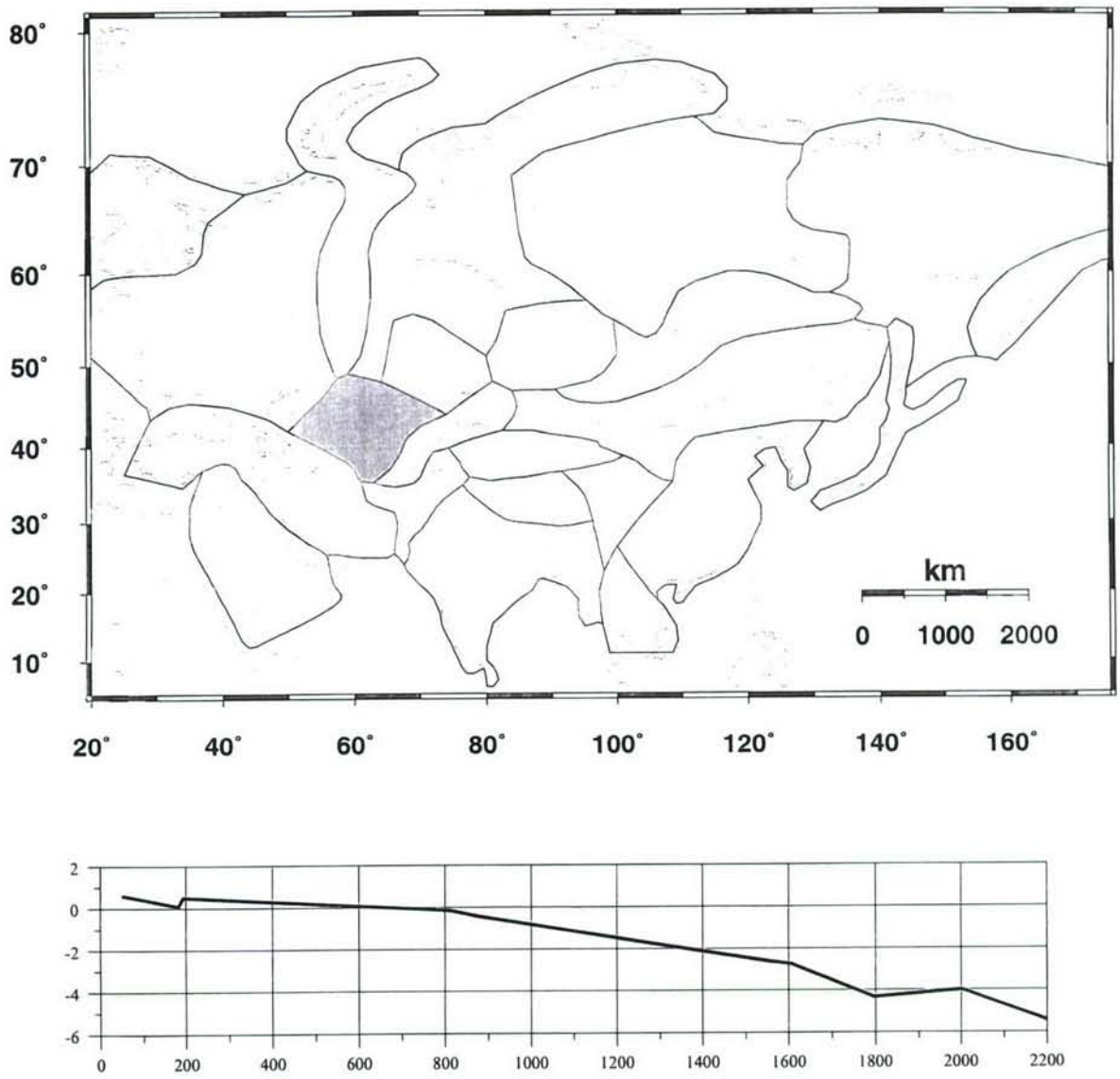


Figure 7. Travel-time residual (in seconds) for the Turan Plateau (Region #5d - IASP91), for first arriving P waves out to 2200 km. Initial travel time model.

3.4.8. Altay-Sayan Folded Region (Region #6)

This is a mountainous area of Caledonian folding that evolved into intensive orogenesis. Seismicity is high in the eastern part (East Sayan) and southern part (Mongol Altay), decreasing to the west and north. Heat flow is average (about 50 mW/m^2), and increasing from west to east. It is

higher than in West and East Siberian platforms and significantly lower than in the Baykal Rift Zone. The relief of the Moho surface in this region is complicated. Average Moho depth is 45 - 50 km, increasing from 42 km in the northwest to 54 km in the southeast. A detailed study of crustal and upper mantle velocity structure for the region was published by V. Sereznev et al.(2000).

Pg waves have an average velocity of 6.10 km/s, increasing up to values in the range 6.20 - 6.25 km/s towards the northwest (West Siberian Plate) and the southeast (Mongolian fold zone). Lg waves have an average velocity of 3.55 km/s, decreasing to 3.50 - 3.45 km/s to the west. Pn velocity just beneath the Moho surface is 8.00 km/s on average, decreasing to 7.9 km/s in the west, north, and east directions; and increasing to 8.15 km/s in the south direction. Very careful studies of regional-phases travel times were conducted by Tsibulchik (1967) and later by Seleznev et al. (2000). We initially used the results summarized below:

Region #6. ALTAY-SAYAN

P waves, first arrivals:

Time equations	Distance
t(Pg) = R/6.13 + 0.3	50 - 200 km
t(Pn1) = R/8.13 + 8.3	200 - 900 km
t(Pn2) = R/8.36 + 11.3	900 - 1600 km
t(Pn3) = R/8.73 + 19.4	1600 - 2000 km
t(P1) = R/9.30 + 33.4	2000 - 2200 km
t(P2) = R/10.1 + 52.2	2200 - 2500 km

Other regional phases:

Time equations	Distance
t(Pg) = R/6.13 + 0.3	50 - 1200 km
t(Sn) = R/4.56 + 12.7	200 - 1200 km
t(Lg) = R/3.57 + 0.5	50 - 2000 km

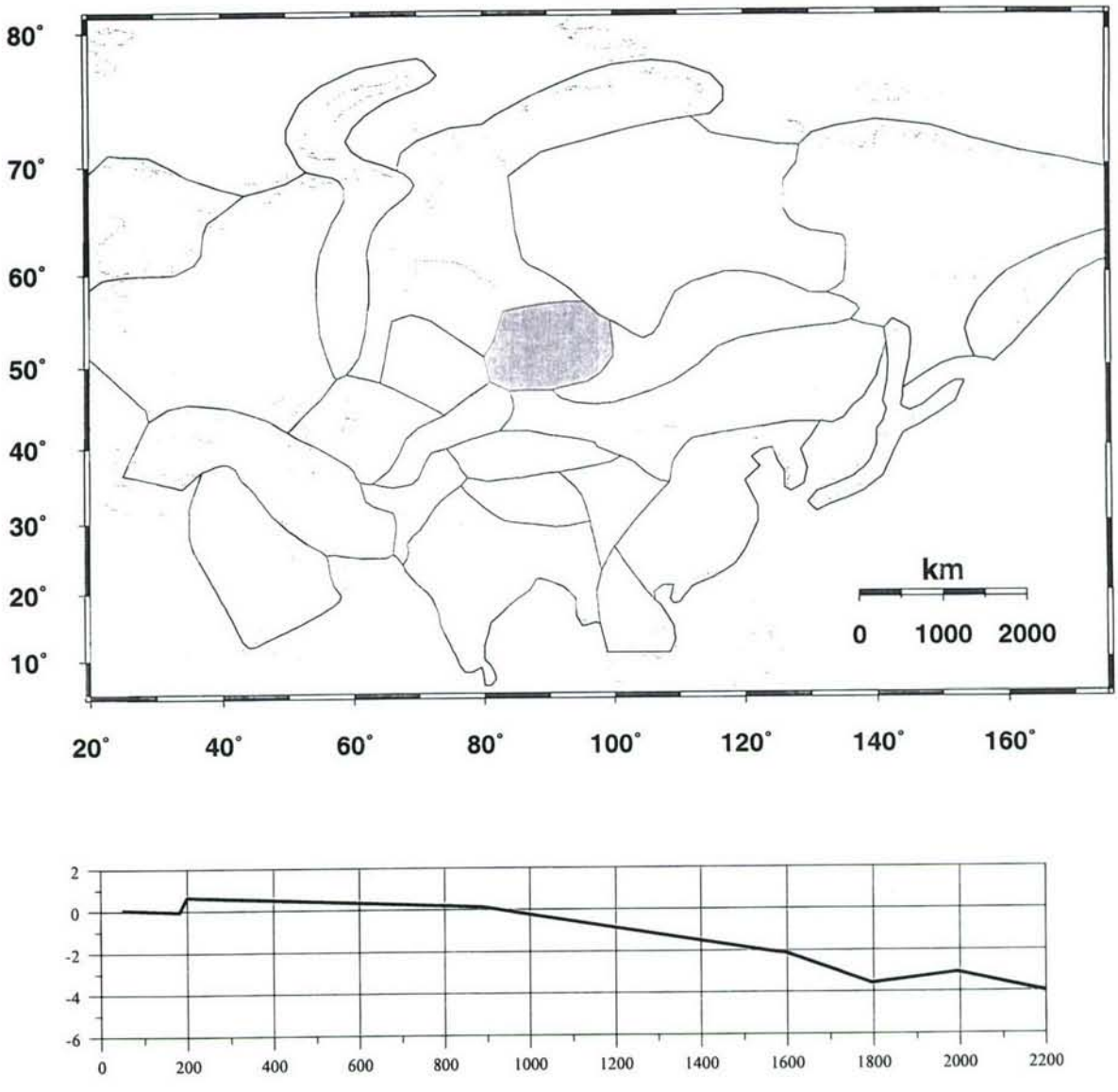


Figure 8. Travel-time residual (in seconds) for the Altay-Sayan (Region #6 - IASP91), for first arriving P waves out to 2200 km. Initial travel time model.

3.4.9. Tian Shan Orogenic Zone (Region #7)

The Tian Shan Orogenic Zone is located between the stable Eurasian plate and mobile regions involved in movements associated with the collision by the India sub-continent. The Earth's crust in this region has been subjected to lateral compression and has undergone considerable

thickening. It is a region of linear folding with upthrusted and overthrusted sheets. Seismicity is high in this region; there have been many historic earthquakes with magnitude 7 and a few with magnitude 8. The present level of deformation within the Tian Shan is anomalously high for an intracontinental zone. Heat flow is high, reaching about 120 - 150 mW/m^2. The average crustal thickness is 48 - 54 km. The Moho depth increases from 42 km at the northern part of the Tian Shan (at the border with the Kazakh Massif) to 60 km in the southern Tian Shan.

Velocity structures of the Tian Shan are described by Molnar and Tapponier (1975, 1979), Roecker et al. (1993), and Hamburger et al. (1998). Evidence of low velocity layers has been found in the crust and upper mantle, but their depth and thickness are different in the eastern and western parts of the Tian Shan. The western part (approximately west of 70^o E) is simpler than the eastern part. This is clearly seen from isostatic gravity anomalies (which are high), geothermal observations (heat flow is low), and velocity observations (travel times are about 2 s shorter). The lithosphere in the western part is thick (80 - 160 km), and the asthenosphere is not clearly seen. In the eastern part the asthenosphere is thicker (between 90 - 150 km). Some authors propose that two low velocity layers exist there: one directly under the Moho or at depths of 20 - 35 km beneath it, and another between 100 to 200 km depth. We suppose that regional variability in the depth of the first low velocity zone explains the significant variations in Pn velocity at distances in the range 200 to 400 km — from 7.0 km/s in East Tian Shan (Sabitova, 1989), then 7.35 km/s (Gorbuova, 1990; Shatsilov, 1989), and up to 7.8 - 8.0 km/s in West Tian Shan (Atabaev and Butovskaya, 1986).

Travel-time data have been obtained mostly from seismological observations and to some extent from Deep Seismic Sounding. We summarize the results of seismological observations by local networks. Average travel-time relations for eight local areas at distances up to 250 km for Pg, Lg and Sn waves:

$t(Pg) = R/6.06 + 0.5$	50 - 250 km
$t(Lg) = R/3.51 + 1.2$	50 - 250 km
$t(Sn) = R/4.58 + 16.2$	50 - 250 km

The average travel-time relations at different distances for Pn waves, taken from 5 publications where data were obtained for distances in the range 600 - 1000 km (V.I. Bune et el., 1955; T.M.

Sabitova. 1989; V.I.Ulomov and A.B.Aronov, 1977; I.L. Nersesov, 1960; I.V. Gorbunova, 1990) are the following:

t(Pn1) = R/7.72 + 8.6	200 - 400 km
t(Pn2) = R/8.00 + 10.4	400 - 800 km

Also, from a DSS long profile (Ryaboy 1985) we find:

t(Pn1) = R/7.87 + 8.6	200 - 400 km
t(Pn2) = R/8.20 + 10.7	400 -1200 km
t(Pn3) = R/8.46 + 16.0	1300 -1700 km

Travel-time data were also extracted from Bune and Butovskaya (1995), Hamburger and Ghose (1998), Khamrabaev (1977), Molnar and Tapponier (1975), Molnar and Tapponier (1979), Roecker et al. (1993), Ryaboy (1985), Sabitova (1989), Shatsilov (1989), and Ulomov and Aronov (1977). If we average all available data (recognizing that there are differences within the region) the following time relations are the result:

t(Pn1) = R/7.75 + 8.6	225 - 400 km
t(Pn2) = R/8.03 + 10.4	400 - 800 km
t(Pn3) = R/8.13 + 11.1	800 - 1300 km
t(Pn4) = R/8.26 + 14.1	1300 - 1800 km

For travel times for events having one end of the ray path (source or station) in the Tian Shan and the other end more than 200 - 300 km outside it, then the following relations are proposed:

t(Pn1) = R/8.13 + 9.2	300 - 900 km
t(Pn3) = R/8.36 + 12.2	900 - 1600 km
t(Pn4) = R/8.73 + 19.7	1600 - 2000 km

The travel time relations summarizing all these observations for the Tian Shan, which we used in our initial work, are as follows:

Region #7. TIAN SHAN OROGENIC ZONE

Case A: epicenter and station located within the zone

P waves, first arrivals:

Time equations	Distance
t(Pg) = R/6.06 + 0.5	0 - 225 km
t(Pn1) = R/7.75 + 8.6	225 - 400 km
t(Pn2) = R/8.03 + 10.4	400 - 800km
t(Pn3) = R/8.13 + 11.6	800 - 1300 km
t(Pn4) = R/8.26 + 14.1	1300 - 1800 km

Other regional phases:

Time equations	Distance
t(Pg) = R/6.06 + 0.5	0 - 600km
t(Lg) = R/3.51 + 1.2	0 - 1500 km
t(Sn) = R/4.58 + 16.2	225 - 1000 km

Case B. For transit rays, when source or station is located more than 200 - 300 km from the zone, and the other end of the ray is within the zone, then

P waves, first arrivals:

Time equations	Distance
t(Pn1) = R/8.13 + 9.2	300 - 900 km
t(Pn2) = R/8.36 + 12.2	900 - 1600 km
t(Pn3) = R/8.73 + 20.3	1600 - 2000 km

Other regional phases:

Time equations	Distance
t(Pg) = R/6.06 + 0.5	0 - 600 km
t(Lg) = R/3.51 + 1.2	0 - 1500 km

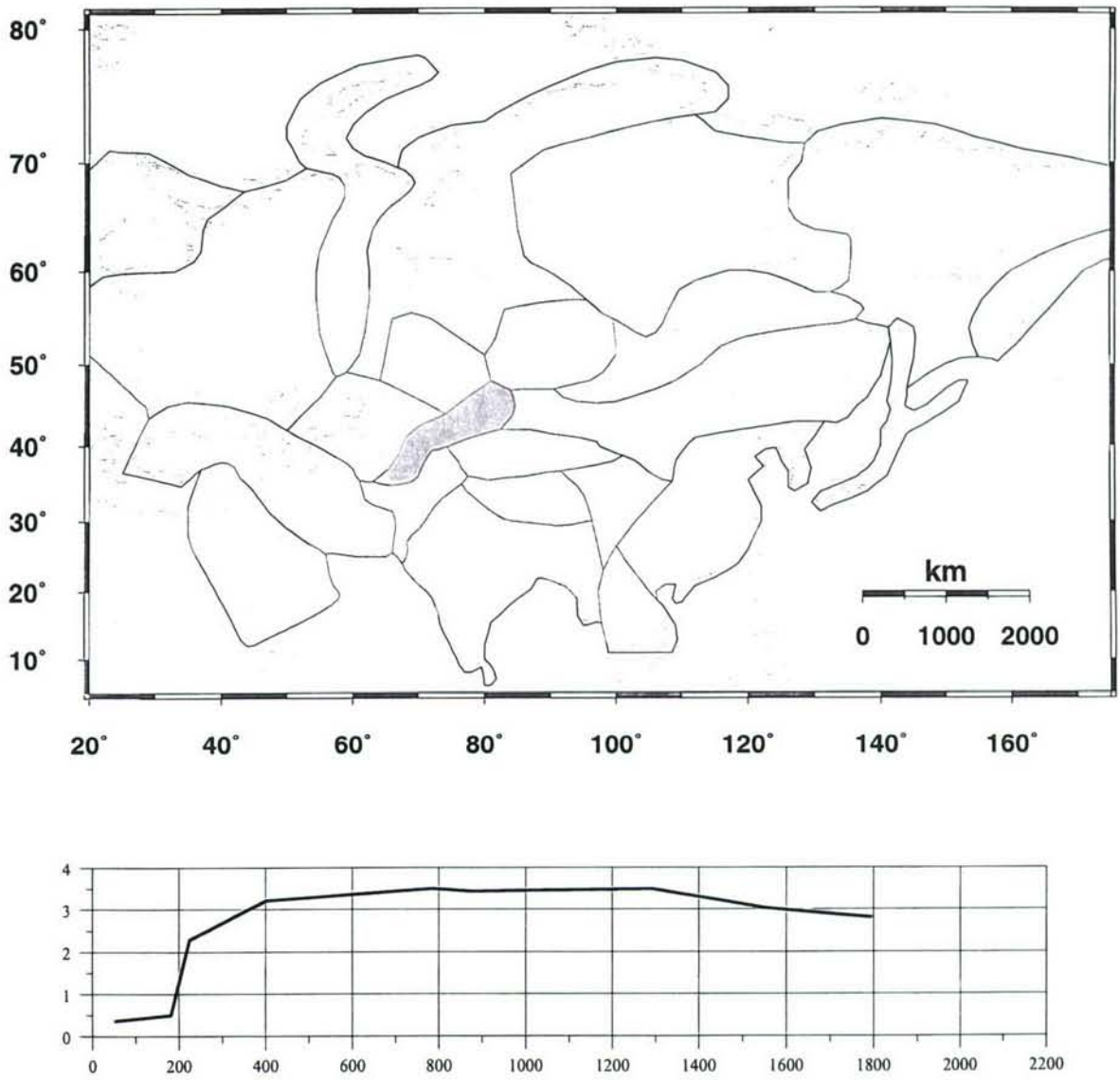


Figure 9. Travel-time residual (in seconds) for the Tian Shan Orogenic Zone (Region #7 - IASP91), for first arriving P waves out to 2200 km. Initial travel time model. Unusually for the territory of Russia and Central Asia, this region has travel times for Pn that are significantly greater than those of the IASP91 travel time model.

3.4.10. Baykal-Mongolian Fold Zone (Region #12)

This zone combines two subareas with different crustal and upper mantle structures: the Baykal rift zone, and the Mongolian-Okhotsk fold zone. We describe below some of the data pertinent to each

subarea. However, in our initial regionalization (used for the May 2002 CCB proposal, Richards et al., 2002), we used the travel times of Kirichenko and Kraev (2000).

#12a. BAYKAL RIFT ZONE

The Baykal rift zone extends from the south-western shore of Lake Baykal, along the lake axis, to its north-eastern shore, and then for a few hundred additional km gradually changing trend from northeast to east. The rift zone has a total length of about 1400 km, about twice as long as the lake itself. This narrow zone is located between the East Siberian Platform to the northwest and the Trans-Baykal part of the extended Mongolian-Okhotsk fold zone to the southeast. The rift zone is 200 - 300 km wide and 1400 km long. The area of low velocity in the crust and mantle, and of high heat flow, is even narrower (150 - 200 km). The crustal thickness is mostly within the range 36 - 42 km. This is an area of quite high levels of seismicity. Epicenters are concentrated along the axis of the rift zone (i.e., continuing a few hundred km east of the northeast edge of the lake).

The average velocity just beneath the Moho is anomalously low, that is, about 7.7 - 7.8 km/s. The layer with this low velocity has thickness about 20 - 30 km. The velocity beneath the low velocity layer is standard, that is, 8.0 - 8.1 km/s. Lithosphere thickness with this velocity is only 50 - 70 km. The more deeply located asthenosphere has thickness 100 km or greater.

The heat flow varies significantly from place to place. On average it is about 75 mW/m^2, but reaches 200 - 500 mW/m^2 in the central part of Lake Baykal and in some other regions along the axis of the rift zone. The temperature is about 800 - 1200° C at the base of the crust in the central part of the rift, and 500 - 700° C at the base of the crust in surrounding regions.

The results of regional seismological observations are based on data acquired not only along the rift zone (from southwest to northeast) but also on paths that cross the Baykal rift zone.

Golenetsky (1974 and 1978) fit data with the following travel-time relations:

t(Pg) = R/6.15 + 0.6	20 - 600 km
t(Pn) = R/8.04 + 7.2	180 - 600 km
t(Lg) = R/3.56 + 1.0	20 - 600 km
t(Sn) = R/4.59 + 12.5	20 - 600 km

Krilov et al. (1974) obtained from Deep Seismic Sounding and from seismological observations the following results for P-wave first arrivals:

t(Pg) = R/6.12 + 0.8	0 - 185 km
t(Pn1) = R/7.75 + 7.1	185 - 370 km
t(Pn2) = R/8.10 + 9.1	370 - 1000 km

These results were obtained only for traces along the rift axis itself, and have been supported by later publications. The following travel times, for paths within the Baykal Rift Zone, having epicentral distances less 1000 km, summarize the observations:

Region #12a. BAYKAL RIFT ZONE.

P waves, first arrivals:

Time equations	Distance
t(Pg) = R/6.12 + 0.8	0 - 185 km *
t(Pn1) = R/7.75 + 7.1	185 - 370 km
t(Pn2) = R/8.07 + 9.0	370 - 1000 km

* This same straight line fits Pg observed out to several hundred km.

#12b. MONGOLIAN-OKHOTSK FOLD SYSTEM

This is a long and mountainous fold system lying between the Altay-Sayan on the west and Okhotsk Sea on the east, and between the Baykal Rift Zone and East Siberian Platform on the north and the North Chinese Platform on the south. It is high land with moderate seismic activity in some areas. Geophysical data for this region are sparse. The crust thickness is about 36 - 44 km.

For the Mongolian part of this zone, regional phase velocity was estimated by Anikonova (1995). In North Mongolia, she obtained the following fit to travel-time data for Pg and Lg waves:

t(Pg) = R/6.25 + 0.2	50 - 200 km
t(Lg) = R/3.63 + 1.2	50 - 200 km

We have no data at greater distances. However, this region is the eastward continuation of the Altay-Sayan region and both regions are similar in tectonic history. So, the travel-time relations for the Altay-Sayan region (Region # 6) could be taken to apply also to the #12b region:

Region #12b. MONGOLIAN-OKHOTSK FOLD SYSTEM

P waves, first arrivals:

Time equations	Distance
t(Pg) = R/6.13 + 0.3	50 - 200 km
t(Pn1) = R/8.13 + 8.3	200 - 900 km
t(Pn2) = R/8.36 + 11.3	900 - 1600 km
t(Pn3) = R/8.73 + 19.4	1600 - 2000 km
t(P1) = R/9.30 + 33.4	2000 - 2200 km
t(P2) = R/10.1 + 52.2	2200 - 2500 km

Other regional phases:

Time equations	Distance
t(Pg) = R/6.13 + 0.3	50 - 1200 km
t(Sn) = R/4.56 + 12.7	200 - 1200 km
t(Lg) = R/3.57 + 0.5	50 - 2000 km

We concluded that, for our initial model, it is appropriate to apply the travel-time relations proposed by Kirichenko and Kraev (2000), which are as follows:

Time equations	Distance
t(Pg) = R/6.13 - 0.9	400 - 1200 km
t(Pn) = R/8.21 + 6.8	400 - 2000 km
t(Sn) = R/4.64 + 12.4	400 - 2000 km
t(Lg) = R/3.48 - 6.4	400 - 2500 km

3.4.11. East Siberian Platform (Region #15)

This platform is located between two younger structures, the West Siberian Plate and Northeast folding region. The natural borders are the Enisey River to the west and the Lena River to the east. To the south the East Siberian Platform borders on the Altay-Sayan, the Baykal Rift zone, and the eastern continuation of the Mongolian-Okhotsk fold system. This highland region is a stable aseismic craton of Proterozoic age. Continental crust of the region developed in early Precambrian time. There are two old (Pre-Riphean) shields in the East Siberian Platform: the Anabar Shield to the north and the Aldan Shield to the south.

Heat ow values are low; about 30 mW/m^2 is typical for most areas of the craton, with only 20 mW/m^2 in the Anabar shield. Heat flow values increase from north to south, reaching 60 mW/m^2 and more, close to the Baykal Rift Zone. These low heat flow values provide evidence for some of the lowest temperatures in Eurasia at the depth of 100 km (600 - 700° C) and 150 km (900 - 1000° C) (Mooney et.al., 2001).

The average lithosphere thickness (200 km) is the greatest in Eurasia. The asthenosphere on average is located at depths between 200 - 280 km. These properties are related to the observation that a high Pn velocity is observed starting at a distance of around 220 km, and continuing out as far as 1100 km. Crustal thickness is 40 - 48 km with average P velocity 6.6 - 6.7 km/s. The average velocity just beneath the Moho is also high: 8.25 - 8.40 km/s. In some areas of Yakutia, anomalous values of Pn velocity as high as 8.8 - 8.9 km/s have been observed.

The lack of seismicity means that only Deep Seismic Sounding data can be used to obtain travel-time relations. Results have been published by many authors, but only a few of them gave the actual travel-time data, namely Ryaboy (1985), Barkhin et al. (1987), and Egorkin et al. (1987). For most publications typically the Pn velocity is high (8.3 - 8.5 km/s), right from the initial distances (220 - 240 km) at which Pn is observed. The summary of available travel-time relations, used in our initial work, is given below:

Region #15. EAST SIBERIAN PLATFORM

P waves, first arrivals:

Time equations	Distance

t(Pg) = R/6.24 + 0.5	50 - 220 km
t(Pn1) = R/8.43 + 9.7	220 - 1100 km
t(Pn2) = R/8.61 + 12.4	1100 - 2000 km
t(P1) = R/9.30 + 29.6	2000 - 2200 km
t(P2) = R/10.0 + 46.2	2200 - 2500 km

Other regional phases:

Time equations	Distance
t(Pg) = R/6.24 + 0.5	50 - 1200 km
t(Sn) = R/4.77 + 17.0	600 - 2000 km
t(Lg) = R/3.53 + 0.7	250 - 2500 km

3.4.12. Northeast Territory and Chukot Peninsula (Region #16)

For this region we initially used the Kirichenko and Kraev (2000) travel-time relations:

Region #16. NORTH-EAST TERRITORY AND CHUKOT PENINSULA

P waves, first arrivals:

Time equations	Distance
t(Pg) = R/6.19 + 1.6	50 - 205 km
t(Pn) = R/8.29 + 10.0	205 - 2000 km

Other regional phases:

Time equations	Distance
t(Pg) = R/6.19 + 1.6	100 - 1000 km
t(Sn) = R/4.51 + 6.6	500 - 2200 km
t(Lg) = R/3.50 + 0	200 - 2500 km

3.5. Our Regionalization of China and Surrounding Areas

Initially we used regional travel times in and around China that differed from IASP91 for the Tarim Basin (Region 8 of Figure 2), Tibet (Region 10), Northern China (Region 11), and Sechuan-Yunnan (also called Sikkam, Region 20a). We initially retained IASP91 for the remaining areas of China (Region 13). Our initial travel time relations for these Regions 8, 10, 11, and 20a are given below in Sections 3.5.1 through 3.5.3.

Subsequently, we revised this regionalization as described in Section 3.5.4, entailing subdivisions of Regions 11 and 13.

3.5.1. Tarim and North Chinese Platforms (Regions #8 and #11)

We initially applied the same travel-time relations for both these cratonic regions of northwest and northeast China. This is a mostly stable region, composed mainly of cratonic terrains that were accreted to Southern Asia prior to the India-Eurasia collision. Seismic tomography for this region indicates that it typically has higher Pn velocity, than does Southeastern China (region #13) (Hearn and Ni, 2000).

The Chinese test site (Lop Nor) is located in the Tarim basin. Travel-time data of regional phases for events located in this region were obtained by Khalturin et al. (1978). Records were analyzed from many stations of the Complex Seismological Expedition (CSE), located in East and South-east Kazakhstan and South Siberia. Sources of these signals were located in Dzungaria, Xinjiang, Kuen Lun, and other areas of China and Mongolia at epicentral distances from 800 km to 2400 km. All phases in P, Sn and Lg wave groups were measured on these records, with results as follows:

Travel-time table of Pn, Sn, S and Lg waves

P waves, first arrivals:

Time equations	Distance
t(Pg) = R/6.18 + 0	0 - 220 km
t(Pn1) = R/8.16 + 8.5	200 - 1000 km
t(Pn2) = R/8.47 + 12.9	1000 - 1800 km
t(Pn3) = R/8.85 + 22.0	1800 - 2000 km

t(P1) = R/9.52 + 38.0	2000 - 2100 km
t(P2) = R/10.39 + 56.4	2100 - 2500 km
S waves, first arrivals	
t(Sn) = R/4.74 + 18.7	800 - 1600 km
t(S1) = R/5.68 + 99.1	1300 - 1900 km
t(S2) = R/5.75 + 103.1	1900 - 2400 km
First arrivals of Lg1 and Lg2 waves	
t(Lg1) = R/3.57 + 0.2	800 - 2300 km
t(Lg2) = R/3.36 - 6.0	800 - 2400 km

Comments:

(a) In some cases both waves Sn and S (regional and teleseismic) are observed on records in the 1400 - 1600 km distance range. Sn wave is shorter period (a few hz), S is long period (1 - 3 sec) and propagates beneath the asthenosphere. The time interval between Sn and S can be 20 - 30 sec and its regional variations are large. In general, regional variability of S (or Sn) velocity is several times larger than regional variability of P (or Pn) velocity;

(b) The Lg1 phase becomes weaker at distances greater than 2000 km, and Lg2 dominates;

(c) The Lg2 wave is not stable, but is observed on most records beyond 1000 km. The Lg2 wave has lower frequency content than Lg1.

We initially (May 2002, CCB proposal, Richards et al., 2002) used the following travel time relations:

Regions #8 and #11. TARIM PLATFORM AND NORTH CHINESE PLATFORM

P waves, first arrivals:

Time equations	Distance
t(Pg) = R/6.18 + 0	50 - 215 km
t(Pn1) = R/8.16 + 8.5	215 - 1000 km
t(Pn2) = R/8.47 + 12.9	1000 - 1800 km

t(Pn3) = R/8.85 + 22.0	1800 - 2000 km
t(P1) = R/9.52 + 38.0	2000 - 2100 km
t(P2) = R/10.39 + 56.4	2100 - 2500 km

Sn, S and Lg waves, first arrivals:

Time equations	Distance
t(Sn) = R/4.74 + 18.7	800 - 1600 km
t(S) = R/5.68 + 99.1	1300 - 1900 km
t(S) = R/5.75 + 103.1	1900 - 2400 km
t(Lg) = R/3.57 + 0.2	800 - 2400 km

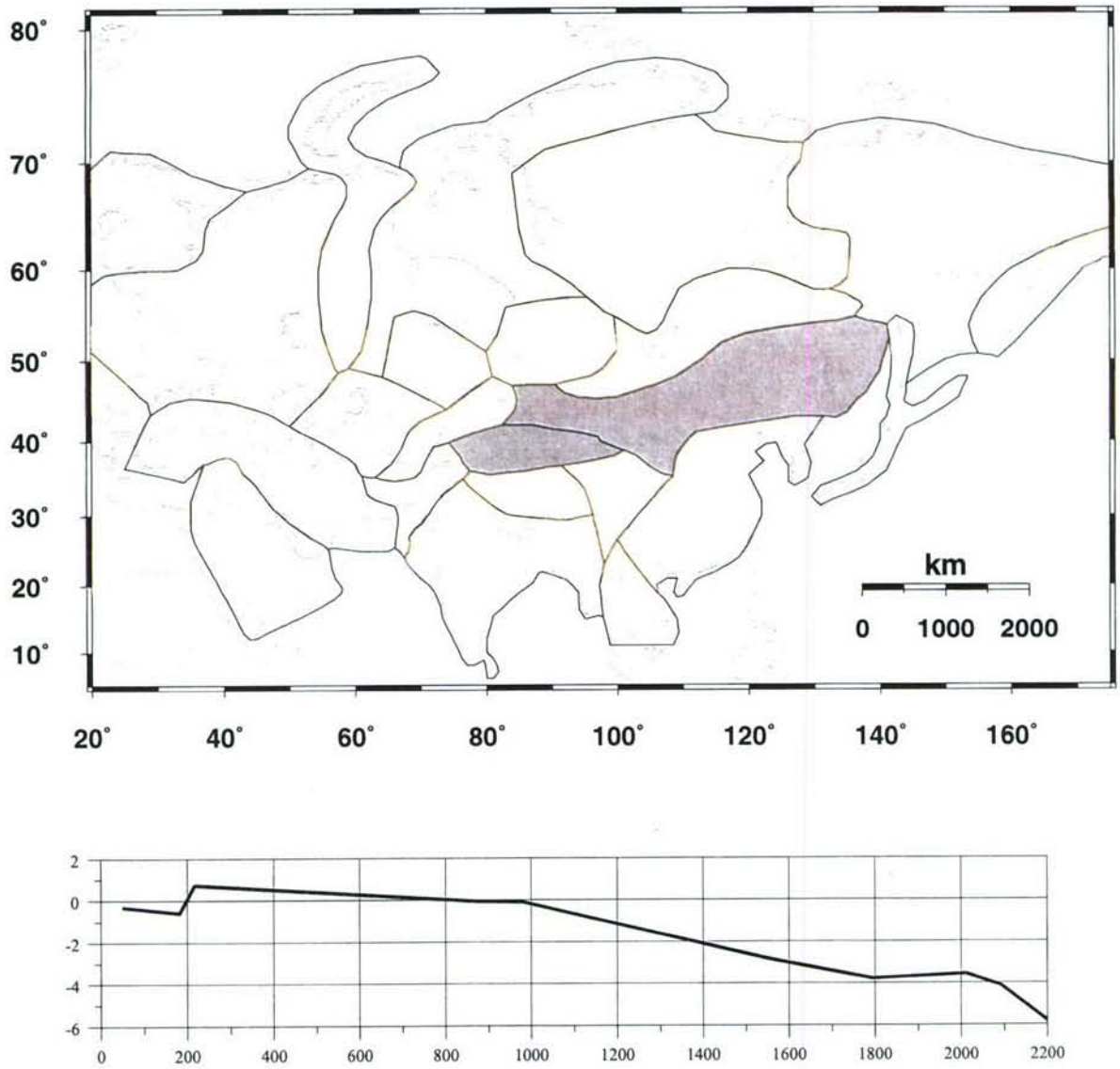


Figure 10. Travel-time residual (in seconds) for the Tarim Platform and the North Chinese Platform (Region #8 or 11 - IASP91), for first arriving P waves out to 2200 km. Initial travel time model.

3.5.2. Tibetan Plateau (Region #10)

The Tibetan massif has many geological and geophysical anomalies, associated with the India-Eurasia collision. The Earth's crustal thickness reaches 70 km. Gravitational anomalies, shear wave and surface wave attenuation, and velocity anomalies, are very significant for this region. The crust and upper mantle beneath Tibet are characterized by low Q as well as by low shear wave

velocity. P waves are not so anomalous. These phenomena can be explained by unusually high temperatures in the lower crust and upper mantle, down to about 200 - 250 km depth. The north and south borders of Tibet completely block the propagation of Lg waves. This effect was first described by Khalturin et al. (1977). Lg and Sn waves have low propagation efficiency within Tibet. The influence of anomalous structure on Pn propagation is lower, but still significant (Zhao & Xie, 1993).

The travel times of regional phase propagation within Tibet (to a distance of 1100 km) have been described in a publication of the Chinese Seismological Bureau (Xiu et al., 1989) as follows:

Time equations	Distance
t(Pg1) = R/5.55 + 0.1	Pg1 wave is a first arrival at 0 - 75 km
t(Pg2) = R/6.53 + 2.1	Pg2 wave is a first arrival at 75 - 368 km
t(Pn1) = R/7.99 + 12.3	Pn1 wave is a first arrival at 368 - 640 km
t(Pn2) = R/8.29 + 15.2	Pn2 becomes first arrival after 640 km till observations end at 1100 km
t(Sg1) = R/3.26 + 0.3	Lg1 wave is a first S arrival at 0 - 75 km
t(Sg2) = R/3.76 + 3.2	Lg2 wave is a first S arrival at 75 - 378 km
t(Sn1) = R/4.55 + 20.7	Sn1 wave is a first S arrival at 378 - 650 km
t(Sn2) = R/4.69 + 25.0	Sn2 wave is a first S arrival beyond 650 km till observations end at 1100 km

The principal special features of these travel times are that:

(a) Pg and Lg waves with standard velocities 6.10 and 3.55 km/s are not observed. Pg and Lg waves at distances of 0 to 75 km propagate with velocity 11% lower than standard values typical for other regions;

(b) Pg and Lg waves are observed as first arrivals out to 370 km! This is almost twice as far as for stable regions. These waves propagate in the distance range 75 - 370 km with a velocity that is 7% higher than standard values typical for other regions;

(c) Pn waves propagate with velocity about 8.0 km/s in the distance range 370 - 650 km. This is close to the Pn velocity observed in other mobile and active regions, such as the Tian Shan;

(d) The Pn velocity 8.3 km/s observed at distances greater than 650 km is similar to that of other tectonically active regions;

(e) The time delay for Pn arrivals in the distance range 800 - 1200 km for Tibet is 5 - 7 s greater than for stable regions!

In summary we initially used the following travel-time relations for the Tibetan Plateau:

Region #10. TIBETAN PLATEAU

P waves, first arrivals:

Time equations	Distance
t(Pg1) = R/5.55 + 0.1	0 - 75 km
t(Pg2) = R/6.53 + 2.1	75 - 368 km
t(Pn1) = R/7.99 + 12.3	368 - 640 km
t(Pn2) = R/8.29 + 15.2	640 - 1100 km

Lg or Sn first arrivals:

Time equations	Distance
t(Lg1) = R/3.26 + 0.3	0 - 75 km
t(Lg2) = R/3.76 + 3.2	75 - 378 km
t(Sn1) = R/4.55 + 20.7	378 - 650 km
t(Sn2) = R/4.69 + 25.0	650 - 1100 km

3.5.3. Sikkam, Sichuan-Yunan Region (Region #20a)

This region is a transition zone between the Tibetan plateau to the west and the Yangtze continental platform to the east. The zone is a consequence of the Indian-Eurasian plate collision. The Moho depth increases from southwest to northwest: it is about 38 - 40 km in the south and reaches 56 km

in the north (Yunnan). This is an area with a high level of seismicity. Many earthquakes having magnitude greater than 7.0 have occurred here during the last thirty years.

According to W. Chan et al. (2001), the average crust velocity is 6.25 km/s. The average velocity just beneath the Moho is only 7.75 km/s. This low value is related to high temperatures, possibly associated with the intrusion of melted materials into the lower crust. Sn waves were not observed. Available travel-time data can be fit by the following travel-time relations for the distance interval 0 - 600 km:

t(Pn) = R/7.9 + 8.5

t(Pg) = R/6.06 + 1.0

t(Lg) = R/3.52 + 1.5

To extend these Pn travel times to greater distances, for example up to 1000 - 1200 km, orogenic areas like the Tian Shan or the Pamirs can be identified as analogs. The average Pn velocity in the range 600 - 1200 km for these regions is 8.13 km/s. So the following travel-time relations are proposed for the Sikkam region for distances 600 - 1200 km:

t(Pn2) = R/8.13 + 10.7

Our initial set of travel times for this region was as follows:

Region #20a. SIKKAM (Sichuan-Yunan region)

P waves, first arrivals:

Time equations	Distance
t(Pg) = R/6.06 + 1.0	0 - 195 km
t(Pn1) = R/7.9 + 8.5	195 - 600 km
t(Pn2) = R/8.13 +10.7	600 - 1200

Other regional phases:

Time equations	Distance
t(Pg) = R/6.06 + 1.0	0 - 600 km
t(Lg) = R/3.52 + 1.5	0 - 600 km

3.5.4. Our Revision of Travel Times and Velocity Models for China

During the period June 2002 - March 2003 we worked extensively with phase picks for approximately 14,000 earthquakes documented in the Annual Bulletin of Chinese Earthquakes (described further in Section 4, below). We also worked with Chinese seismologists on relocation of 6500 earthquakes in central-western China. As part of these studies we refined the initial regionalization given above for the North China platform (Region 11), and for Southeastern China (Region 13, for which we had initially used IASP91) (see Figure 2 for the location of these regions and our initial numbering system).

Our modi cation of region boundaries for China is shown in Figure 11. The issue here is that extensive work in China has led to 1D regional velocity models, developed for earthquake location purposes by operators of provincial seismographic networks (see Xiu et al., 1989; and Jih, 1998). But these models are usually called by the name of a province or geographical region, and have not been clearly associated with region boundaries de ned in terms of geophysical or geological units. We therefore needed to make a determination of the boundaries within which to apply a particular set of travel times from Xiu et al. (1989), and the associated 1D velocity model. Our new choice of boundaries was make by taking four types of information into consideration, namely the areal extent of particular provinces (associated with travel times and 1D velocity models in Xiu et al., 1989), tectonic units, Moho topography, and seismicity. Figure 12 shows these types of information, together with our new set of regions boundaries. Table 6 gives the 1D models.

In this revision for our final results in this three-year project, region 11 has been divided into sub-regions 11a and 11b (Figure 11). The travel-time versus distance functions previously applied to region 11 (see Section 3.5.1) are now applied to subregion 11a. The velocity model "NE China A" (Jih, 1998) has been assigned to subregion 11b. Region 13 has been divided into subregions 13a,b,c (Figure 11). Velocity models "SE China" and "E China A" (Jih, 1998) have been assigned to subregions 13a and 13c, respectively. In the case of subregion 13b the velocity structure is based on a 1D model for the two provinces of Sichuan and Yunnan (Zhi-xian Yang, personal communication, developed in association with a major project between Chinese scientists and the Lamont Consortium, to relocate 6500 earthquakes in central-western China, as described in Yang et al. 2003).

Independent geophysical and geological data provided by the U.S. Geological Survey, and derived from volumes on the regional geology of the China provinces published by the Geological Publishing House (Beijing, 1984-1993), are used to verify the existing and revised regionalized velocity models for China.

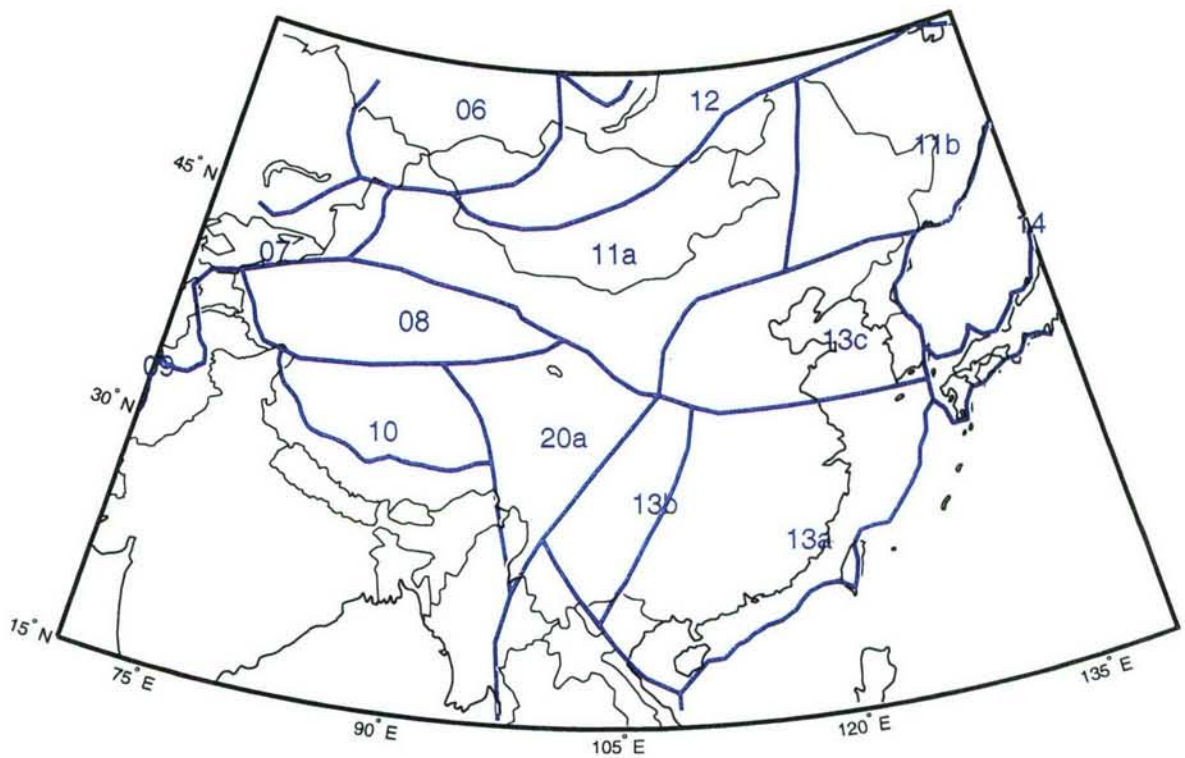


Figure 11. Boundaries of 1D velocity models for China and surrounding areas.

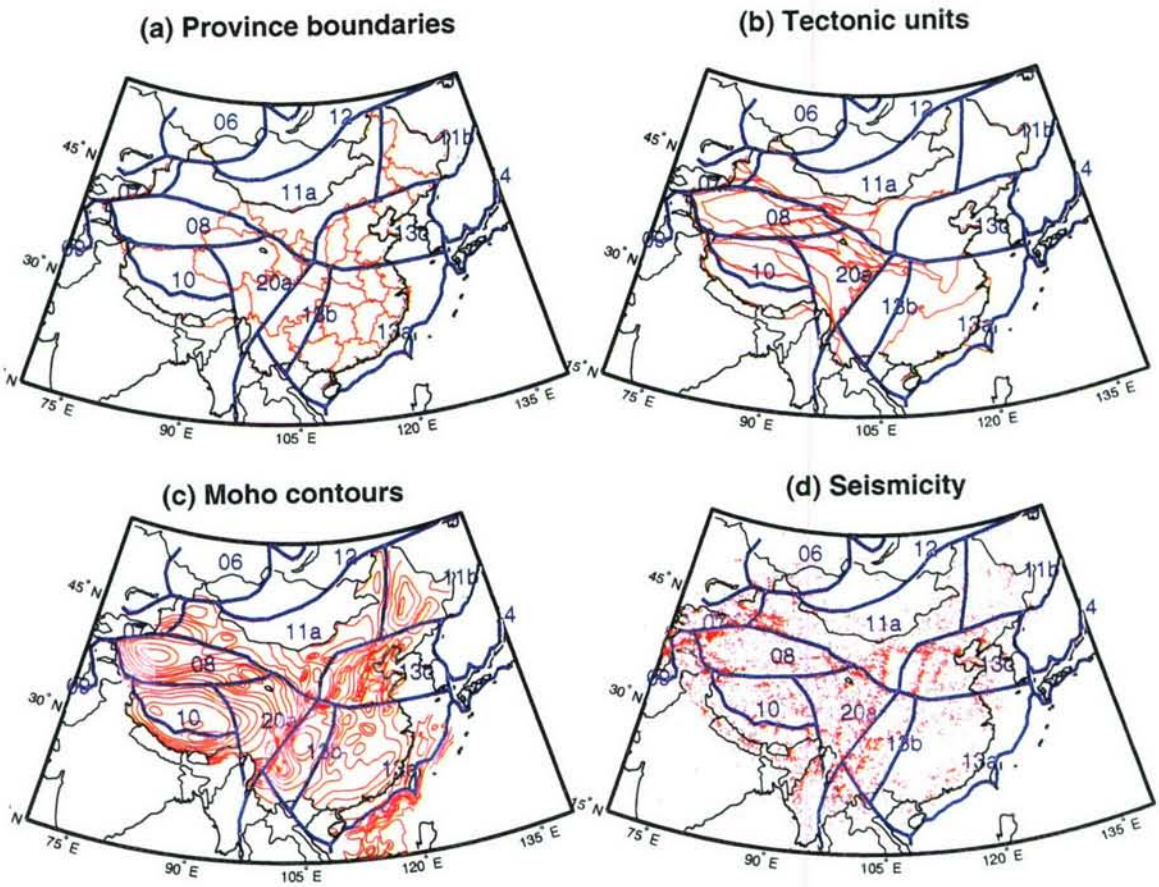


Figure 12. The boundaries shown in Figure 11 are superimposed on province boundaries (a), tectonic units (b), Moho topography (contoured at 2 km depth intervals) (c), and seismicity (d).

Table 6. Refined P-velocity models for sub-regions of China.

11b NE China		13a SE China		13b* Sichuan-Yunnan		13c E China	
depth	km/s	depth	km/s	depth	km/s	depth	km/s
0	5.95	0	6.01	0	5	0	6.16
17	5.95	21.4	6.01	7.5	5	10	6.16
17	6.5	21.4	6.88	7.5	5.48	10	6.56
33	6.5	32.4	6.88	16	5.48	26	6.56

Table 6. Re ned P-velocity models for sub-regions of China.

11b NE China		13a SE China		13b* Sichuan-Yunnan		13c E China	
depth	km/s	depth	km/s	depth	km/s	depth	km/s
33	7.8	32.4	7.98	16	5.93	26	7.05
75	7.8	75	7.98	20	5.93	32	7.05
				20	6.43	32	8
				30	6.43	75	8
				30	6.6		
				50	6.6		
				50	8.3		
				75	8.3		

*) from Zhi-xian Yang (China Seismological Bureau)

3.6. Our Regionalization of the Indian Subcontinent

Initially we used regional travel times different from IASP91 for the Pamir/Hindu Kush/Himalaya area (Region 9 of Figure 2), and retained IASP91 for the remaining and very extensive area of the Indian subcontinent (Region 19). Our initial travel time relations for Region 9 are given below in Section 3.6.1. These were used for our CCB proposal of May 2002 (Richards et al., 2002). Subsequently, we revised this regionalization as described, below, in Section 3.6.2, entailing extensive subdivisions of Region 19.

3.6.1. Pamir, Hindu Kush and Himalaya (Region #9)

This is a very complicated high-mountain region, with high levels of seismicity. As a preliminary step we took this region as a southeast continuation of the Tian Shan orogenic zone. The crustal thickness is high and reaches 60 - 65 km. We initially adopted, for this region #9, the region #7 travel times, with the following relations:

Region #9. PAMIR, HINDU KUSH AND HIMALAYA

Travel time of rst arrivals for paths within the region

P waves, rst arrivals:

Time equations	Distance
t(Pg) = R/6.06 + 0.5	0 - 225 km
t(Pn1) = R/7.75 + 8.6	225 - 400 km
t(Pn2) = R/8.03 + 10.4	400 - 800km
t(Pn3) = R/8.13 + 11.1	800 - 1300 km
t(Pn4) = R/8.26 + 14.1	1300 - 1800 km

Other regional phases:

Time equations	Distance
t(Pg) = R/6.06 + 0.5	0- 600km
t(Lg) = R/3.51 + 1.2	0 - 1500 km
t(Sn) = R/4.58 + 16.2	225 - 1000 km

3.6.2. Our Revision of Velocity Models for the Indian Subcontinent

Since submitting our May 2002 CCB proposal (Richards et al., 2002), personnel with the URS Greiner group (Chandan Saikia and Bradley Woods) have worked as part of the Lamont Consortium to develop eight regionalized velocity models for the Indian subcontinent. These models are for the following regions: the Peninsular and central shields, the Himalayas (replacing our initial model, given above in Section 3.6.1), the Gangetic plains, the west Ganga basin, the Shillong plateau/Assam/NE India, the Cambay- and Sanchor-basin region of western-most India, and Burma. These models are given in Table 7, and region names together with our numbering system are shown in Figure 13. The region numbers range from 19a to 19h and these are included in the Table. A P-to S-velocity ratio of 1.75, the average found in direct P and S studies throughout the region, is used to supply missing parameter data. Further details are as follows:

The velocity model for peninsular shield India (Region 19a) is based on the average of the Arora (1971), Dube et al. (1973) and Srivastava et al. (1984) body-wave models, which were all in close agreement both in terms of velocities and layer thicknesses. Surface-wave models for this region were all derived by forward modeling, and their exactness and resolution are less certain than are

models derived from body-wave studies. That the body-wave studies yielded consistent results, suggests that the structure of this region is well constrained, probably better than for other parts of India.

For the central Indian shield or plateau (Region 19b), we directly use Bhattacharya's (1981) surface-wave based model; it has layer thickness, and P- and S- velocities, compatible with the composite body-wave based peninsular shield model, although there are slight differences. It is useful for modeling body-waves as well as surface waves, and is nearly as well constrained as the peninsular shield model.

For the central and eastern Gangetic plains (Region 19c) the Dube and Bhayana (1974) model is directly used. This model has many similarities with the shear velocity model of the region by Chaudhury (1966), but is again used alone as the final model since the body wave study should provide better resolution of both shear and compressional velocities. We use Chun's (1986) model for the western Ganga basin (Region 19g). His surface-wave based model was determined from a robust stochastic inversion method, and impressive fits of dispersion data provide a good basis for its application; further, distinct differences in the character of surface-wave waveforms between the western Ganga basin and the Gangetic plains to the east supports his contention of a fundamentally different crustal structure, characteristic of old oceanic platforms.

Our model for the Himalayan region (Region 19f) is based on a combination of the deep sounding reflection study of the mountain range by Hauck et al. (1998) for the P velocity and the surface wave study of Hwang and Mitchell (1984) for the corresponding shear velocities. This model is unique amongst these composite regional models in that the crustal thickness is approximately 70 km and the Moho boundary is transitional, with a velocity gradient rather than a first-order discontinuity.

Our model for the westernmost lowlands of India (Region 19h), including the Cambay and Sanchor basins, is taken from a deep sounding profile of this region (Kaila et al., 1990); shear velocities were calculated from the compressional velocity.

Our model for the northeast region of India (Region 19e), including the Shillong Plateau, was developed by combining Singh's (1994) surface wave model for the region with a P- and S-wave

based model of Mukhopadhyay et al. (1997) for the Shillong Plateau. It is considered one of the two more poorly constrained regional models due to the lack of relatively high-resolution body wave information for the entire crust. Further, one study (Kayal and De, 1987) has found exceptionally high Moho velocities of 8.57 km/s on average; as this was not born out in the surface wave model, it was not included in our final composite model.

Our final regional model for the Indian sub-continent is for Burma (Region 19d); it is taken directly from Singh's (1984) model for the region. Part of the lower apparent crust is assigned a very low Vp/Vs ratio of 1.56; this feature is thought to be due to either underplating of the crust or the phase transition of crustal material to that with quasi-mantle seismic characteristics. No body-wave based models were found for this region, and this is the least well-constrained of our composite models.

Table 7. Our layered velocity models for subregions of the Indian subcontinent

P-Wave Km/s	S-Wave km/s	Density gm/cc	Thickness km
Peninsular India Model, region 19a			
5.76	3.43	2.85	17.6
6.56	3.98	3.01	18.9
8.16	4.61	3.32	-.-
Central India, region 19b			
5.78	3.53	2.85	20.4
6.58	3.92	3.02	18.3
8.19	4.61	3.34	61.3
8.3	4.61	3.36	40.0
8.4	4.62	3.38	-.-
Gangetic Plains Model, region 19c			
2.71	2.0	2.24	3.7
5.64	3.45	2.83	15.2
6.44	3.85	2.99	21.4
8.06	4.61	3.31	-.-
Burma Model, region 19d			

Table 7. Our layered velocity models for subregions of the Indian subcontinent

P-Wave Km/s	S-Wave km/s	Density gm/cc	Thickness km
4.06	2.55	2.66	3.0
5.31	3.5	2.72	7.0
5.8	3.7	2.75	8.0
6.4	3.9	2.98	8.0
6.57	4.2	3.0	8.0
6.7	4.5	3.2	11.0
6.89	4.7	3.29	11.0
8.15	4.9	3.3	30.0
8.26	5.1	3.42	70.0
8.30	4.85	3.42	150.0
8.5	5.1	3.45	60.0
8.7	5.3	3.45	-.-
North East India, region 19e			
4.06	2.75	2.66	2.0
5.9	3.4	2.88	10.5
6.4	3.55	2.98	14.5
6.89	3.98	3.29	9.0
8.15	4.7	3.30	10.0
8.26	4.72	3.42	30.0
8.3	4.75	3.42	30.0
8.4	4.75	3.44	-.-
Himalayan Model, region 19f			
5.0	2.7	2.7	4.0
6.0	3.35	2.9	22.0
7.0	3.96	3.1	4.0
6.4	5.80	2.98	37.5
6.67	3.82	3.03	2.5

Table 7. Our layered velocity models for subregions of the Indian subcontinent

P-Wave Km/s	S-Wave km/s	Density gm/cc	Thickness km
6.94	3.96	3.09	2.5
7.21	4.11	3.14	2.5
7.48	4.27	3.19	2.5
7.75	4.42	3.24	2.5
8.02	4.57	3.29	2.5
8.29	4.73	3.34	2.5
8.55	4.87	3.41	-.-
West Gangetic Model, region 19g			
4.06	2.34	2.66	4.0
5.31	3.06	2.72	6.0
6.57	3.80	3.00	10.0
6.89	3.98	3.08	20.0
7.83	4.52	3.29	80.0
8.08	4.66	3.34	80.0
7.97	4.6	3.32	-.-
Westernmost Model, region 19h			
2.15	1.5	2.13	2.0
3.2	2.0	2.34	3.0
5.95	3.4	2.89	4.0
5.5	3.14	2.80	2.0
6.3	3.6	2.96	7.0
6.75	3.86	3.05	6.0
7.35	4.2	3.17	8.0
8.0	4.57	3.30	-.-

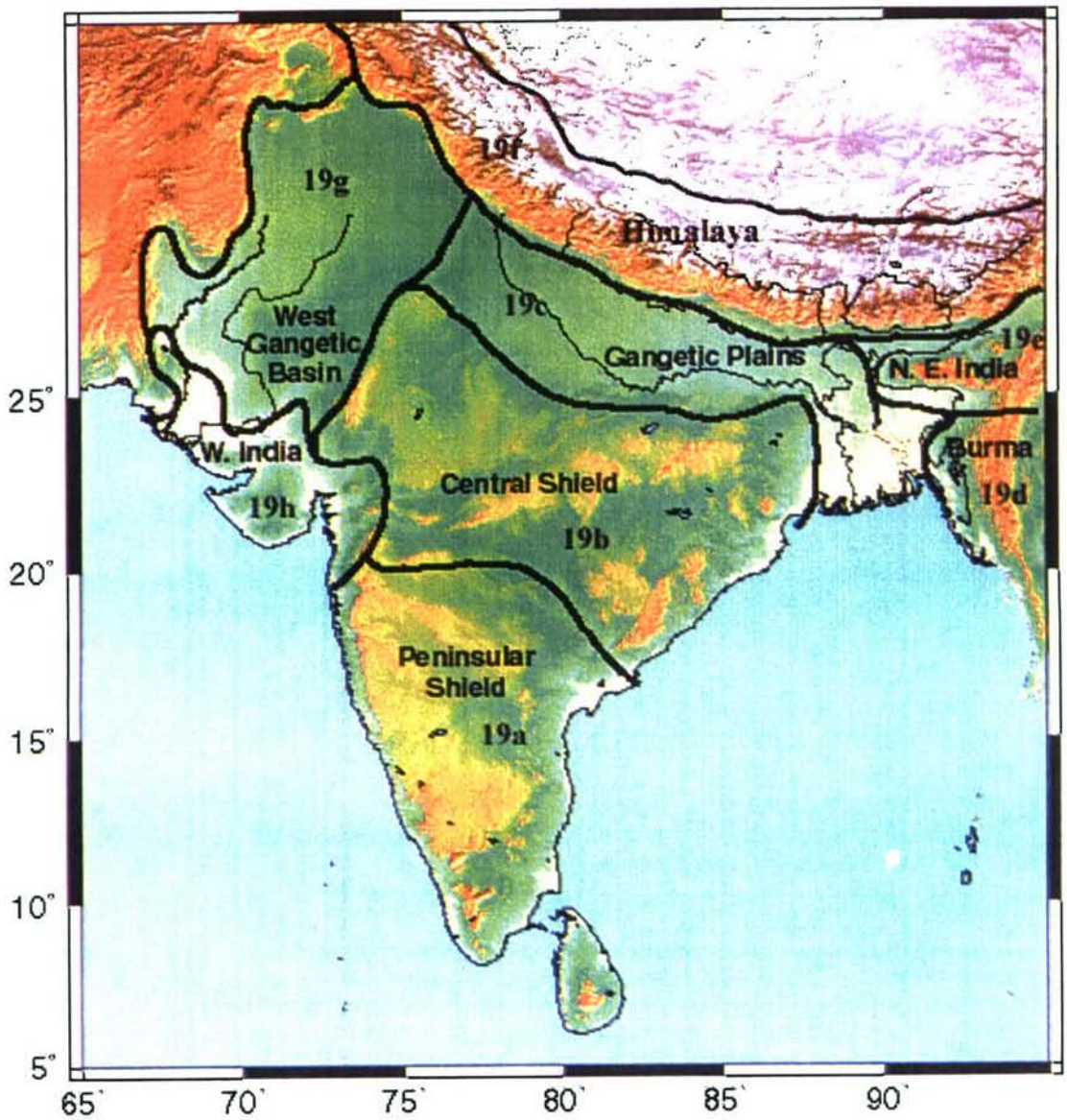


Figure 13. Region names and numbers, for the 1D structures used in our model of the Indian sub-continent.

3.7. The Continent/Ocean Boundary

In our original regionalization, shown in Figure 2, it was tacitly assumed that oceanic structures lie seaward of the coastline. However, numerous studies have demonstrated that the continent/ocean boundary is poorly represented by present-day coastlines.

In the context of our East Asia study, shallow seas surround much of the coastline, and in practice Lg waves propagate efficiently out to significant distances in what may be regarded as continental crust overlain by shallow water. For example, the Yellow Sea between China and the Korean peninsular supports efficient Lg propagation.

Figure 14 shows how parts of the continental regions originally specified in Figure 2 have been revised in our final regionalization, which takes the boundary between continental and oceanic structures as the 200 m bathymetric contour.

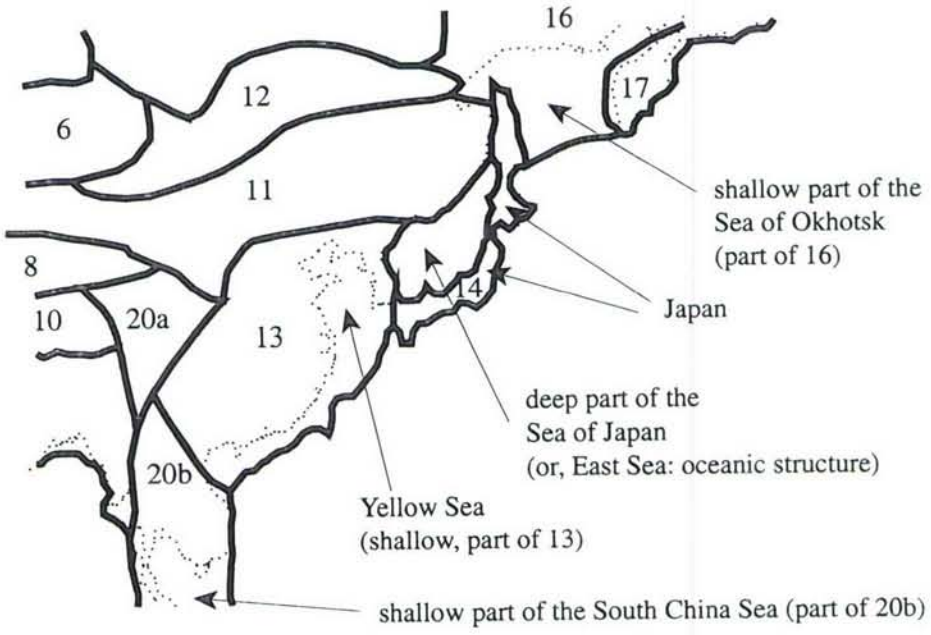


Figure 14. Here are shown the seaward extent of regions, previously defined as continental, which characterize shallow seas to the east and south of East Asia.

Section 4 Data Sets

Our general approach to developing SSSCs has been to pursue two paths somewhat independently in the early stages, that are brought together in the work of validation. Thus, (1) we have generated velocity models as described in Section 3 that enable an approach based on modeling Earth structure; and (2) we have sought as many high-quality reference events that we could find or generate that enable an empirical approach. This Section describes our principal data sets associated with these reference events.

We decided to emphasize high-quality (GT5 or better, though using a few GT10 events where nothing better could be found), rather than develop a long list of low quality reference events (GTn with $n > 10$), since in practice the latter have little impact on location improvement.

The Soviet-era PNEs and underground nuclear explosions (UNTs) at weapons test sites were recorded by hundreds of stations within the territory of the former Soviet Union, that typically did not report these signals in the open literature. Arrival times of these events were reported to the International Seismological Centre (ISC) by hundreds of stations in Eastern Asia. And of course many of the PNEs and some of the UNTs were very well recorded by hundreds of temporary field stations deployed in long profiles within the U.S.S.R. We have built a number of data sets from these travel times that can be used to obtain SSSCs quite directly from observations. The principal work of building these phase pick data sets entails resolving numerous questions on

- what to do when different analysts pick different arrivals from the same waveform, and
- what to do when different station coordinates are listed by different organizations for the same station.

4.1. Kitov Data Set of Soviet-Era Underground Nuclear Explosions

Dr. Ivan Kitov and staff of the Institute of Dynamics of the Geosphere (IDG) have made an important contribution to location calibration by gathering and making available the phase data from 83 Soviet Peaceful Nuclear Explosions (PNEs), 35 underground nuclear weapon tests (UNT) at the Novaya Zemlya Test Site, and 80 underground nuclear explosions at Semipalatinsk Test Site. There are 129 Soviet station locations associated with arrival picks in the data and it is necessary to decide how these should be merged with the reports of the same events given at 915 stations

(east of 20°E and north of 5°N) for which IDG has also collated phase data derived from the ISC bulletin. These data in total provide quite dense coverage.

We obtained a copy of the initial version of the data from a Harvard website (http:// www.seismology.harvard.edu/~ekstrom/Research/FSU_data/FSU_data.html), but to use them we needed to resolve the following issues:

1) There are duplicate station codes that have different locations and presumably are different stations.

2) The station list file has 1044 stations (129 Soviet + 915 derived from ISC) but 944 stations when duplicate code names are removed.

3) In case of phase picks for PNEs, there are 106 stations with more than 20 observations and 236 stations with fewer than 20 picks. We have examined all of these 106 stations and have used numerous contacts with knowledgeable sources of information in the former Soviet Union to decide the best station locations.

4) The ISC station list and the principal Soviet station list contain different station codes for the same station, as well as the same code for different stations, which must all be resolved.

5) Finally, when the station database is constructed, operation start time and end time have to be entered in the case of several stations that were moved, and the best information from station operators has to be used. Our database is described further in Appendix C.

The outcome of this major effort, is a groomed list of 355 station coordinates in which we have confidence, for stations that reported the vast majority of the phase pick data for Soviet PNEs and UNTs. For purposes of calibration, we have used 156 events and 2626 Pn arrival times from the initial dataset obtained from Harvard. For brevity, we refer to these data as Kitov's dataset (though they were derived from many sources and were substantially groomed by members of the Lamont Consortium). Figure 15 shows a map of the event locations (red stars) and the stations that recorded them (triangles), along with great circle paths between events and stations (blue curves). This map illustrates that the source regions, station sites, and paths sample very diverse and

extensive geological structures throughout Asia, making this dataset extremely valuable for model validation as well as providing empirical data that may be used quite directly to generate SSSCs.

Comparison with the Ground Truth Database at the former Center for Monitoring Research revealed that 126 events from Kitov's dataset are in the GT database. Of these 126 events, 32 events are considered GT0 quality (0 km location accuracy), 66 events are GT1 (1 km accuracy), 13 events are GT5 (5 km accuracy), and 15 events are GT10 (10 km accuracy). The CMR Ground Truth database is described by Yang and Romney (1999).

4.2. Additional Explosion Reference Events, used in our May 2002 CCB Proposal and for the Present Study

We augmented Kitov's data set with 18 additional GT explosion events, also shown in Figure 15. This data set includes seven underground chemical explosions (UCE) conducted at the Semipalatinsk test site, all in the CMR GT database with GT0 quality. We also added eleven underground nuclear explosions (UNEs) conducted at the Lop Nor test site in western China, eight of which have associated Pn arrivals at regional stations. Fisk (2002) describes these nuclear explosions and how IKONOS satellite imagery and seismic data were used to obtain GT1 locations for these events. The data set is completed with two more UNEs conducted in India and Pakistan and described by Barker et al. (1999).

The green curves in Figure 15 indicate the great circle paths for these 18 explosions, along with paths for PNEs recorded by BRVK (Borovoye) for which we have made our own phase picks from digital waveforms.

Note that BRVK began digital recording of underground nuclear explosions in 1966. Prior to formation of the Lamont Consortium in March 2000 for the present project, Lamont personnel had worked for several years (since 1991) with scientists in Russia and Kazakhstan to salvage digital waveform data from Soviet-era magnetic tapes and to make the BRVK data generally available in a modern format. More than 700 digital data sets (CSS 3.0 format) have been constructed, each containing different channels of waveform data from one nuclear explosion. This BRVK archive, and an archive also of earthquakes, may result in BRVK becoming the best calibrated of all IMS stations.

We note that although our principal interest is in calibrating the thirty IMS stations (Group 1) in East Asia, we have also gathered phase picks to enable calibration of the additional stations listed in Table 2. Although these other stations are not part of the IMS network, they are useful for validating our regionalized model and the computational methods for generating SSSCs, as demonstrated below.

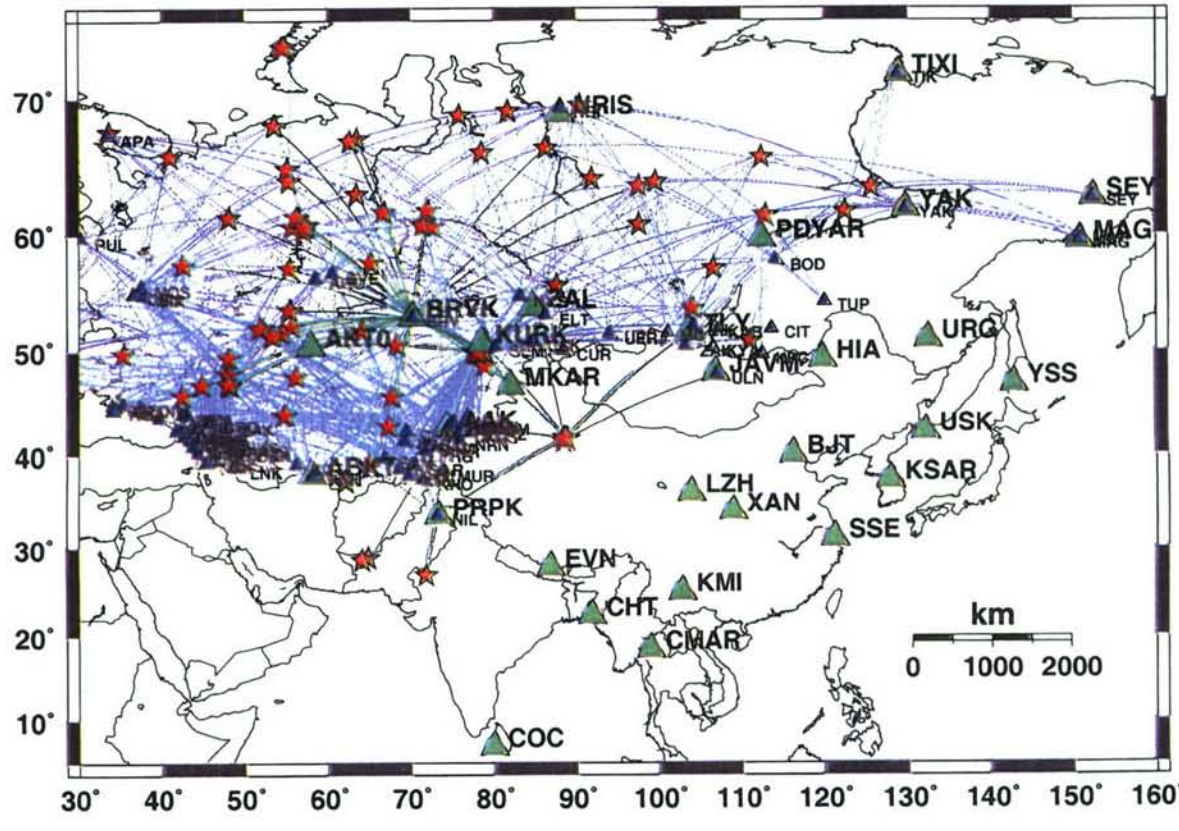


Figure 15. Map showing locations of GT explosions (red stars) and recording seismographic stations (blue triangles) used for validation tests in support of our May 2002 CCB proposal. Also shown are great circle paths between events and stations.

4.3. Data from Field Stations Used to Record 19 Soviet-Era PNEs

The Deep Seismic Sounding program successfully probed for Earth structure for decades using chemical explosions, but it began to use nuclear explosions in 1977. So far, we have mentioned PNEs in the Soviet Deep Seismic Sounding program only in the context of explosion signals

recorded at standard seismographic stations. But these explosions were also recorded at thousands of temporary stations, as described further in Appendix C.

Thus, 19 of the many PNEs on Soviet territory were dedicated to DSS studies. Typically, several hundred field stations were deployed on a long line for each shot, with horizontal as well as vertical sensors. The principal technical objective was to determine crustal thickness and its variability along the set of field stations. The idea was to record P arrivals (on the vertical component), and the Moho P-to-S conversion denoted as Ps (on the horizontal component). The time difference between Ps and P is easily converted into crustal thickness. In practice, however, the seismic data along these profiles have turned out to supply far more information than just crustal thickness. They provide significant information on deep Earth structure, going down more than 400 km to the transition zone between the upper and lower mantle. For our purpose in location calibration, these data (most notably, the first arriving P waves) can be used to validate our model of travel times.

In March 2002 and September 2002, Dr. Igor Morozov, then at the University of Wyoming and under sub-contract to the Lamont Consortium, provided us with phase picks from the DSS (Deep Seismic Sounding) profiles in northern Eurasia (Figure 16). These seven DSS profiles based on 19 PNEs were conducted between July 26, 1977 and September 6, 1988. The best known ground truth data for these PNEs are from Sultanov et al. (1999). The data have been picked originally by seismologists in Russia, but our picks were redone by Igor Morozov and Elena Morozova at the University of Wyoming especially for the Lamont Consortium.

There are 8,411 phase picks in our data set, of which 4,761 are P phases and 3,650 picks are S arrivals. P, Pn and Pg phases are picked at 3,141 stations, whereas S, Sn and Lg arrivals are picked at 2,570 stations. Note that the apparent dark lines on Figure 16 are actually an agglomeration of many points, one for each station.

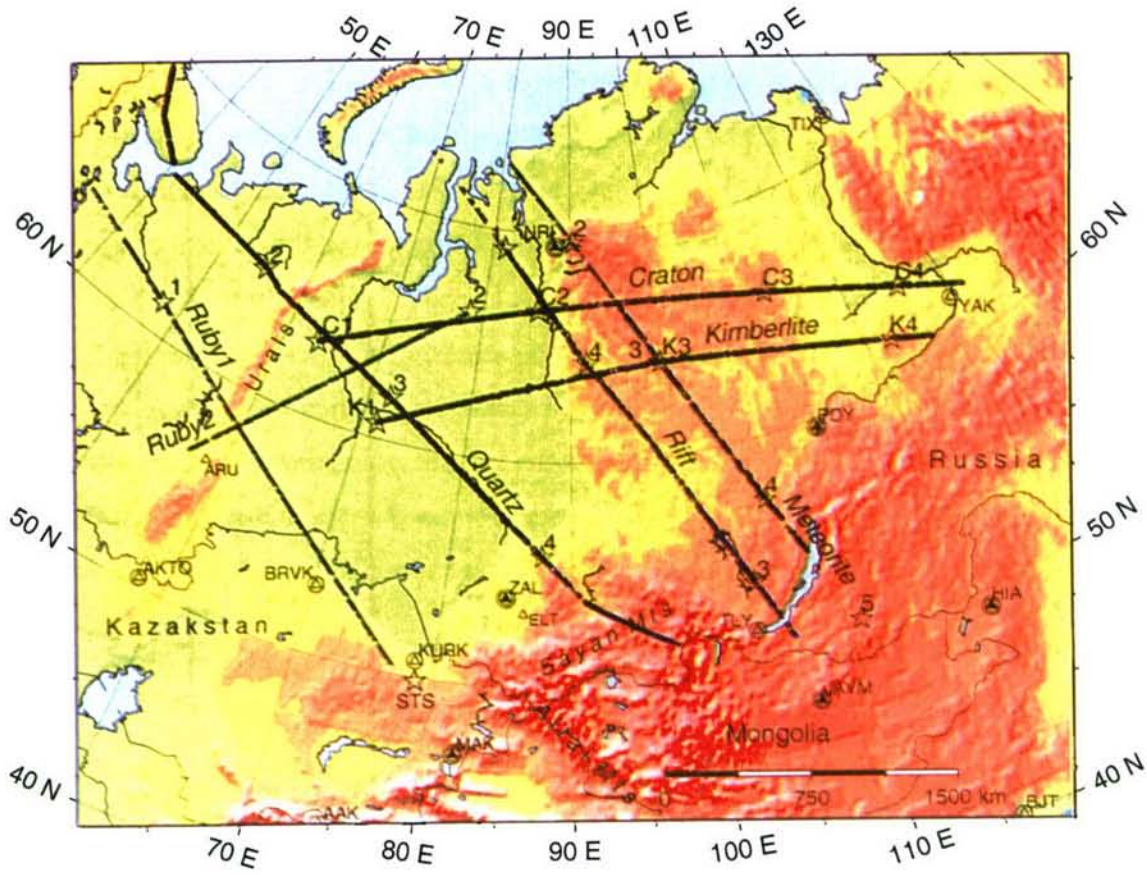


Figure 16. Seven "Deep Seismic Sounding" (DSS) profiles in Northern Eurasia. 19 PNEs (stars) were used to acquire these data. The many small dots (appearing as dark lines along the profiles) give the location of more than 3000 temporary seismographic stations for the DSS experiments carried out in the former Soviet Union from 1977 to 1988.

There was some uncertainty regarding origin times and locations of the PNEs used to derive these travel time data. The basic problems here, are that (1) at the time these 19 PNEs were carried out, the source locations and origin times were classified information in the Soviet system so that ways to communicate the data were developed that did not rely upon this information; and (2) the desired technical results from the DSS program did not require absolute locations for sources and stations, nor did they require absolute origin times. Rather, the community of users of DSS data became accustomed to working with relative locations and relative times (for example, use of offset — which is the distance between source and stations; and use of the time differences between arrival of the same phase at different stations — that is, the slope of the travel time curve, which is all that is needed to determine velocity as a function of depth along the profile).

When scientific publications analyzing these DSS data began to appear in the western scientific literature, it was quite common for maps (in these papers) to indicate source locations (of the PNEs) more than 100 km different from their actual locations.

We have conducted a preliminary analysis of the DSS phase data, and have associated information on absolute times and absolute source and station locations, to ensure that the phase picks (absolute times) and other information are consistent with all that we know about these sources. Thus, when we have plotted arrival time minus origin time (equals travel time), against offset, it is clearly problematical when the Pg travel time appears not to go to zero as the offset goes to zero.

It is understood that the GEON Center in Moscow (the present custodian of all DSS data) provided seismic waveform data to the University of Wyoming, and that each seismic record starts at a reference time relative to the PNE shots. Offset in meters from the shot point, and station coordinates (usually up to four significant decimal digits), are given in each trace header.

Researchers at the University of Wyoming picked P and S wave arrivals relative to the reference time. If the reference time for each PNEs is correct, then these picks are the correct travel times. Arrival times of these phases are obtained by adding the travel times to the origin times given in Sultanov et al. (1999).

We found out that for about half of the PNEs, reported absolute arrival times appear to be consistent with the GT1 or GT2 quality event location given in Sultanov et al. (1999). These PNEs are marked as "A" in the penultimate column of Table 8. We also found that arrival time data from certain PNEs suggest some constant time offsets in the corresponding set of phase picks, amounting to few seconds. These PNEs are marked as "B" and may be due to use of poor absolute times by the agency (GEON) which now has responsibility for these data. There are a few PNEs whose event parameters are not well constrained. These are GT10 or worse quality according to Sultanov et al. (1999) and are marked as "C" in Table 8.

It may be noted that several PNEs can be used as reverse profiles, because several segments of the DSS profiles are recorded twice by shots at the beginning and end of the profiles.

In summary: the good news is that approximately half the PNE profiles appear to have high quality timing and source/station locations in our data sets. The remaining profiles are somewhat questionable. (They are still useful for investigating Earth structure and other subjects. It may turn out on further analysis that some of the profiles to which we have assigned quality B, may be associated with shots in anomalous material that causes the apparent delay that we see as Pg branches which do not go to zero as distance goes to zero. These profiles may be promoted to higher quality on the basis of additional investigations.)

Table 8. The list of 19 PNEs for which we have acquired empirical phase picks. The penultimate column indicates the quality of available information on absolute timing and absolute source and station location for these profiles.

Date (mo/dy/year)	Origin time (hh:mm:ss)	Name	Location quality	Data quality	Offset (possible)
07/26/1977	17:00:00.22	Meteorite-2	GT1	A	
08/10/1977	22:00:00.10	Meteorite-5	GT1	B	
08/20/1977	22:00:00.78	Meteorite-3	GT1	A	
09/10/1977	16:00:00.18	Meteorite-4	GT1	A	
08/09/1978	18:00:00.79	Craton-4	GT1	B	-2.5 s
08/24/1978	18:00:00.35	Craton-3	GT1	A	
09/21/1978	15:00:00.19	Craton-2	GT1	A	
10/17/1978	14:00:00.16	Craton-1	GT1	B	
08/12/1979	18:00:00.21	Kimberlite-4	GT1	A	
09/06/1979	18:00:00.31	Kimberlite-3	GT1	A	
10/04/1979	16:00:00.03	Kimberlite-1	GT1	B	-1.2 s
07/30/1982	21:00:00.00	Rift-3	GT10	C	
09/04/1982	18:00:00.06	Rift-1	GT10	C	-5.0 s
09/25/1982	18:00:00.18	Rift-4	GT10	C	
08/11/1984	19:00:00.20	Quartz-2	GT10	D	
08/25/1984	19:00:00.33	Quartz-3	GT10	C	-1.6 s
09/17/1984	21:00:00.03	Quartz-4	GT1	A	
08/22/1988	16:20:00.07	Ruby-2	GT1	B	-3.0 s
09/06/1988	16:19:59.94	Ruby-1	GT1	A	

4.4. The Annual Bulletin of Chinese Earthquakes

This Bulletin, known as the ABCE, exists in many forms. Notably, these include hard copy books, published each year (we have them for 1996, 1997, 1998), the corresponding electronic files (we have them for 1985, 1986, and 1991 through 1995), and various electronic files in formats somewhat different from what is published. We have mainly uses a version of the ABCE based on what are known as z-files, for the period 1985 to 1999, one file for each month (180 files, z8501 - z9912). Approximately 14,000 earthquakes and other seismic sources, in and near China, are characterized in these files. They include regional phase pick data for all Lop Nor nuclear explosions during this period (13 UNEs). The IASPEI organization has made these 180 monthly files generally available on a CD, accompanying Part B of the International Handbook of Earthquake and Engineering Seismology (Lee et al. editors, 2003).

Concerning station locations, first we note that for the years 1985 to 1999 there are 170 stations in and near China for which there are phase pick and amplitude data in our files for the period from 1985 to 1999. Numerous additional stations, not near China, provide this information through the U.S. Geological Survey's Earthquake Data Report (EDR), and we our files z8501 - z9912 contain the additional information that appears to be derived from the EDR, as well as from the 170 stations in and near China.

Of the 170 stations in and near China, there are 11 stations in Taiwan, 4 in Thailand, 3 in each of Kygyzstan, India, Nepal, Tadjikistan, Uzbekistan, 2 in each of Kazakhstan, Pakistan, and 1 in each of Bangladesh, Russia, and Vietnam. Coordinates for all of these 37 stations are available for example from the U.S.G.S.

For the remaining 133 stations, all in China, we have not checked to see which have been listed by the ISC. (We also note that station coordinates can be obtained from the published ABCE, since these hard copy publications include the Jeffreys-Bullen residual for each phase pick. These are perfect data for locating stations.) We have long had coordinates for these 133 stations, which recently we have been able to compare with locations provided as the result of a GPS survey. In most cases, there is less than 1 km difference between the different locations we have for a particular station. Also, we note that for purposes of applying the double difference method for event relocation, an error in a station location is not serious provided it does not result in a

significant difference in the azimuth angle between source location and station direction. But of course for purposes of locating earthquakes one at a time, and for tomography, station location errors can be significant

4.5. Additional Information on GT Events Used in this Study

We have written five documents that give considerable detail on the more than 800 GT events used by our consortium to calibrate the Group 1 IMS stations. The first of these is a scientific paper characterizing a set of earthquakes in the Xiuyan region of Liaoning Province, China (Schaff and Richards, 2003). The second is a technical report on methods used to develop 64 GT5 events in China, which appears as Appendix A of this document. The third is an expanded version of Appendix A, written as a scientific paper (Waldhauser and Richards, 2003), which in addition to developing GT events explores the use of ABCE data to obtain empirical SSSCs and their uncertainty. The fourth, is a technical report summarizing the parameters of the more than 800 GT events we have used for validation of our SSSCs and which appears as Appendix B of this document. In addition to our studies resulting in GT events in China, Appendix B notes our work to obtain a few additional (earthquake) GT events in Central Asia, Japan, Kyrgyzstan, Taiwan, and South Korea. The fifth, is a scientific paper we have written jointly with Chinese scientists (Yang, Waldhauser, Chen, & Richards, 2003) which relocates more than 6500 earthquakes in central-west China on the basis of data recorded by 193 stations (most of them in Yunnan and Sichuan provinces).

Section 5 Model Revision and Computation of SSSCs

SSSCs represent travel-time corrections to a standard travel-time model (now almost universally taken as IASP91), as a function of source position, for a particular station and a given seismic phase. The method of calculation of SSSCs adopted by the Lamont consortium entailed four steps. Thus, it began with (1) application of the method of Bondár (1999) to first compute travel times for regional phases that cross region boundaries, using the initial set of boundaries and travel-time models described above in Sections 3.4, 3.5.1 through 3.5.3, and 3.6.1. For regions not explicitly assigned regional travel times in these Sections, the IASP91 travel-time model was assumed. Then (2) we developed a 3D ray-tracing approach to replace the Bondár method, and (3) made a set of small adjustments to our set of velocity models in each subregion in order to make our final computation of travel times from the necessary grid points and thus to obtain our final set of model-based SSSCs.

Our nal step has been (4) to use phase arrival data from GT events in a kriging algorithm to refine the SSSCs empirically. At each grid point, the SSSCs are updated by an optimal linear combination of travel-time residuals, weighted by a distance-dependent correlation function. In addition to the updated correction grid, the kriging algorithm estimates a corresponding uncertainty grid. The spatial distribution of the calibration points determines how much weight each calibration datum contributes to the correction surface, and the relative magnitude of the uncertainty surface. For well-calibrated locations — that is, locations near many calibration points — the correction surface converges to the mean of the data close to that location and the uncertainty (variance) surface converges to the variance of nearby data, which we call the residual variance. For locations far from calibration points, the correction surface converges to the model-based SSSC value, with larger uncertainty equal to the sum of the residual variance and the calibration variance, which is the variance of the travel-time means averaged over all well-separated locations.

We next describe each of these four steps in more detail.

5.1. The Bondár Method of SSSC Computation

The model-based approach of Bondár (1999) relies on regionalization and corresponding one-dimensional (1D) regional travel times as a function of distance within each region. It does not

need a velocity model, since computation of travel times for a path that crosses more than one region is accomplished without ray tracing. In this method, a weighted average is formed, of the travel times as if the signals had traveled the full distance in each of the separate sub-regions, the weights being essentially the proportion of the path in each sub-region.

This method has been applied successfully to regional phases at stations in Fennoscandia (Yang et al., 2001) and at stations in North America (Bondár et al., 1998; Yang et al., 2001). The SSSCs and the corresponding modeling errors are defined at points of a user-defined rectangular grid. Additional information on the Bondár's method and the results of using the SSSCs for model validation is provided in Burlacu et al. (2002).

In May 2002 the Lamont consortium successfully presented a CCB proposal (Richards et al., 2002) based on use of the Bondár method applied to the data depicted in Figure 15, and kriging, for a subset of 14 of the Group 1 stations. These kriged SSSCs, for 14 IMS stations in Russia and Central Asia, led us to the following preliminary results:

- median mislocation error reduced from 12.2 km to 2.7 km,
- error ellipse areas reduced by 20% or more for 97% of events,
- median error ellipse reduced from 1,596 to 196 km^2, while achieving 100% coverage.

These metrics indicate that very significant improvement in location capability can be achieved with application of our preliminary SSSCs. But we could not use the same approach for more than half the Group 1 stations, because as shown in Figure 15 the PNE and other explosion data do not apply to the remaining stations.

In order to complete the work of calibrating all the Group 1 stations, it is clearly necessary to work with the additional GT data associated with earthquakes — and, in particular, earthquakes in and near China. It was for this purpose that we developed the results mentioned above in Section 4.5 and described in Appendices A and B.

In practice, to obtain SSSCs for all the Group 1 stations, we made two additional changes as well as using earthquake data. First, we took the major step of using 3D ray-tracing rather than relying upon the Bondár method; and second, we obtained results using S-waves as well as P-waves.

5.2. Our Method of 3D Ray-Tracing in Heterogeneous Structures

In order to compute travel times for paths that cross different 1D regions, we made an application of methods described by Menke (2002) in which a 3D velocity model is specified with a cartesian grid. This necessitated, first, the derivation of velocity models for each of the 1D regions we had identified. (Note that with the Bondár method for obtaining travel times across different regions, there is no need to develop a velocity model because the travel time is derived directly from a weighted average of travel times in the 1D structures.) Second, we needed to generate an overall 3D model by aggregating the 1D models; and third we needed to compute travel times from each of the stations listed in Table 1 (30 IMS stations) and Table 2 (128 additional stations), out to all the 1^{o} x 1^{o} grid points at which model-based SSSCs are needed (up to 20^{o} from each station).

Our first steps in obtaining velocity models, for each 1D region for which we had travel time relationships, were taken by M. West at Lamont in mid-2002. Using a least squares fitting procedure, he inverted the observed Pn travel times, given above in Section 3, for 22 of the regions shown in Figure 2 (further details are given at http://geophysics.nmsu.edu/west/AS). Figure 17 shows how well his model travel times fit the observed travel time relationships. The velocity in each of the 22 regions was constrained to vary continuously with depth — that is, there are no first-order discontinuities. This choice of velocity model is well-suited to the method of ray tracing we adopted. Our initial 3D velocity model was obtained by smoothing over a zone 100 km wide between the adjacent 1D regions shown in Figure 2.

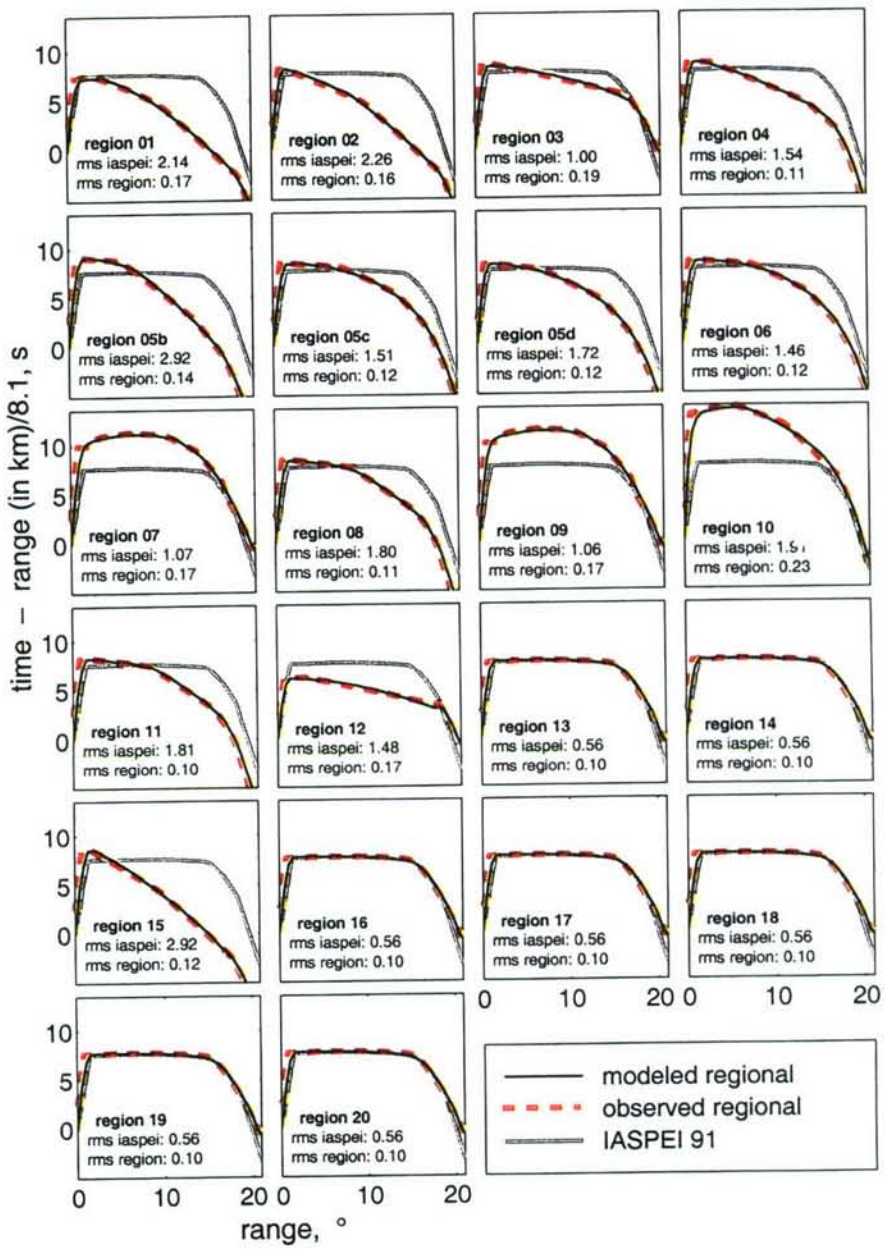


Figure 17. Reduced travel time curves are shown for 22 of the regions depicted in Figure 2. The dashed line ("observed regional") in each case represents the Pn travel-time relationship for the region, as given above in Section 3. The gray line is the IASP91 standard Pn travel time. The dark line ("modeled regional") is the travel time in a 1D structure comprised of a series of layers, in each of which the P-wave velocity increases linearly with depth. The rms misfit is smaller than 0.25 s in all cases. This figure indicates very significant departures from the IASP91 travel times for Pn propagation in different parts of East Asia.

To carry out the travel time computations, the velocity models, initially defined as functions of latitude, longitude and depth, were sampled by a 3D grid tracking the spherical shape of the Earth, with each grid point specified in a cartesian coordinate system. Earth flattening is not needed. (The method can directly handle the Earth's departure from spherical shape, by using a standard ellipsoid or the geoid as the outer surface, sampled by points in the cartesian grid. However, we did not do this because the ellipticity correction is significantly smaller than the typical differences we found between model times and observed times.) Model input formats were converted to enable application of a 3D ray tracing code originally developed by W. Menke (available from www.ldeo.columbia.edu/users/menke/software.html). In our analysis, the grid was discretized at 0.5^{o} x 0.5^{o}. Each parallelepiped of eight nodes (specified by cartesian coordinates) was then divided into five tetrahedra with velocity defined at each vertex. These four velocities can be fit by a linear gradient superimposed on an average velocity. The ray path in such a medium is an arc of a circle, and the travel-time along such an arc can be computed analytically. The limitation of this method, as currently implemented, is that it requires a non-zero velocity gradient in each tetrahedron and it does not allow velocity discontinuities. Figure 18 shows schematically how the grid was set up, and how a ray path follows an arc of a circle in each tetrahedron. Use of tetrahedra essentially allows the total travel time to be obtained analytically as a sum of contributions from each circular arc, although of course there are all the usual problems of finding the right path between a particular pair of end points.

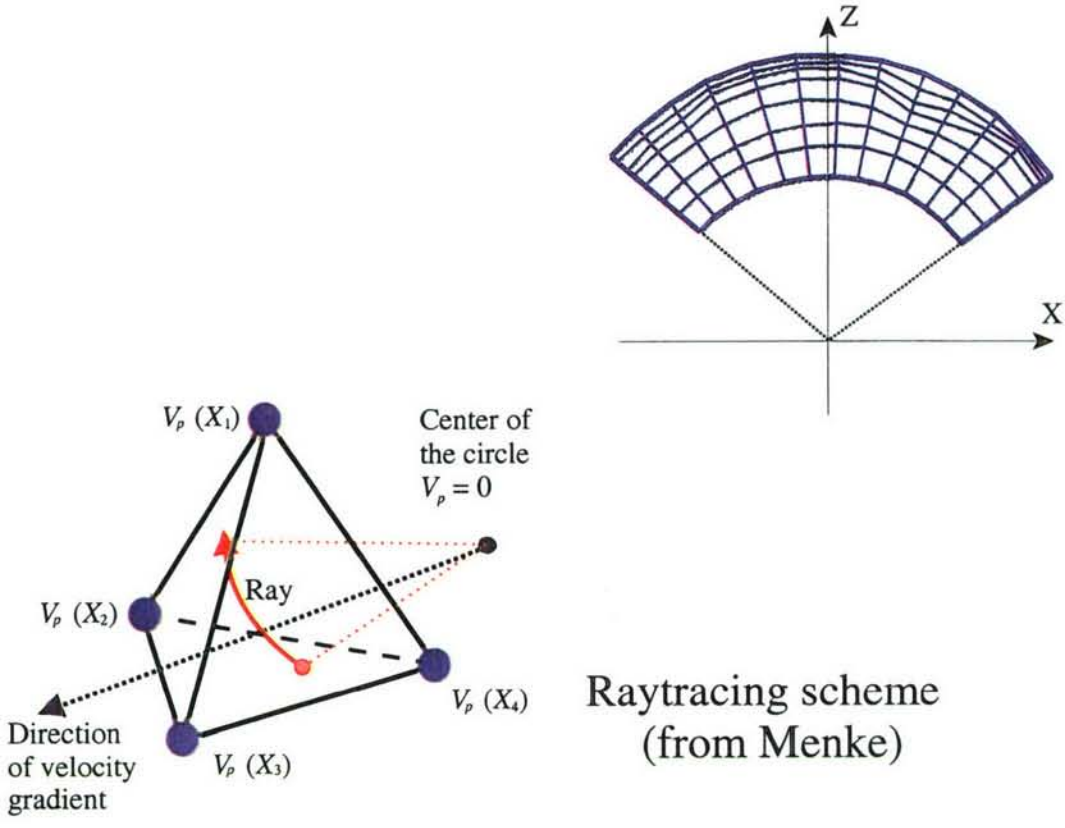


Figure 18. On the upper right, is shown the system of grid points that allows layer numbers to be identified for a laterally-varying Earth model. Each grid point, or node, is specified by its cartesian coordinates. Lower left, shows a tetrahedron within which the velocity has a linear gradient, so that the ray path follows the arc of a circle.

As noted by Cormier and Stroujkova (2002), the error of this method is comprised of two major effects. The first source of error is the tetrahedral parameterization of the Earth, which for example implies an approximation of the surface of the Earth by a multifaceted surface. It is possible roughly to estimate the magnitude of this error. Figure 19a shows a simplified 2-D geometry for this case, with one facet of the tetrahedron approximating part of the spherical surface. The deviation of the model (tetrahedron) surface from the surface of the sphere at both source and receiver is

$$dz = R \{1 - [\cos(\delta/2)/\cos(\delta/2 - \gamma)]\},$$

where R is the radius of the Earth, δ is the angular distance between nodes of the grid, and γ is the angular distance to the nearest node. This leads to a travel time perturbation given by

$dt = dz \cos i/V_0$, where V_0 is the velocity at the source or receiver and i is the corresponding takeoff or arrival angle. This type of error is largest in the center of a grid cell (where $\gamma = \Delta/2$), gets smaller toward its nodes, and goes to zero at the nodes themselves.

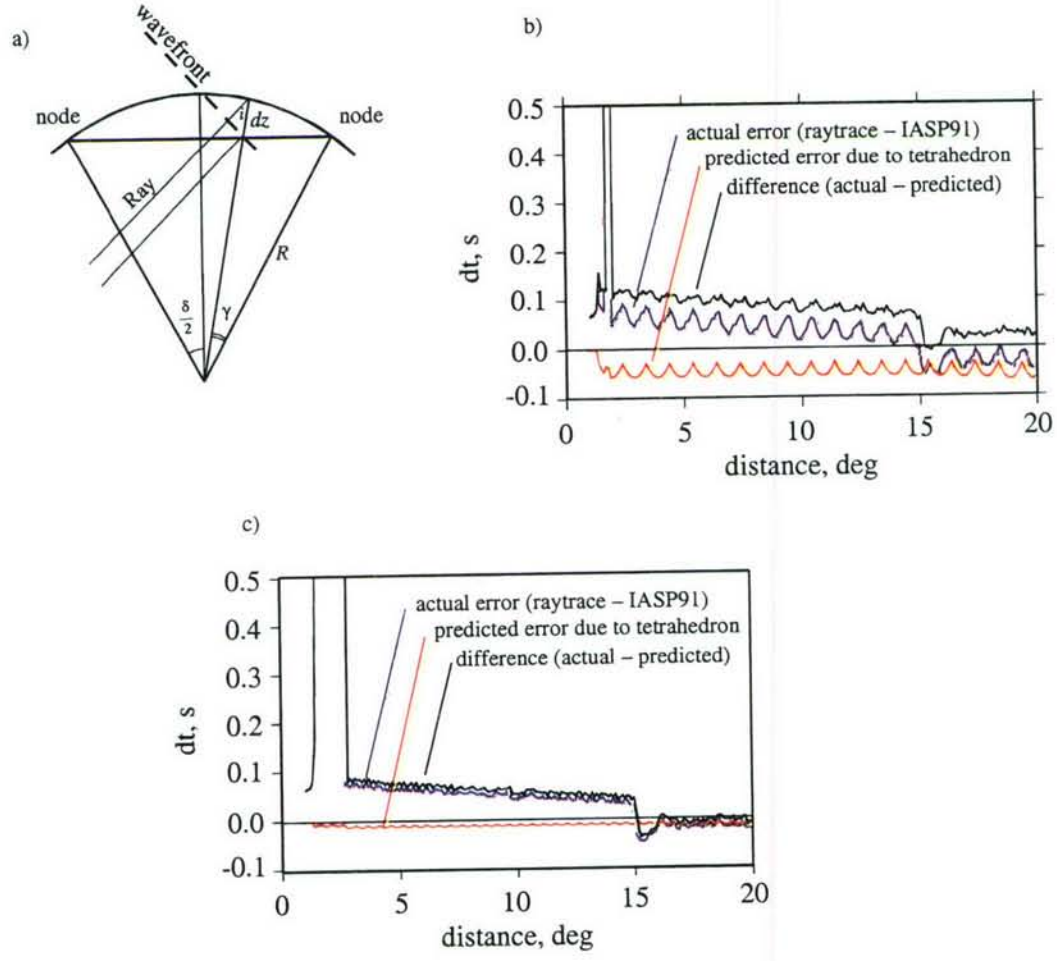


Figure 19. a) Geometry of a ray near the surface in the spherical Earth approximated by tetrahedra. Angles δ and γ are much smaller than shown, in practice. b) Difference between computed travel times and IASP91 travel times, for a 1^o x 1^o grid. Blue line shows the difference between the actual computed time (ray traced in tetrahedra) and the IASP91 travel time. Red line shows predicted error due to surface approximation (see text). Black line is the difference between actual and predicted error (blue - red). c) Same as b), except node spacing is reduced to 0.5^o. This error is negligible beyond 2^o.

The second error comes from the velocity approximation itself — that is, how well an inhomogeneous model is characterized by the discrete grid points and the interpolation rule for determining velocity between the grid points (which may differ from the velocity in the inhomogeneous model). To examine the relative importance of these two types of errors we applied our method of tetrahedral sampling and ray tracing, to the IASP91 velocity model. The results are shown in Figure 19b and Figure 19c for grid samplings of 1° and 0.5° respectively. Subtraction of the theoretical error from the observed error yields the error caused by velocity approximation, which in the case of 1° grid spacing was below 0.1 s for distances between 2° and 15°. For distances less than 2° it can be as large as 2 s, and beyond 15° it gets less than 0.05 s. For a 0.5° x 0.5° grid the error beyond 2° stays less than about 0.07 s. We used 0.5° x 0.5°grids in our subsequent work. The velocity approximation error however stays large for distances less than about 2°. In practice this did not matter in our analysis of Pn and Sn signals, for which almost all data came from greater distances. (We focused on the use of Pn, and did not use Pg data in our location calibration. To incorporate Pg would entail a separate analysis for each station, of the appropriate Pg travel time relation. Fortunately, this has smaller variability from station to station, than is the case for Pn.)

The practical work of applying Menke's (2002) method to the computation of our final set of model-based SSSCs was largely done by Anastasia Stroujkova, a member of the Lamont Consortium working with Vernon Cormier at the University of Connecticut. Her work was often done while changes were being made to our initial regionalization shown in Figure 2. For example, in Sections 3.5.2 and 3.6.2 we describe our revisions to travel-time models and velocity models for India and China, and in Section 3.7 our revisions to give a better treatment of the continent/ocean boundary. We also found it was appropriate to make some small revisions to our initial travel-time model for Russia and Central Asia, as we next discuss.

5.3. Final Development of Model-Based SSSCs

With the initial regionalization shown in Figure 2, together with revisions for China, India and the continent/ocean boundary, a 3D velocity model was derived by the methods described in Section 5.2. It was found that the travel-time residuals at a set of 97 stations for the Kitov dataset (see Section 4.1) had a quite consistent sign and magnitude in most of the regions.

Such residuals can be remedied by applying average velocity corrections in corresponding regions. However, regions 7, 12 and 16 were found to have significant residuals of both signs. For region 7 (the Tian Shan Orogenic Zone) the stations with negative and positive residuals (between -2.7s and +2.4s) were all mixed, making it impossible to separate sub-regions with different apparent velocities. Either local velocity variations or station timing errors may cause such large differences. The residuals in region 12 (Baykal-Mongol fold zone) were clearly separated for the northern (Baykal rift) part and the southern part and varied from -3.4 s (south) to 2s (north). Therefore we divided region 12 into two sub-regions (12ab) and performed a velocity adjustment separately for each one. Similarly, region 16 was separated into two regions.

Together with previous revisions, this led to a total of 36 different regions for our 3D model of East Asia and its surroundings (out to a distance of 2000 km from the East Asian perimeter). Our final set of region boundaries is shown in Figure 20, and described in further detail in Appendix D.

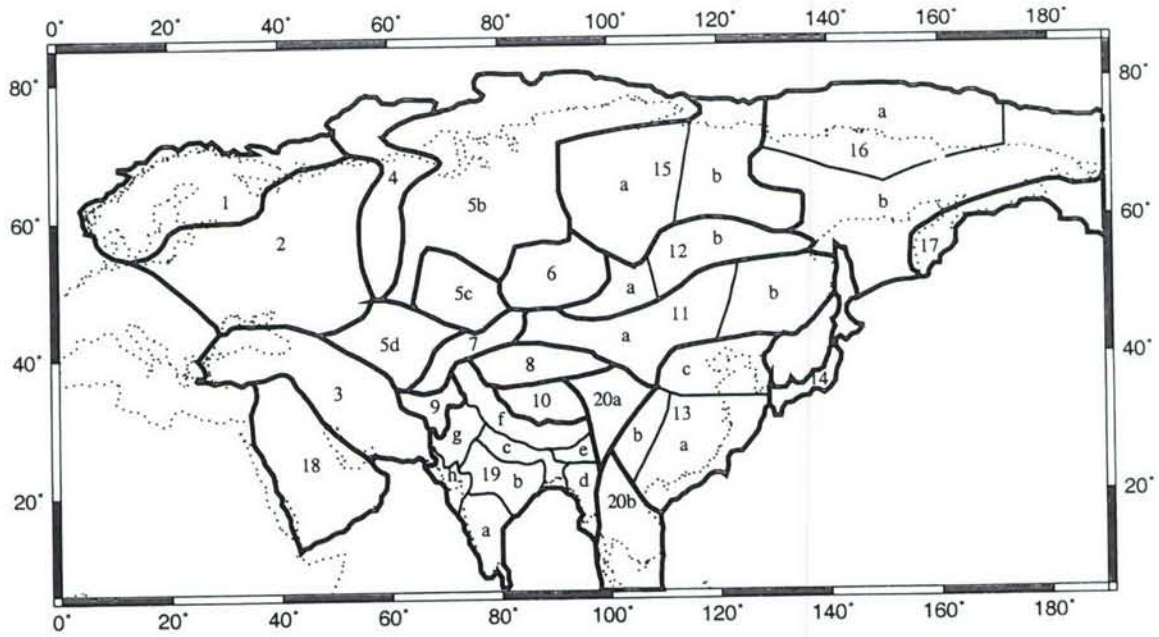


Figure 20. The region boundaries and numbering system used for 36 1D regions in East Asia and surrounding areas, which together make up the 3D velocity model in which 3D ray tracing was used to give our model-based SSSCs. Appendix D provides the lat/long values which specify these boundaries.

The velocity changes needed to reduce residuals for Kitov's data set were quite small — in almost all cases less than 0.1 km/s. (The same velocity change for a particular region was applied for every layer.) The resulting mean travel-time residuals (Δt) are shown in Table 9, together with a velocity change that is derived from differentiating

V_p = distance / (travel time) to give ΔV_p = - distance x Δt / (travel time)^2.

The values of Δt and ΔV_p in the Table are averages for all the sources and stations associated with the region. The value of ΔV_p before adjustment is indicative of how big an adjustment in velocity was applied to obtain our final models, which are listed in Appendix D.

To obtain S-wave travel times, we observed that the slopes of the Pn and Sn travel time curves for all the regional travel-time relations given in Section 3 had a ratio lying between 1.74 and 1.78. It therefore appears that with only minor error, we can take the Poisson ratio of our 3D model as effectively constant, with P-wave speed everywhere equal to 1.76 times the S-wave speed. Therefore, we have concluded we can simply take the P-wave model travel time x 1.76 as a first estimate of the S-wave model travel time.

Table 9. Mean travel time residuals and velocity corrections for each region

	Before adjustment		After adjustment	
Region	Δt (s)	ΔV_p (km/s)	Δt (s)	ΔVp (km/s)
R01	-2.10	0.070	-1.20	0.026
R02	-1.23	0.054	-0.17	0.001
R03	-0.98	0.060	0.07	-0.011
R04	0.36	-0.022	0.14	-0.013
R05b	-0.34	0.000	-0.19	0.000
R05c	0.10	-0.003	0.75	-0.033
R05d	0.02	-0.016	0.01	-0.011
R06	-0.90	0.052	-0.39	0.024
R07	0.48	-0.038	0.15	-0.017
R09	0.45	-0.025	0.34	-0.021

Table 9. Mean travel time residuals and velocity corrections for each region

Region	Before adjustment		After adjustment	
	Δt (s)	ΔV_p (km/s)	Δt (s)	ΔVp (km/s)
R12a	-2.14	0.073	-0.66	0.021
R12b	1.90	-0.105	0.35	-0.01
R13b	-1.50	0.049	-0.92	0.029
R15b	-0.39	0.018	-0.07	-0.001
R16a	-0.93	0.035	-0.70	0.025
R16b	-0.40	0.021	-0.41	0.021

As a check on our overall P-velocity model, the residuals for a number of PNEs were obtained (observed arrival time, minus the arrival time computed by 3D ray tracing) for shots that are indicated in Table 8. Figure 21 shows a histogram of these results, for six explosions for which Table 8 indicates the field data are of highest quality. In most cases the residuals are within 1s. For Ruby 1, they are within - 2 s to 0. These are very satisfactory results, given that no adjustments were made to the 3D model to achieve these small residuals. Not shown in this Figure, are results for the Meteorite 5 PNE. This shot was carried out on the border of region 12b, and we have found that residuals amount to several seconds, indicating our 3D velocity model is somewhat too fast for the paths recording this shot.

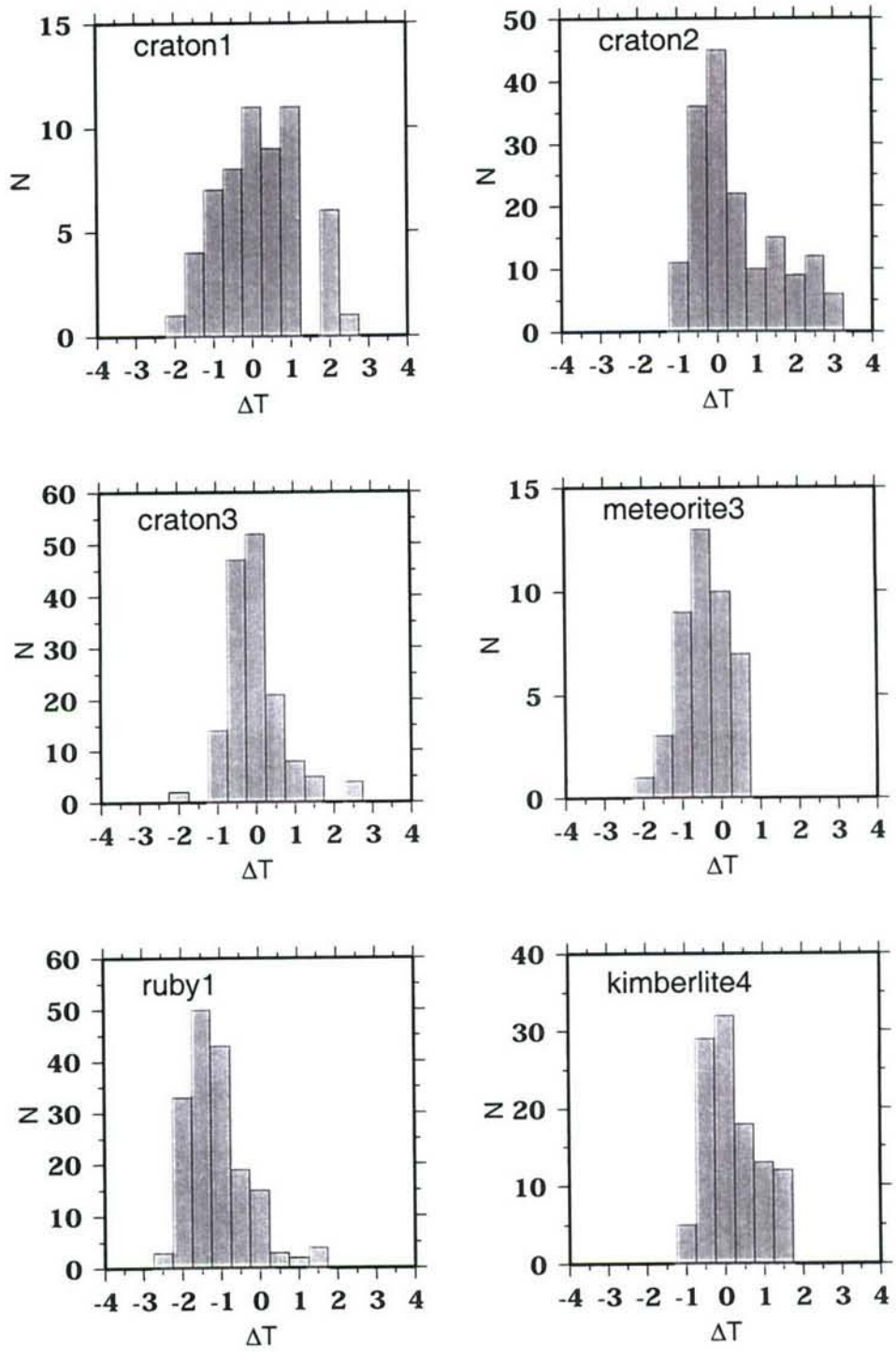


Figure 21. Residuals (observed arrival times minus times expected on the basis of GT information and travel times computed for the model shown in Figure 20), for the field station data associated with six PNEs in Russia for which our observed arrival times and GT information are believed to be of highest quality (see Table 8).

5.4. Model Errors and Model-Based SSSCs

Model error must be quantified in order to estimate the contribution of our uncertainty of Earth structure to the eventual size of error ellipses. Our model error is expected to be smaller than the generally accepted model error for IASP91 since this standard travel-time model is a global average and we have taken care to model the major travel-time departures from the standard. We can be guided by the average absolute travel-time misfits to our model-based SSSCs. The latter are binned by distance for Pn in Figure 22, and for Sn in Figure 23 (green curves). We have chosen to use 0.7 x the IASP91 model error for Pn and 0.9 x the IASP91 model error for Sn (magenta curves) as the model errors in our analysis. While there are differences between the average misfit values and our modeling error curves, they are not significant with respect to the uncertainties. Furthermore, the validity of the error model was ultimately demonstrated by achieving appropriate coverage statistics.

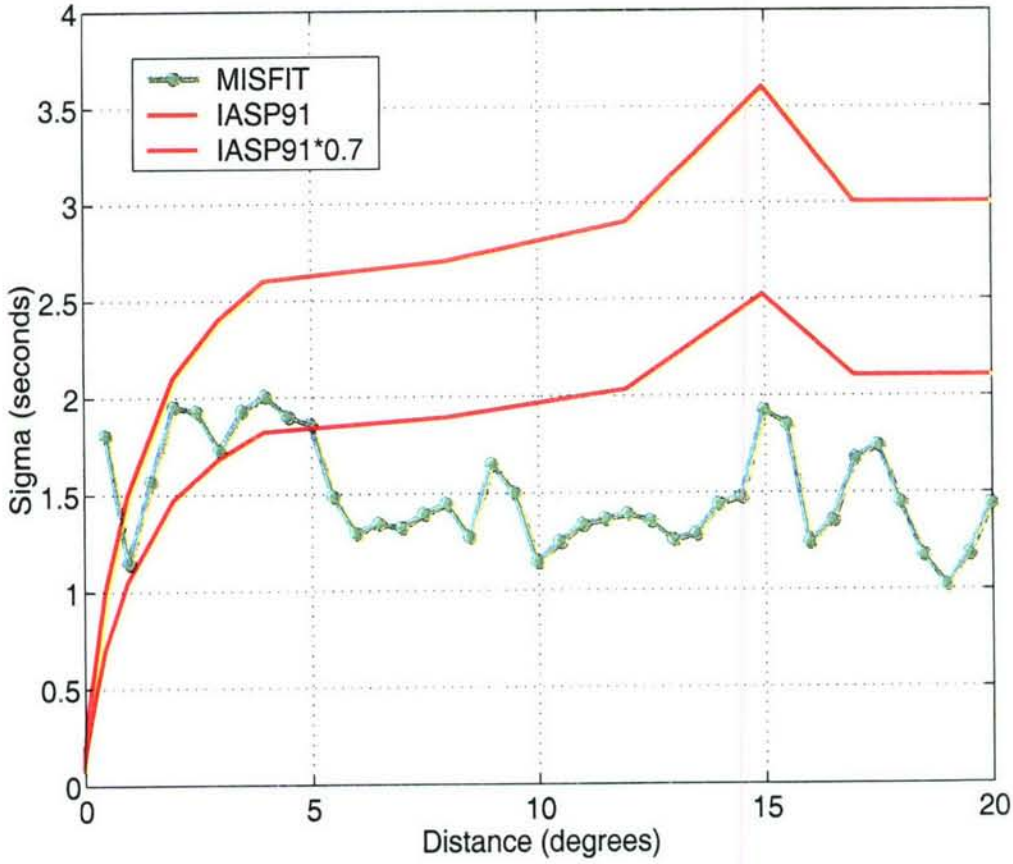


Figure 22. Pn modeling errors as functions of epicentral distance (total path length from event to station) for IASP91 (red curve) and our regionalized model (magenta curve). Also shown are travel-time misfits to the model-based SSSCs, binned by distance, for Pn phase arrivals (green markers).

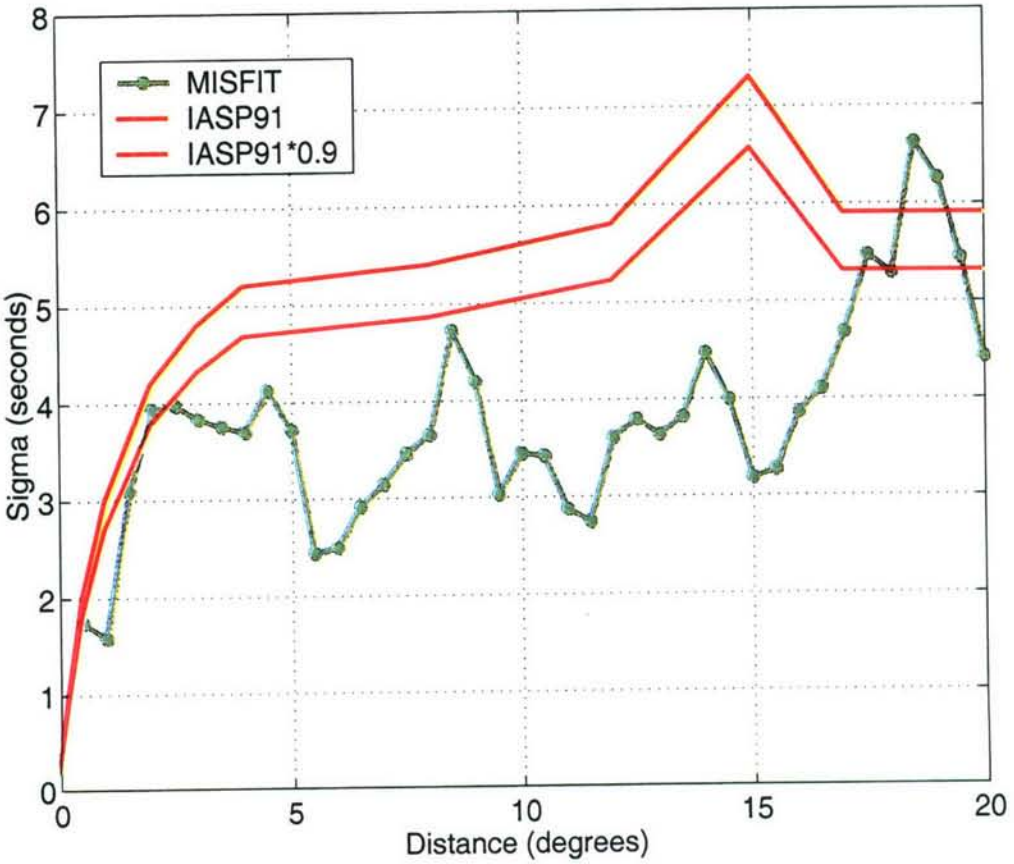


Figure 23. Sn modeling errors as functions of epicentral distance.Markers are defined as in Figure 22.

The Pn SSSC grid for BRVK that is computed by 3D ray tracing is shown in Figure 24. The associated modeling-error grid is shown in Figure 25. These figures also show the Pn travel-time residuals, after applying the SSSCs, for the events recorded at BRVK. These residuals are quantified below, after describing the kriging algorithm. It can be seen from Figure 24 that the Pn SSSC for BRVK consists mostly of negative travel-time corrections, by as much as 7.6 seconds in some areas. The estimated modeling errors, depicted in Figure 25, are typically about 1.5 to 2.5 seconds. Figure 26 and Figure 27 show the Sn SSSC for BRVK and the corresponding modeling errors, respectively. The travel-time corrections vary between -27 and +4 seconds. The modeling errors in the Sn case reach values in excess of 6 seconds.

It is some interest that the general region of the Kara Sea has the maximum SSSC for both Pn and Sn at BRVK. The small earthquake of 1997 August 17 in the Kara Sea was observed at BRVK with travel times that support these large departures from IASP91.

No corrections or modeling errors are obtained for distances beyond 20 degrees from the station.

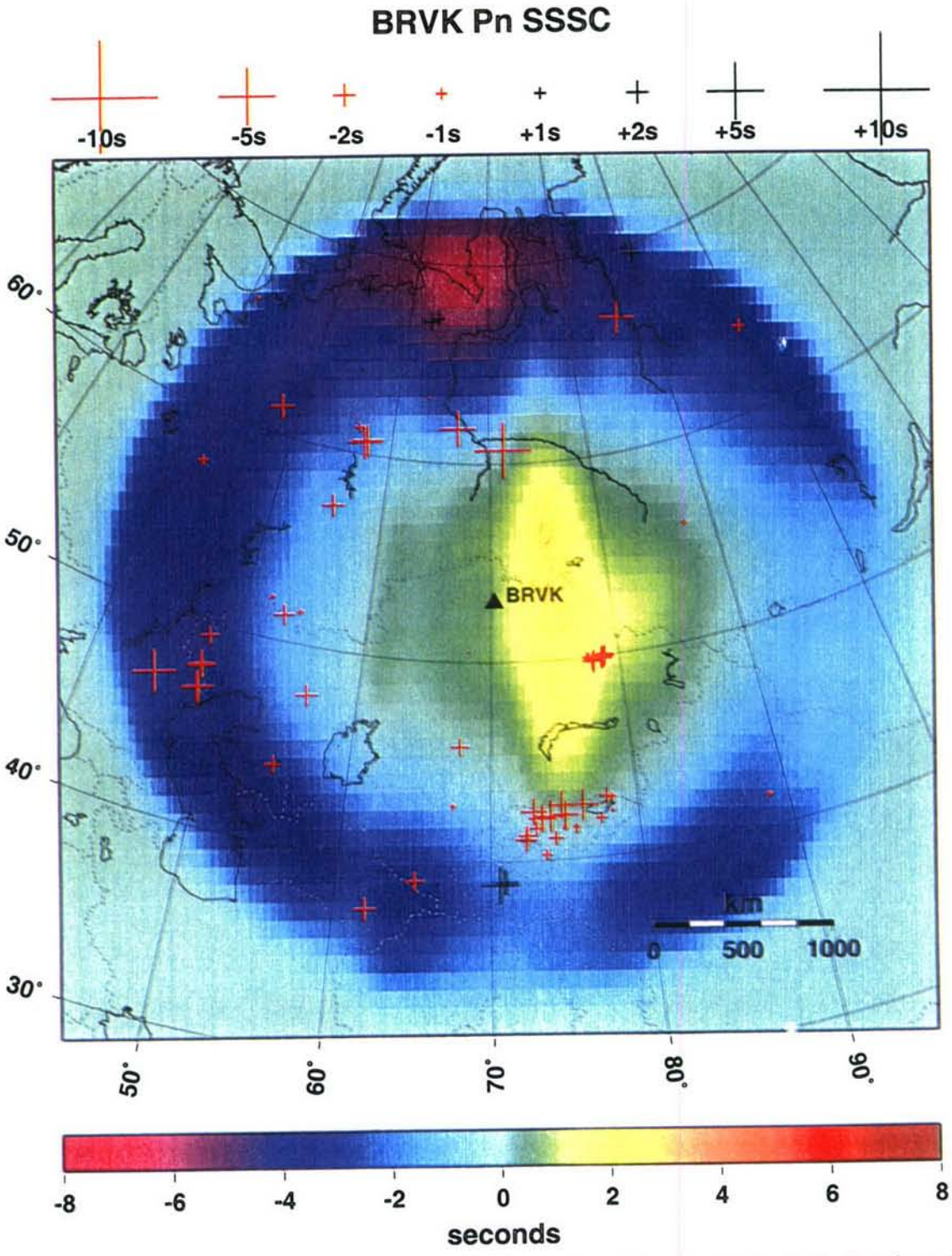


Figure 24. Model-based Pn SSSC for station BRVK. The markers (plus signs) indicate the locations of the calibration events. Black and red markers represent positive and negative residuals, respectively, with marker size proportional to the travel-time residual relative to the predicted travel times by 3D ray tracing.

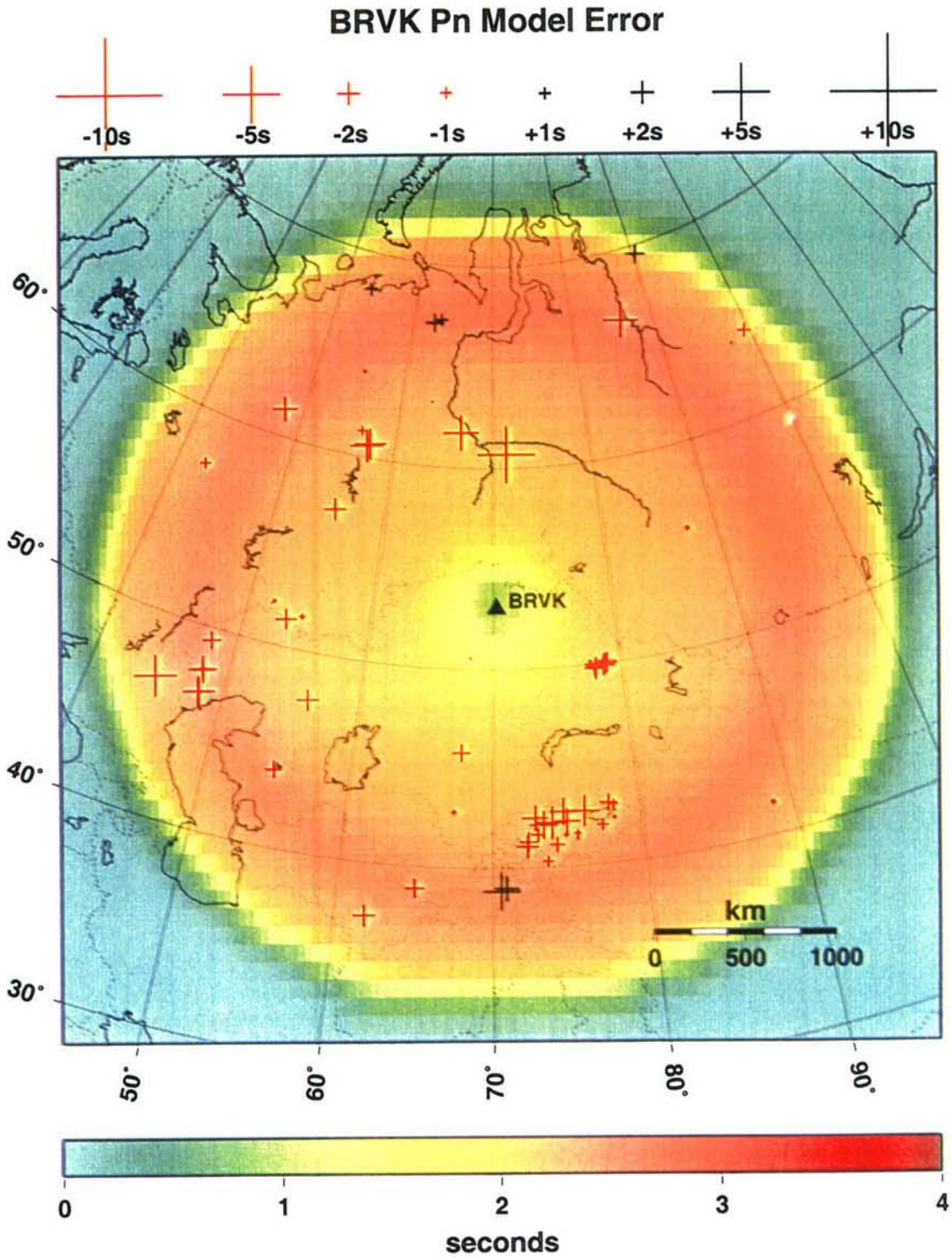


Figure 25. Modeling errors associated with the Pn SSSC computed using 3D ray tracing for station BRVK. Markers are defined as in Figure 24.

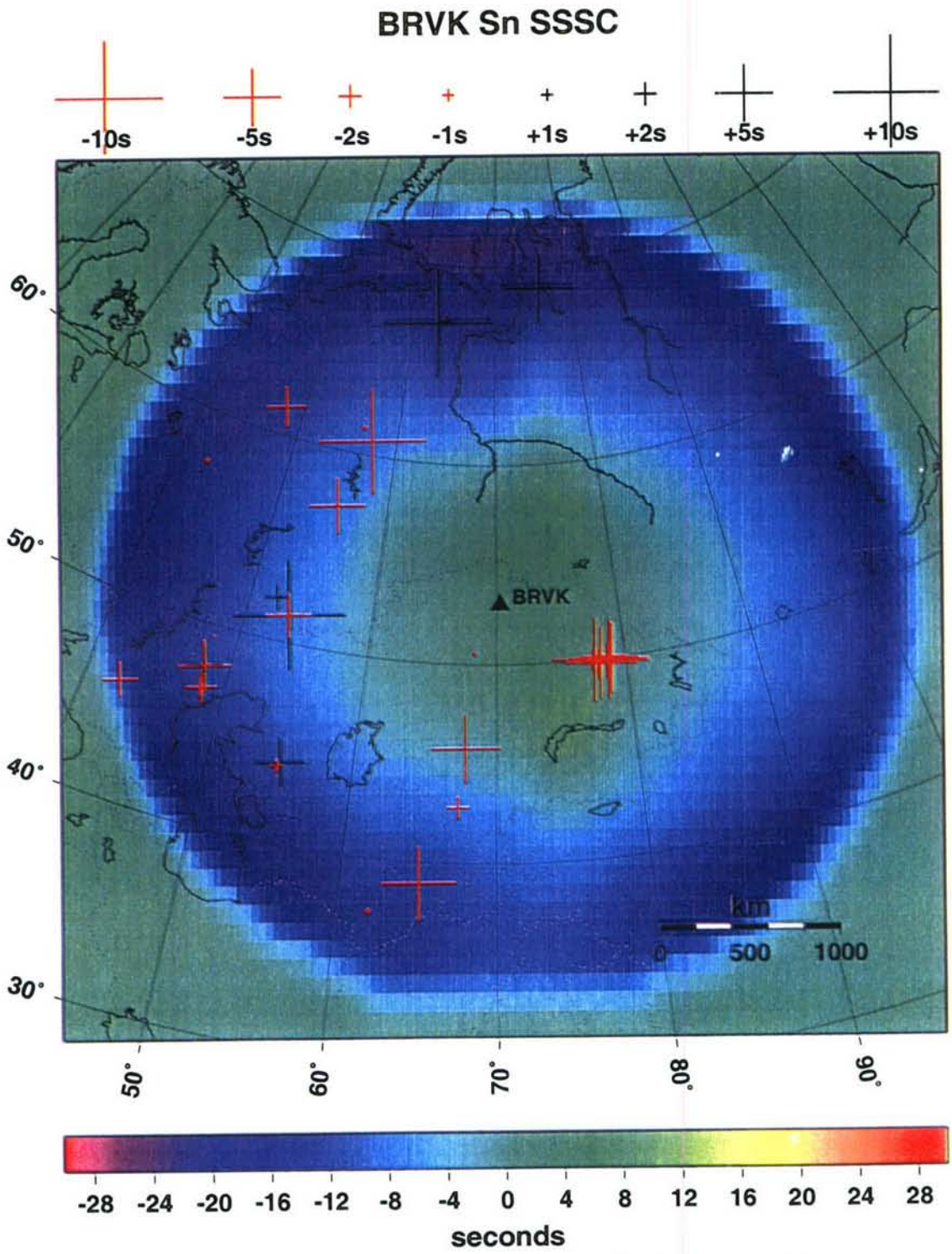


Figure 26. Model-based Sn SSSC for station BRVK. Markers are defined as in Figure 24.

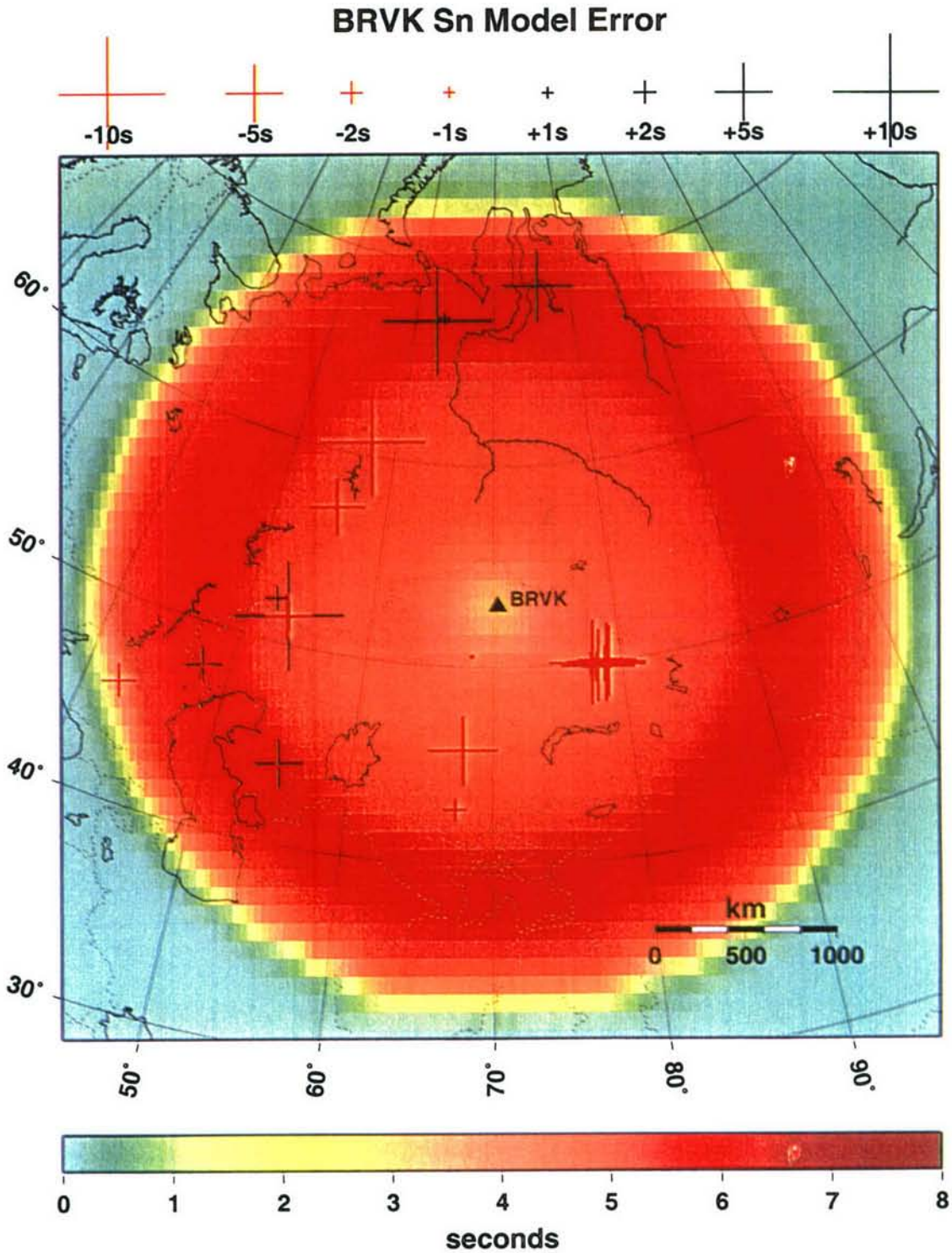


Figure 27. Modeling errors associated with the Sn SSSC computed using 3D ray tracing for station BRVK. Markers are defined as in Figure 24.

5.5. Kriging

We now turn to the issue of incorporating empirical travel-time data into our SSSCs. The procedure known as kriging allows the use of such data, which are all that may be needed to obtain travel times for a new event in the vicinity of events for which reliable travel-time data already exist. Kriging also allows us to assess the region of applicability, of previously observed travel times, at distances that differ from where the empirical data were obtained.

Kriging is a method of optimal spatial prediction, which generally refers to making inferences at a new location, given previously measured data at N separate locations, in a way that minimizes the uncertainty of that prediction under given statistical assumptions. It is a minimum variance, linear estimation technique that models nonuniformly distributed data as a continuous surface with uncertainty estimates that depend on second-order (covariance) properties (Rogers et al., 1999). It assumes that the spatial data result from a random process, meaning that samples are considered as outcomes of a random variable that is a function of spatial coordinates. Given reference data, kriging provides optimal prediction at a new location expressed as a weighted linear combination of data, with greater weight conferred to data that are spatially closer to the prediction location. The predictions at a set of spatial points may be used as a prediction (or correction) surface.

Given N data values, $x(\mathbf{s}_1), \ldots, x(\mathbf{s}_N)$, at locations $\mathbf{s}_1, \ldots, \mathbf{s}_N$ (in our case $x(\mathbf{s}_i)$ is the measured travel-time residual at position $\mathbf{s}_i$), the kriging optimal predictor for the mean at a location $\mathbf{s}_0$ is given by the weighted linear combination of data:

$$\hat{\mu}(\mathbf{s}_0) = \sum_{i=1}^{N} w_i x(\mathbf{s}_i) .$$

The set of all predictions, $\hat{\mu}(\mathbf{s}_0)$, over all $\mathbf{s}_0$, provides a prediction, or correction, surface. A corresponding uncertainty surface, $\sigma^2(\mathbf{s}_0)$, also results from the calculation.

The weights w_i and the kriged variance, $\sigma^2(\mathbf{s}_0)$, depend on the correlations, ρ_{ij}, between the means of data located at $\mathbf{s}_i$ and $\mathbf{s}_j$, the calibration variance, σ_c^2, and residual variance, σ_r^2:

$$w_i = F(\sigma_c^2, \sigma_r^2, \rho_{ij}); \; \sigma^2(s_0) = G(\sigma_c^2, \sigma_r^2, \rho_{ij}) .$$

The correlations, ρ_{ij}, between the means located at $\mathbf{s}_i$ and $\mathbf{s}_j$, are assumed to depend only on the distance $\Delta(\mathbf{s}_i,\mathbf{s}_j)$ between $\mathbf{s}_i$ and $\mathbf{s}_j$, and are taken to be given by the exponential function

$$\rho_{ij} = \exp(-\Delta(\mathbf{s}_i, \mathbf{s}_j) /\alpha),$$

where α is the correlation length.

Required input parameters for the kriging algorithm are σ_c^2, σ_r^2, and α. In practice these parameters are estimated from data using the variogram, which is defined by

$$2\gamma(h) = \mathrm{var}(x_i - x_j),$$

and is assumed to depend only on the distance h separating the locations of x_i and x_j. If we model data x_i at location $\mathbf{s}_i$ as

$$x_i = x(\mathbf{s}_i) = \mu_i + e_i,$$

where μ_i is the mean of the data at $\mathbf{s}_i$ with covariance $\rho_{ij}\sigma_c^2$ and e_i has mean zero and variance σ_r^2 and is uncorrelated with μ_i, it can be shown that the semivariogram, $\gamma(h)$, is given by

$$\gamma(h) = \sigma_r^2 + \sigma_c^2[1 - \exp(-h/\alpha)], \; h > 0.$$

The parameters, σ_c^2, σ_r^2, and α, can be estimated by computing the covariance of all data pairs with separations approximately equal to h, for various values of h. The resulting set of values as a function of h can then be fit with the semivariogram equation to estimate σ_c^2, σ_r^2, and α.

In our application of kriging, the spatial reference data are travel-time residuals for GT events at a given station, relative to the model-based SSSC value for that station and event location. The kriged correction surface, when added to the model-based SSSC, corresponds to an updated travel-time correction grid in the same form as the model-based SSSCs. The resulting kriged correction surface approaches the local mean of data with small uncertainty, equal to the residual variance, for well calibrated areas, and approaches the SSSC background model with large uncertainty, equal to the sum of the residual and calibration variances, for areas far from any calibration data.

An example of a kriged grid of Pn SSSCs for BRVK is shown in Figure 28. The superimposed plus signs indicate the Pn travel-time residuals of the calibration events relative to the predicted travel-times. Marker size is proportional to the size of the residuals, red for negative values and black for positive values. The corresponding modeling errors obtained by kriging are shown in Figure 29, which indicates that they are comparable to those in Figure 25, except near calibration data, where the estimated modeling errors after kriging are generally lower. The kriged grid of Sn SSSCs for BRVK and the modeling errors after kriging are shown in Figure 30 and Figure 31.

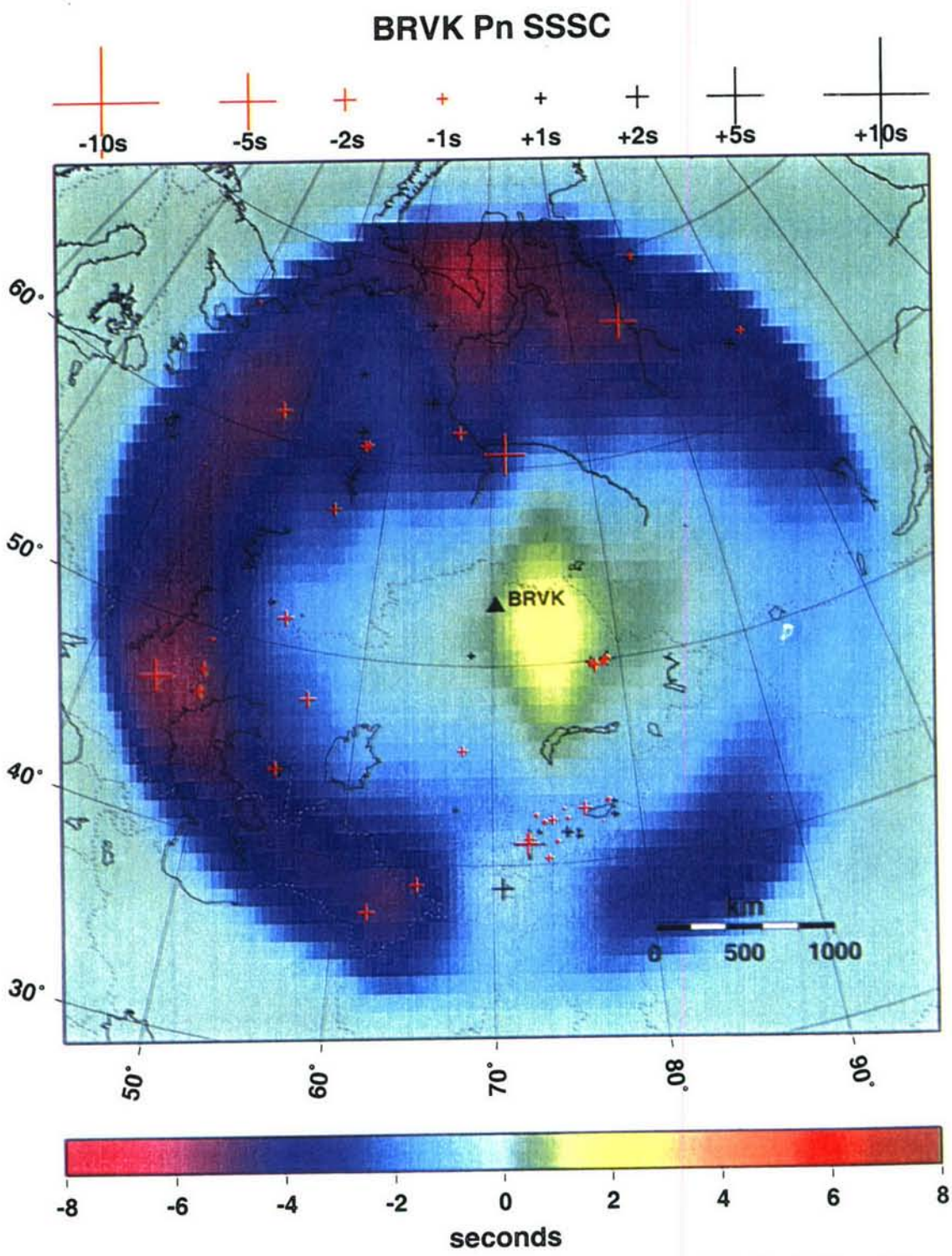


Figure 28. Model-based and kriged Pn SSSC for station BRVK. Markers are defined as in Figure 24.

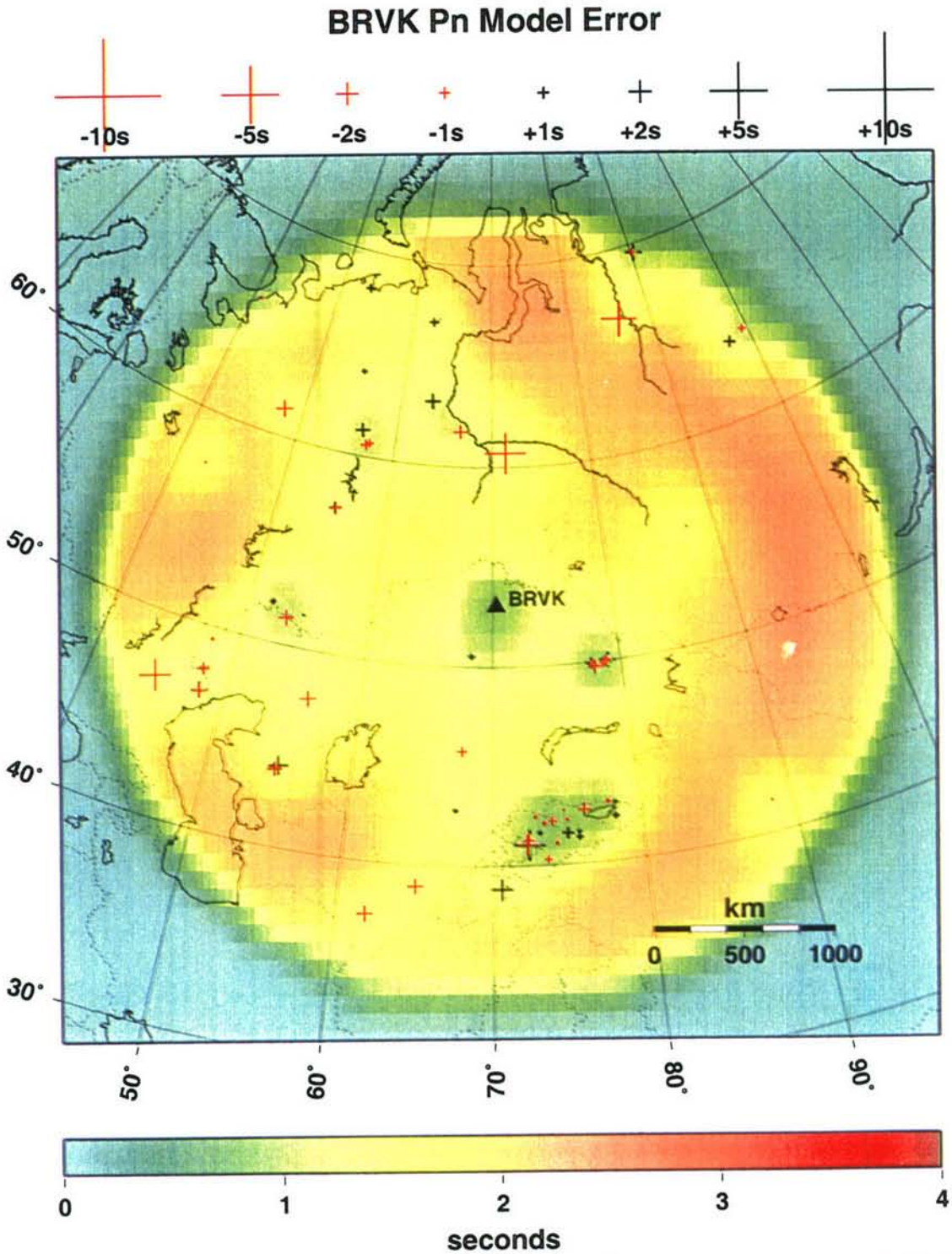


Figure 29. Grid of kriged modeling errors associated with the Pn SSSC computed for station BRVK. Markers are defined as in Figure 24.

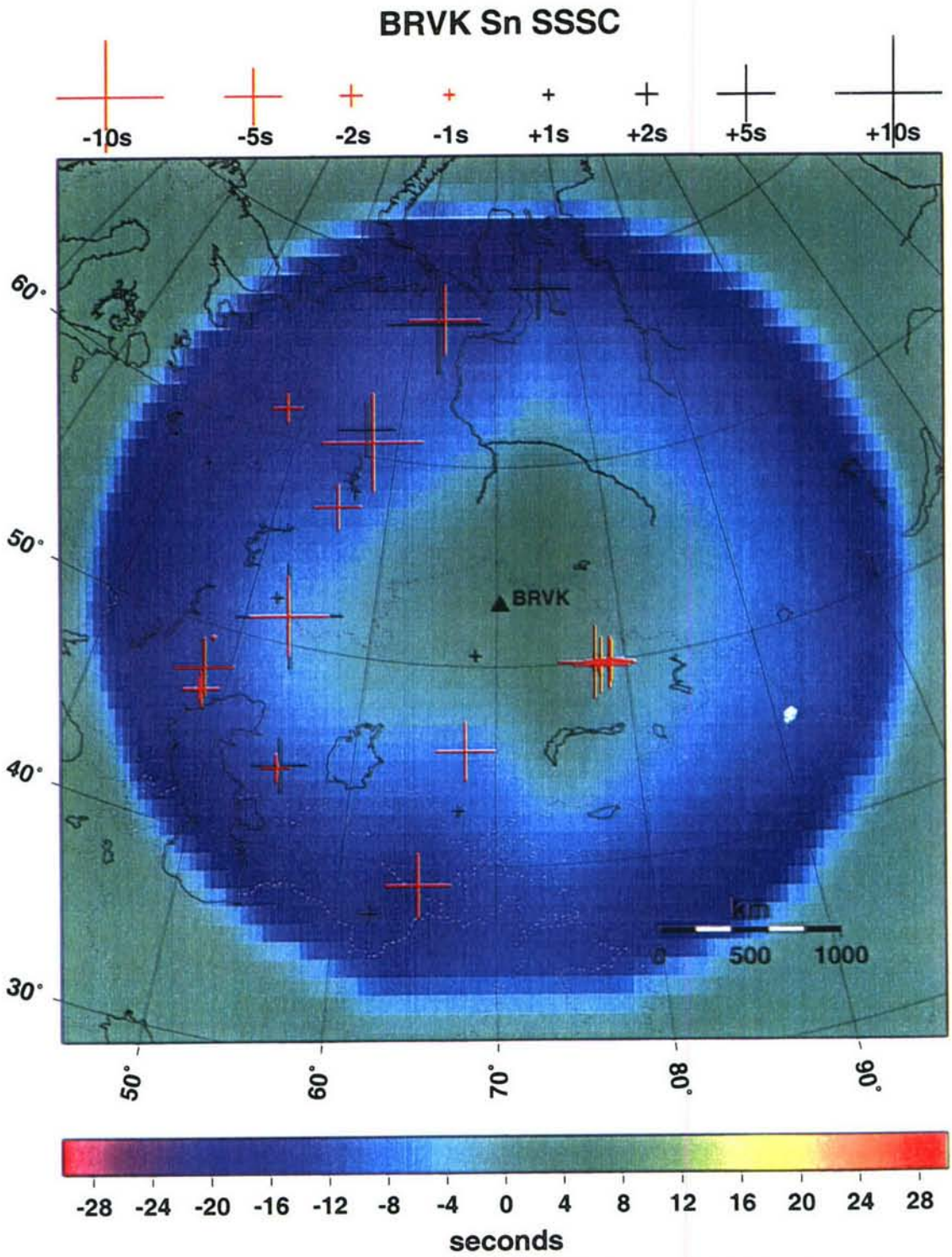


Figure 30. Model-based and kriged Sn SSSC for station BRVK. Markers are defined as in Figure 24.

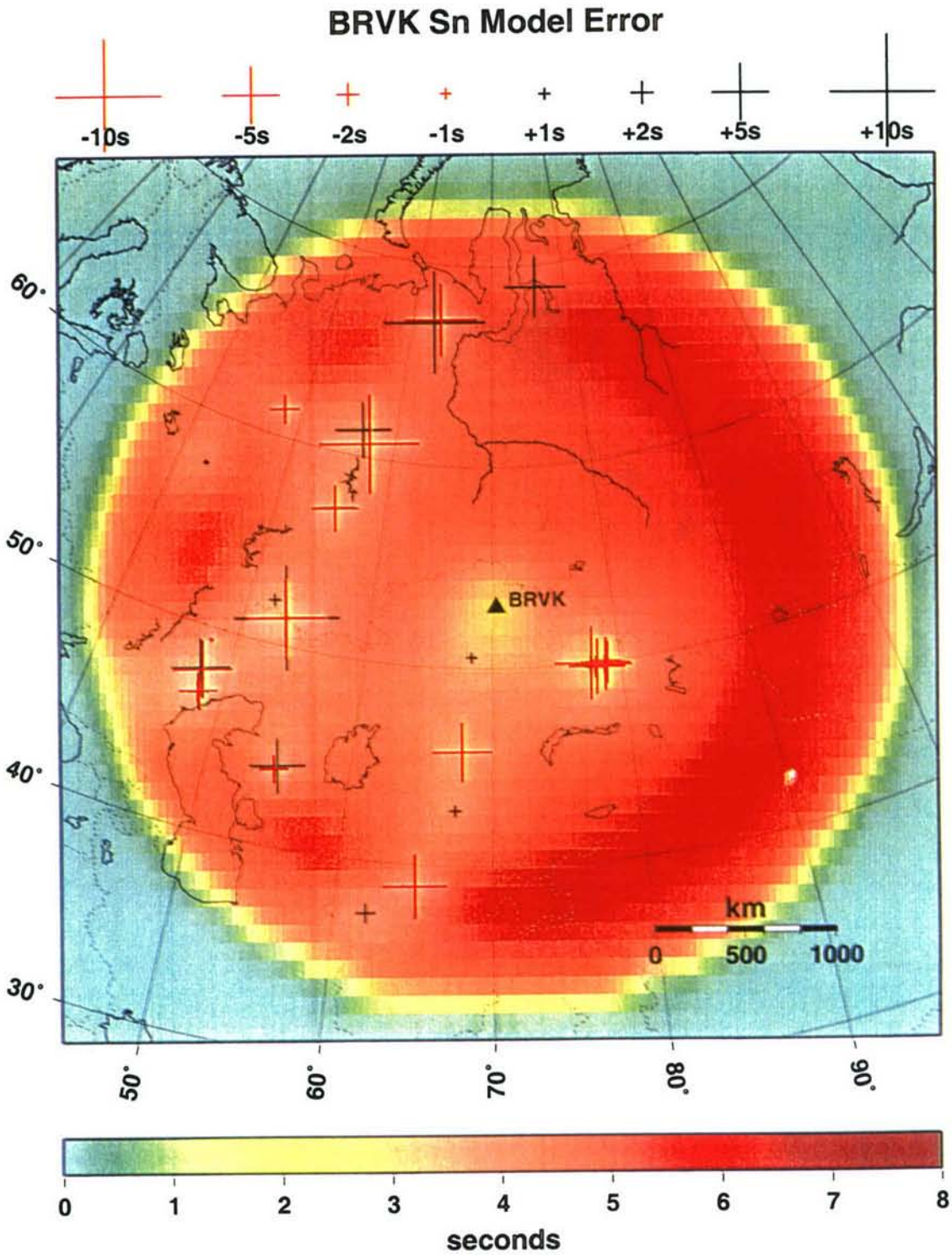


Figure 31. Grid of kriged modeling errors associated with the Sn SSSC computed for station BRVK. Markers are defined as in Figure 24.

It is informative to compare the travel-time residuals before and after applying either the model-based or kriged SSSCs. Figure 32 shows travel-time residuals at station BRVK. The residuals are relative to IASP91 without corrections. Figure 33 illustrates the residuals after applying the model-based SSSCs computed by 3D ray tracing. It is clear the model-based SSSCs generally reduce the travel-time residuals. Figure 34 shows a similar plot using the Pn SSSCs computed by 3D ray tracing and kriging, which shows that application of kriging provides further reduction of the Pn travel-time residuals at BRVK.

These results are quantified in Table 10 in terms of the mean and standard deviation of the Pn travel-time residuals. Both the mean travel-time bias and the standard deviation of the travel-time residuals are progressively reduced by applying the model-based Pn SSSCs and the model-based plus kriged SSSCs. Table 10 also presents the results for the Sn case. While the mean is reduced by applying the model-based Sn SSSCs and the model-based plus kriged SSSCs, the standard deviation does not change much (2.99 s vs. 2.97 s) suggesting that the Sn arrival picks are not so accurate.

Table 10. Comparison of Pn and Sn travel-time residuals for station BRVK.

Case	IASP91		Model-Based SSSCs		Model + Kriged SSSCs	
	$\mu_{\Delta T}$(s)	$\sigma_{\Delta T}$(s)	$\mu_{\Delta T}$(s)	$\sigma_{\Delta T}$(s)	$\mu_{\Delta T}$(s)	$\sigma_{\Delta T}$(s)
Pn	-1.50	2.38	-1.00	0.99	-0.07	0.79
Sn	-5.24	5.79	-1.30	2.99	-0.03	2.97

Although these results for BRVK were shown because of the geographical distribution of GT events and the quantity and quality of the Pn phase picks, which we carefully reviewed by inspection of the waveforms, they are qualitatively representative of the reductions in mean travel-time bias and residual variance that we obtain at other stations in Asia. Figure 35 and Figure 36 present the mean and standard deviation of the Pn travel-time residuals for all the stations that recorded at least 3 GT events (126 stations) and Figure 37 and Figure 38 present the mean and standard deviation of the Sn travel-time residuals for all the stations that recorded at least 3 GT events (74 stations).

Table 11 shows the RMS for mean and standard deviation of the Pn and Sn travel-time residuals for all the stations that recorded at least 3 GT events. (For each station, a mean and standard deviation of the travel-time residuals is computed. Each type of these values, for example the mean, is then squared, averaged over all stations with equal weight, and the square root is taken.)

From this Table, we see that a very significant reduction of residuals is obtained by kriging.

Table 11. RMS of mean and standard deviation of Pn and Sn travel-time residuals for all the stations that recorded at least 3 GT events.

	IASP91		Model-Based SSSCs		Model + Kriged SSSCs	
Case	$\mu_{\Delta T}(s)$	$\sigma_{\Delta T}(s)$	$\mu_{\Delta T}(s)$	$\sigma_{\Delta T}(s)$	$\mu_{\Delta T}(s)$	$\sigma_{\Delta T}(s)$
Pn	1.89	1.77	1.33	1.48	0.22	1.01
Sn	6.08	4.24	3.08	3.76	1.34	3.76

Appendix E provides plots of the explicit SSSCs, and modeling errors, for thirty seismographic stations in East Asia. These plots show the residuals we obtained, using our ground truth data (hypocenter information, and observed arrival times). The density of such residuals, shown on each plot, allows one to gain an impression of the extent of empirical calibration data, for each station and each source region.

In the next Section, we assess the degree to which location capability is improved, for East Asia, by use of our SSSCs (both model-based, and kriged).

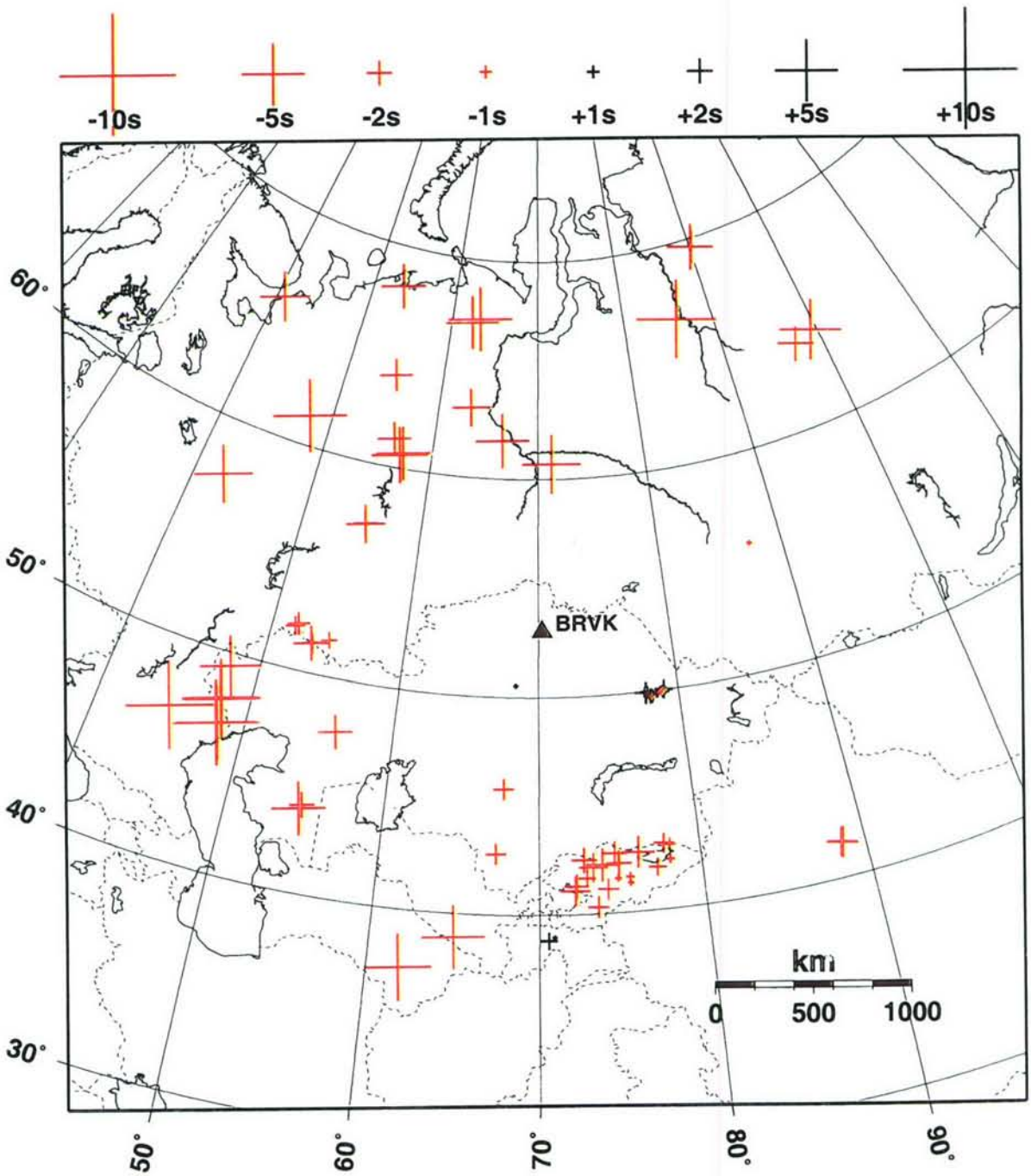


Figure 32. Pn travel-time residuals for station BRVK, before applying model-based Pn SSSCs (IASP91).Black and red markers represent positive and negative residuals, respectively, with marker size proportional to the travel-time residual relative to the predicted travel times.

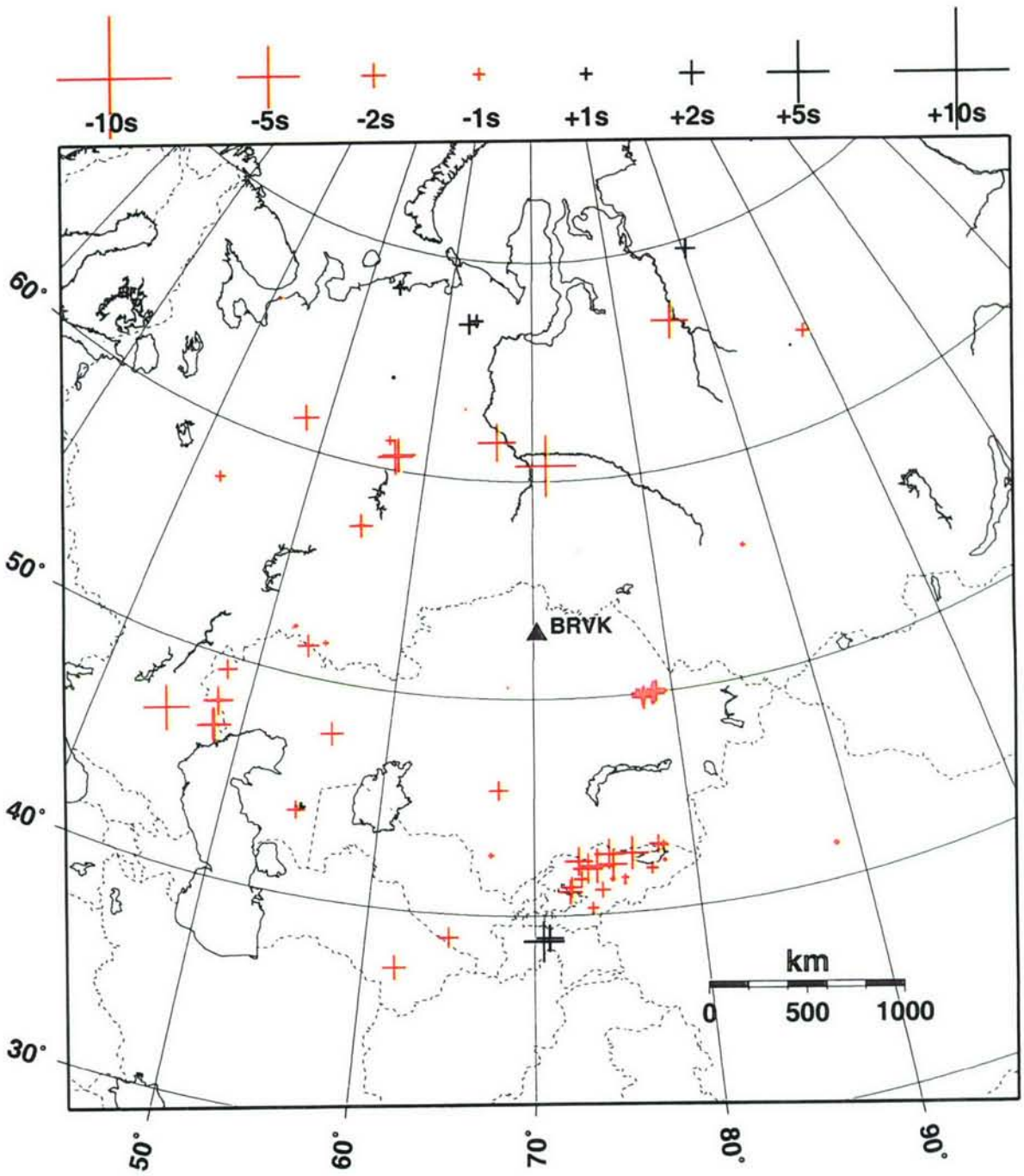


Figure 33. Pn travel-time residuals for station BRVK, after applying model-based Pn SSSCs. Markers are defined as in Figure 32.

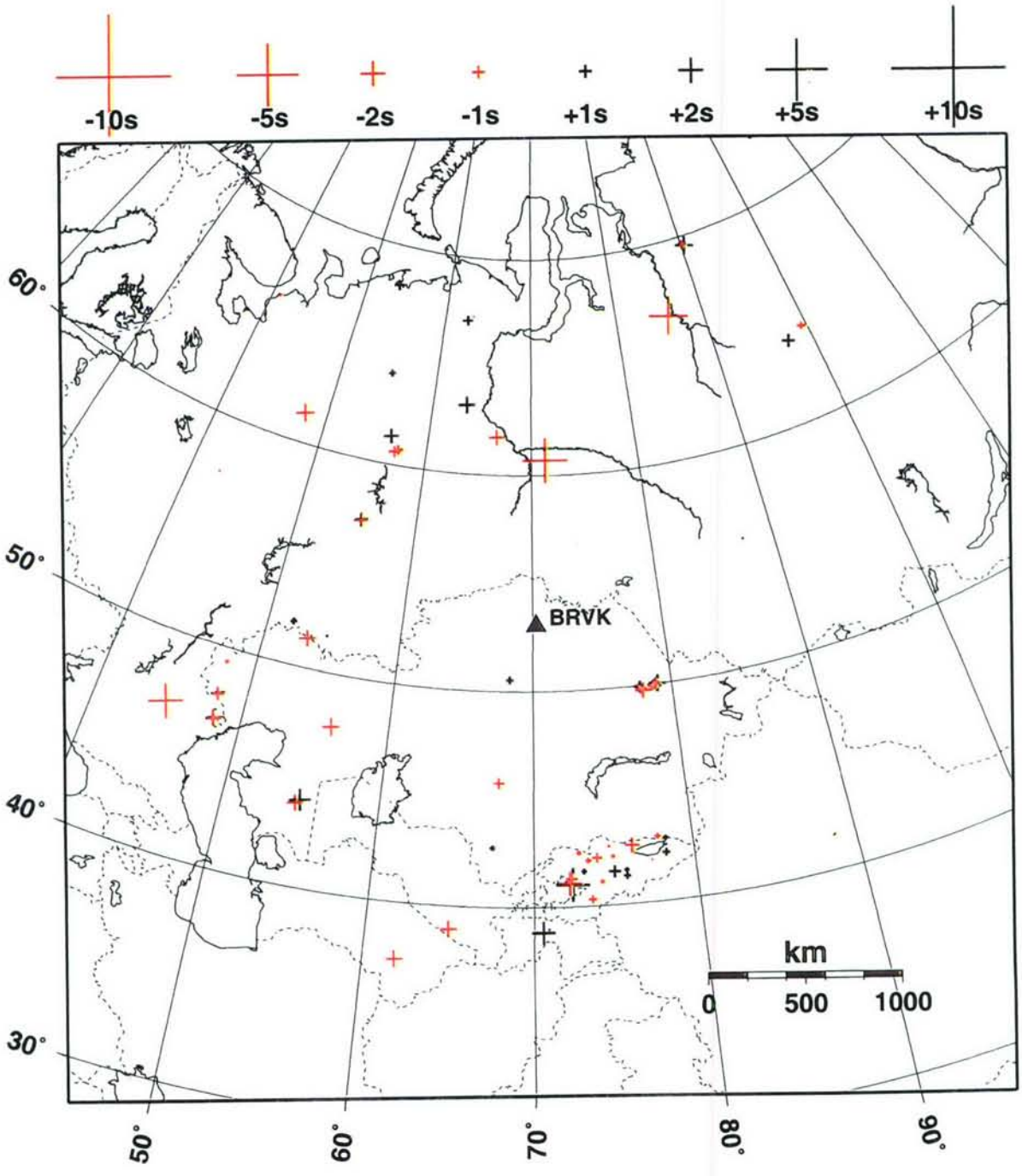


Figure 34. Pn travel-time residuals for station BRVK, after applying model-based plus kriged Pn SSSCs. Markers are defined as in Figure 32.

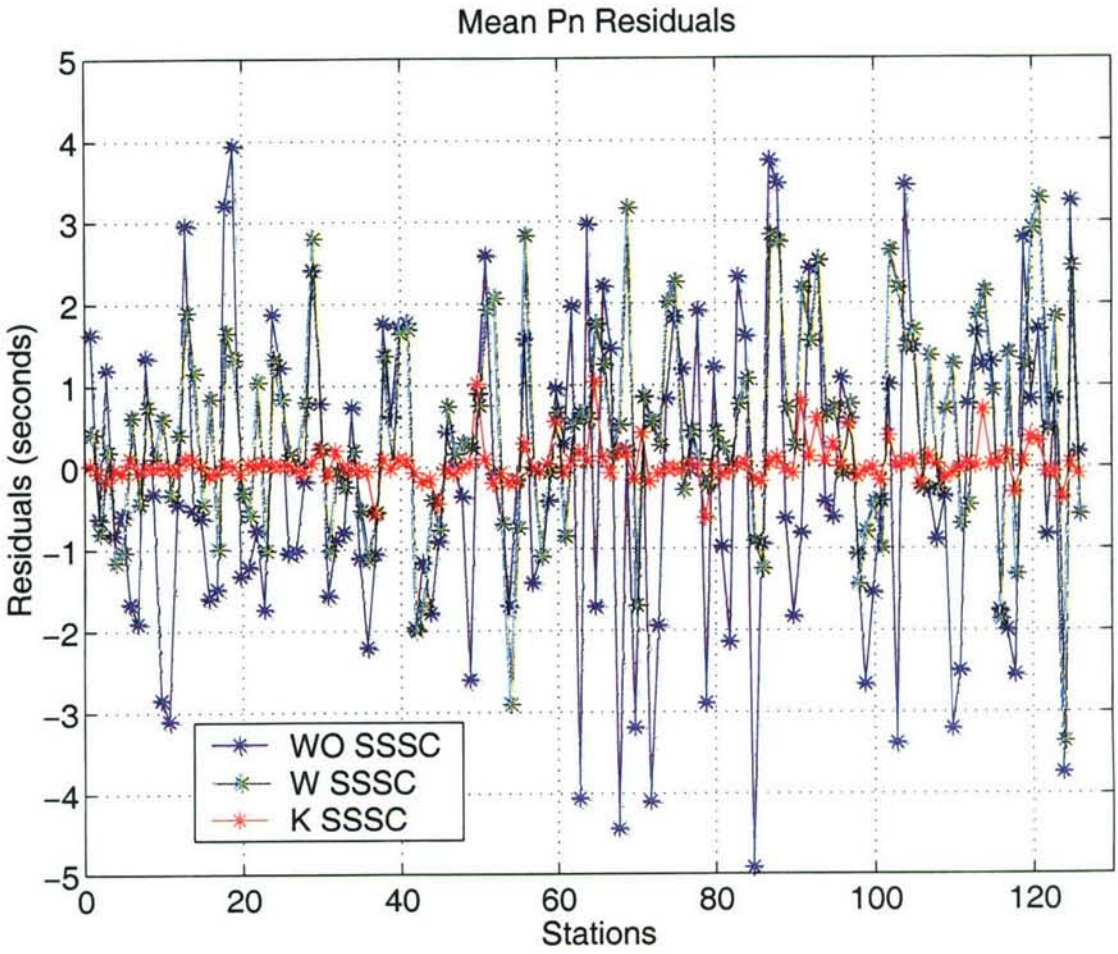


Figure 35. Mean Pn travel time residuals for all the stations that recorded at least 3 GT events. Blue markers and curve represent the residuals by station without SSSCs (IASP91), green markers and curve represent the residuals by station when model-based SSSCs were applied, and magenta markers and curve represent the residuals by station when model-based SSSCs and kriging were applied.

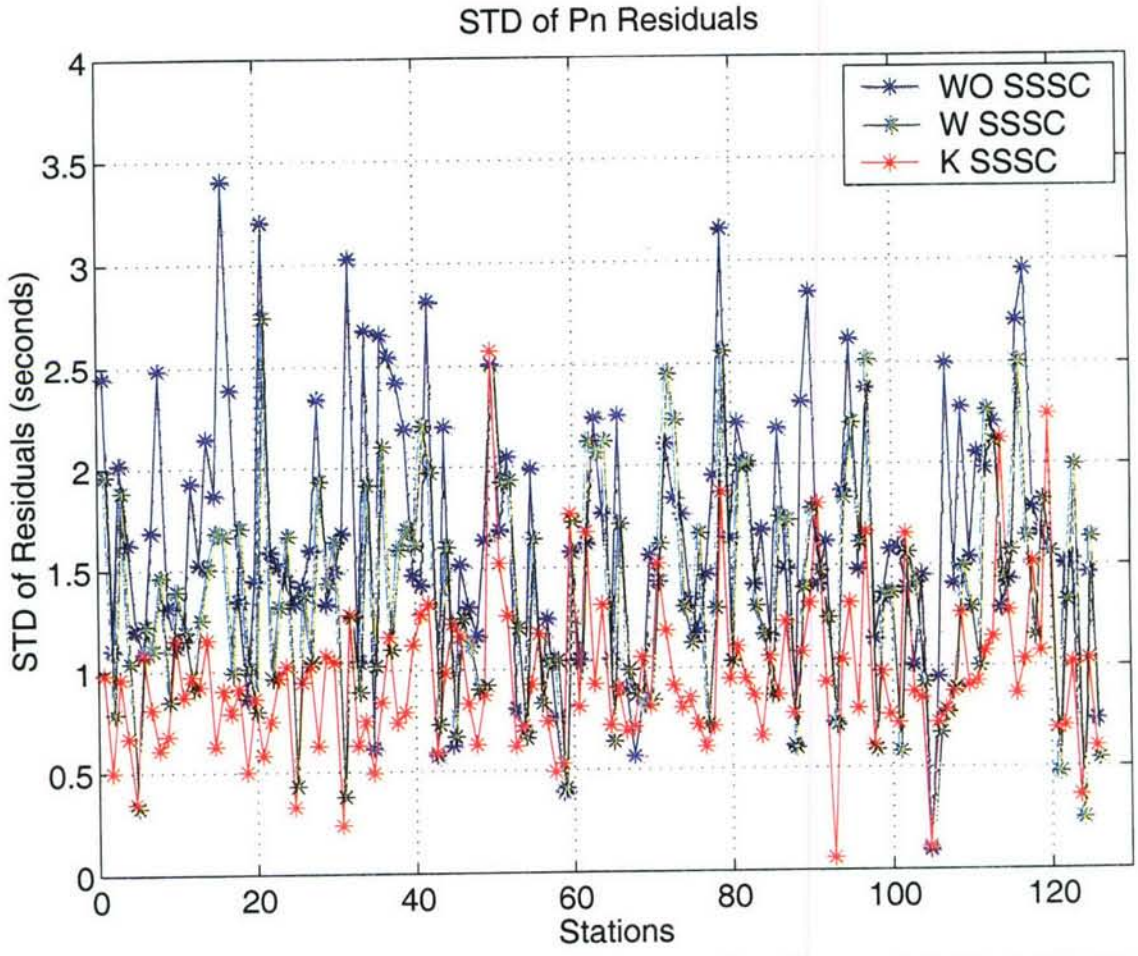


Figure 36. Standard deviation of the Pn travel times for all the stations that recorded at least 3 GT events. Markers are defined as in Figure 35.

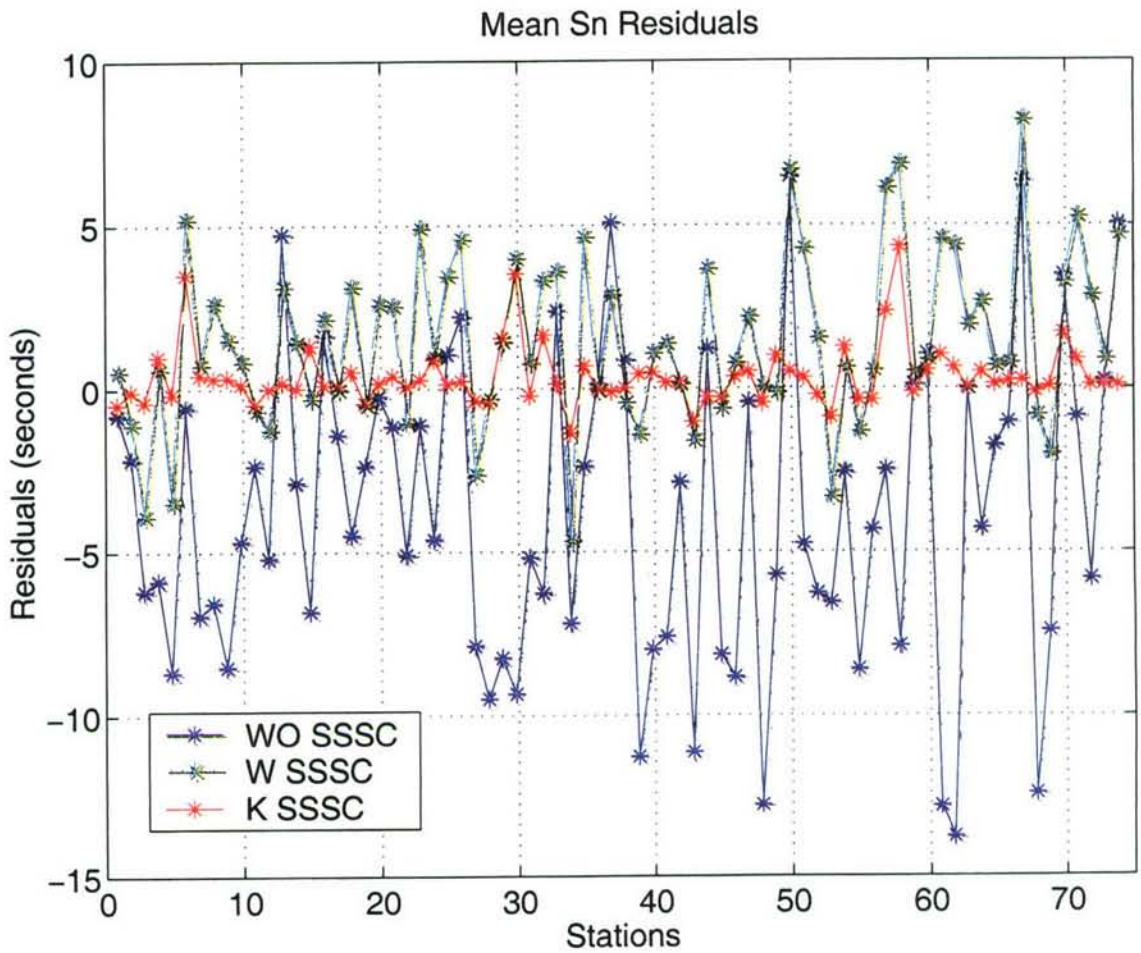


Figure 37. Mean Sn travel time residuals for all the stations that recorded at least 3 GT events. Markers are defined as in Figure 35.

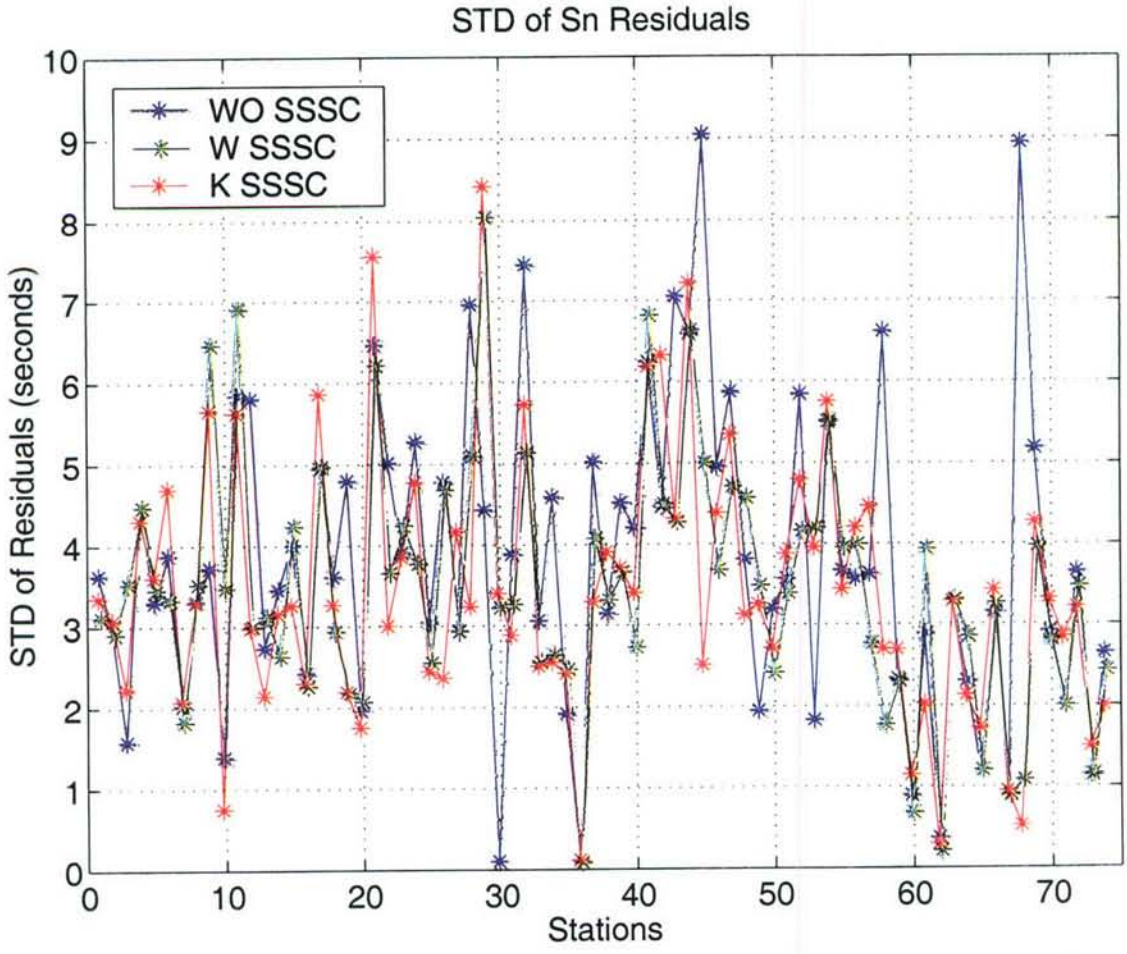


Figure 38. Standard deviation of the Sn travel times for all the stations that recorded at least 3 GT events. Markers are defined as in Figure 35.

Section 6 Validation Testing and Performance Metrics

6.1. Introduction

Validation testing of Pn and Sn SSSCs for East Asia consists mainly of relocating events to demonstrate improvements in location performance relative to using IASP91 travel times. Using the CMR location software *EvLoc*, relocations are computed with and without the SSSCs to assess the impact of these corrections on location and error ellipse estimation. Improvements are quantified using standard evaluation metrics of mislocation errors, error ellipse area, 90% error ellipse coverage, and standard deviations of the phase arrival-time observations.

There are two main objectives of the validation tests: (1) model validation and (2) evaluation of the kriged SSSCs. The first is to validate the regionalized travel-time model and model-based SSSCs computed by 3D ray tracing. The model-based SSSCs were computed by 3D ray tracing through a structural model, derived from combining regionalized 1D travel-time curves for Asia based on published studies. By relocating events with the model-based SSSCs, we can demonstrate reductions in mislocations and error ellipse size, while maintaining adequate coverage of the error ellipses with the GT locations. The goal is to show that this model provides an effective representation of travel times in East Asia. This is a critical step in the validation process because events may occur at locations far from calibration points used by the kriging algorithm, where the grids are effectively equivalent to the model-based SSSCs.

The second main objective is to assess location performance using the kriged SSSCs. To do this, we relocate the events using the kriged SSSCs with a leave-one-out procedure (to avoid using the same events to both compute and test the grids), and quantify the results in terms of the same performance metrics used in the model validation. The results are compared to those in which the relocations were performed without SSSCs and with the SSSCs computed by 3D ray tracing.

To perform these tests we use 525 GT events from the data sets described in Section 4. Although many of the stations associated with the data sets are not in the IMS, they are especially useful for validating our regionalized model over a very broad and diverse range of geological conditions.

6.2. Model Validation

For model validation we use 525 events recorded at 140 stations. The test consists of relocating these events using Pn (5677 picks) and Sn (1586 picks) arrivals. All the relocations are performed with depth fixed at the surface. Figure 39 shows the distributions of events and seismographic stations used in this analysis. Also shown in Figure 39 are great circle Pn paths between events and stations. The great circle Sn paths are presented in Figure 40. The relocation procedure is first applied using the IASP91 travel-time tables, without any SSSCs. This is followed by relocating the same events using the SSSCs. Both sets of relocation results are saved in a database at the CMR. Executing *EvLoc* with and without SSSCs resulted in 525 events with location estimates that converged.

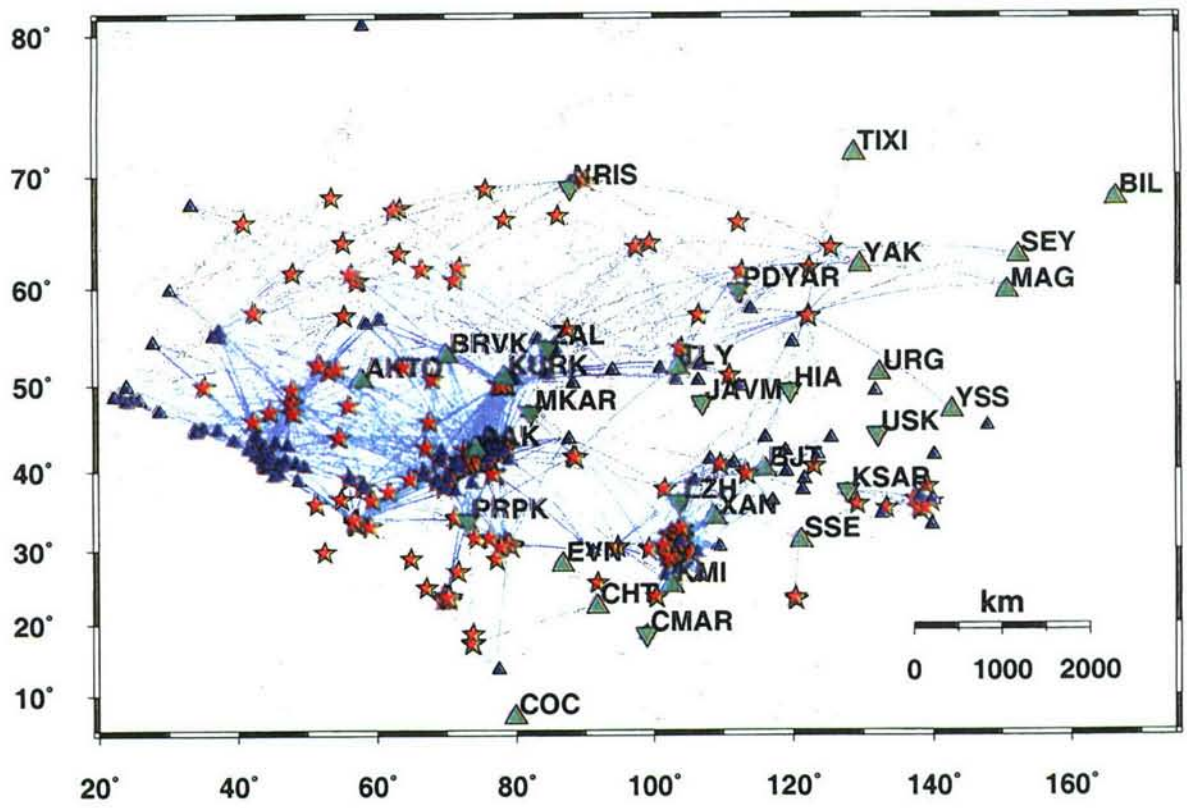


Figure 39. Map of events (red stars) and recording seismic stations (blue triangles) of the data set used for model validation.The green triangles represent the 30 IMS stations that our consortium was tasked to calibrate. Also shown are great circle Pn paths between events and station.

Relocation performance is quanti ed using evaluation metrics that conform with the guidelines from the 1999 Location Workshop (CTBT/WGB/TL-2/18) held in Oslo, Norway, which include the following:

- the median mislocation of GT events should be signi cantly reduced;
- mislocation should be reduced by 20% or more for the majority of events;
- median confidence ellipses should be reduced in area, and the coverage should be the same or better;
- confidence ellipses should be reduced by 20% or more for the majority of events;
- the variance of travel-time residuals should be similar or smaller.

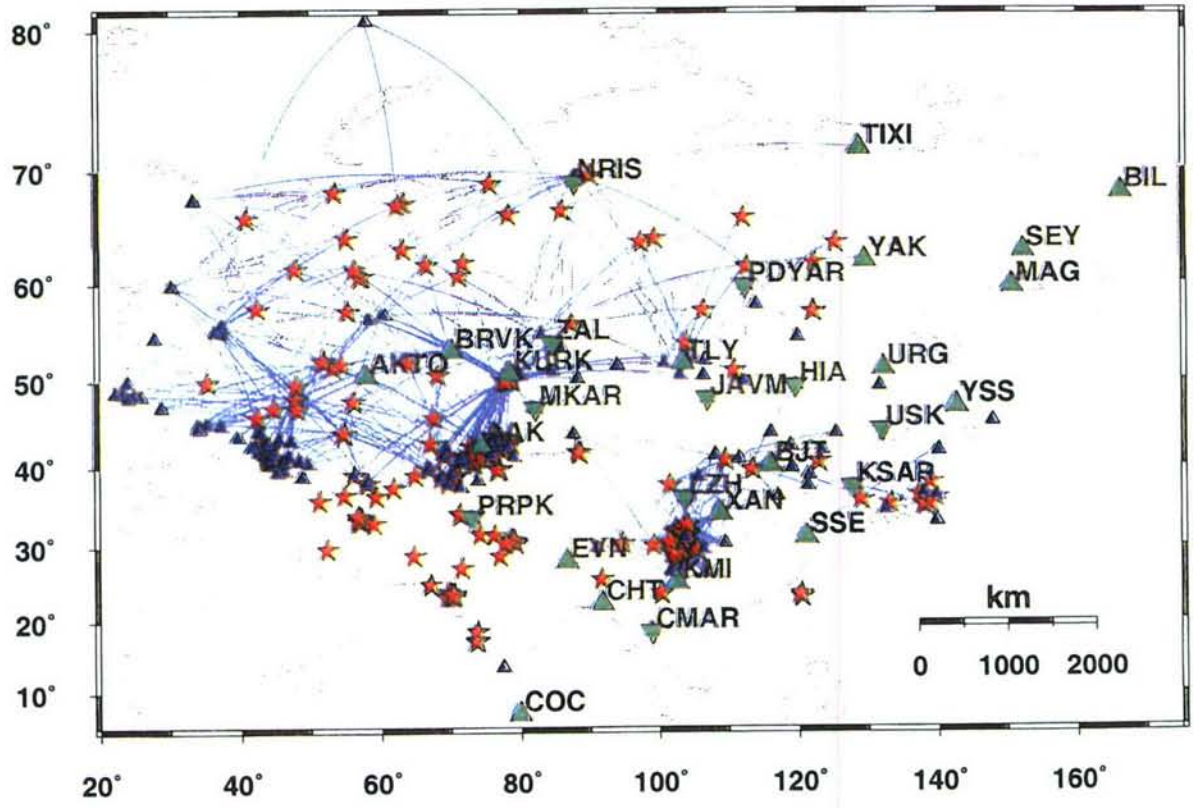


Figure 40. Map of events (red stars) and recording seismic stations (blue triangles), IMS stations (green triangles) and great circle Sn paths. Markers are defined as in Figure 39.

6.2.1. Mislocation

Mislocation is expressed as the difference in distance between the GT location and the location obtained by *EvLoc*. Of the 525 events, the locations using SSSCs improved for 348 events (66%) and deteriorated for 177 events (34%). The median mislocation was reduced from 16.9 km to 11.4

km. For 276 events (53%) the solutions improved by more than 20%, while for 140 events (27%) the deterioration is more than 20%. Figure 41 shows the mislocation results. The green symbols represent the events for which the relocation with SSSCs is closer to the GT location than without SSSCs. The red symbols show the events for which the mislocation without SSSCs is smaller than with SSSCs.

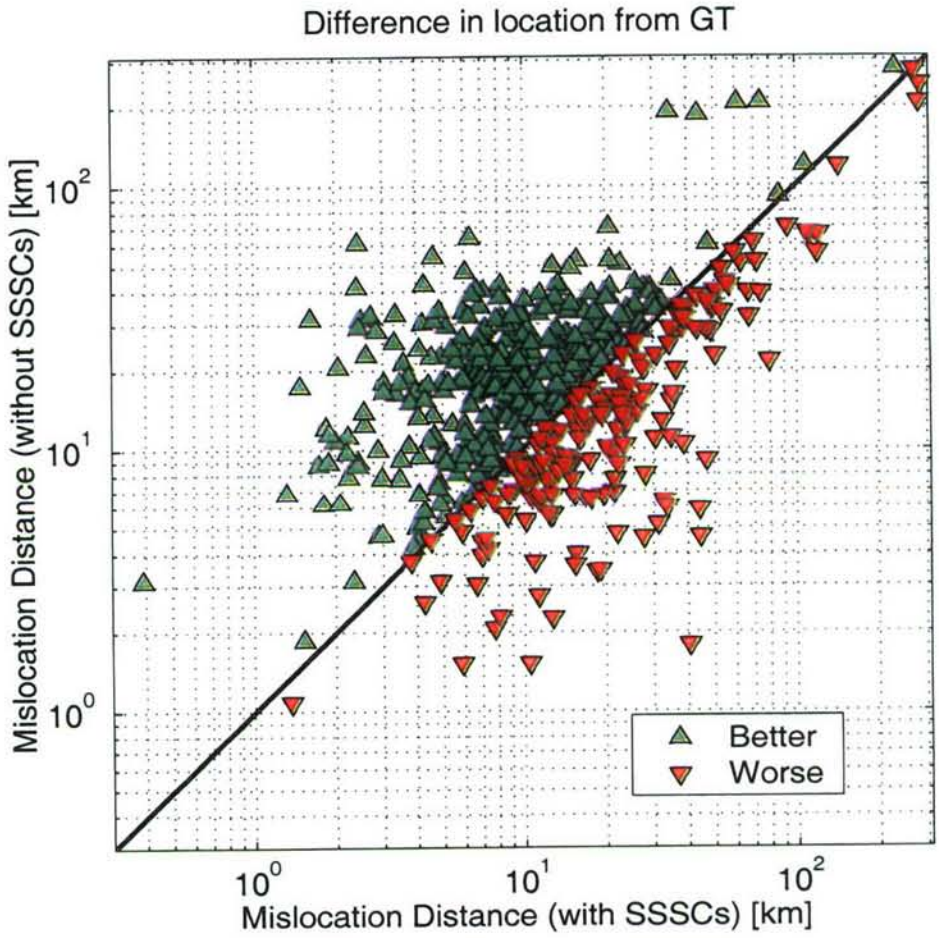


Figure 41. Mislocation distances with and without using model-based SSSCs with respect to corresponding GT locations. The green symbols show the events for which the mislocation error is smaller using SSSCs than without. Red symbols show the events for which the mislocation errors are smaller without using SSSCs. The bisecting line corresponds to equivalent mislocation errors for the two solutions (with and without SSSCs).

Figure 42 shows the map distribution of the mislocation results. The green circles represent the events for which the relocation with SSSCs is closer to the GT location than without SSSCs. The red squares show the events for which the mislocation without SSSCs is smaller than with SSSCs. In general, there is a uniform spatial distribution of the two types of solutions represented by green circles and red squares, respectively.

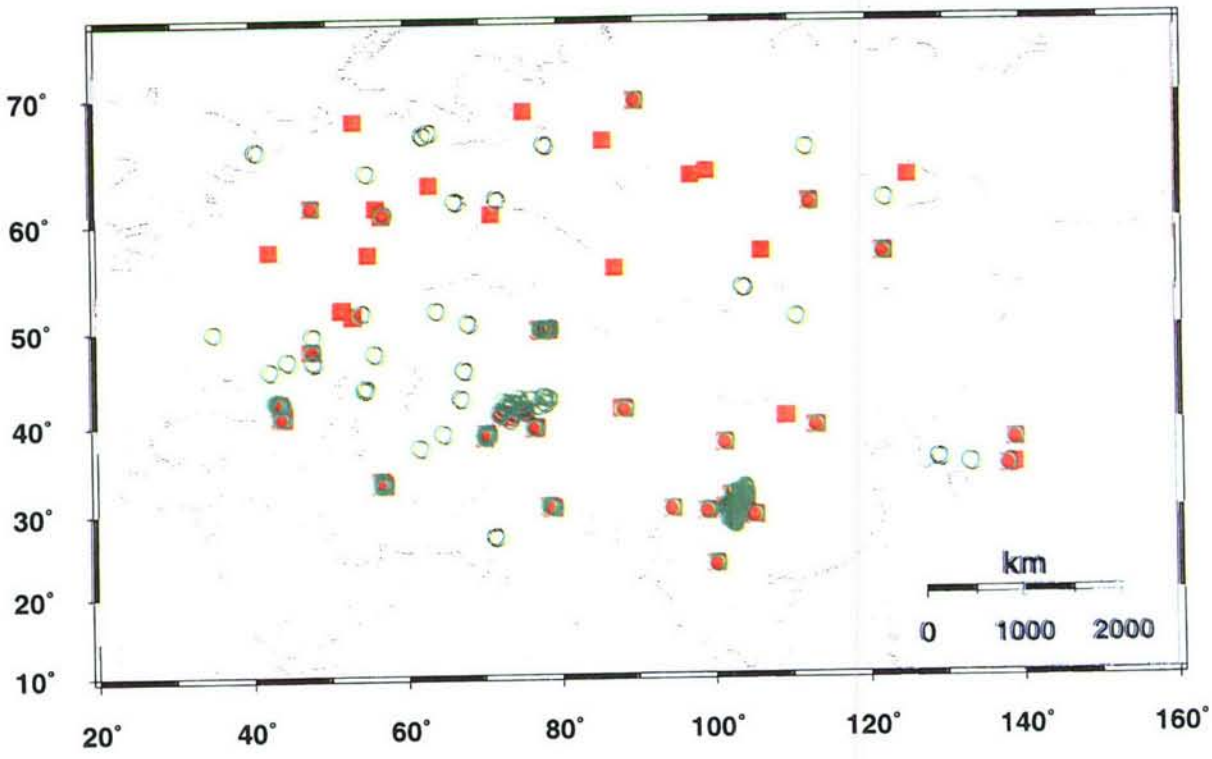


Figure 42. Map showing the distribution of the mislocation results for IASP91 and model-based SSSCs. The green circles show the events for which the mislocation error is smaller using SSSCs than without while the red squares represent the events for which the mislocation errors are smaller without using SSSCs.

6.2.2. Error Ellipse Area and Coverage

The error ellipses have systematic reduction in area for almost all events, when SSSCs are applied. Thus, using model-based SSSCs, error ellipse area is reduced for 522 of 525 solutions (99%), 498 of which (95%) are improved by more than 20%. Only 3 solutions (1%) do not have smaller error ellipses. The decrease in the median error ellipse area is 953 km^2 (from 2,616 km^2 to 1,633 km^2). Figure 43 shows the scatter plot of error ellipse areas computed with and without SSSCs.

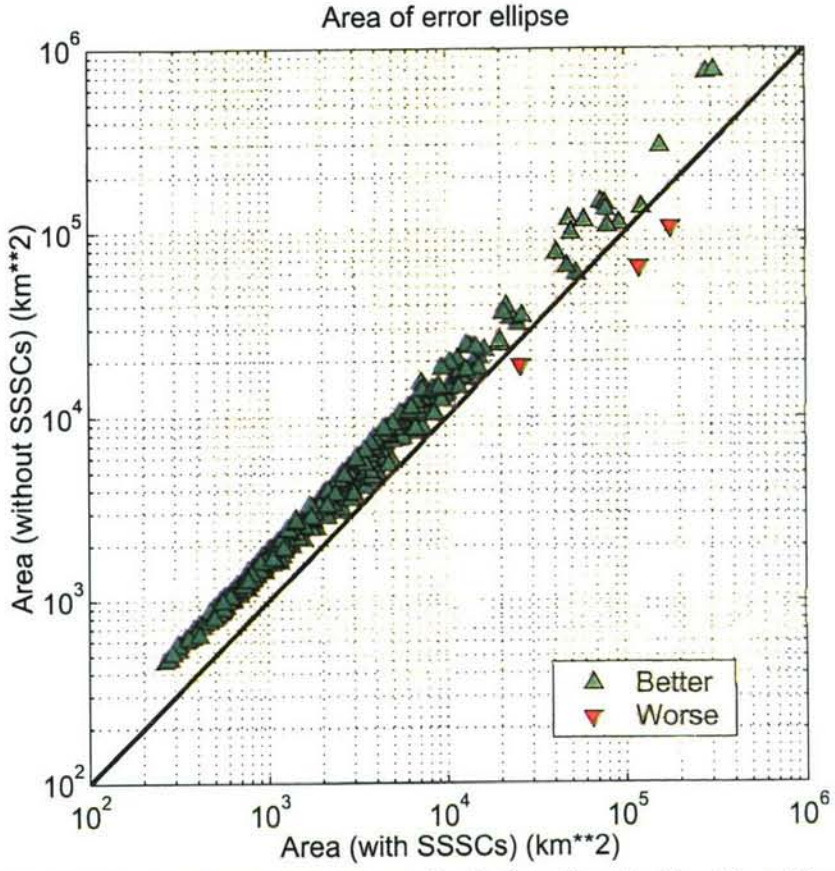


Figure 43. Scatter plot of error ellipse areas computed with (x-axis) and without (y-axis) using model-based SSSCs. Green symbols represent error ellipse areas that are smaller when using the SSSCs than without.

Error ellipse coverage is de ned as the percentage of GT event locations that fall within the corresponding 90%-confidence error ellipse. For relocation solutions without using SSSCs, 466 events (89%) have 90%-confidence ellipses that contain the GT locations. Using SSSCs, 476 events (91%) have 90%-confidence ellipses that contain the GT locations. In both cases the coverage is near the target of 90%, while the median area of the error ellipses is reduced significantly when relocating with SSSCs.

6.2.3. Standard Error of Observations

The standard error of observations, a measure of the t that depends on the root-mean-squared (rms) travel-time residuals, shows improvement for 304 solutions (58%) and deterioration for 221 solutions (42%). 186 solutions (35%) are improved by more than 20% and 147 solutions (28%) deteriorated by more than 20%.

6.2.4. Discussion

The relocation results using the model-based SSSCs show the following:

- 66% of the events are located closer to the GT location than without using SSSCs;
- error ellipse area is smaller by 20% or more for 95% of the events;
- the coverage of the error ellipses is 91%.

Given the large number of source regions, stations, and ray paths that sample very diverse and extensive geological structures we expect that SSSCs computed by 3D ray tracing for other stations in East Asia will, on average, perform as well as for the stations used to compile these evaluation metrics.

6.3. Evaluation of Kriged SSSCs

We now evaluate location performance using the kriged SSSCs. At locations near calibration data, the kriged corrections converge to the mean of the nearby data values and the uncertainty converges to the residual (i.e., local) variance. For grid points far from calibration data, the correction surface asymptotically approaches the model-based SSSC, with larger uncertainty that is the sum of the calibration and residual variances. Thus, the kriged SSSCs should perform at least as well as the model-based SSSCs, and much better for locations close to calibration points.

In this analysis, we use a "leave-one out" procedure in which the event to be relocated is excluded from the kriging calculation of the SSSCs. We then relocate each of the 525 events with kriged SSSCs that are re-computed for each event so that we do not use the same data to both compute and test the SSSCs. The new SSSCs and the relocation processing are executed by a script, *run_lv1out.csh*, that includes the following steps:

- start a loop based on origin IDs of the events in the le *ORID.lst*
- for each *orid* do a loop by phase (phase names are kept in le *PH.lst*)
- for each phase do a loop over stations in the le *STA.lst*
- if there are picks at the station for the given *orid* and phase, omit the picks from the data le and apply kriging to the SSSCs computed with 3D ray tracing for that station
- repeat for all the stations that have arrivals for the given *orid* and phase
- at the end of the loop over stations and phase, reformat the SSSCs into PIDC format and install the SSSCs in the appropriate directory

- execute the script *run_evloc_wk* for the selected *orid*, relocating the event with the updated SSSCs (parameter *sssc_level*=1 in the *EvLoc* par le)
- repeat for all the events in *ORID.lst*

The location solutions are stored in the database and are used to compute the same location performance metrics, as above. The metrics are compared to those obtained using the model-based SSSCs and without any SSSCs (i.e., using IASP91). The following subsections describe the metrics for mislocation, error ellipse area, coverage, and standard errors of observations.

As an example, Figure 44 shows relocation results without SSSCs, with model-based SSSCs, and with kriged SSSCs for a PNE, Meridian-2, that was conducted on 19 September 1973 in the Former Soviet Union. The kriged SSSCs reduce the mislocation error from 20.8 km to 6.6 km and reduce the error ellipse area from 710 km^2 to 357 km^2. For this event, the relocation results do not differ significantly when using the model-based or kriged SSSCs. Also, the error ellipses are smaller when using either version of the SSSCs, and contain the GT location, unlike the error ellipse based on IASP91 without SSSCs. Another case, depicted in Figure 45, shows that kriging, when calibration points are near the event to be located, can have a significant impact. In this case the error ellipse based on IASP91 without SSSCs does not include the GT location, as in the previous case. What is different in this case is that there are 23 GT events inside a 4 deg radius around the Azgir-10 PNE and only one in the previous case (Meridian-2). With magenta squares we display in Figure 45 the nearby GT reference events. The residuals of the 23 GT events are being used in the kriging process. The kriged SSSCs, used in relocation, contribute to a solution that is 1 km in distance from the GT location compared to 6.8 km when model-based SSSCs are used in the relocation process.

The improvement of results shown in Figure 45, compared to the results in Figure 44, is an indication of the effectiveness of empirical data, in a situation where such data are available.

6.3.1. Mislocation

Of the 525 GT events, 445 solutions (85%) have smaller mislocation errors using kriged SSSCs than those obtained using just the IASP91 travel-time tables. Of these, 410 events (78%) have mislocation errors that are reduced by more than 20%. Only 80 solutions (15%) deteriorated and 53 solutions (10%) deteriorated by more than 20%. The median mislocation is reduced from 16.9

km to 6.5 km when kriged SSSCs are used. Figure 46 shows a scatter plot of the mislocation distances, relative to the GT locations, obtained with (x-axis) and without (y-axis) using the SSSCs. As in Figure 41, the green symbols represent events for which location estimates using the kriged SSSCs are closer to the GT locations, while the red symbols show solutions that are better without using SSSCs.

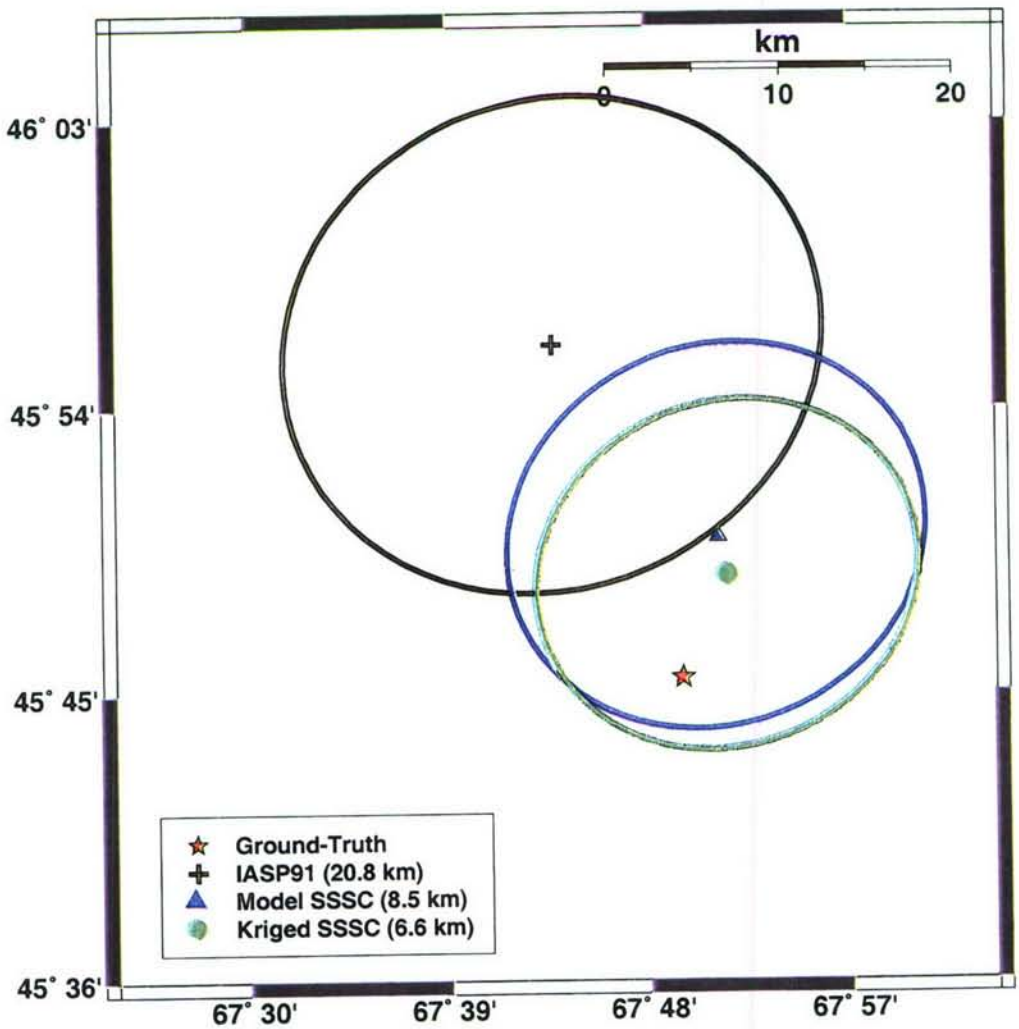


Figure 44. Relocation results, with and without using SSSCs, for a PNE (Meridian-2) in the Former Soviet Union on 19 September 1973. Mislocation errors relative to the ground-truth location are 20.8 km without using SSSCs, 8.5 km using model-based SSSCs, and 6.6 km using kriged SSSCs. The error ellipse areas are 710 km^2 without using SSSCs, 425 km^2 using model-based SSSCs, and 357 km^2 using kriged SSSCs.

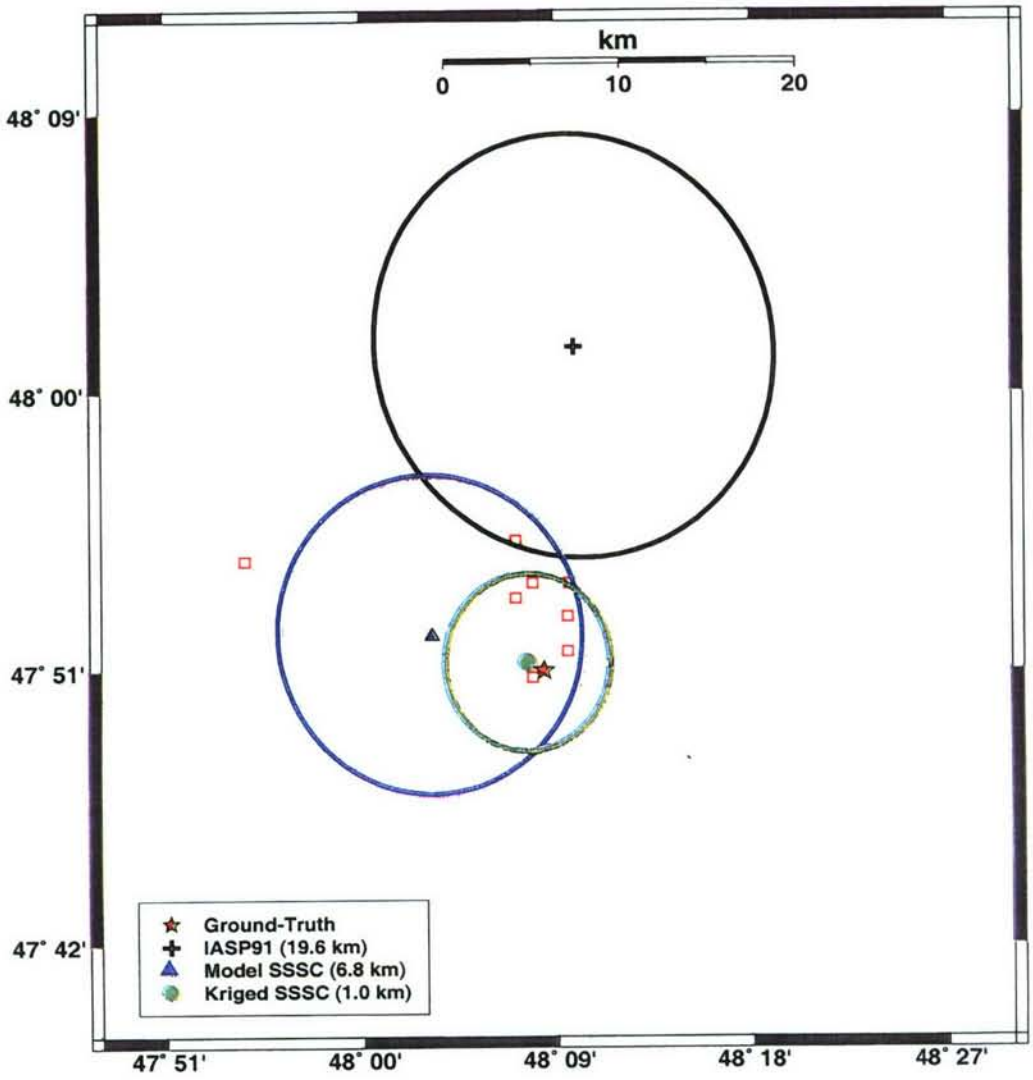


Figure 45. Relocation results, with and without using SSSCs, for a PNE (Azgir-10) in the Former Soviet Union on 24 October 1979. Mislocation errors relative to the ground-truth location are 19.6 km without using SSSCs, 6.8 km using model-based SSSCs, and 1.0 km using kriged SSSCs. Magenta square markers represent calibration points. The error ellipse areas are 455 km^2 without using SSSCs, 264 km^2 using model-based SSSCs, and 79 km^2 using kriged SSSCs.

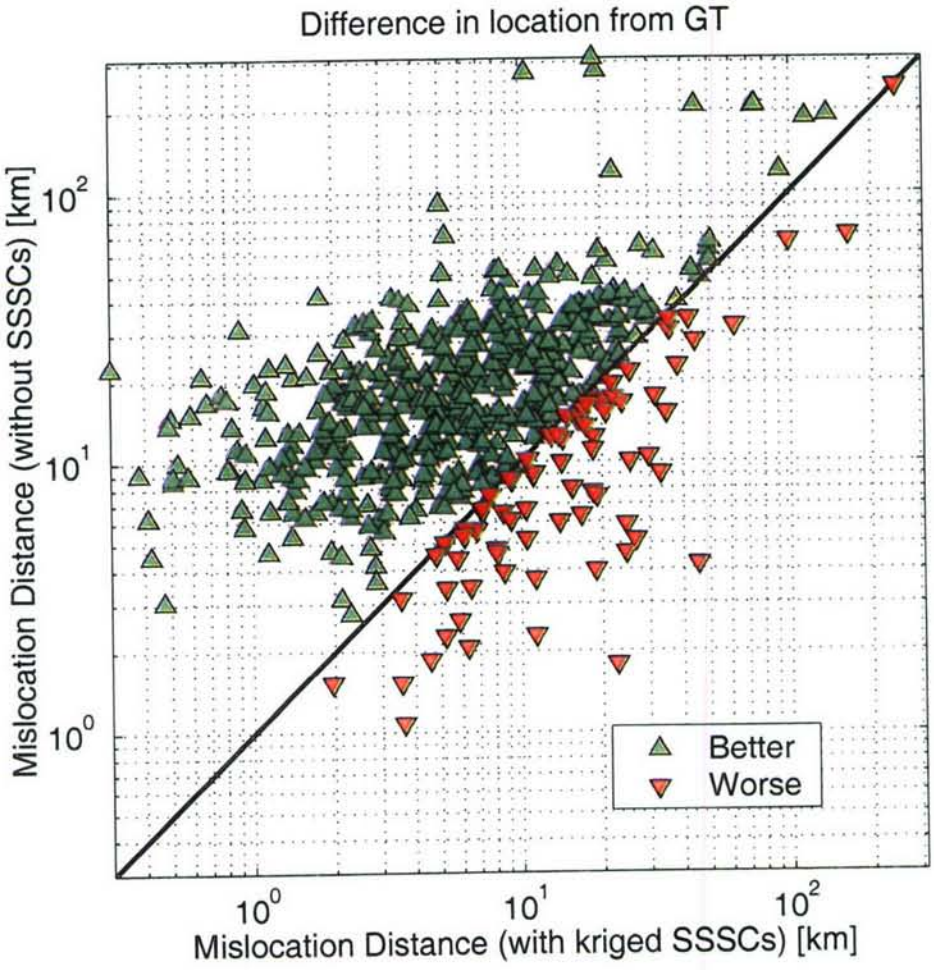


Figure 46. Mislocation distances with and without using kriged SSSCs with respect to corresponding GT locations. Markers and the line are defined as in Figure 41.

As in the model-based SSSC case, we present in Figure 47 the mislocation results in map view. The green circles represent the events for which the relocation with model-based SSSCs and kriging is closer to the GT location than without SSSCs. The red squares show the events for which the mislocation without SSSCs is smaller than with SSSCs.

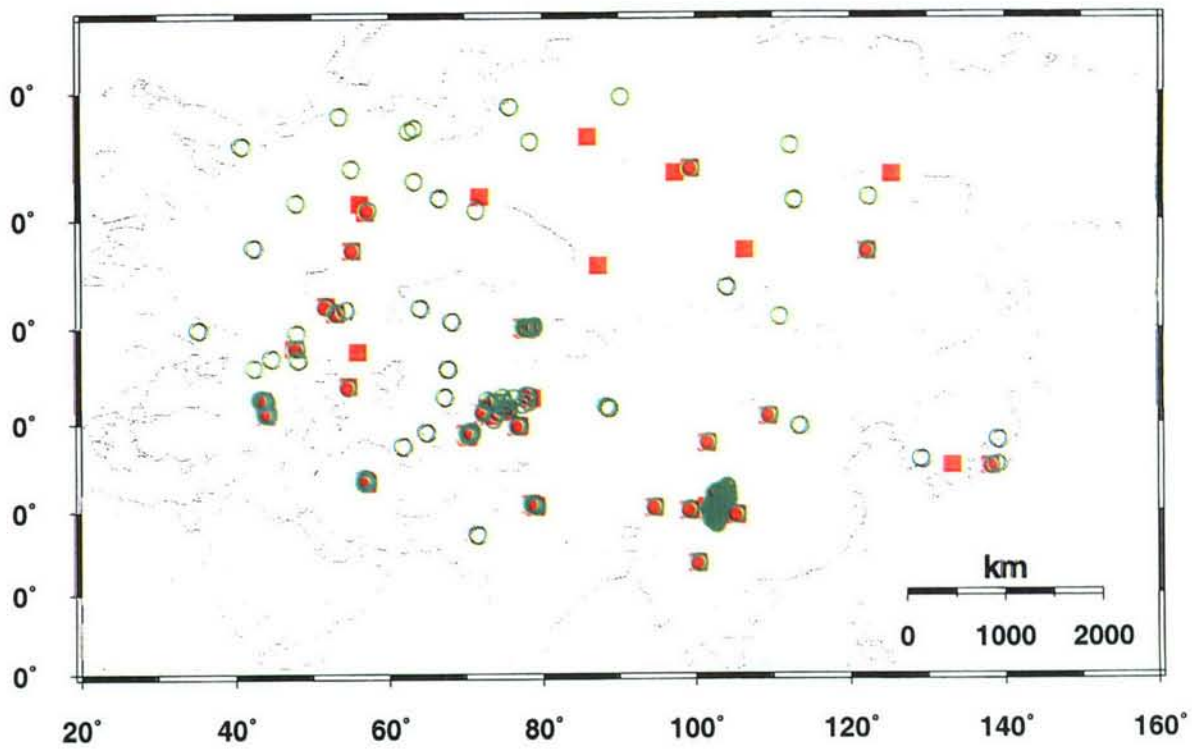


Figure 47. Map showing the distribution of the mislocation results for IASP91 and model-based SSSCs and kriging. Markers are defined as in Figure 42.

6.3.2. Error Ellipse Area and Coverage

Using kriged SSSCs, error ellipse area is reduced for all the 525 solutions (100%), 523 of which (99.6%) are improved by more than 20%. The median ellipse area is reduced from 2,616 km^2 to 722 km^2. The results are shown in Figure 48. Error ellipse coverage, computed as the percentage of GT event locations contained within the 90%-confidence error ellipses, is 92% (483 GT events) when using the kriged SSSCs, as compared to 89% (466 GT events) without using SSSCs (i.e., using IASP91 only).

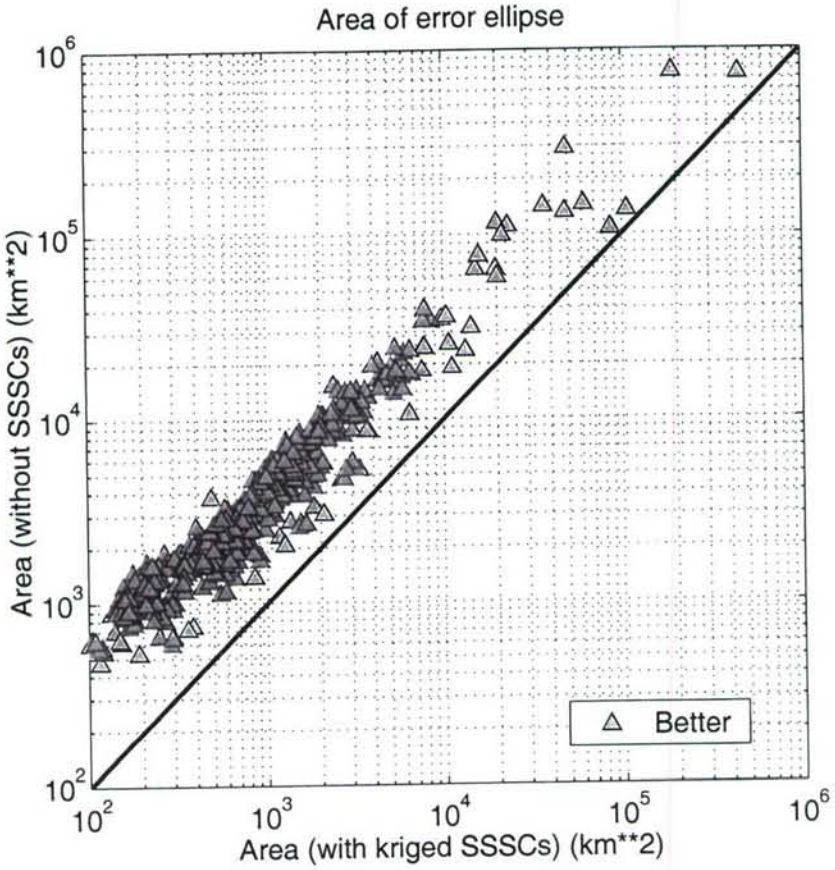


Figure 48. Scatter plot of error ellipse areas computed with (x-axis) and without (y-axis) using kriged SSSCs. Markers are defined as in Figure 43.

In Figure 49 we show the cumulative probability distribution of the coverage parameter without SSSCs (red curve), with model-based SSSCs (green curve), model-based SSSCs and kriging (magenta curve), and the theoretical 90 percentile χ^2 distribution with two degrees of freedom. Values of less than one for the coverage parameter indicate the GT location is inside the actual error ellipse when relocation is done with or without SSSCs. The curves in Figure 49 also suggest that the *a priori* modeling errors for Pn and Sn (Figure 22 and Figure 23) are rather conservative (see cases with model-based SSSCs — green curve, and model-based SSSCs and kriging — magenta curve).

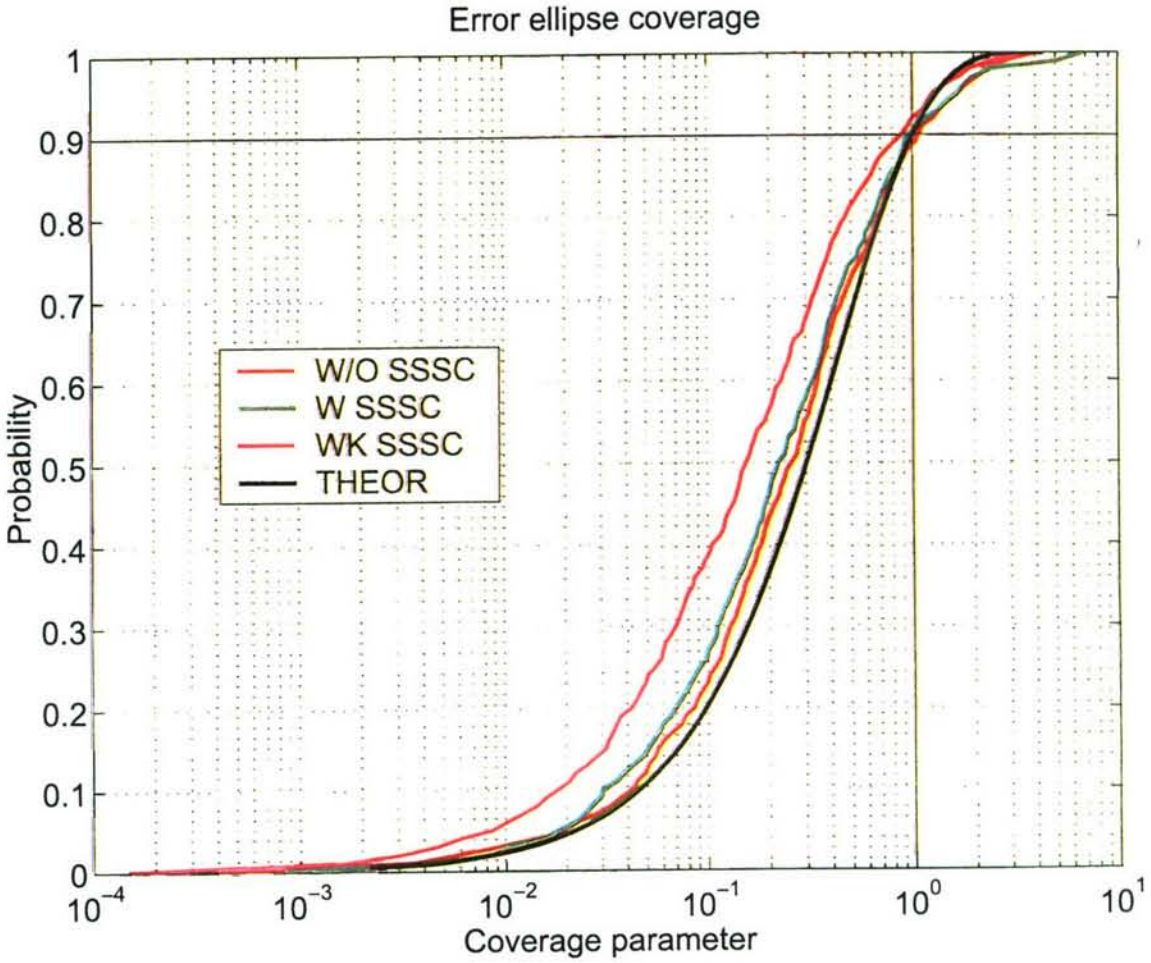


Figure 49. Cumulative probability distribution of the coverage parameter without SSSCs (red), with model-based SSSCs (green), with model-based SSSCs and kriging (magenta, and the theoretical 90 percentile χ^2 distribution with two degrees of freedom (black).

6.3.3. Standard Error of Observations

The results presented in Figure 50 show that 75% (393 GT events) of the solutions have smaller standard errors of the travel-time observations (62% improved by more than 20%) and 25% deteriorated.

6.3.4. Discussion

The relocation results using kriged SSSCs show significant improvements for all location performance metrics. Specifically,

- 85% of the events are located closer to the GT location with median mislocation errors reduced from 16.9 km to 6.5 km;
- error ellipse area is reduced by 20% or more for 99.6% of the events;
- median error ellipse area is reduced from 2,616 km^2 to 722 km^2, while achieving 92% coverage of the error ellipses with the GT event locations.

These results are very encouraging and show that our regionalized travel-time model of East Asia, and the combined computational methods of 3D ray tracing and kriging, yield useful Pn and Sn SSSCs and modeling errors for stations in this region. It is important to note that location performance of events in areas far from existing calibration data should be, on average, comparable to the results obtained using the model-based SSSCs (i.e., without kriging).

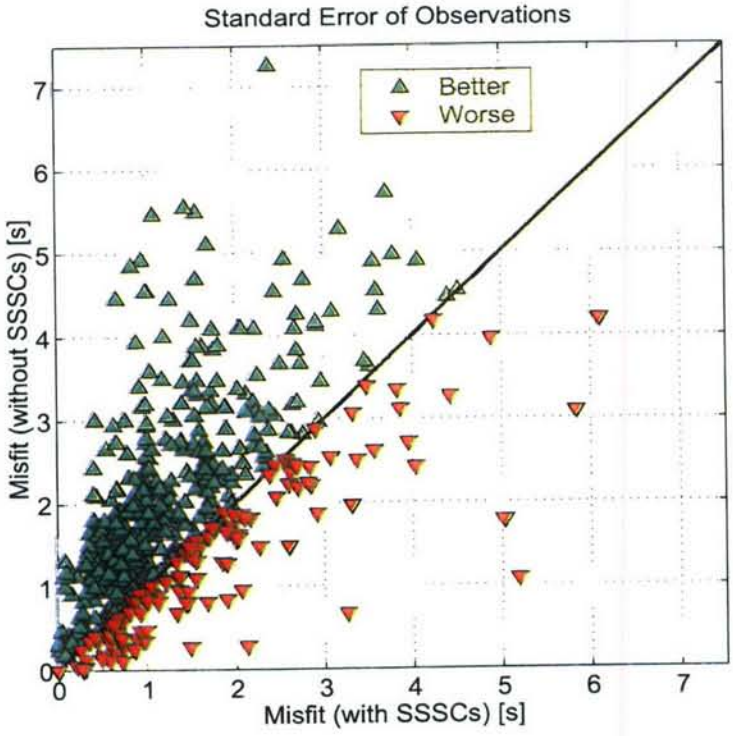


Figure 50. Scatter plot of the standard error of observations with (x-axis) and without (y-axis) using kriged SSSCs. The green symbols represent solutions with smaller standard errors using SSSCs, while the red symbols show the solutions with smaller standard errors without using SSSCs.

In Table 12 we summarize the main location performance metrics when Pn and Sn arrivals were used with and without SSSCs.

Table 12. Location performance metrics for Pn and Sn.

Case	IASP91	Model-Based SSSCs	Model + Kriged SSSCs
Median mislocation (km)	16.9	11.4	6.5
Events with reduced mislocation		66%	85%
Median error ellipse area (km^2)	2,616	1,663	722
Events with smaller ellipses		99%	100%
90% coverage	89%	91%	92%

6.4. Results for Pn only

We repeated the above analysis using Pn arrivals only. The results, shown in Table 13, are not much different from those based on Pn and Sn.

There are several reasons for the similarity. First, 40% of the solutions were identical (due to the fact that there were no Sn phases for those events). Second, it was generally true that the number of Pn phases was greater than the number of Sn phases. And third, the measurement and modeling

Table 13. Location performance metrics for Pn alone.

Case	IASP91	Model-Based SSSCs	Model + Kriged SSSCs
Median mislocation (km)	15.7	11.6	6.4
Events with reduced mislocation		63%	84%
Median error ellipse area (km^2)	3,089	1,727	786
Events with smaller ellipses		98%	99%
90% coverage	89%	92%	94%

errors, which are used as a weighting factor in the location process, were greater for Sn than for Pn, making the Sn contribution less important.

6.5. Variability of Location Quality

It is generally understood that the quality of event location will vary depending on the number of defining phases used for each event (Ndef), and depending also on the azimuthal distribution of detecting stations. The latter characteristic is crudely characterized by the value of the "Gap," that is, the largest azimuthal separation between stations that report an arrival.

In order to gain an appreciation of the way in which location quality varies in practice, for the 525 events for which we have GT information, Figures 51, 52, 53, and 54 show the size of the 90% confidence ellipses as a function of Gap, for four different ranges of Ndef; and Figures 55, 56, 57, and 58 show the size of the confidence ellipses as a function of Ndef, for four different ranges of Gap. Thus, in Figure 51 is shown the dependence on Gap, for a set of events (typically, of low magnitude) for which there are few defining phases (Ndef < 10). Figure 54 shows the dependence on Gap, for events with far more defining phases (30 < Ndef < 40). As would be expected, Figures 51, 52, 53, and 54 are in order of increasing capability as the range of Ndef values increases; and Figures 55, 56, 57, and 58 are in general order of decreasing capability as the Gap range increases from low values, 65° to 75° in Figure 55, to values greater than 200° for Figure 58.

In each of these eight Figures, we see that there is significant improvement in location (that is, smaller error ellipses compared to the results of using IASP91 travel times), when model-based SSSCs are applied; and further improvement when kriged SSSCs are applied. With kriged SSSCs, it is still necessary to have more than 15 defining phases in order to have high confidence of error ellipses smaller than 1000 km^2.

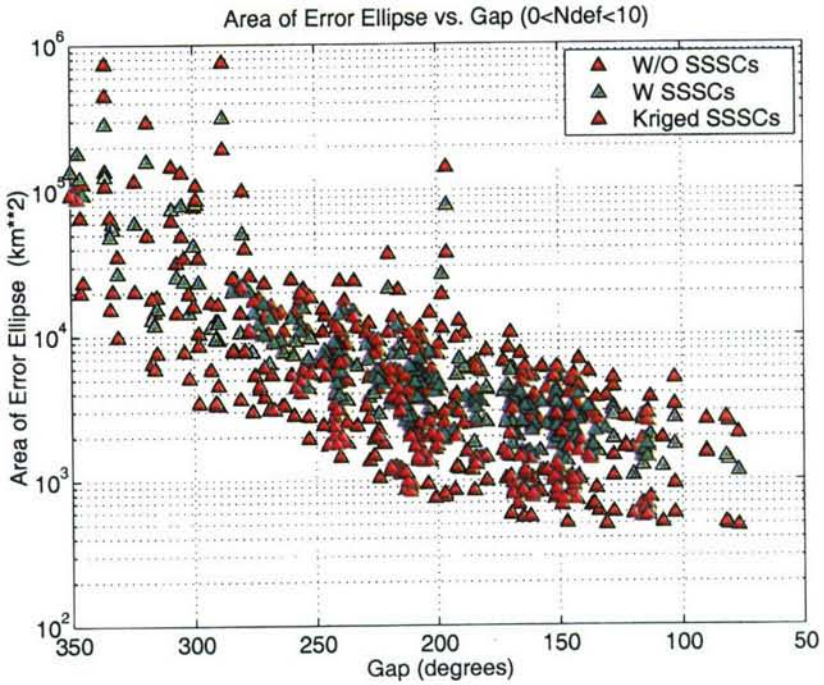


Figure 51. Area of the 90% confidence ellipses, as a function of azimuthal gap, for events that have fewer than 10 defining phases.

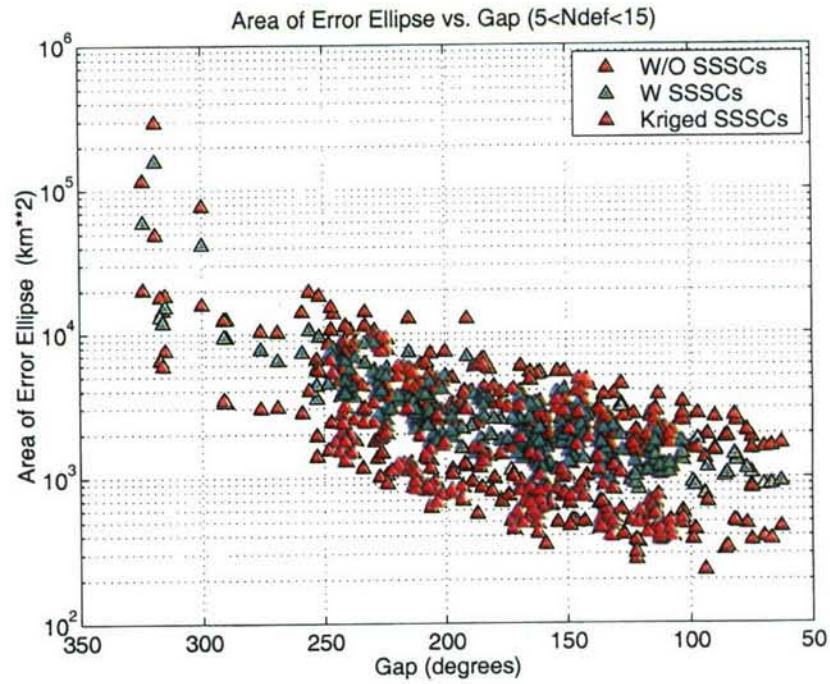


Figure 52. Area of the 90% confidence ellipses, as a function of azimuthal gap, for events that have between 5 and 15 defining phases.

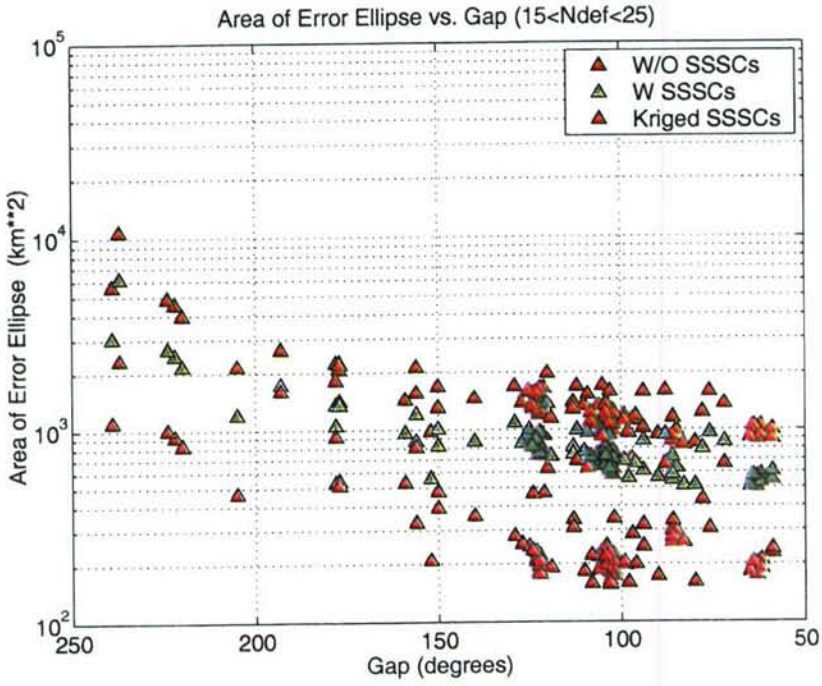


Figure 53. Area of the 90% confidence ellipses, as a function of azimuthal gap, for events that have between 15 and 25 defining phases.

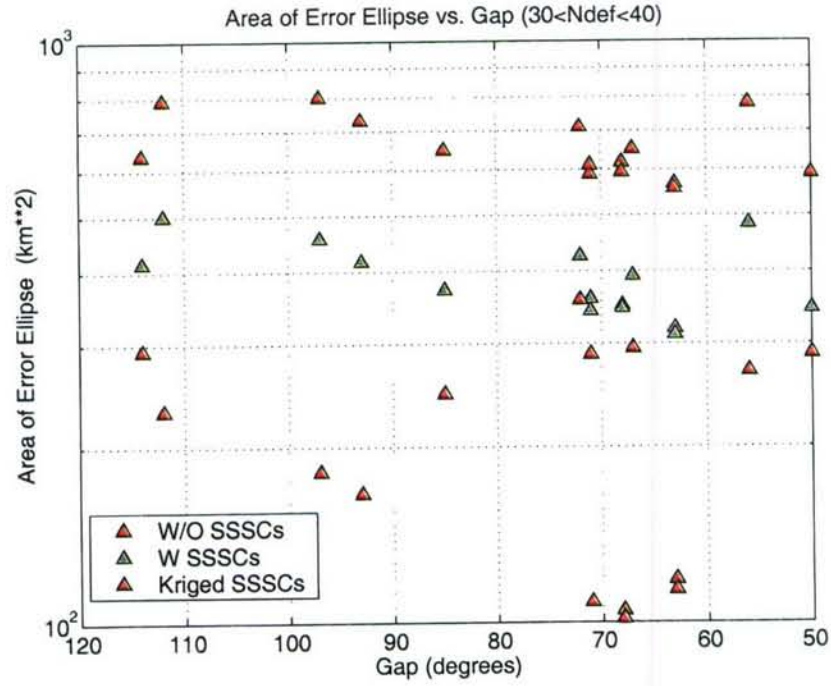


Figure 54. Area of the 90% confidence ellipses, as a function of azimuthal gap, for events that have between 30 and 40 defining phases.

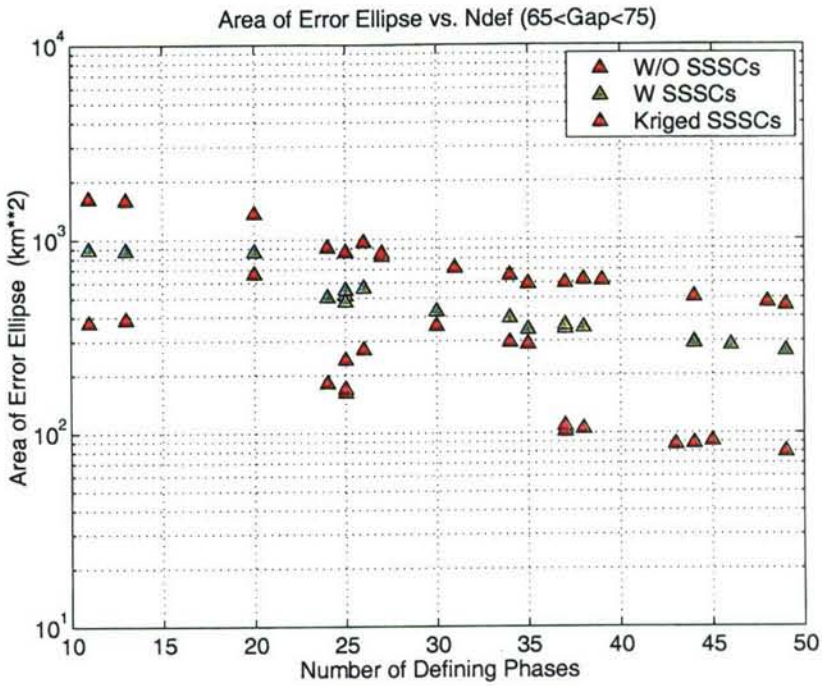


Figure 55. Area of the 90% confidence ellipses, as a function of the number of defining phases, for events that have an azimuthal gap lying between 65° and 75°.

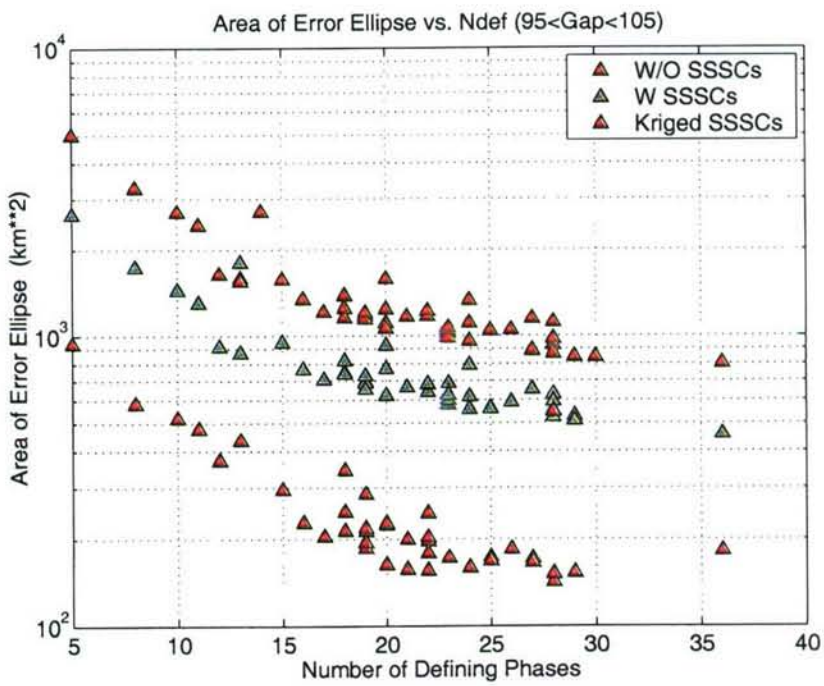


Figure 56. Area of the 90% confidence ellipses, as a function of the number of defining phases, for events that have an azimuthal gap lying between 95° and 105°.

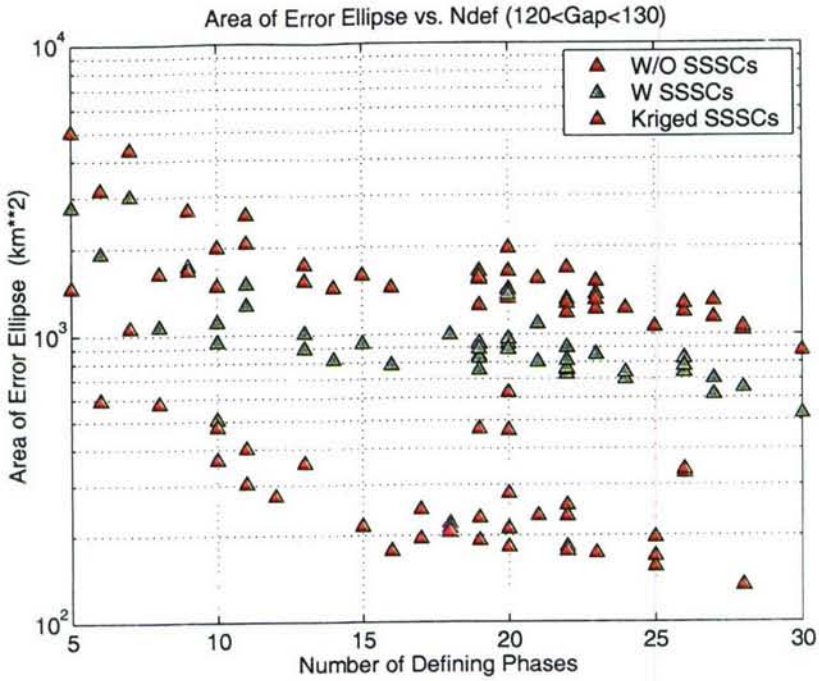


Figure 57. Area of the 90% confidence ellipses, as a function of the number of defining phases, for events that have an azimuthal gap lying between 120° and 130°.

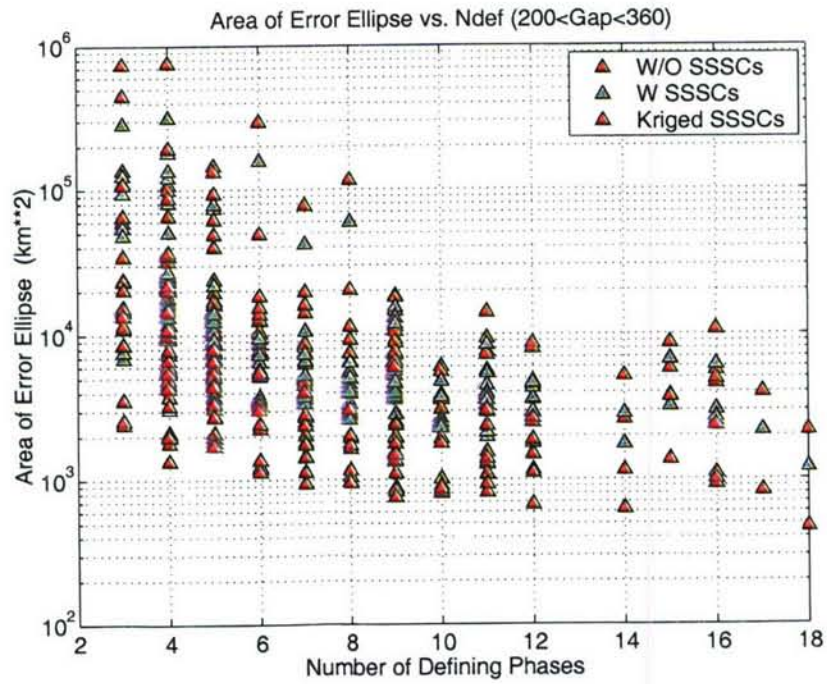


Figure 58. Area of the 90% confidence ellipses, as a function of the number of defining phases, for events that have an azimuthal gap greater than 200°. These events thus have a poor station distribution.

Section 7 Conclusions and Recommendations

The goal of the tests presented in this report was to validate our regionalized travel-time model of East Asia and evaluate the effectiveness of the regional Pn and Sn SSSCs developed by the Lamont Consortium for Group1 IMS stations. As the regionalization is an important part of our current SSSC computation, a significant portion of the report was also devoted to specifying the boundaries of the subregions and reviewing a wide variety of data and literature to obtain the best available estimates of the travel times, as a function of distance, within each subregion.

The SSSCs were computed for each station using 3D ray tracing and refined by spatially correcting the travel-time residuals at each grid point using kriging. The kriging approach assures that the correction converges to the mean of nearby calibration data for areas with ground truth, and the uncertainty converges to the residual variance of the local data. Far from empirical calibration data, the correction surface reverts to the background model-based SSSC, with larger uncertainty that is the sum of the residual and calibration variances.

To quantify improvements in location performance due to our Pn and Sn SSSCs, we performed two series of tests on the data sets. The main objective of the first test was to validate the regionalized travel-time model and demonstrate that the resulting SSSCs improve location performance. To directly test the validity of the model, we first performed relocation tests that did not use kriging to re ne the model-based SSSCs. To evaluate the additional benefit of kriging, we performed a second set of relocation tests using kriged model-based SSSCs. Although kriging significantly enhances the calibration of the SSSCs, as shown, a direct test of the model is important to demonstrate that even in areas and at stations without empirical calibration data, the model-based SSSCs provide useful improvements in location performance.

We relocated 525 events recorded by various combinations of 140 regional stations, with and without using SSSCs. The results show reductions in mislocations for 66% of events when the model-based SSSCs were used, and 85% when using model-based SSSCs refined by kriging. The median mislocation improved from 16.9 km to 11.4 km and 6.5 km, respectively. The median area of the error ellipses was reduced from 2,616 km^2 to 1,663 km^2 and 722 km^2, respectively. Error ellipse coverage, as a percentage of GT event locations within the corresponding error ellipses, is 89% without using SSSCs, 91% using model-based SSSCs, and 92% using kriged SSSCs. These

results were obtained for source locations, stations, and paths that sample very extensive and diverse geological provinces throughout East Asia (Figure 39). Thus, we believe the results indicate the general validity of the model and the resulting SSSCs for this region.

In all cases, the results demonstrate that the regionalization and travel-times curves, developed by the Lamont Group 1 consortium, along with the computational methods of 3D ray tracing and kriging, have produced Pn and Sn SSSCs and modeling errors that improve the location performance and reduce uncertainty estimates in East Asia. We expect that these SSSCs will perform, on average, as well as indicated by the validation test results for the model-based SSSCs, and substantially better for regions where empirical data are available, including the areas surrounding the Lop Nor, Semipalatinsk, Indian and Pakistani nuclear test sites.

We note that the degree of location improvement using our SSSCs significantly exceeds the criteria developed at Location Workshops held in 1999, 2000, 2001, 2002, and 2003 in Oslo, Norway (see for example CTBT/WGB/TL-2/18 for 1999). In part, this is a reflection of the fact that the IASP91 travel times are a poor representation of regional travel times in much of the region we have studied. We therefore recommend that our SSSCs be considered for seismic event location in East Asia by any users of regional signals recorded by the Group 1 stations (Table 1) and other stations that we have calibrated (Table 2). In particular, we recommend that our SSSCs be considered for use in operational systems that interpret seismic arrival-time data from these stations.

Finally, we note that our overall method (of first obtaining model travel times and then kriging with empirical data) is well suited to calibration of any stations in East Asia which have a significant archive of reliably measured arrival times. For stations that already have arrivals from a substantial subset of the GT events we have obtained in this project, the calibration (using kriging) is particularly simple.

Section 8 References

Anikanova, G. Thickness of the crust in the Western Khubsugul region. Russian Geology and Geophysics, 36, N12, 128-130, 1995.

Antonenko, A.N. The Deep Structure of the Kazakhstan Earth Crust (from seismic data). Nauka Publ. House, Alma-Ata, 242 pages, 1984 (in Russian).

Arora, S. K. A study of the Earth's crust near Gauribidanur in Southern India, Bull. Seism. Soc. Amer., 61, 671-683, 1971.

Atabaev, Kh. A., E.M. Butovskaya. Regional travel-time tables for some regions of Central Asia. Institute of Geophysics and Geology, Uzbek National Academy of Science, Tashkent, report, 36 pages, 1986 (in Russian).

Barker, B., M. Clark, P. Davis, M. Fisk, M. Hedlin, H. Israellson, V. Khalturin, W.-Y. Kim, K. McLaughlin, C. Meade, J. Murphy, R. North, J. Orcutt, C. Powell, P. Richards, R. Stead, J. Stevens, F. Vernon, and T. Wallace, Monitoring nuclear tests, Science, 281, 1967-1968, 1999.

Barkhin, G.S., L.N. Nikitina, V.Z. Ryaboy. Study of the structure of the upper mantle based on DSS profile observations. VINITI, 65 pages, 1987.

Båth, M. Earthquakes in Sweden, 1951-1976. Travel times of regional phases in Scandinavia region for H = 0 km and H = 12 km. Uppsala, 1977.

Beloussov, V.V. et al. (editors). Deep structure of the USSR territory. Moscow, Nauka, 1991.

Beloussov, V.V., N.I. Pavlenkova and G.N. Kvyatkovskaya (editors), Structure of the Crust and Upper Mantle of the USSR, International Geology Review, V.34, N4, 213-445, 1992.

Bhattacharya, S. N. Observation and inversion of surface wave group velocities across central India, Bull. Seism. Soc. Amer. 71, 1489-1501, 1981.

Bocharov, V.S., S.A. Selentov and V.N. Mikhailov, Characteristics of 92 Underground Nuclear Explosions at the Semipalatinsk Test Site, Atomnaya Energia, Vol.87, Issue 3, 1989 (in Russian).

Bondár, I. Combining 1-D models for regional calibration, in Proceedings of a Workshop on IMS Location Calibration, Oslo, January 1999.

Bondár, I., X. Yang, K. McLaughlin, R. North, V. Ryaboy, and W. Nagy. Source Specific Station Corrections for Regional Phases at IMS Stations in North America and Fennoscandinavia, EOS Trans., AGU, 79 (45), Fall Meet. Suppl., F839, 1998.

Bondár, I., V. Ryaboy. Regional travel-time tables for the Baltic Shield region. Technical report CMR-97/24, 34 pages, 1997.

Bottone S., M.D. Fisk, and G.D. McCartor. Regional seismic event characterization using a Bayesian formulation of simple kriging, Bull. Seism. Soc. Amer. 92, 2277-2296, 2002.

Bune, V.I., E.M. Butovskaya. Travel-time curves and Earth's structure studied by records of large explosions. Proceedings of Geophysical Institute, N32, 142-153, 1955 (in Russian).

Burlacu, V., M. D. Fisk, V. I. Khalturin, W-Y. Kim, P. G. Richards, J. Armbruster, I. Morozov, E. Morozova. Validation Test Report: Off-line Testing of a Regionalized Travel-Time Model and Source-Specific Stations Corrections for Asia, 2002.

Chan, W.W., C.Y. Wang, and W.D. Mooney. 3-D Crustal structure in southwestern China. 23rd Seismic Research Review, Wyoming, v.1, 12-20. 2001.

Chaudhury, H. M. Seismic surface wave dispersion and the crust across the Gangetic basin, Geophys. J., 23, 129-138, 1966.

Chun, K.-Y. Crustal block of the western Ganga basin: A Fragment of oceanic affinity? Bull. Seism. Soc. Amer. 76, 1687-1698, 1986.

Cormier, V., and A. Stroujkova. Source-specific Station Corrections modeled by dynamic ray tracing in 3-D Earth models, 24th Seismic Research Review, Ponte Vedra, Florida, 2002.

Dube, R. K., J. C. Bhayana, and H. M. Chaudhury. Crustal structure of Peninsular India, Pure Appl. Geophys. 109, 1718-1727, 1973.

Dube, R. K. and J. C. Bhayana. Crustal Structure in the Gangetic Plains of the Indian sub-continent from body waves, Bull. Seism. Soc. Amer. 64, 571-579, 1974.

Egorkin, A.V., et al. Structure and properties of the Upper Mantle on the USSR territory. Moscow, Nauka Publ. House, 1980.

Egorkin, A.A., et al. Results of lithospheric studies from long-range profiles in Siberia. Tectonophysics, v. 140, 29-47, 1987.

Fedorov, S.A. (editor). Gazli earthquakes. Geological and geophysical nature of the source zones. Moscow, Nauka Publ. House, 200 pages, 1984.

Fisk, M.D. Accurate locations of nuclear explosions at the Lop Nor test site using alignment of seismograms and Ikonos satellite imagery, Bull. Seism. Soc. Amer., 92, 2911-2925, 2001.

Golenetskiy, S.I. Travel time tables of seismic waves from Baykal region earthquakes. In the book: Seismicity and Deep Structure of Baykal Area. Novosibirsk, Nauka Publ. House, pages 30-38, 1978.

Golenetskiy, S.I., F.B. Novomeyskaya, and G.I. Perevalova. Travel times of seismic waves and Earth's crust thickness in the North-East part of Baykal zone. Geology and Geophysics, Novosibirsk, N2, 40-57, 1974.

Gorbunova, I.V. Average travel time of P wave first arrivals for Central Asia and South Kazakhstan regions. Annual book: Earthquakes in the USSR in 1988. Moscow, Nauka Publ. House, pages 59-63, 1990 (in Russian).

Hamburger, M.W., and S. Ghose. Velocity structure beneath the Northern Tien Shan, J. Geophys. Res., v103, 2725-2748, 1998.

Hauck, M. L., K. D. Nelson, L. D. Brown, Wenjin Zhao, and A. R. Ross. Crustal structure of the Himalayan orogen at ~90 deg east longitude from Project INDEPTH deep reflection profiles, Tectonics 17, 481-500, 1998.

Hearn, T.M., J. Ni. Tomography and location problems in China using regional travel-time data, 22nd Seismic Research Symposium, New Orleans, v.2, pages 155-160, 2000.

Hwang, H.-J. and B. J. Mitchell. Shear velocities, Q_β, and the frequency dependence of Q_β in stable and tectonically active regions from surface wave observations, Geophys. J. R. astr. Soc. 90, 575-613, 1987.

IDC Documentation IDC7.1.5 - Event Location Software, 2001.

Jih, R.-S. Location Calibration Efforts in China, in Proceedings of the 20th Annual Seismic Research Symposium, Santa Fé, September 21 - 23, 1998.

Kaila, K. L., H. C. Tewari, V. G. Krishna, M. M. Dixit, D. Sarkar, and M. S. Reddy. Deep seismic sounding studies in the north Cambay and Sanchor basins, India, Geophys. J. Int. 103, 621-637, 1990.

Kayal, J. R. and Reena De. Pn Velocity study using a temporary seismographic network in the Shillong Plateau, northeast India, Bull. Seism. Soc. Amer., 77, 1718-1727, 1987.

Karus, E.V. (editor). Investigation of the Earth's crust and upper mantle in the seismic active zone of the USSR. Moscow, Nauka Publ. House, 1984 (in Russian).

Kennett, B.L.N. (editor). IASPEI 1991 Seismological Tables, Research School of Earth Sciences, Australian National University, Canberra, Australia, 1991.

Khalturin, V.I. Regional version of Nersesov-Rautian (1964) travel-time table (unpublished report), 1974.

Khalturin, V.I., et al. Propagation of Lg waves and lateral variations in crustal structure. J. Geophys. Res., v82, #2, 307-316. 1977.

Khalturin, V.I, A.A. Lukk, A.I. Ruzaykin. Regional phase velocities and fine structure of its travel time curves from CSE stations observations of seismic events in North-West China at the distances 800-2400 km (part of unpublished CSE report to Soviet Military), Dec. 1978.

Khalturin, V.I., T.G. Rautian, P.G. Richards. A study of small earthquakes and small explosions during 1961-1989 at the Semipalatinsk Test Site. Technical report to DOE/LLNL, 64 pages, 1994.

Khalturin, V.I., T.G. Rautian, P.G. Richards. A study of small magnitude seismic events during 1961-1989 on and near the Semipalatinsk Test Site, Kazakhstan, Pure and Applied Geophysics, v. 158, pages 143-172, 2001.

Khamrabaev, I.Kh. (editor). Earth's crust and upper mantle of Central Asia. Nauka Publ.House, Moscow, 210 pages, 1977.

Kirichenko, V.V., Y.A. Kraev. Development of regional travel-time tables for different geotectonic provinces of Northern Eurasia. Proceedings of 22nd Annual DoD/DOE Seismic Symposium, New Orleans, pages 305-315, 2000.

Kirichenko, V. V., and Y. A. Kraev. Results of 1-D location calibration studies related to the territory of Northern Eurasia, Proceedings of the 23rd Seismic Research Review, 2001.

Kosminskaya, I.P. et al. (editors). Seismic models of the lithosphere of the main Geostructures in USSR territory. Moscow, Nauka Publ. House, 191 pages, 1980 (in Russian).

Krasnopevtseva, G.V. Deep structure of the Caucasus seismoactive region. Nauka, Publ. House, Moscow, 109 pages, 1984.

Krilov, S.V. et al. Seismic cross-section of the lithosphere at the Baykal Rift Zone. Geology and Geophysics, Novosibirsk, N3, 1975.

Lomakin, V.S, V.V. Kolmogorova, G.I. Parygin. Travel time table of seismic waves in Ural region. In the book: Seismic waves from mining explosions and study of the Earth's crust in the Ural. Ural Scientific Center of Acad. Sci. USSR, Sverdlovsk, pages 14-20, 1978.

Lukk, A.A., I.L. Nersesov. Deep Pamir-Hindu Kush earthquakes. Earthquakes in the USSR in 1966, Nauka Publ. House, 1967 (in Russian).

Menke, W. Case studies of seismic tomography in a regional context, in Seismic Data Analysis and Imaging With Global and Local Arrays, Alan Levander and Guust Nolet, Eds., American Geophysical Union, submitted 2002.

Mooney, W., et al., 2001. A review of new seismic constraints of crust and mantle from China and India. Proceedings of the 23rd Seismic Research Review. Wyoming, pages 90-99, 2001.

Molnar, P., and P. Tapponier. Cenozoic tectonics of Asia: effects of tectonic collision, Science, v 189, 419-426, 1975.

Molnar, P., and P. Tapponier. Active faulting and Cenozoic tectonics of the Tien Shan, Mongolian and Baykal regions, J. Geophys. Res., v84, 3425-3459, 1979.

Mukhopadhyay, S., R. Chander, and K.N. Khattri. Crustal properties in the epicentral tract of the Great 1897 Assam earthquakes, Northeast India, Tectonophysics, 283, 311 - 330, 1997.

Nersesov, I.L. Structure of the Earth's Crust. In the book: Methods of the Detailed Study of the Seismicity, Chapter 3. Moscow. Publ. House of Academy of Science, Moscow, pages 30-46. 1960 (in Russian).

Nersesov, I.L. (editor). Deep Structure of the low seismicity regions of the USSR. Moscow, Nauka Publ.House, 223 pages, 1987 (in Russian).

Nersesov, I.L., T.G. Rautian. Kinematics and dynamics of seismic waves at epicentral distances less than 3,500 km. Proceedings of the Institute of the Physics of the Earth, N32, pages 63-84, 1964 (in Russian).

Pavlenkova, N.I. Crust and upper mantle structure in Northern Eurasia from seismic data. Advances in Geophysics, v. 37, Academic Press, 1996.

Richards, P. G., V. Burlacu, and M. D. Fisk. Pn SSSCs for IMS and Surrogate Stations in Asia, CCB-PRO-02/04 Rev. 1, 2002.

Roecker, S.W., et al. Three-dimensional velocity structure of the Western and Central Tien Shan, J. Geophys. Res., v99, 15779-15795, 1993.

Ryaboy, V.Z. Lower lithosphere and asthenosphere of the Central and Eastern regions of Northern Eurasia based on seismic data. Physics of the Solid Earth (English edition), Soviet Academy of Sciences, v.21, N2, pages 100-110, 1985.

Ryaboy, V.Z. Upper mantle structure studies by explosion seismology in the USSR. Delphic Associates, 154 pages, 1989.

Ryaboy, V.Z. The Earth's crust and upper mantle structure and lateral inhomogeneities beneath Northern Eurasia. Nuclear monitoring research at the Center for Seismic Studies. Sci. Report N1, 64 pages, 1991.

Sabitova, T.M. Seismic wave velocities in Northern Kyrgizia and their use for epicenter location. Seismicity of Tien-Shan, ILM Publ.House, Frunze, pages 27-49, 1989.

Schaff, D., and P.G. Richards. Lg-wave cross correlation and double-difference location: application to the 1999 Xiuyan, China, sequence, Bull. Seism. Soc. Amer., submitted for publication, June, 2003.

Schultz, C.A., S.C. Myers, J. Hipp, and C.J. Young. Nonstationary Bayesian Kriging: A predictive technique to generate spatial corrections for seismic detection, location and identification, Bull. Seism. Soc. Amer., 88, 1275-1288, 1998.

Seismic Models of the Lithosphere of the main Geostructures in territory of the USSR, Moscow, Nauka Publ. House, 311 pages, 1980 (in Russian).

Seleznev, V.S., V.M. Solovyev, I.V. Zhemchugova. Deep structure of Altay-Sayan region from the seismological systems of observations. Seismology in Siberia. Novosibirsk, Nauka Publ.House, pages 222-228, 2000 (in Russian).

Shatsilov, V.I. Methods of Evaluating Seismic Hazard, Nauka Publ. House, Alma-Ata, pages 65-78, 1989.

Shatsilov, V.I., et al. Velocity Models of the Earth's Crust in Kazakhstan, Eurasia Publ. House, Almaty, 105 pages, 1993 (in Russian).

Singh, D. D. Shear wave velocity structure over the eastern Indian subcontinent, Tectonophysics 230, 127-134, 1994.

Srivastava, H. N., R. K. Verma, G. S. Verma, and H. M. Chaudhury. Crustal studies of the Koyna region using explosion data from deep seismic sounding, Tectonophysics 110, 61-72, 1984.

Starovoit, O.E., et al. in Proceedings of a Workshop on IMS Location Calibration, Oslo, March 2000.

Sultanov, D.D., J.R. Murphy, and Kh.D. Rubinstein. A Seismic Source Summary for Soviet Peaceful Nuclear Explosions, Bull. Seism. Soc. Amer., 89, vol.3, 640-647, 1999.

Travel time table of regional phases for several Chinese regions. Chinese Seismological Bureau. Beijing, 178 pages, 1989 (in Chinese).

Tsibulchik, G.M. Travel time data of the regional phases and the Earth's crustal structure in the Altay-Sayan region. In the book: Regional Geophysical Studies in Siberia. Novosibirsk, Nauka Publ. House, pages 159-169, 1967 (in Russian).

Ulomov, V.I., A.B. Aronov. Travel-time table of main P and S phases for seismic waves observed in Uzbekistan at epicentral distances up to 1000 km, Technical report, 1977.

Volvovsky, B. Probabilistic Geophysical Models of the Earth's Crust of the main structure of Central Asia. Moscow, Nauka Publ. House, 1991 (in Russian).

Waldhauser, F., and P.G. Richards. Reference events and empirical Source Specific Station Corrections for regional phases at IMS stations in China, Bull. Seism. Soc. Amer., submitted for publication, June 6, 2003.

Working Group B, Recommendations for seismic event location calibration development, CTBT/ WGB/TL-2/18, 1999.

Xiu, J.-G., C. Zhang, and K.-X. Qiu. Development of Regionalized Travel-Time Tables in China, Department of Science, Technology, and Monitoring, State Seismological Bureau, Seismology Publisher (Beijing, China), 1989.

Xu, Shaoxie. A Review of Information on Seismic Event Location in China, in Proceedings of the Second Workshop on IMS Location Calibration, Oslo, Norway, March 2000.

Yang, X., I. Bondár, K. McLaughlin, and R. North. Source Specific Station Corrections for Regional Phases at Fennoscandinavian Stations, Pure Appl. Geophys., 158, 35-57, 2001.

Yang, X., I. Bondár, K. McLaughlin, R. North, and W. Nagy. Path-Dependent Phase Travel-Time Corrections for the International Monitoring System in North America, Bull. Seism. Soc. Amer., 91, 1831-1850, 2001.

Yang, X. and C. Romney. PIDC Ground Truth (GT) Datatbase, CMR Technical Report, CMR-99/15, May 1999.

Yang, X., R. North, C. Romney, and P. G. Richards. Worldwide Nuclear Explosions, in press for the International Handbook of Earthquake and Engineering Seismology, Part B, edited by W.H.K. Lee, H. Kanamori, P. Jennings, and C. Kisslinger on behalf of the International Association of Seismology and Physics of the Earth's Interior, Academic Press, 2003.

Yang, Z.-X., F. Waldhauser, Y.-T. Chen, and Paul G. Richards, Relocation of Earthquakes in Central-Western China using the Double-Difference Earthquake Location Algorithm, ms. submitted for publication, Journal of Seismology, 2003.

Yakovleva, I.B. Travel times for West Uzbekistan. In the book: Seismology and Seismogeology of Uzbekistan. FAN Publ. House, Tashkent, pages 52-60, 1971.

Zhao, L.S., J. Xie. Lateral variations in compressional velocities beneath the Tibetan Plateau from Pn travel time tomography, Geophys. J. Int., v115, pages 1970-1984, 1993.

Zunnunov, F.K. Lithosphere of Central Asia from seismic data. Tashkent, FAN Publishing House, 208 pages, 1985 (in Russian).

Appendix A Compilation of Seismic Reference Events in Asia

Overview

Effective verification of the Comprehensive Nuclear-Test-Ban Treaty (CTBT) critically depends on the availability of seismic reference events in the area monitored. Such reference events, or ground truth (GT) events, are seismic events with well-determined hypocenter locations and origin times. They improve International Data Centre (IDC) monitoring capabilities for nearby events by providing accurate travel time corrections relative to the standard Earth model IASP91 (Kennett and Engdahl, 1991) at surrounding stations of the International Monitoring System (IMS).

A critical step in collecting reference events for seismic monitoring purposes is the assessment of the location uncertainty, generally referred to as the GTn level of an event (n = horizontal location uncertainty in km). GT0 reference events, for example, have perfectly known locations and origin times, and are typically obtained from peaceful nuclear or chemical explosions. Since the global distribution of man-made sources with well known source parameters is sparse, data from moderate size earthquakes must also be used to obtain empirical travel times from seismically active areas to IMS stations within 20° distance. The location of earthquakes, however, is generally less well known, resulting in events of GT5 quality or lower. Only in a few cases, such as well monitored aftershock sequences, is GT1 achieved. The quality of earthquake locations depends on several factors, including the distribution of seismic stations (network geometry), the quality of the phase arrival time picks, and knowledge of the Earth structure (e.g. Pavlis, 1986; Gomberg et al., 1990).

During the course of this project we have compiled 809 seismic reference events that were used to calibrate IMS stations in eastern Asia (Figure A1). The hypocentral parameters of these reference events are listed in Appendix B, and are provided with additional information as an electronic supplement in CSS3.0 format. The following is a brief summary of the collected events:

- Peaceful Nuclear Explosions (PNE) in Russia (80 events)

- Underground Nuclear Explosions (UNE) at
  Semipalatinsk test site (76 events in 1 cluster)
  Lop Nor test site (9 events in 1 cluster)
  Indian test site (1 event)
  Pakistan test site (1 event)
- Chemical Explosions in
  Jilin Province, NE China (4 events in 1 cluster)
  Semipalatinsk Test Site (7 events in 1 cluster)
- Earthquakes from local networks in
  Sichuan Province, China (119 events in 4 clusters)
  Liaoning Province, China (16 events in 1 cluster)
  southeastern Korea (1 event)
  Kyrgyzstan (27 events)
  Taiwan (4 events)
  Japan (9 events)
  Nilore, Pakistan (44 sources)
- Earthquakes from the ABCE regional network in China (64 events in 7 clusters) (see below)
- Earthquakes from regional and global network (347 events in 9 clusters)

A great variety of data sets and techniques were employed to accurately locate these events and/or to determine their location uncertainty. Appendix B includes detailed information on the method of location and their performance when applied to the individual events. Figure A2 gives an overview of the quality levels of the reference events collected.

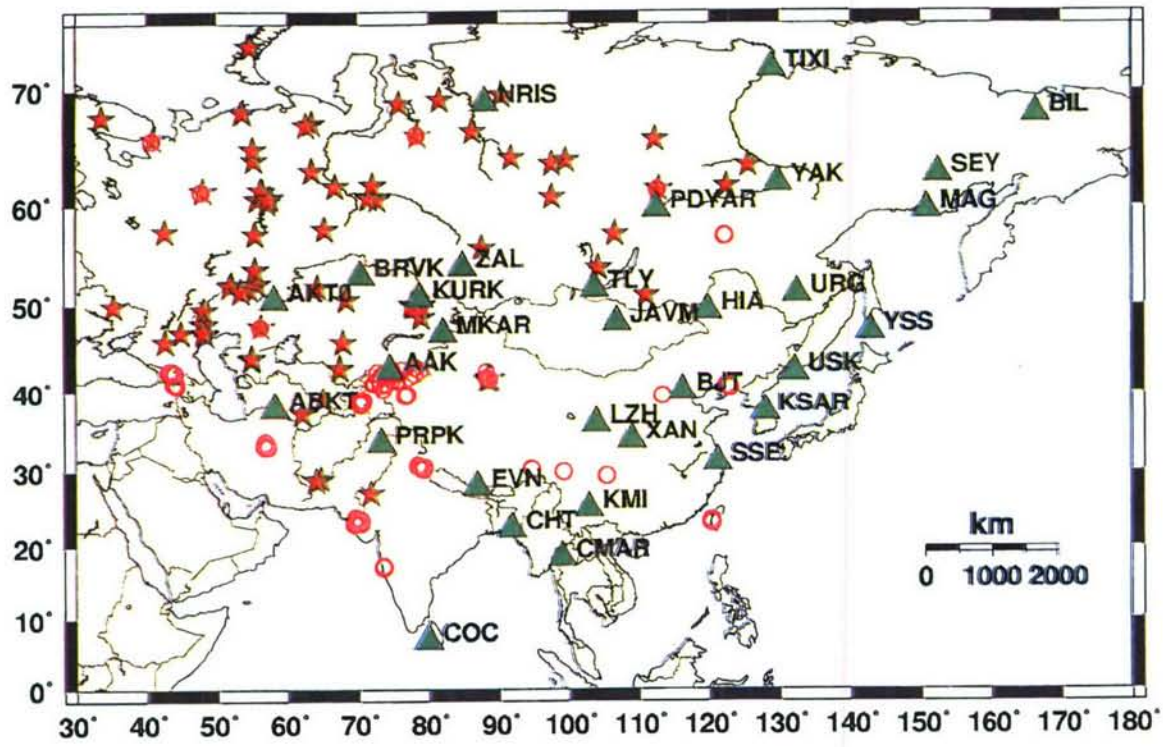


Figure A1. Map of GT event locations. Stars are nuclear explosions, magenta circles are earthquakes, triangles are IMS stations.

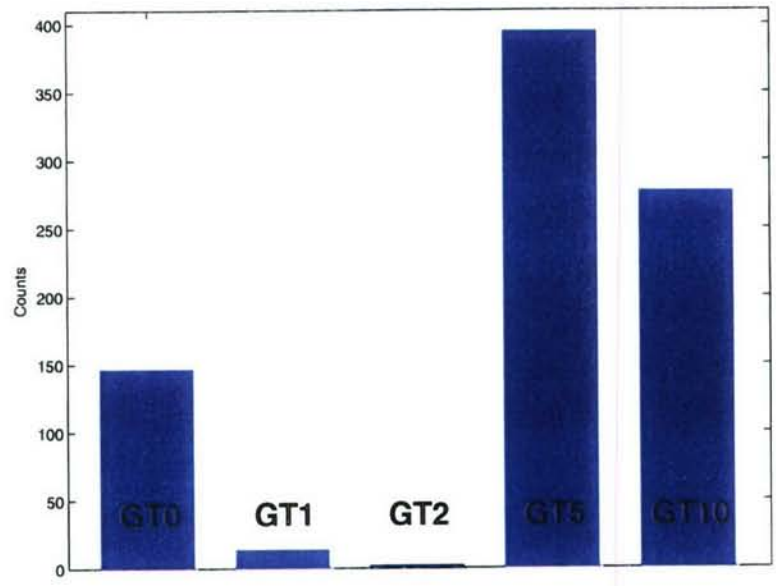


Figure A2. Distribution of GT quality of reference events collected in this study.

In the case of chemical and peaceful nuclear explosions (PNEs), the location and origin time, and thus the seismic travel times to a specific IMS station that recorded the event, are fairly well known (e.g., Sultanov et al., 1999). Many of these PNE reference events are considered ground truth data at the GT0 and GT1 level; i.e. locations that are precisely known (GT0) or known within 1 km of their given location (GT1). Many reference events, though, were obtained from careful analysis of seismic, satellite imagery, and/or geologic data to obtain hypocentral parameters of earthquakes at the GT5 to GT10 level (i.e., events with locations accurate to within 5 to 10 km). Many of these earthquake locations are obtained with a local/regional seismic network that fulfills the evaluation metrics for GT5 candidate events established by the monitoring research community at the 1999 Oslo Location Workshop (CTBT/WGB/TL-2/18,1999). These metrics at the 95% confidence level are:

- at least 10 stations within 250 km from the epicenter,
- maximum primary azimuthal gap $\leq 110°$ at stations within 250 km,
- maximum secondary azimuthal gap $\leq 160°$ at stations within 250 km,
- at least one station within 30 km.

Standard earthquake location algorithms such as *HYPOINVERSE* (Klein, 2002) or the *LocSat* program (Bratt and Bache, 1988), currently used for monitoring purposes at the IDC in Vienna, were employed to solve for many of the hypocenter locations and associated location uncertainties, in particular those that fulfill the GT5 candidate criteria. In China, which lacks sufficient high-quality reference events to empirically calibrate IMS stations, moderate to large size earthquakes occur frequently, but available seismic data for these earthquakes are sparse. To determine reference events for this region, we use a regional seismic data set, the Annual Bulletin of Chinese Earthquakes (ABCE) with about 10,000 events from 1985 to 1999. None of the events in the ABCE fulfill the GT5 candidate criteria, but they can be relocated to obtain precise relative locations of clustered events. The increased resolution in the relocated seismicity sharpens the spatial relationship to mapped fault information at the surface, allowing the assessment of the accuracy of the absolute locations. The following section describes this approach, which produces 64 GT5 events that are distributed in 7 clusters throughout central and eastern China, providing travel time information for *Pg*, *Pn*, *Sg*, and *Sn* phases to at least one of the six planned IMS stations; BJI, LHR, LZH, KMI, SSE, and XAN.

Reference Events in China Derived from Cluster Analysis and Fault Data

Data and Method

The electronic version of the Annual Bulletin of Chinese Earthquakes (ABCE) (z-files, included in the IASPEI International Handbook of Earthquake and Engineering, Part B, 2003) includes about 14,000 events in and near China with magnitudes up to M 6.8 which occurred during 1985-1999, with more than 10,000 events located in mainland China (Figure A3). P-and S-phase picks of remarkable consistency are available for 170 regional stations in and near China. In general, Pn-phase picks are reported to a tenth of a second, epicentral locations are rounded to the nearest tenth of a degree (introducing, presumably randomly distributed, location uncertainties of up to 5 km), and depths for about 50% of the events appear to be fixed at 10, 15, or 33 km. Comparison with event locations from local data and our own relocation results (see below) indicate that the average uncertainty of the ABCE locations is probably about 10 km, but may be larger in some areas.

Due to uncertainties of this order in ABCE locations we can not extract high-quality reference events directly from the catalog, but accurate event locations may be determined by relocating the events. The effect of model error can be minimized by using relative earthquake location methods such as the double-difference technique (Waldhauser and Ellsworth, 2000). By taking the difference in phase travel times between nearby events observed at a common station and inverting for event separation, common mode travel time errors are reduced without the use of station corrections. The double-difference algorithm is most efficient for clusters of events where hypocenters can be linked to their nearest neighbors over short distances, and a network of such links can connect events across large areas. The performance of the double-difference approach, therefore, depends on a sufficiently dense distribution of seismicity. The method can be applied to relocate events distributed over a wide area, which is not the case with other multiple-event location algorithms such as JHD (Douglas, 1967) or HDC (Jordan and Sverdrup, 1981) which employ station corrections that are fixed for a particular cluster.

Relocation of the ABCE data for the purpose of obtaining reference events is problematic because of the sparse station distribution for most of the events. Also, the presence of severely mislocated events in the ABCE may hamper the inversion, since the linearization of the non-linear double-difference location problem (which solves for adjustments to initial locations) requires the initial

locations to be close to the true value. To stabilize the inversion we search for clusters of well linked event pairs (at least 10 stations), and iteratively solve the system of double-difference equations by careful damping of the solution vector using the double-difference algorithm *hypoDD* (Waldhauser, 2001). Convergence to a stable solution is greatly helped by the high quality of the ABCE phase picks, and little contamination by outliers. A search of the ABCE for clusters of events that are most suitable for double-difference relocation in terms of network geometry and event density resulted in 36 clusters, ranging in size between 20 and 344 earthquakes. This analysis was done by searching about 460,000 *P*- and *S*-phase picks. For the 36 clusters, *P*- and *S*-phase pairs at common stations out to 2000 km distance are formed, and the differential data is inverted for event separation by means of weighted least squares. Regional 1-D layered velocity models are used to predict the travel time differences and partial derivatives. These models were adapted from the models used for routine locations at Chinese provincial seismic networks (Jih, 1998).

In many of the 36 clusters the high resolution relocations reveal detailed structural information about the active fault on which they occur, such as dip and strike. It is possible to validate the absolute location accuracy of such an event cluster by comparing the relocated seismicity with independent surface information. Extremely detailed fault data for mainland China have been prepared by the U.S. Geological Survey, derived from volumes on the regional geology of Chinese provinces published by the Geological Publishing House (Beijing, 1984-1993). The location of these fault lines are subject to uncertainties due to inconsistencies in the published maps and/or uncertainties related to the digitizing and GIS mapping process. In general the uncertainties range from a few hundreds of meters to a few kilometers in some rare cases. Specifically, the information on deep faults used in this study were drawn with very thick lines on the published Chinese maps, which translate to a possible maximum uncertainty of 0.5 km in the digital map provided by the USGS.

In order to extract potential reference events for the purpose of IMS station calibration from any of the 36 clusters, we have defined the following three criteria: The relocated seismicity

- indicates fault structure such as strike and dip,
- correlates with a nearby major, if possible isolated, fault mapped at the surface,
- and includes events of $M \geq 3.5$ that have small relative errors and are recorded at IMS stations within 2000 km distance.

Seven clusters that include a total of 289 events fulfill these criteria. These clusters are located in central and eastern China in the provinces of Sichuan, Shanxi, Tibet, Qinghai, Yunnan, and Meimongol (Figure A3).

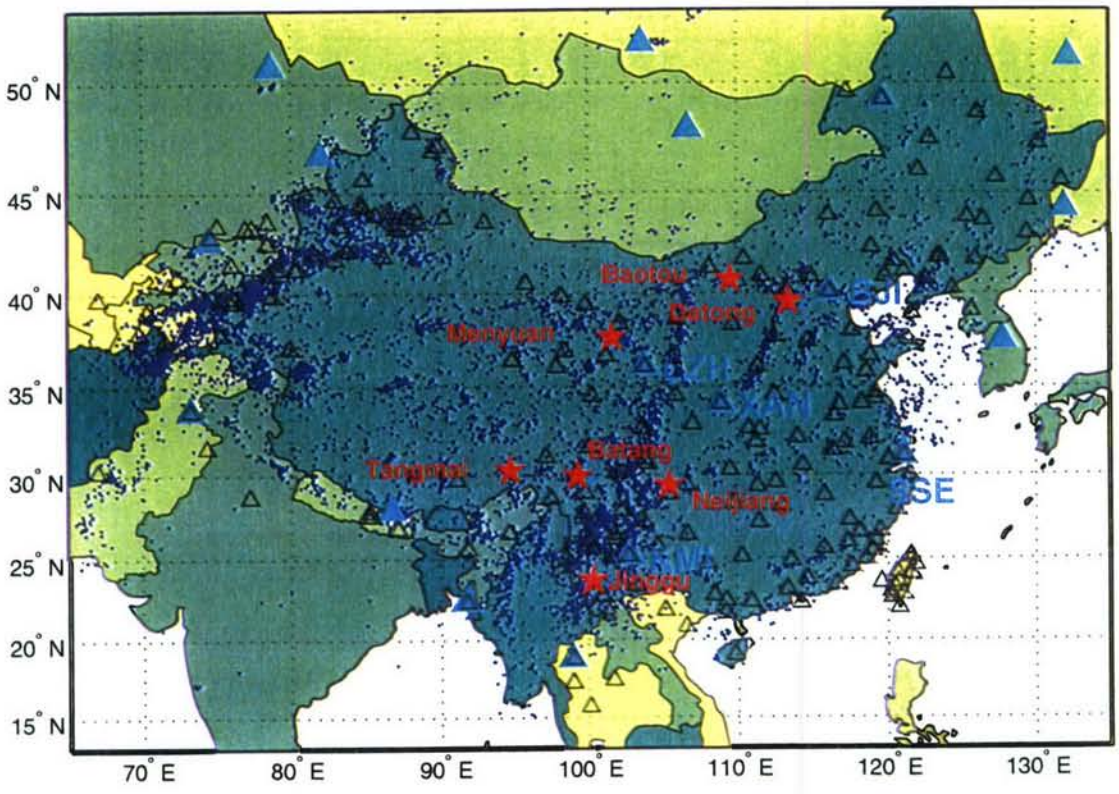


Figure A3. Events (blue dots) and Chinese stations (open triangles) listed in the Annual Bulletin of Chinese Earthquakes. IMS stations (solid cyan triangles) are indicated. Red stars indicate locations at which GT5 events were obtained.

Generation of GT5 Reference Events in Central and Eastern China

We start with a detailed description of the derivation of reference events in the cluster near Neijiang (Sichuan Province), followed by a summary of results obtained from 6 additional clusters. The Neijiang cluster (named after its closest city) in Sichuan Province includes 61 well linked events that were recorded at 31 stations between 1989-1999 (Figure A4). The largest

azimuthal gap is 83° and the closest station is more than 100 km away. Table A1 shows the regional velocity model used for relocation.

Table A1: 1-D *P*-velocity model for Neijiang cluster

Top of layer [km]	Vp, km/s
0.0	5.00
7.50	5.48
16.0	5.93
20.0	6.43
30.0	6.60
50.0	8.30

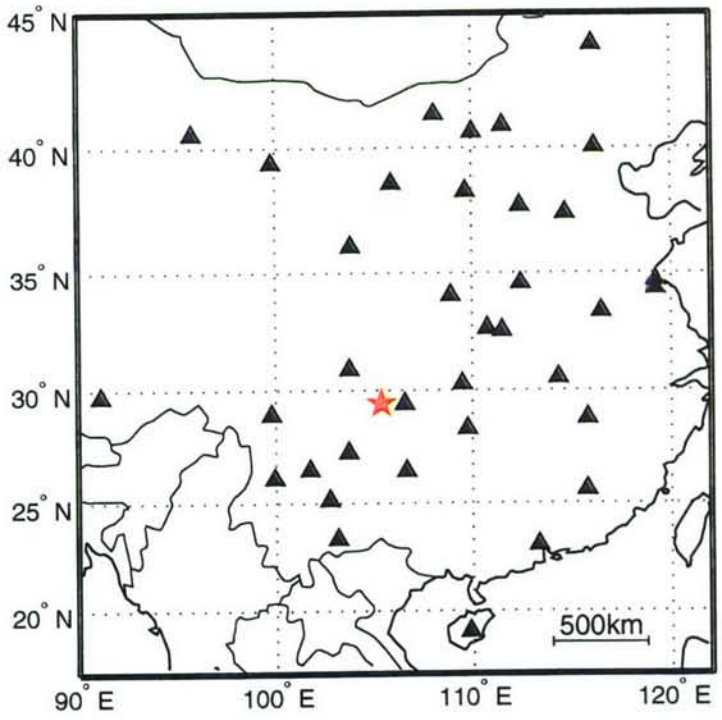


Figure A4. Stations (triangles) that recorded the 61 events near Neijiang, Sichuan Province. Red star indicates the location of the cluster

Figure A5 compares the double-difference epicenter locations with the locations listed in the ABCE. The double-difference locations indicate a much tighter distribution compared to the ABCE, and concentrate near a deep reverse fault mapped at the surface by Chinese scientists. Shifts between ABCE and double-difference locations range from 0.5 to 40 km, with a mean of about 13 km. Shifts in origin times range from -4.9 to 4.3 s, with a mean of -0.08 s and a standard deviation of about 2 s. The root mean square (*rms*) residual after relocation is 0.7 s, down 72% from the initial value. A bootstrap analysis of the remaining differential time residuals (see Waldhauser and Ellsworth, 2000, for details) has been performed to assess the relative location uncertainty of the double-difference locations. These errors are indicated in Figure A6 in map view and in fault-perpendicular cross section. The error ellipses and crosses (in map view and cross section, respectively) contain 90% of the 200 bootstrap samples derived for each event. The *rms* values for semi-major and minor axes are 1.5 km and 0.85 km, respectively, and 1.5 km for errors in depths, for all 61 events.

The relocated seismicity images a ~25 km deep northwest dipping fault which correlates well with a mapped surface trace described as a deep reverse fault on the digital fault map (Figure A6). Eight events with $M \geq 4$ appear to locate on this fault, for which the inferred downward projection is indicated by a dashed line. A ninth $M \geq 4$ event, having larger uncertainty, locates to the southeast away from the fault. Considering the uncertainty in relative locations being smaller than 2 km for the eight $M \geq 4$ events, and the juxtaposition with independently mapped surface information, we select these eight larger events as reference events of GT5 quality (see Appendix B for hypocentral parameters). Note that the cluster centroid of the double-difference locations has not been shifted to line up with the surface trace of the fault. The fault information is considered independent data that validates the absolute location of the GT5 events.

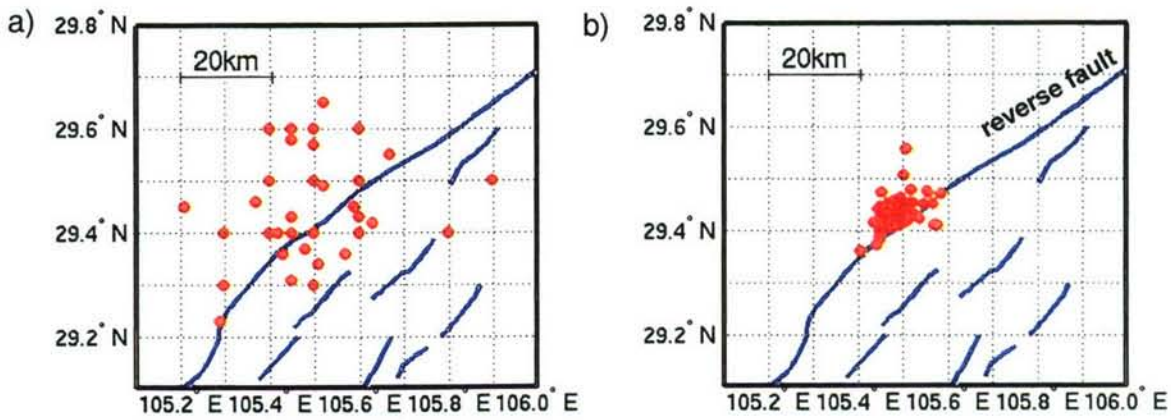


Figure A5. Map view of (a) ABCE locations and (b) double-difference locations (red dots). Blue lines indicate mapped surface traces of deep reverse faults.

Several tests were performed to verify that the northwest dipping trend of the seismicity and its correlation with the surface trace are robust. The tests included the use of different models (including the IASP91 tables), the use of only a selected number of stations (e.g., stations only within 600 km distance, and a station set with the closest station removed), and repeated relocation of the cluster with one event removed in each run. The results from these tests indicate changes in hypocenter locations not more than a couple of hundred meters, and in each case the relocated GT5 events locate on a northwest dipping structure consistent with surface observations.

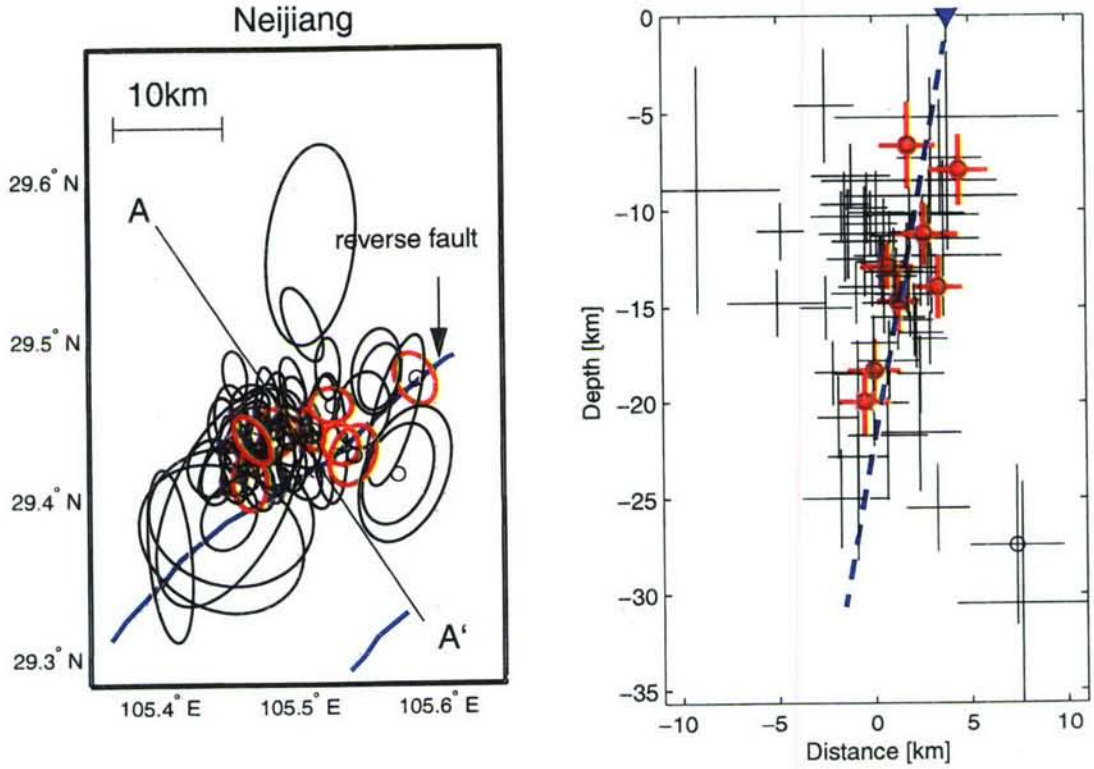


Figure A6. Relocated events in (a) map view and (b) fault perpendicular cross section along A-A'. Ellipses and crosses indicate bootstrap errors at the 90% confidence level. Events in red are selected to be of GT5 quality. Blue line indicates fault at the surface, blue triangle its projection on the cross section. Blue dashed line indicates assumed fault dip based on seismicity. Black open circles denote events with M>4. Dotted ellipses indicate approximate areas associated with GT5 and GT10 events.

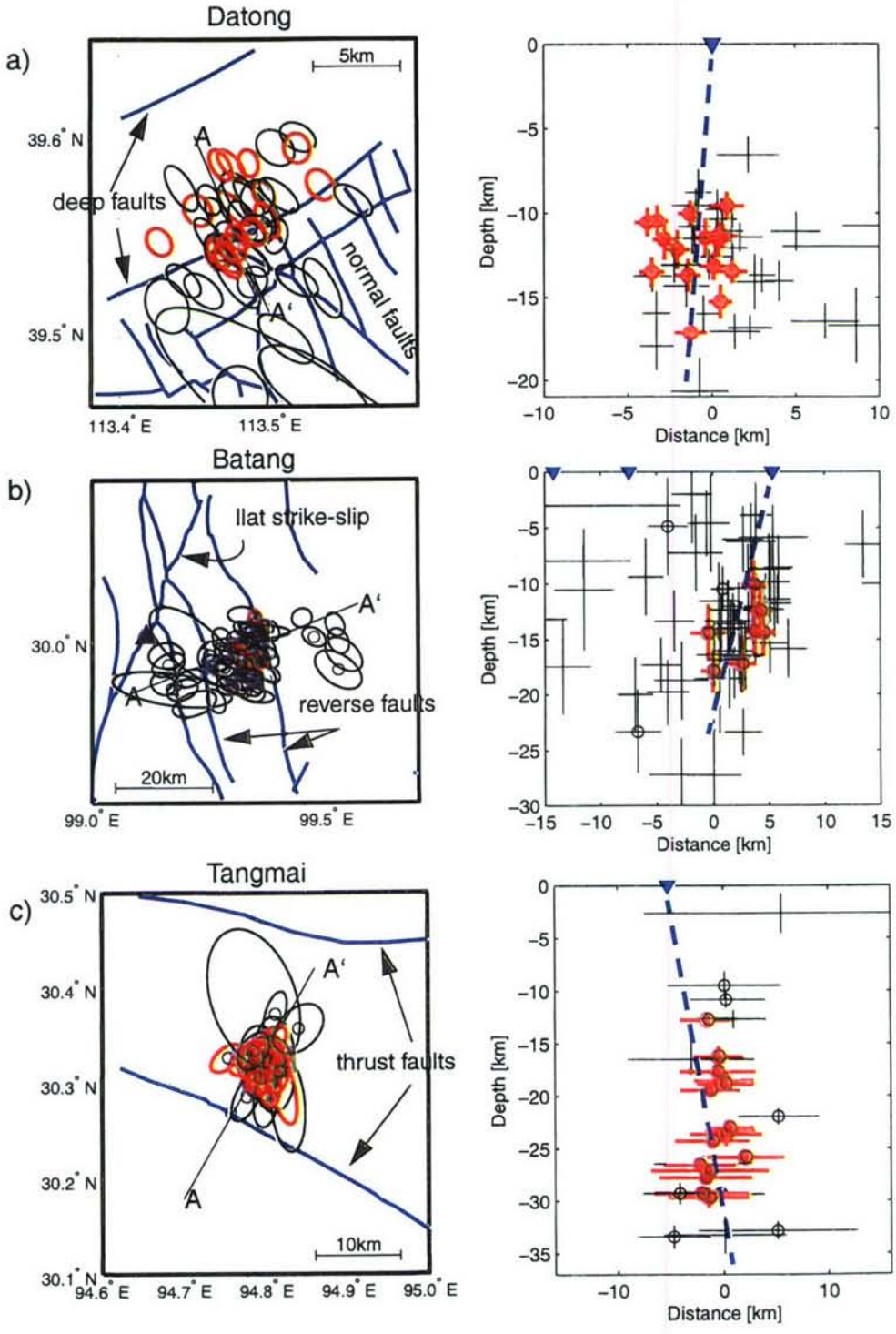
We have investigated the spatial relationship between high-precision seismicity location and mapped surface traces in six additional clusters (see Figure A3 for location). A total of 64 reference events (including the Neijiang events) are assigned GT5 quality (Appendix B), based on event magnitudes (they are large enough for far-regional detections), their relative error estimates, and their alignment with mapped surface structures:

- 8 events near Neijiang, Sichuan province (see Figure A6a)
- 16 events near Datong, Shanxi province (Figure A7a)
- 7 events near Batang, Sichuan province (Figure A7b)
- 16 events near Tangmai, Tibet (Figure A7c)
- 5 events near Menyuan, Qinghai Province (Figure A7d)
- 7 events near Jimggu, Yunnan Province (Figure A7e)

- 5 events near Baotou, Meimongol (Figure A7f).

Figures 7a-f show map views and cross sections of the relocated events in each of the clusters. Relative error estimates are at the 90% confidence level. The average relative travel time residual for the 64 events decreases by 50% after relocation. Lines in map views indicate fault trace, and triangles in cross sections indicate the approximate projection of the fault trace. Open circles in cross sections indicate events with $M \geq 3$, except in the Batang cluster ($M \geq 5$), and the Tangmai cluster ($M \geq 4.5$). No magnitudes are available for events in the Datong cluster. Solid circles indicate reference events of GT5 quality for which hypocentral parameters are listed in Appendix B. Faults are labeled as indicated on the digital fault map, for example the type of faulting, whether they are deep reaching, and in some cases the direction of fault dip. Note that for some events in the Tangmai, Jinggu, and Baotou clusters, relative depth errors are smaller than errors in the horizontal directions. The somewhat large horizontal errors are caused by azimuthal gaps in nearby stations, while relative depths are still well constrained by downgoing ray paths of *Pn* phases observed at great distances.

For the first three clusters listed above, the relocated seismicity supports the characterization of the corresponding faults given in the digital fault data base. For the seventh cluster (Baotou, Figure A7f) the correlation between seismicity and surface data is less clear, but we still consider the events to be of GT5 quality given the isolated location of the corresponding deep fault. For the Menyuan and Jinggu clusters a shift of the cluster centroid was necessary to align the seismicity with the mapped tectonic structures. The shift for the Menyuan cluster centroid was about 0.05° to the north and 0.035° to the east. For the Jinggu cluster it was 0.01° and 0.09° to the south and east, respectively, to correlate with a deep fault and a possible step-over configuration (Figure A7e). These significant shifts (> 5km) applied to the ABCE absolute locations before relocation could be verified with available data from a printed version of the ABCE for events that occurred in 1985 and 1986, and in the years 1991-1995. The printed ABCE reports earthquake locations to the nearest hundredth of a degree. Comparison between the printed and the electronic ABCE data for the rest of the clustered reference events indicate shifts smaller than 5 km.


Datong
a)
5km
39.6° N
39.5° N
A
A'
deep faults
normal faults
113.4° E
113.5° E
Depth [km]
Distance [km]
Batang
b)
llat strike-slip
A'
A
30.0° N
reverse faults
20km
99.0° E
99.5° E
Depth [km]
Distance [km]
Tangmai
c)
30.5° N
30.4° N
30.3° N
30.2° N
30.1° N
A'
A
thrust faults
10km
94.6° E
94.7° E
94.8° E
94.9° E
95.0° E
Depth [km]
Distance [km]

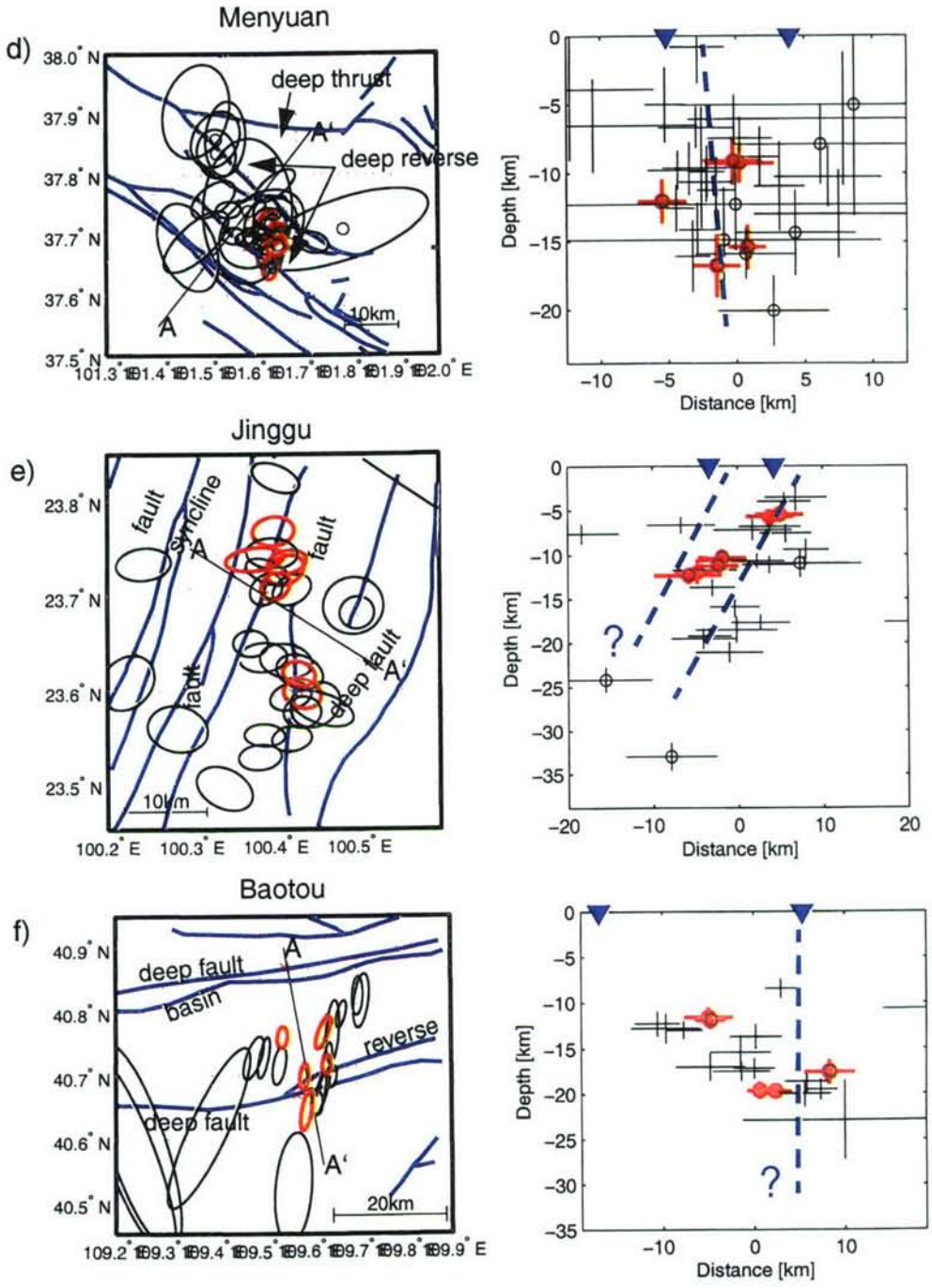


Figure A7. Double-difference locations of events near (a) Datong, (b) Batang, (c) Tangmai, (d) Menyaun, (e) Jinggu, (f) Baotou. See text and caption to Figure A6 for description.

Evaluation of Solution Quality

Although the double-difference algorithm is somewhat sensitive to absolute locations through a chosen model, we keep the initial cluster centroid fixed during inversion. Thus we assume that systematic biases in the ABCE locations are smaller than 5 km, and that the short period mislocations (such as rounding errors) are randomly distributed. Although we used surface information to validate the absolute location of the clusters and the reference events they include, we are not able to quantify absolute location errors in a standard approach using the ABCE data alone. For the Neijiiang cluster we are fortunate to have *P*- and *S*-phase travel time data between 1992-1999 from a dense local seismic network in the Yunnan/Sichuan provinces (Zhi-xian Yang, pers. communication). To investigate absolute location uncertainty of the Neijiang-GT5 events we simultaneously invert these data for hypocenter adjustments, 1-D velocity model corrections, and station corrections using the program *velest* (Roecker, 1977; Kissling et al., 1994). Figure A8a shows the station distribution used for relocation, with the closest station at a distance of about 50 km to the east. We choose only events that have 20 readings or more, and a maximum station gap that is smaller than 120 degrees, to offset convergence problems due to the unreliable initial locations (indicated by open circles in Figure A8b). 20 events were relocated, and two of them (1997/02/24 and 1997/08/13) are among the 8 GT5 events selected from the DD locations. The relocated events, shown as solid circles in Figure A8b, cluster near the fault, similar to the double-difference locations using ABCE data (Figure A5). For the two reference events, the differences between the *hypoDD* (solid red squares) and *velest* (solid red circles) locations are smaller than 3 km, indicating that the 2 *hypoDD* locations are indeed of GT5 quality, and therefore also the 6 additional *hypoDD* locations since they were precisely relocated relative to the two. Note that the formal error estimates of the *velest* locations are 1.2 km and 0.9 km in EW and NS direction, respectively, and do not overlap with the relative location errors. It is likely that the absolute *velest* errors are underestimated.

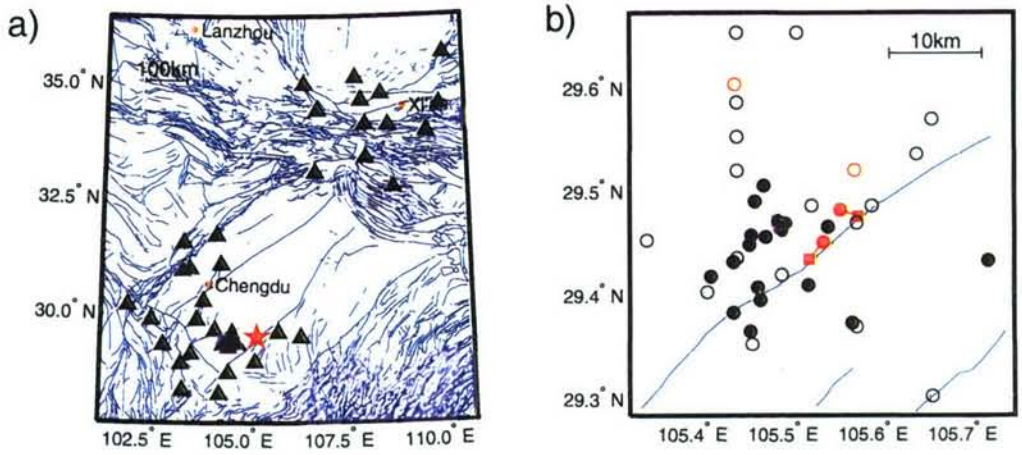


Figure A8. a) Distribution of local network stations (Zhi-xian Yang, pers. communication) that recorded 20 events in the Neijiang cluster with a azimuthal gap less than 120 degrees. The closest station is about 50 km away from the cluster centroid (indicated by a red star). Fault lines (blue) are from the digital fault map of China. b) Initial locations (open circles) and *velest* locations (solid circles) are shown. Red squares are *hypoDD* locations with assigned GT5 quality, red solid circles are the velest locations of the same events. Red lines indicate shifts between the two locations.

To obtain more robust absolute location errors for the GT5 events we use the location procedure *LocSat* that is currently used for nuclear test monitoring at the IDC. Event locations in this approach are determined via an iterative non-linear inverse technique, essentially that of Jordan and Sverdrup (1981) extended to include azimuth and slowness data. We apply the *LocSat* algorithm to both data sets, the ABCE data to locate all of the 8 GT5 events, and to Yunnan/ Sichuan local network data to locate 4 of the 8 GT5 events. In both studies the IASP91 tables are used to compute travel times and partial derivatives. Figure A9a shows the results from the ABCE data. The average in major and minor 95% error ellipse axes are 4.9 and 3.5 km, respectively, with the major axis predominantly oriented in northwest direction perpendicular to the fault. Differences between the *LocSat* and *hypoDD* locations range from 0.2 km to 13.6 km, with a mean of 7 km. In 3 of the 8 cases the differences are smaller than 5 km. *LocSat* locations are systematically shifted to the east, although a systematic shift in absolute locations can not be ruled out. Figure A9b shows *LocSat* locations for 4 events using the local Yunnan/Sichuan (YS) data. Average in major and minor axis are 5.2 km and 3.3 km, respectively, and shifts between *LocSat* and *hypoDD* locations are 3.4, 5.6, 6.1, 7.3 km for the 4 events located. A systematic shift to the

south is seen. Shifts between the mean of the ABCE/*hypoDD* locations and the mean of the ABCE/*LocSat* and the YS/*LocSat* locations are, in both cases, smaller than 5 km. Furthermore, in the case of the YS/*LocSat* locations, where we have better data coverage, the shifts are perpendicular to the fault, a direction that is less well constrained by the seismic data, but quite well constrained by the fault data. The average shift along the fault is only about 1 km. This verifies the GT5 solution quality of our 8 double-difference locations based on ABCE data and surface information.

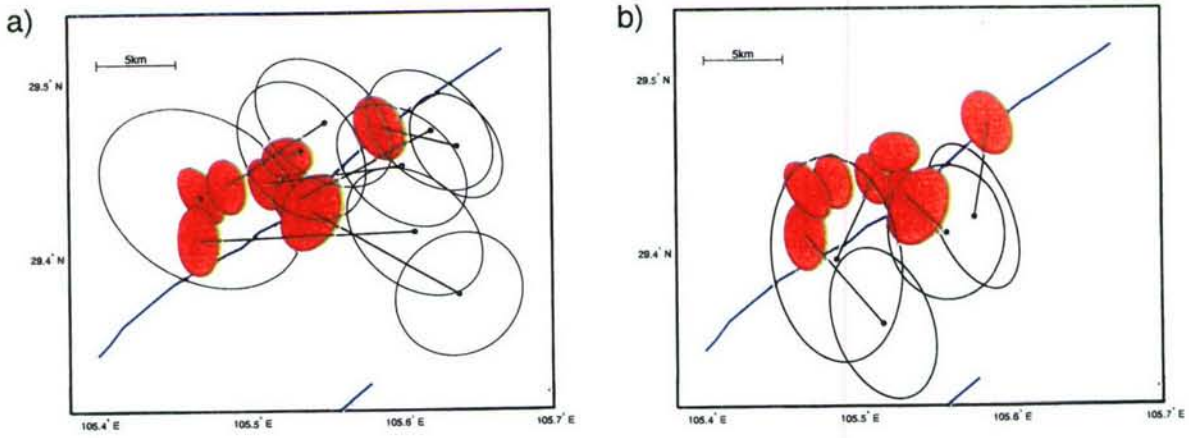


Figure A9. *hypoDD* (red solid ellipses) and *LocSat* (black open ellipses) locations of the eight Neijiang GT5 events using (a) the ABCE phase picks and (b) the Sichuan/Yunnan local earthquake data. Error ellipses are at the 95% confidence level. Only 4 events could be relocated in (b). Black lines indicate the shift between *LocSat* and *hypoDD* locations. Blue lines indicate mapped fault traces.

GT5 Travel Times to IMS Stations

Figure A10 shows the P-wave paths from each cluster of reference events to each IMS station that recorded at least one event. Figure A11 shows 192 GT5 travel time residuals relative to the median travel time of each cluster for each source-IMS station pair, for double-difference (solid circles) and ABCE (open circles) solutions. A significant reduction in residual scatter is observed, with the standard deviation decreasing from 1.27 s before to 0.61 s after relocation. Such residual clustering is consistent with the more compact double-difference locations compared to the ABCE locations (see Figure A5). The double-difference cluster analysis enabled the detection of eight apparent phase pick outliers (solid squares in Figure A11) (mostly events in the Neijiang and Menyuan

clusters) that were removed from further processing. These extreme outliers may indicate timing problems. Note that such outliers are generally downweighted or removed during the relocation process, and stations other than the IMS stations were used to relocate the events.

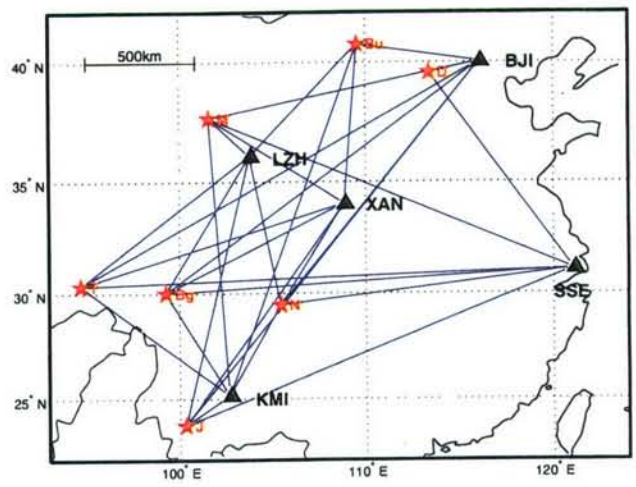


Figure A10. Paths of *P*-waves generated by clustered reference events (red stars) and observed at IMS stations (black triangle). N: Neijiang; D: Datong; Bg: Batang; T: Tangmai; M: Menyuan; J: Jimggu; Bu: Baotou.

P-wave travel time residuals that accumulate at each IMS station are shown in Figure A12, for each cluster of events and each station. Double-difference (solid circles) and ABCE (open circles) residuals are computed with respect to the IASP91 travel times. The somewhat larger spread of residuals seen in the Tangmai cluster may result from the 20 km depth range of the double-difference locations and a crustal velocity that may be faster than the IASP91 prediction (see Figure A7c). Most of the residuals lay in positive territory, in some cases reaching 5 seconds of travel time delay relative to the IASP91 model. These observations are consistent with tomographic results by Hearn and Ni (2000) that show slow sub-Moho velocities across eastern China, although a systematic shift in origin times can not be ruled out as a possible cause for the observed travel time delays. Negative *Pg*-residuals are observed at station BJI for nearby events in the Datong cluster, indicating that the true crustal velocity may be significantly faster than the IASP91 prediction.

Conclusions

We have generated GT5 solutions for 64 reference events in central and eastern China, an area with high seismic activity but sparse seismic data that does not fulfill the GT5 candidate event criteria. We obtained precise relative event locations from double-difference analysis of the Annual Bulletin of Chinese Earthquakes, and combined them with available fault information at the surface to validate absolute locations. The new reference events can be used to validate 3-D models and to support calculation of source-station path corrections relative to a standard Earth model for regional seismic phases recorded by IMS and surrogate stations in Asia.

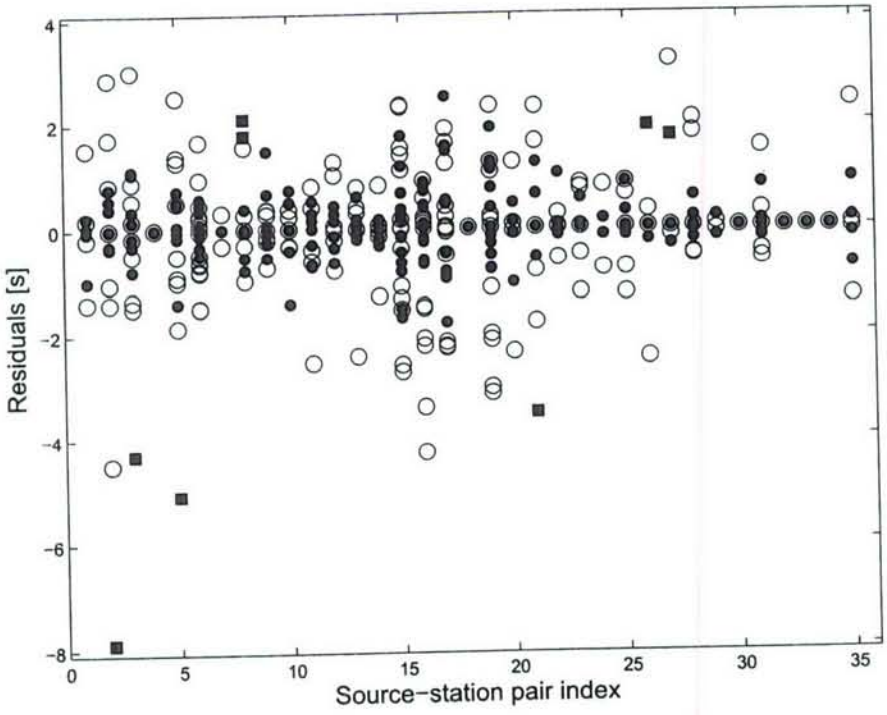


Figure A11. Deviations from the median travel time plotted for each cluster and station. Solid circles indicate GT5 travel time residuals, open circles residuals from the ABCE locations. Squares indicate phase picks that are considered outliers. The standard deviation for the GT5 residuals, after removing the outliers, is 0.61 sec. For the ABCE residuals it is 1.27 sec.

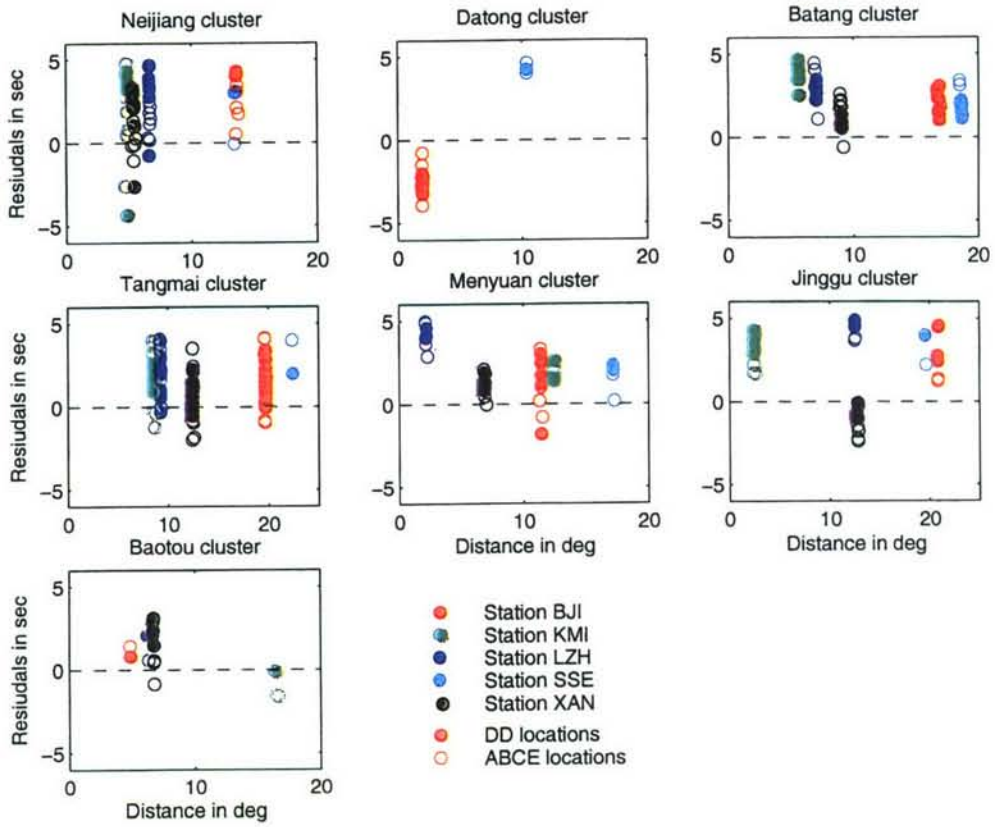


Figure A12. First arriving P-travel time residuals with respect to the IASP91 times displayed as a function of distance from each of the cluster centroid. Solid circles represent double-difference residuals, open circles ABCE residuals.

References

Bratt, S., and T. Bache, Locating events with a sparse network of regional arrays, *Bull. Seism. Soc. Amer.*. 78, 780-798, 1988.

Douglas, A., Joint epicenter determination, *Nature*, 215, 47-48, 1967.

Engdahl, E.R., R. van der Hilst, and R. Buland, Global teleseismic earthquake relocation with improved travel times and procedures for depth determination, *Bull. Seism. Soc. Amer.*, 88, 722-743, 1998.

Appendix B Seismic Reference Events

Date	Time	Lat	Lon	Depth	Mag	Src	GT	Met	Ref	Location	Footnote
1965/10/14	04:00:00.20	49.991	77.636	0.048	-	PNE	0	CS	SMR99	Sary-Uzen, Russia	1
1968/05/21	03:59:11.98	38.918	65.031	2.440	5.4	PNE	0	CS	SMR99	Pamuk, Russia	1
1968/07/01	04:02:00.50	47.909	47.912	0.597	5.5	PNE	5	CS	SMR99	Azgir, Russia	1
1969/09/02	04:59:58.61	57.220	55.393	1.212	4.8	PNE	0	CS	SMR99	Grifon-1, Russia	1
1969/09/08	04:59:58.70	57.220	55.417	1.208	4.8	PNE	0	CS	SMR99	Grifon-2 , Russia	1
1969/09/26	06:59:58.14	45.848	42.600	0.712	5.6	PNE	0	CS	SMR99	Stavropol, Russia	1
1969/12/06	07:02:59.85	43.867	54.800	0.407	5.8	PNE	0	CS	SMR99	Mangishlak-1, Ru	1
1970/12/12	07:00:59.83	43.850	54.800	0.497	6.0	PNE	5	CS	SMR99	Mangishlak-2, Ru	1
1970/12/23	07:00:59.76	44.025	54.933	0.470	6.0	PNE	0	CS	SMR99	Mangishlak-3, Ru	1
1971/03/23	06:59:58.38	61.400	56.200	0.127	5.5	PNE	5	CS	SMR99	Taiga, Russia	1
1971/07/02	17:00:01.13	67.283	63.467	0.542	4.7	PNE	0	CS	SMR99	Globe-4, Russia	1
1971/07/10	17:00:01.38	64.167	55.267	0.465	5.2	PNE	0	CS	SMR99	Globe-3, Russia	1
1971/09/19	11:00:01.08	57.508	42.643	0.610	4.5	PNE	0	CS	SMR99	Globe-1, Russia	1
1971/10/04	10:00:00.14	61.358	48.092	0.595	4.6	PNE	0	CS	SMR99	Globe-2, Russia	1
1971/12/22	06:59:59.00	47.897	48.133	0.986	6.0	PNE	10	CS	SMR99	Azgir, Russia	1
1972/04/11	06:00:01.92	37.350	62.050	1.720	4.9	PNE	5	CS	SMR99	Krater, Russia	1
1972/07/09	07:00:01.25	49.800	35.400	2.483	4.8	PNE	5	CS	SMR99	Fakel, Russia	1
1972/08/20	03:00:00.01	49.400	48.142	0.489	5.7	PNE	0	CS	SMR99	Region-3, Russia	1
1972/09/21	09:00:00.31	52.118	52.068	0.485	5.0	PNE	0	CS	SMR99	Region-1, Russia	1
1972/10/03	09:00:00.18	46.853	44.938	0.485	5.6	PNE	0	CS	SMR99	Region-4, Russia	1
1972/11/24	09:00:00.04	51.990	51.867	0.675	4.5	PNE	0	CS	SMR99	Region-2, Russia	1
1972/11/24	10:00:00.23	51.842	64.210	0.423	5.2	PNE	0	CS	SMR99	Region-5, Russia	1
1973/08/15	02:00:00.02	42.775	67.408	0.600	5.3	PNE	0	CS	SMR99	Meridian-3, Ru	1
1973/08/28	03:00:00.04	50.527	68.323	0.395	5.2	PNE	0	CS	SMR99	Meridian-1, Ru	1
1973/09/19	03:00:00.18	45.758	67.825	0.615	5.1	PNE	0	CS	SMR99	Meridian-2, Ru	1
1973/09/30	05:00:00.35	51.650	54.550	1.145	5.2	PNE	5	CS	SMR99	Sapphir-2, Russia	1
1974/08/14	15:00:00.19	68.903	75.823	0.534	5.4	PNE	0	CS	SMR99	Horizon-2, Russia	1
1974/08/29	15:00:00.39	67.085	62.625	0.583	5.0	PNE	0	CS	SMR99	Horizon-1, Russia	1
1975/09/29	11:00:00.43	69.578	90.337	0.834	4.8	PNE	0	CS	SMR99	Horizon-3, Russia	1
1976/07/29	05:00:00.50	47.870	48.150	1.000	5.9	PNE	5	CS	SMR99	Azgir, Russia	1
1976/11/05	03:59:59.98	61.458	112.860	1.522	5.3	PNE	0	CS	SMR99	Oka, Russia	1
1977/07/26	17:00:00.22	69.575	90.375	0.850	5.0	PNE	0	CS	SMR99	Meteorite-2, Ru	1
1977/08/10	22:00:00.10	50.955	110.983	0.494	5.0	PNE	0	CS	SMR99	Meteorite-5, Ru	1
1977/08/20	22:00:00.78	64.108	99.558	0.600	5.0	PNE	0	CS	SMR99	Meteorite-3, Ru	1
1977/09/10	16:00:00.18	57.251	106.551	0.550	4.8	PNE	0	CS	SMR99	Meteorite-4, Ru	1
1977/09/30	06:59:58.43	47.897	48.161	1.500	5.0	PNE	0	CS	SMR99	Azgir, Russia	1
1978/08/09	18:00:00.79	63.678	125.522	0.567	5.6	PNE	0	CS	SMR99	Kraton-4, Russia	1
1978/08/24	18:00:00.35	65.925	112.338	0.577	5.1	PNE	0	CS	SMR99	Kraton-3, Russia	1
1978/09/21	15:00:00.19	66.598	86.210	0.886	5.2	PNE	0	CS	SMR99	Kraton-2, Russia	1
1978/10/17	04:59:59.06	47.850	48.120	1.040	5.8	PNE	0	CS	SMR99	Azgir, Russia	1
1978/10/17	14:00:00.16	63.185	63.432	0.593	5.5	PNE	0	CS	SMR99	Kraton-1, Russia	1
1978/12/18	07:59:58.50	47.860	48.160	0.630	5.9	PNE	5	CS	SMR99	Azgir, Russia	1
1979/01/17	07:59:58.50	47.920	48.120	0.995	6.0	PNE	5	CS	SMR99	Azgir, Russia	1
1979/07/14	04:59:58.00	47.880	48.120	0.849	5.6	PNE	5	CS	SMR99	Azgir, Russia	1
1979/08/12	18:00:00.21	61.803	122.430	0.982	4.9	PNE	0	CS	SMR99	Kimberlite-4, Ru	1
1979/09/06	18:00:00.31	64.110	99.562	0.599	4.9	PNE	0	CS	SMR99	Kimberlite-3, Ru	1
1979/10/04	16:00:00.03	60.675	71.455	0.837	5.4	PNE	0	CS	SMR99	Kimberlite-1, Ru	1
1979/10/24	05:59:59.00	47.850	48.140	0.915	5.8	PNE	5	CS	SMR99	Azgir, Russia	1
1980/10/08	06:00:00.29	46.757	48.275	1.050	5.2	PNE	0	CS	SMR99	Vega-1, Russia	1

1980/12/10	07:00:00.06	61.750	66.750	2.485	4.6	PNE	5	CS	SMR99	Angara, Russia	1
1981/05/25	05:00:00.32	68.200	53.500	1.511	5.5	PNE	5	CS	SMR99	Pyrite, Russia	1
1981/09/26	05:00:00.28	46.790	48.313	1.050	5.2	PNE	0	CS	SMR99	Vega, Russia	1
1981/09/26	05:03:59.94	46.771	48.304	1.050	5.3	PNE	0	CS	SMR99	Vega, Russia	1
1981/10/22	14:00:00.36	63.800	97.550	0.581	5.1	PNE	5	CS	SMR99	Shpat-2, Russia	1
1982/07/30	21:00:00.00	53.800	104.150	0.554	5.0	PNE	5	CS	SMR99	Rift-3, Russia	1
1982/10/10	05:00:00.23	61.550	112.850	1.502	5.3	PNE	5	CS	SMR99	Neva-1, Russia	1
1982/10/16	06:00:00.15	46.759	48.247	0.947	5.2	PNE	0	CS	SMR99	Vega, Russia	1
1982/10/16	06:05:00.08	46.752	48.258	0.991	5.2	PNE	0	CS	SMR99	Vega, Russia	1
1982/10/16	06:10:00.10	46.766	48.288	1.100	5.2	PNE	0	CS	SMR99	Vega, Russia	1
1982/10/16	06:15:00.17	46.760	48.300	1.057	5.4	PNE	0	CS	SMR99	Vega, Russia	1
1983/07/10	03:59:59.99	51.363	53.306	0.907	5.3	PNE	0	CS	SMR99	Lira, Russia	1
1983/07/10	04:04:59.94	51.367	53.327	0.917	5.3	PNE	0	CS	SMR99	Lira, Russia	1
1983/07/10	04:09:59.85	51.380	53.340	0.841	5.3	PNE	0	CS	SMR99	Lira, Russia	1
1983/09/24	05:00:00.03	46.783	48.315	1.050	5.2	PNE	0	CS	SMR99	Vega, Russia	1
1983/09/24	05:05:00.00	46.788	48.297	1.050	5.1	PNE	0	CS	SMR99	Vega, Russia	1
1983/09/24	05:10:00.08	46.767	48.310	0.920	5.0	PNE	0	CS	SMR99	Vega, Russia	1
1983/09/24	05:15:00.14	46.749	48.303	1.100	5.2	PNE	0	CS	SMR99	Vega, Russia	1
1983/09/24	05:19:59.93	46.754	48.289	0.950	5.4	PNE	0	CS	SMR99	Vega, Russia	1
1983/09/24	05:25:00.00	46.766	48.274	1.100	5.3	PNE	0	CS	SMR99	Vega, Russia	1
1984/07/21	02:59:59.81	51.358	53.319	0.846	5.4	PNE	0	CS	SMR99	Lira, Russia	1
1984/07/21	03:04:59.71	51.371	53.337	0.955	5.3	PNE	0	CS	SMR99	Lira, Russia	1
1984/07/21	03:09:59.85	51.391	53.351	0.844	5.4	PNE	0	CS	SMR99	Lira, Russia	1
1984/08/25	19:00:00.33	61.900	72.100	0.726	5.3	PNE	5	CS	SMR99	Quartz-3, Russia	1
1984/08/28	02:59:59.84	60.300	57.100	2.065	4.4	PNE	5	CS	SMR99	Helium, Russia	1
1984/08/28	03:04:59.90	60.700	57.500	2.075	4.4	PNE	5	CS	SMR99	Helium, Russia	1
1984/09/17	21:00:00.03	55.834	87.526	0.557	5.0	PNE	0	CS	SMR99	Quartz-4, Russia	1
1985/07/18	21:15:00.29	65.994	41.038	0.772	5.1	PNE	0	CS	SMR99	Agate, Russia	1
1987/04/19	04:00:00.01	60.600	57.200	2.015	4.5	PNE	5	CS	SMR99	Helium, Russia	1
1987/10/03	15:15:00.03	47.600	56.200	1.002	5.3	PNE	5	CS	SMR99	Batholith-2, Ru	1
1988/08/22	16:20:00.07	66.280	78.491	0.829	5.3	PNE	0	CS	SMR99	Ruby-2, Russia	1
1988/09/06	16:19:59.94	61.361	48.092	0.820	4.8	PNE	0	CS	SMR99	Ruby-1, Russia	1
1997/06/25	18:50:23.48	35.803	129.248	14.2	4.3	EQ	5	HI	LDEO	Kyungju, Korea	3
1998/08/12	15:00:08.18	42.865	128.223	0.000	3.0	EX	2	CS	FW	Jilin, China	4
1998/08/18	14:00:06.69	42.914	129.324	0.000	3.0	EX	0	CS	FW	Jilin, China	4
1998/08/19	15:00:07.79	42.091	128.739	0.000	3.0	EX	0	CS	FW	Jilin, China	4
1998/08/25	15:00:07.46	42.427	126.748	0.000	3.0	EX	2	CS	FW	Jilin, China	4
1993/08/20	06:37:54.64	29.440	105.485	18.4	4.5	EQ	5	DD	LDEO	Neijiang, China	2
1994/04/14	17:57:06.24	29.441	105.511	14.7	4.4	EQ	5	DD	LDEO	Neijiang, China	2
1995/12/26	03:31:08.15	29.456	105.526	12.9	4.2	EQ	5	DD	LDEO	Neijiang, China	2
1996/01/16	00:08:15.86	29.408	105.467	6.7	4.2	EQ	5	DD	LDEO	Neijiang, China	2
1997/02/24	18:43:04.24	29.431	105.532	14.0	4.5	EQ	5	DD	LDEO	Neijiang, China	2
1997/08/13	08:13:29.83	29.473	105.587	11.2	4.8	EQ	5	DD	LDEO	Neijiang, China	2
1998/02/18	06:20:57.43	29.435	105.469	20.0	4.0	EQ	5	DD	LDEO	Neijiang, China	2
1999/08/17	10:41:05.03	29.425	105.541	7.9	4.8	EQ	5	DD	LDEO	Neijiang, China	2
1989/10/18	15:15:25.59	39.563	113.478	17.1	NA	EQ	5	DD	LDEO	Datong, China	2
1989/10/18	17:01:33.10	39.562	113.454	12.2	NA	EQ	5	DD	LDEO	Datong, China	2
1989/10/18	18:20:46.04	39.546	113.428	13.7	NA	EQ	5	DD	LDEO	Datong, China	2
1989/10/18	19:37:49.40	39.585	113.476	13.5	NA	EQ	5	DD	LDEO	Datong, China	2
1989/10/19	10:29:02.70	39.585	113.469	10.5	NA	EQ	5	DD	LDEO	Datong, China	2
1989/10/19	12:32:15.48	39.541	113.467	15.3	NA	EQ	5	DD	LDEO	Datong, China	2
1989/10/19	13:59:58.75	39.586	113.488	10.5	NA	EQ	5	DD	LDEO	Datong, China	2
1989/10/19	17:56:47.80	39.570	113.498	10.0	NA	EQ	5	DD	LDEO	Datong, China	2
1989/10/19	23:54:31.40	39.594	113.520	11.6	NA	EQ	5	DD	LDEO	Datong, China	2

1989/10/20	11:41:41.47	39.575	113.536	11.5	NA	EQ	5	DD	LDEO	Datong, China	2
1989/10/23	13:19:33.20	39.557	113.500	13.2	NA	EQ	5	DD	LDEO	Datong, China	2
1989/10/23	17:07:54.20	39.548	113.480	11.4	NA	EQ	5	DD	LDEO	Datong, China	2
1989/10/29	02:22:42.93	39.539	113.471	9.6	NA	EQ	5	DD	LDEO	Datong, China	2
1989/12/08	13:05:13.81	39.543	113.477	11.4	NA	EQ	5	DD	LDEO	Datong, China	2
1989/12/08	23:04:50.50	39.537	113.474	13.5	NA	EQ	5	DD	LDEO	Datong, China	2
1989/12/31	08:24:48.03	39.551	113.491	11.6	NA	EQ	5	DD	LDEO	Datong, China	2
1989/04/16	18:25:50.26	29.977	99.319	14.4	5.1	EQ	5	DD	LDEO	Batang, China	2
1989/04/25	02:13:22.08	29.993	99.320	17.9	6.2	EQ	5	DD	LDEO	Batang, China	2
1989/04/30	23:05:26.82	29.964	99.353	17.2	5.1	EQ	5	DD	LDEO	Batang, China	2
1989/05/03	05:53:00.94	30.020	99.362	14.4	6.1	EQ	5	DD	LDEO	Batang, China	2
1989/05/03	15:41:30.94	29.966	99.365	14.3	5.8	EQ	5	DD	LDEO	Batang, China	2
1989/05/03	17:28:21.44	30.047	99.354	12.5	5.3	EQ	5	DD	LDEO	Batang, China	2
1989/05/04	05:30:46.27	29.963	99.364	10.1	5.1	EQ	5	DD	LDEO	Batang, China	2
1985/07/18	17:40:13.12	30.335	94.795	23.3	4.9	EQ	5	DD	LDEO	Tangmai, China	2
1985/07/19	02:38:09.24	30.323	94.811	23.6	4.7	EQ	5	DD	LDEO	Tangmai, China	2
1985/07/20	18:31:45.28	30.323	94.819	23.0	4.6	EQ	5	DD	LDEO	Tangmai, China	2
1986/10/10	08:59:19.63	30.324	94.779	19.4	4.8	EQ	5	DD	LDEO	Tangmai, China	2
1986/10/12	16:29:11.59	30.343	94.809	25.8	4.7	EQ	5	DD	LDEO	Tangmai, China	2
1987/09/17	01:34:47.26	30.328	94.788	16.2	4.9	EQ	5	DD	LDEO	Tangmai, China	2
1987/09/19	18:59:38.84	30.313	94.797	29.7	4.7	EQ	5	DD	LDEO	Tangmai, China	2
1991/07/18	13:25:00.11	30.317	94.796	24.3	5.0	EQ	5	DD	LDEO	Tangmai, China	2
1991/07/20	18:52:24.48	30.305	94.807	27.8	4.5	EQ	5	DD	LDEO	Tangmai, China	2
1991/07/20	19:02:31.24	30.323	94.808	18.5	4.8	EQ	5	DD	LDEO	Tangmai, China	2
1991/07/23	16:51:53.74	30.327	94.802	18.9	4.7	EQ	5	DD	LDEO	Tangmai, China	2
1991/07/24	06:06:45.19	30.305	94.795	26.6	4.8	EQ	5	DD	LDEO	Tangmai, China	2
1991/07/25	01:52:44.31	30.319	94.783	12.7	4.8	EQ	5	DD	LDEO	Tangmai, China	2
1991/07/28	23:58:20.64	30.327	94.754	29.3	4.9	EQ	5	DD	LDEO	Tangmai, China	2
1991/07/29	03:20:16.14	30.302	94.821	27.1	4.6	EQ	5	DD	LDEO	Tangmai, China	2
1993/09/06	20:57:22.42	30.311	94.819	17.7	4.7	EQ	5	DD	LDEO	Tangmai, China	2
1986/08/26	09:43:00.03	37.773	101.674	8.9	6.2	EQ	5	DD	LDEO	Menyuan, China	2
1986/08/26	10:30:00.16	37.756	101.703	14.7	5.4	EQ	5	DD	LDEO	Menyuan, China	2
1986/08/26	13:11:24.46	37.752	101.687	9.6	5.0	EQ	5	DD	LDEO	Menyuan, China	2
1986/08/27	13:15:23.17	37.701	101.685	11.7	4.3	EQ	5	DD	LDEO	Menyuan, China	2
1987/06/28	01:16:37.46	37.735	101.695	16.6	4.9	EQ	5	DD	LDEO	Menyuan, China	2
1993/05/30	10:01:10.33	23.715	100.501	11.5	NA	EQ	5	DD	LDEO	Jinggu, China	2
1993/05/30	21:49:02.14	23.746	100.483	13.0	NA	EQ	5	DD	LDEO	Jinggu, China	2
1993/06/04	01:04:00.94	23.707	100.500	11.4	4.5	EQ	5	DD	LDEO	Jinggu, China	2
1993/06/10	20:38:28.68	23.691	100.490	12.2	4.6	EQ	5	DD	LDEO	Jinggu, China	2
1993/10/25	08:32:46.55	23.582	100.523	5.9	NA	EQ	5	DD	LDEO	Jinggu, China	2
1994/03/18	16:16:47.64	23.606	100.521	5.7	NA	EQ	5	DD	LDEO	Jinggu, China	2
1994/11/07	22:40:50.12	23.720	100.464	12.9	4.0	EQ	5	DD	LDEO	Jinggu, China	2
1996/05/03	03:32:46.42	40.645	109.600	17.6	5.5	EQ	5	DD	LDEO	Baotou, China	2
1996/05/03	06:04:41.85	40.698	109.595	19.7	NA	EQ	5	DD	LDEO	Baotou, China	2
1996/05/07	23:47:02.12	40.767	109.635	11.6	NA	EQ	5	DD	LDEO	Baotou, China	2
1996/05/08	02:03:55.79	40.760	109.550	11.9	3.9	EQ	5	DD	LDEO	Baotou, China	2
1996/05/10	09:12:42.98	40.717	109.641	19.6	NA	EQ	5	DD	LDEO	Baotou, China	2
1992/08/24	06:30:14.39	31.165	103.725	25.0	NA	EQ	10	DD	LDEO	Chengdu, China	8
1992/12/18	10:55:59.66	30.942	103.637	17.0	NA	EQ	10	DD	LDEO	Chengdu, China	8
1993/03/02	13:36:37.59	30.593	103.377	13.2	NA	EQ	10	DD	LDEO	Chengdu, China	8
1993/03/30	09:18:10.02	31.317	103.903	14.3	NA	EQ	10	DD	LDEO	Chengdu, China	8
1993/04/22	07:32:55.11	31.656	103.703	21.3	NA	EQ	10	DD	LDEO	Chengdu, China	8
1994/03/04	19:03:05.32	31.463	104.070	10.6	NA	EQ	10	DD	LDEO	Chengdu, China	8
1994/06/07	07:25:20.97	31.166	103.796	13.2	NA	EQ	10	DD	LDEO	Chengdu, China	8

1994/06/09	21:31:01.16	31.631	102.390	13.2	NA	EQ	10	DD	LDEO	Chengdu, China	8
1994/07/01	22:39:49.32	31.829	102.425	15.2	NA	EQ	10	DD	LDEO	Chengdu, China	8
1994/07/03	15:28:21.47	30.035	103.123	11.1	NA	EQ	10	DD	LDEO	Chengdu, China	8
1994/08/23	04:17:21.92	31.559	104.079	18.7	NA	EQ	10	DD	LDEO	Chengdu, China	8
1994/09/25	18:29:20.32	31.580	104.069	19.6	NA	EQ	10	DD	LDEO	Chengdu, China	8
1994/10/17	23:00:36.36	30.042	103.145	23.1	NA	EQ	10	DD	LDEO	Chengdu, China	8
1994/10/24	13:00:26.10	30.522	102.721	13.5	NA	EQ	10	DD	LDEO	Chengdu, China	8
1994/11/11	15:45:15.96	30.032	103.188	17.3	NA	EQ	10	DD	LDEO	Chengdu, China	8
1995/02/01	05:17:27.37	30.995	103.458	15.6	NA	EQ	10	DD	LDEO	Chengdu, China	8
1995/02/02	22:54:48.94	31.003	103.456	11.7	NA	EQ	10	DD	LDEO	Chengdu, China	8
1995/02/03	04:28:04.82	31.003	103.455	12.8	NA	EQ	10	DD	LDEO	Chengdu, China	8
1995/06/08	06:04:51.75	29.381	103.315	13.0	NA	EQ	10	DD	LDEO	Chengdu, China	8
1995/06/10	05:08:53.95	31.711	104.176	15.6	NA	EQ	10	DD	LDEO	Chengdu, China	8
1995/06/11	04:08:03.99	31.744	104.175	15.5	NA	EQ	10	DD	LDEO	Chengdu, China	8
1995/06/12	03:37:31.64	31.759	104.139	16.8	NA	EQ	10	DD	LDEO	Chengdu, China	8
1995/06/18	04:34:10.08	29.449	103.471	7.8	NA	EQ	10	DD	LDEO	Chengdu, China	8
1995/06/23	11:51:24.70	32.084	102.776	12.9	NA	EQ	10	DD	LDEO	Chengdu, China	8
1995/07/08	01:05:10.88	31.726	102.790	6.7	NA	EQ	10	DD	LDEO	Chengdu, China	8
1995/09/09	01:19:24.66	31.344	103.909	14.9	NA	EQ	10	DD	LDEO	Chengdu, China	8
1995/09/22	12:13:19.58	30.653	102.832	23.3	NA	EQ	10	DD	LDEO	Chengdu, China	8
1995/09/27	06:56:13.67	31.543	104.127	16.5	NA	EQ	10	DD	LDEO	Chengdu, China	8
1995/10/09	14:08:12.78	31.847	102.580	14.5	NA	EQ	10	DD	LDEO	Chengdu, China	8
1996/01/10	21:45:50.12	30.098	103.364	8.8	NA	EQ	10	DD	LDEO	Chengdu, China	8
1996/01/11	10:22:24.96	30.112	103.373	7.6	NA	EQ	10	DD	LDEO	Chengdu, China	8
1996/01/18	16:17:13.89	31.859	103.915	24.8	NA	EQ	10	DD	LDEO	Chengdu, China	8
1996/01/25	02:27:37.08	30.659	102.802	32.9	NA	EQ	10	DD	LDEO	Chengdu, China	8
1996/02/02	01:52:45.17	30.407	103.026	14.0	NA	EQ	10	DD	LDEO	Chengdu, China	8
1996/03/18	15:03:28.51	29.961	102.373	25.9	NA	EQ	10	DD	LDEO	Chengdu, China	8
1996/03/23	16:12:09.27	29.954	103.175	19.1	NA	EQ	10	DD	LDEO	Chengdu, China	8
1996/05/04	00:15:58.86	29.963	103.191	20.0	NA	EQ	10	DD	LDEO	Chengdu, China	8
1996/05/04	17:10:02.22	29.953	103.192	15.6	NA	EQ	10	DD	LDEO	Chengdu, China	8
1996/05/09	15:03:38.84	31.235	103.560	17.7	NA	EQ	10	DD	LDEO	Chengdu, China	8
1996/05/20	08:44:29.28	30.029	102.803	19.6	NA	EQ	10	DD	LDEO	Chengdu, China	8
1996/07/08	07:33:08.67	30.328	102.697	15.0	NA	EQ	10	DD	LDEO	Chengdu, China	8
1996/08/09	07:56:02.50	31.524	102.391	13.4	NA	EQ	10	DD	LDEO	Chengdu, China	8
1996/08/19	05:14:22.45	29.976	103.152	23.6	NA	EQ	10	DD	LDEO	Chengdu, China	8
1996/09/06	13:04:19.96	31.596	102.383	14.2	NA	EQ	10	DD	LDEO	Chengdu, China	8
1996/10/05	03:30:48.57	30.658	102.820	25.3	NA	EQ	10	DD	LDEO	Chengdu, China	8
1996/10/18	12:28:38.25	31.808	102.598	11.2	NA	EQ	10	DD	LDEO	Chengdu, China	8
1996/11/18	12:07:05.06	29.829	103.215	14.6	NA	EQ	10	DD	LDEO	Chengdu, China	8
1996/11/19	02:46:05.52	30.655	102.891	17.5	NA	EQ	10	DD	LDEO	Chengdu, China	8
1996/12/31	11:35:39.92	30.421	102.981	17.4	NA	EQ	10	DD	LDEO	Chengdu, China	8
1997/02/17	19:02:49.32	32.233	103.551	12.5	NA	EQ	10	DD	LDEO	Chengdu, China	8
1997/03/10	03:12:23.89	29.318	103.050	18.1	NA	EQ	10	DD	LDEO	Chengdu, China	8
1997/04/01	05:57:11.27	29.316	103.039	16.6	NA	EQ	10	DD	LDEO	Chengdu, China	8
1997/04/23	02:31:06.21	32.270	103.719	9.7	NA	EQ	10	DD	LDEO	Chengdu, China	8
1997/04/28	07:59:06.78	30.660	102.833	27.4	NA	EQ	10	DD	LDEO	Chengdu, China	8
1997/05/05	09:39:46.55	31.579	102.915	18.8	NA	EQ	10	DD	LDEO	Chengdu, China	8
1997/05/06	14:16:10.41	31.559	102.903	18.4	NA	EQ	10	DD	LDEO	Chengdu, China	8
1997/05/24	17:08:57.08	31.483	104.151	22.8	NA	EQ	10	DD	LDEO	Chengdu, China	8
1997/06/11	16:33:38.74	29.873	103.330	25.6	NA	EQ	10	DD	LDEO	Chengdu, China	8
1997/06/13	14:15:22.92	32.055	103.537	12.1	NA	EQ	10	DD	LDEO	Chengdu, China	8
1997/08/07	03:12:44.27	29.771	102.533	16.6	NA	EQ	10	DD	LDEO	Chengdu, China	8
1997/08/15	02:11:00.99	31.538	104.165	13.6	NA	EQ	10	DD	LDEO	Chengdu, China	8

1997/09/17	06:11:29.41	30.657	102.837	16.0	NA	EQ	10	DD	LDEO	Chengdu, China	8
1997/09/23	11:01:03.60	30.646	102.823	23.0	NA	EQ	10	DD	LDEO	Chengdu, China	8
1997/10/11	15:09:51.14	31.267	103.743	14.3	NA	EQ	10	DD	LDEO	Chengdu, China	8
1997/10/12	16:59:32.77	31.268	103.213	14.0	NA	EQ	10	DD	LDEO	Chengdu, China	8
1997/10/18	03:13:53.87	30.500	102.690	24.4	NA	EQ	10	DD	LDEO	Chengdu, China	8
1997/10/28	21:15:43.08	29.298	103.299	15.9	NA	EQ	10	DD	LDEO	Chengdu, China	8
1997/12/09	16:18:13.66	30.257	102.967	26.0	NA	EQ	10	DD	LDEO	Chengdu, China	8
1997/12/14	15:47:08.12	31.463	104.133	17.2	NA	EQ	10	DD	LDEO	Chengdu, China	8
1998/01/20	14:02:26.90	31.717	104.267	19.7	NA	EQ	10	DD	LDEO	Chengdu, China	8
1998/04/17	12:58:00.25	31.708	103.954	15.8	NA	EQ	10	DD	LDEO	Chengdu, China	8
1998/04/17	13:23:58.12	31.711	103.951	14.5	NA	EQ	10	DD	LDEO	Chengdu, China	8
1998/05/07	14:09:14.87	32.264	103.738	11.6	NA	EQ	10	DD	LDEO	Chengdu, China	8
1998/05/15	13:17:28.09	30.138	103.016	29.3	NA	EQ	10	DD	LDEO	Chengdu, China	8
1998/08/01	20:08:45.16	30.692	103.339	16.3	NA	EQ	10	DD	LDEO	Chengdu, China	8
1998/09/22	14:47:02.94	31.588	104.036	24.5	NA	EQ	10	DD	LDEO	Chengdu, China	8
1998/11/01	18:26:32.24	31.239	103.739	16.3	NA	EQ	10	DD	LDEO	Chengdu, China	8
1998/11/02	22:07:15.96	32.271	103.744	11.4	NA	EQ	10	DD	LDEO	Chengdu, China	8
1998/11/24	20:28:22.86	30.083	102.737	14.8	NA	EQ	10	DD	LDEO	Chengdu, China	8
1999/03/17	01:24:26.18	30.427	103.075	9.8	NA	EQ	10	DD	LDEO	Chengdu, China	8
1999/03/23	02:47:56.00	31.297	104.320	14.7	NA	EQ	10	DD	LDEO	Chengdu, China	8
1999/09/23	07:57:08.09	31.309	103.790	19.0	NA	EQ	10	DD	LDEO	Chengdu, China	8
1999/10/11	20:07:57.74	30.865	103.475	15.3	NA	EQ	10	DD	LDEO	Chengdu, China	8
1999/10/19	23:29:46.94	31.579	104.083	16.9	NA	EQ	10	DD	LDEO	Chengdu, China	8
1999/10/28	09:30:30.53	31.575	104.070	18.7	NA	EQ	10	DD	LDEO	Chengdu, China	8
1999/11/07	01:55:04.36	31.462	103.534	14.3	NA	EQ	10	DD	LDEO	Chengdu, China	8
1999/11/10	05:17:25.67	30.724	103.549	18.2	NA	EQ	10	DD	LDEO	Chengdu, China	8
1999/11/12	05:34:09.72	30.728	103.558	19.0	NA	EQ	10	DD	LDEO	Chengdu, China	8
1999/11/16	12:27:12.43	30.603	103.498	26.5	NA	EQ	10	DD	LDEO	Chengdu, China	8
1992/12/05	01:28:27.97	30.097	102.030	14.4	NA	EQ	10	DD	LDEO	Yuexi, China	8
1993/04/01	14:01:24.75	29.754	101.945	23.7	NA	EQ	10	DD	LDEO	Yuexi, China	8
1993/05/04	14:05:18.90	28.666	102.688	15.1	NA	EQ	10	DD	LDEO	Yuexi, China	8
1994/10/12	06:10:06.64	29.061	102.367	23.0	NA	EQ	10	DD	LDEO	Yuexi, China	8
1995/07/23	14:48:33.82	29.057	102.227	22.9	NA	EQ	10	DD	LDEO	Yuexi, China	8
1996/01/05	13:17:18.56	28.955	102.662	9.4	NA	EQ	10	DD	LDEO	Yuexi, China	8
1996/04/23	13:35:25.59	29.542	102.185	15.6	NA	EQ	10	DD	LDEO	Yuexi, China	8
1996/04/27	07:55:30.80	29.314	102.221	10.6	NA	EQ	10	DD	LDEO	Yuexi, China	8
1996/08/13	14:58:59.84	29.112	102.069	19.1	NA	EQ	10	DD	LDEO	Yuexi, China	8
1996/10/05	14:57:01.78	29.154	102.390	27.3	NA	EQ	10	DD	LDEO	Yuexi, China	8
1996/11/25	02:08:47.48	29.271	102.191	16.4	NA	EQ	10	DD	LDEO	Yuexi, China	8
1997/01/18	00:09:08.07	29.090	102.356	25.8	NA	EQ	10	DD	LDEO	Yuexi, China	8
1997/01/25	19:42:25.96	29.212	102.207	18.0	NA	EQ	10	DD	LDEO	Yuexi, China	8
1997/03/02	01:55:09.66	29.305	102.324	24.9	NA	EQ	10	DD	LDEO	Yuexi, China	8
1997/04/22	09:00:28.49	28.795	102.091	14.0	NA	EQ	10	DD	LDEO	Yuexi, China	8
1997/05/28	03:55:23.16	30.164	101.934	16.5	NA	EQ	10	DD	LDEO	Yuexi, China	8
1997/05/31	19:44:08.72	28.318	102.778	25.0	NA	EQ	10	DD	LDEO	Yuexi, China	8
1997/07/11	04:04:36.64	29.175	102.379	17.6	NA	EQ	10	DD	LDEO	Yuexi, China	8
1997/07/21	10:39:55.37	29.697	101.966	16.1	NA	EQ	10	DD	LDEO	Yuexi, China	8
1997/07/25	10:30:40.18	29.168	102.168	13.9	NA	EQ	10	DD	LDEO	Yuexi, China	8
1997/10/04	11:08:32.60	29.595	102.179	14.6	NA	EQ	10	DD	LDEO	Yuexi, China	8
1997/10/04	16:03:00.33	29.593	102.182	14.4	NA	EQ	10	DD	LDEO	Yuexi, China	8
1997/10/24	08:30:30.01	28.598	102.694	25.1	NA	EQ	10	DD	LDEO	Yuexi, China	8
1998/09/17	02:28:55.65	29.006	102.373	27.3	NA	EQ	10	DD	LDEO	Yuexi, China	8
1994/02/25	21:12:36.88	32.696	104.132	14.4	NA	EQ	5	DD	LDEO	Pingwu, China	8
1996/01/20	16:46:15.12	32.439	104.188	13.0	NA	EQ	5	DD	LDEO	Pingwu, China	8

1996/02/19	08:50:00.26	32.619	104.178	12.9	NA	EQ	5	DD	LDEO	Pingwu, China	8
1997/09/22	13:58:45.01	32.733	104.107	12.9	NA	EQ	5	DD	LDEO	Pingwu, China	8
1996/08/26	04:47:44.80	30.445	101.560	20.7	NA	EQ	5	DD	LDEO	Qianning, China	8
1996/10/05	15:14:16.48	30.460	101.603	22.6	NA	EQ	5	DD	LDEO	Qianning, China	8
1995/02/20	08:07:33.77	41.286	72.437	0.000	4.8	EQ	5	LS	LDEO	Kyrgyzstan	5
1995/11/02	23:16:34.41	42.233	75.062	0.000	4.1	EQ	5	LS	LDEO	Kyrgyzstan	5
1995/11/03	11:09:55.43	40.298	73.693	0.000	4.3	EQ	5	LS	LDEO	Kyrgyzstan	5
1995/11/04	18:35:19.17	42.240	75.058	0.000	3.9	EQ	5	LS	LDEO	Kyrgyzstan	5
1995/11/17	10:30:57.58	41.043	72.357	0.000	4.2	EQ	5	LS	LDEO	Kyrgyzstan	5
1995/11/17	13:44:44.99	41.051	72.331	0.000	4.2	EQ	5	LS	LDEO	Kyrgyzstan	5
1996/01/14	18:16:26.49	42.707	74.847	0.000	4.1	EQ	5	LS	LDEO	Kyrgyzstan	5
1996/01/16	18:33:35.77	41.109	72.552	0.000	4.5	EQ	5	LS	LDEO	Kyrgyzstan	5
1996/01/18	09:33:49.55	41.914	77.446	0.000	5.2	EQ	5	LS	LDEO	Kyrgyzstan	5
1996/01/30	10:55:42.44	40.765	73.341	0.000	4.5	EQ	5	LS	LDEO	Kyrgyzstan	5
1996/05/11	10:32:45.72	42.918	78.296	0.000	3.8	EQ	5	LS	LDEO	Kyrgyzstan	5
1996/05/14	12:45:27.50	41.557	74.960	0.000	4.6	EQ	5	LS	LDEO	Kyrgyzstan	5
1996/06/14	22:45:36.88	42.447	72.930	0.000	5.4	EQ	5	LS	LDEO	Kyrgyzstan	5
1996/07/27	15:48:53.30	41.107	72.386	0.000	3.8	EQ	5	LS	LDEO	Kyrgyzstan	5
1996/12/28	07:40:32.12	42.977	77.944	0.000	4.3	EQ	5	LS	LDEO	Kyrgyzstan	5
1997/01/09	13:43:31.84	41.108	74.323	0.000	5.9	EQ	5	LS	LDEO	Kyrgyzstan	5
1997/03/05	09:35:07.68	41.311	75.716	0.000	4.8	EQ	5	LS	LDEO	Kyrgyzstan	5
1997/12/01	20:54:14.69	41.590	75.729	0.000	4.2	EQ	5	LS	LDEO	Kyrgyzstan	5
1997/12/27	04:20:57.88	42.229	78.267	0.000	4.0	EQ	5	LS	LDEO	Kyrgyzstan	5
1998/02/13	13:27:00.14	42.096	73.489	0.000	4.5	EQ	5	LS	LDEO	Kyrgyzstan	5
1998/11/21	11:46:08.83	42.205	74.065	0.000	4.4	EQ	5	LS	LDEO	Kyrgyzstan	5
1999/05/13	20:38:35.28	42.704	78.887	0.000	3.7	EQ	5	LS	LDEO	Kyrgyzstan	5
1999/10/03	12:52:45.27	40.862	74.017	0.000	4.1	EQ	5	LS	LDEO	Kyrgyzstan	5
1999/12/06	07:33:11.42	42.678	76.292	0.000	4.9	EQ	5	LS	LDEO	Kyrgyzstan	5
1999/12/06	08:17:28.67	42.682	76.319	0.000	4.2	EQ	5	LS	LDEO	Kyrgyzstan	5
2000/01/26	18:35:03.61	40.867	73.343	0.000	4.2	EQ	5	LS	LDEO	Kyrgyzstan	5
2000/02/13	09:46:07.26	41.636	73.080	0.000	4.2	EQ	5	LS	LDEO	Kyrgyzstan	5
1999/11/08	23:01:40.64	40.532	123.047	10.275	4.0	EQ	5	DD	CYT	Xiuyan, China	6
1999/11/25	12:47:48.60	40.533	123.030	10.013	3.7	EQ	5	DD	CYT	Xiuyan, China	6
1999/11/25	12:55:04.16	40.533	123.029	9.671	4.2	EQ	5	DD	CYT	Xiuyan, China	6
1999/11/29	04:10:39.15	40.526	123.039	8.184	4.9	EQ	5	DD	CYT	Xiuyan, China	6
1999/11/29	04:45:50.49	40.521	123.035	8.198	4.3	EQ	5	DD	CYT	Xiuyan, China	6
1999/11/29	08:16:48.03	40.540	123.000	8.914	4.4	EQ	5	DD	CYT	Xiuyan, China	6
1999/11/29	23:52:55.80	40.525	123.049	9.595	4.2	EQ	5	DD	CYT	Xiuyan, China	6
1999/11/30	06:06:55.22	40.528	123.029	9.700	4.3	EQ	5	DD	CYT	Xiuyan, China	6
1999/11/30	06:09:36.63	40.524	123.032	7.239	4.0	EQ	5	DD	CYT	Xiuyan, China	6
1999/11/30	17:47:01.48	40.525	123.051	11.052	4.0	EQ	5	DD	CYT	Xiuyan, China	6
1999/11/30	20:33:00.09	40.532	123.011	10.018	NA	EQ	5	DD	CYT	Xiuyan, China	6
1999/12/01	04:45:30.49	40.528	123.037	11.847	4.2	EQ	5	DD	CYT	Xiuyan, China	6
1999/12/12	21:49:30.34	40.522	123.068	9.830	3.8	EQ	5	DD	CYT	Xiuyan, China	6
1999/12/27	11:27:15.20	40.526	123.025	8.901	3.6	EQ	5	DD	CYT	Xiuyan, China	6
2000/01/11	23:43:54.98	40.525	123.045	12.682	5.1	EQ	5	DD	CYT	Xiuyan, China	6
2000/01/12	05:00:31.84	40.516	123.030	10.454	NA	EQ	5	DD	CYT	Xiuyan, China	6
1993/12/15	21:49:43.10	23.213	120.524	12.500	NA	EQ	5	DD	KFM	Taiwan	7
1994/04/06	01:12:11.09	23.532	120.421	13.440	NA	EQ	5	DD	KFM	Taiwan	7
1995/10/31	22:27:06.94	23.291	120.359	10.650	NA	EQ	5	DD	KFM	Taiwan	7
1999/10/22	03:10:17.46	23.533	120.431	16.740	NA	EQ	5	DD	KFM	Taiwan	7
1997/08/03	08:07:20.04	49.941	78.786	0.050	NA	EX	0	CS	NNC/LDEO	Degelen	9
1997/08/31	07:08:38.75	49.884	78.815	0.300	NA	EX	0	CS	NNC/LDEO	Degelen	9
1997/09/28	07:30:15.13	49.879	78.849	0.550	NA	EX	0	CS	NNC/LDEO	Degelen	9

1998/08/22	05:00:18.90	49.767	77.991	0.000	NA	EX	1	CS	NNC/LDEO	Degelen	9
1998/09/17	07:19:40.55	49.981	78.756	0.030	NA	EX	0	CS	NNC/LDEO	Degelen	9
1999/09/25	05:00:05.98	49.782	77.966	0.000	NA	EX	1	CS	NNC/LDEO	Degelen	9
2000/07/29	06:10:04.25	49.782	77.967	0.000	4.0	EX	1	CS	NNC/LDEO	Degelen	9
1990/08/16	04:59:59.40	41.538	88.740	0.000	NA	UNE	1	LS	Fi02	Lop Nor	10
1992/05/21	04:59:59.06	41.542	88.768	0.000	NA	UNE	1	LS	Fi02	Lop Nor	10
1992/09/25	07:59:59.71	41.717	88.377	0.000	NA	UNE	1	LS	Fi02	Lop Nor	10
1993/10/05	01:59:57.92	41.592	88.703	0.000	NA	UNE	1	LS	Fi02	Lop Nor	10
1994/10/07	03:25:59.44	41.574	88.720	0.000	NA	UNE	1	LS	Fi02	Lop Nor	10
1995/05/15	04:05:59.37	41.555	88.752	0.000	NA	UNE	1	LS	Fi02	Lop Nor	10
1995/08/17	00:59:59.34	41.540	88.753	0.000	NA	UNE	1	LS	Fi02	Lop Nor	10
1996/06/08	02:55:59.34	41.578	88.688	0.000	NA	EX	1	LS	Fi02	Lop Nor	10
1996/07/29	01:48:59.31	41.716	88.376	0.000	NA	EX	1	LS	Fi02	Lop Nor	10
1998/05/11	10:13:44.23	27.078	71.719	0.000	5.0	UNE	1	LS	Ba98	Indian	11
1998/05/28	10:16:17.29	28.793	64.946	0.000	4.9	UNE	1	LS	Ba98	Pakistan	11
1967/09/16	04:04:00.30	49.937	77.728	0.230	NA	UNE	0	CS	Bo89	Semipalatinsk	12
1967/09/22	05:04:00.00	49.960	77.691	0.229	NA	UNE	0	CS	Bo89	Semipalatinsk	12
1967/10/17	05:04:00.20	49.781	78.004	0.181	NA	UNE	0	CS	Bo89	Semipalatinsk	12
1967/11/22	04:03:59.90	49.942	77.687	0.227	NA	UNE	0	CS	Bo89	Semipalatinsk	12
1968/01/07	03:46:59.90	49.754	78.030	0.237	NA	UNE	0	CS	Bo89	Semipalatinsk	12
1968/06/19	05:05:59.80	49.980	78.986	0.316	NA	UNE	0	CS	Bo89	Semipalatinsk	12
1968/09/05	04:05:59.60	49.742	78.076	0.162	NA	UNE	0	CS	Bo89	Semipalatinsk	12
1968/09/29	03:43:00.00	49.812	78.122	0.290	NA	UNE	0	CS	Bo89	Semipalatinsk	12
1968/12/18	05:01:59.70	49.746	78.092	0.194	NA	UNE	0	CS	Bo89	Semipalatinsk	12
1969/03/07	08:26:59.80	49.821	78.063	0.214	NA	UNE	0	CS	Bo89	Semipalatinsk	12
1969/05/16	04:02:59.70	49.759	78.076	0.184	NA	UNE	0	CS	Bo89	Semipalatinsk	12
1969/05/31	05:01:59.40	49.950	77.694	0.258	NA	UNE	0	CS	Bo89	Semipalatinsk	12
1969/07/23	02:47:00.20	49.816	78.130	0.175	NA	UNE	0	CS	Bo89	Semipalatinsk	12
1969/11/30	03:32:59.70	49.924	78.956	0.472	NA	UNE	0	CS	Bo89	Semipalatinsk	12
1969/12/28	03:47:00.20	49.937	77.714	0.388	NA	UNE	0	CS	Bo89	Semipalatinsk	12
1970/01/29	07:03:00.00	49.796	78.124	0.214	NA	UNE	0	CS	Bo89	Semipalatinsk	12
1970/06/28	01:58:00.00	49.802	78.107	0.332	NA	UNE	0	CS	Bo89	Semipalatinsk	12
1970/07/21	03:02:59.70	49.952	77.673	0.225	NA	UNE	0	CS	Bo89	Semipalatinsk	12
1970/09/06	04:02:59.91	49.785	78.009	0.250	NA	UNE	0	CS	Bo89	Semipalatinsk	12
1970/11/04	06:02:59.77	49.989	77.762	0.250	NA	UNE	0	CS	Bo89	Semipalatinsk	12
1970/12/17	07:01:00.02	49.746	78.099	0.200	NA	UNE	0	CS	Bo89	Semipalatinsk	12
1971/03/22	04:33:00.27	49.798	78.109	0.300	NA	UNE	0	CS	Bo89	Semipalatinsk	12
1971/04/25	03:32:59.91	49.769	78.034	0.350	NA	UNE	0	CS	Bo89	Semipalatinsk	12
1971/06/06	04:02:59.66	49.975	77.660	0.250	NA	UNE	0	CS	Bo89	Semipalatinsk	12
1971/06/06	04:04:00.14	49.969	77.641	0.250	NA	UNE	0	CS	Bo89	Semipalatinsk	12
1971/06/30	03:56:59.80	49.946	78.980	0.200	NA	UNE	0	CS	Bo89	Semipalatinsk	12
1971/10/09	06:02:59.70	49.978	77.641	0.200	NA	UNE	0	CS	Bo89	Semipalatinsk	12
1971/10/21	06:02:59.73	49.974	77.597	0.250	NA	UNE	0	CS	Bo89	Semipalatinsk	12
1971/12/30	06:21:00.13	49.753	78.000	0.200	NA	UNE	0	CS	Bo89	Semipalatinsk	12
1972/02/10	05:02:59.98	50.024	78.878	0.200	NA	UNE	0	CS	Bo89	Semipalatinsk	12
1972/06/07	01:27:59.98	49.827	78.115	0.250	NA	UNE	0	CS	Bo89	Semipalatinsk	12
1972/11/11	01:27:00.20	49.927	78.817	0.350	NA	UNE	0	CS	Bo89	Semipalatinsk	12
1979/05/06	03:16:59.91	49.763	77.995	0.200	NA	UNE	0	CS	IDG/NNC	Semipalatinsk	12
1979/06/23	02:57:00.00	49.915	78.845	0.350	NA	UNE	0	CS	IDG/NNC	Semipalatinsk	12
1979/08/18	02:51:59.00	49.948	78.919	0.400	NA	UNE	0	CS	IDG/NNC	Semipalatinsk	12
1980/10/12	03:34:16.00	49.968	79.022	0.300	NA	UNE	0	CS	IDG/NNC	Semipalatinsk	12
1981/03/29	04:03:52.00	50.022	78.981	0.250	NA	UNE	0	CS	IDG/NNC	Semipalatinsk	12
1981/09/13	02:17:20.00	49.914	78.894	0.200	NA	UNE	0	CS	IDG/NNC	Semipalatinsk	12
1981/11/29	03:35:11.00	49.902	78.847	0.300	NA	UNE	0	CS	IDG/NNC	Semipalatinsk	12

1981/12/22	04:31:05.26	49.828	78.077	0.200	NA	UNE	0	CS	IDG/NNC	Semipalatinsk	12
1981/12/27	03:43:16.00	49.933	78.780	0.350	NA	UNE	0	CS	IDG/NNC	Semipalatinsk	12
1982/02/19	03:56:13.40	49.813	78.034	0.250	NA	UNE	0	CS	IDG/NNC	Semipalatinsk	12
1982/04/25	03:23:08.00	49.918	78.887	0.350	NA	UNE	0	CS	IDG/NNC	Semipalatinsk	12
1982/09/21	02:57:03.17	49.783	78.136	0.200	NA	UNE	0	CS	IDG/NNC	Semipalatinsk	12
1982/12/26	03:35:17.00	50.068	78.995	0.200	NA	UNE	0	CS	IDG/NNC	Semipalatinsk	12
1983/05/30	03:33:47.13	49.743	78.110	0.200	NA	UNE	0	CS	IDG/NNC	Semipalatinsk	12
1983/10/06	01:47:08.70	49.925	78.757	0.400	NA	UNE	0	CS	IDG/NNC	Semipalatinsk	12
1984/04/15	03:17:12.52	49.749	78.083	0.300	NA	UNE	0	CS	IDG/NNC	Semipalatinsk	12
1984/09/09	02:59:08.76	49.805	78.100	0.200	NA	UNE	0	CS	IDG/NNC	Semipalatinsk	12
1985/07/25	03:11:09.01	49.814	78.010	0.200	NA	UNE	0	CS	IDG/NNC	Semipalatinsk	12
1987/02/26	04:58:24.29	49.829	78.084	0.200	NA	UNE	0	CS	IDG/NNC	Semipalatinsk	12
1987/03/12	01:57:19.70	49.935	78.829	0.334	NA	UNE	0	CS	IDG/NNC	Semipalatinsk	12
1987/04/03	01:17:10.50	49.918	78.780	0.342	NA	UNE	0	CS	IDG/NNC	Semipalatinsk	12
1987/04/17	01:03:07.30	49.879	78.669	0.346	NA	UNE	0	CS	IDG/NNC	Semipalatinsk	12
1987/06/20	00:53:07.40	49.935	78.744	0.328	NA	UNE	0	CS	IDG/NNC	Semipalatinsk	12
1987/07/17	01:17:09.18	49.766	78.029	0.300	NA	UNE	0	CS	IDG/NNC	Semipalatinsk	12
1987/08/02	00:58:09.40	49.881	78.875	0.334	NA	UNE	0	CS	IDG/NNC	Semipalatinsk	12
1987/11/15	03:31:09.20	49.899	78.758	0.345	NA	UNE	0	CS	IDG/NNC	Semipalatinsk	12
1987/12/13	03:21:07.30	49.963	78.793	0.331	NA	UNE	0	CS	IDG/NNC	Semipalatinsk	12
1987/12/20	02:55:08.91	49.775	78.006	0.200	NA	UNE	0	CS	IDG/NNC	Semipalatinsk	12
1987/12/27	03:05:07.30	49.879	78.725	0.350	NA	UNE	0	CS	IDG/NNC	Semipalatinsk	12
1988/02/13	03:05:08.40	49.937	78.864	0.330	NA	UNE	0	CS	IDG/NNC	Semipalatinsk	12
1988/03/22	09:30:09.17	49.793	78.103	0.200	NA	UNE	0	CS	IDG/NNC	Semipalatinsk	12
1988/04/03	01:33:08.30	49.908	78.908	0.323	NA	UNE	0	CS	IDG/NNC	Semipalatinsk	12
1988/05/04	00:57:09.20	49.949	78.750	0.328	NA	UNE	0	CS	IDG/NNC	Semipalatinsk	12
1988/06/14	02:27:08.90	50.019	78.961	0.313	NA	UNE	0	CS	IDG/NNC	Semipalatinsk	12
1988/09/14	04:00:00.00	49.878	78.823	0.334	NA	UNE	0	CS	IDG/NNC	Semipalatinsk	12
1988/11/12	03:30:06.20	50.043	78.969	0.308	NA	UNE	0	CS	IDG/NNC	Semipalatinsk	12
1988/11/23	03:57:08.95	49.773	78.037	0.200	NA	UNE	0	CS	IDG/NNC	Semipalatinsk	12
1988/12/17	04:18:09.40	49.882	78.925	0.320	NA	UNE	0	CS	IDG/NNC	Semipalatinsk	12
1989/01/22	03:57:09.10	49.939	78.819	0.327	NA	UNE	0	CS	IDG/NNC	Semipalatinsk	12
1989/02/12	04:15:09.30	49.919	78.711	0.344	NA	UNE	0	CS	IDG/NNC	Semipalatinsk	12
1989/02/17	04:01:09.08	49.823	78.069	0.200	NA	UNE	0	CS	IDG/NNC	Semipalatinsk	12
1989/07/08	03:47:00.10	49.868	78.780	0.353	NA	UNE	0	CS	IDG/NNC	Semipalatinsk	12
1989/09/02	04:16:59.80	50.006	78.986	0.312	NA	UNE	0	CS	IDG/NNC	Semipalatinsk	12
1989/10/19	09:49:59.70	49.922	78.908	0.328	NA	UNE	0	CS	IDG/NNC	Semipalatinsk	12
1996/06/12	21:57:00.40	36.082	139.884	54.700	NA	EQ	5	JHD	CTBT98	Japan	13
1996/06/15	02:10:00.90	35.250	133.384	11.300	NA	EQ	5	JHD	CTBT98	Japan	13
1997/07/05	06:27:09.30	35.015	138.311	25.000	NA	EQ	5	JHD	CTBT98	Japan	13
1997/07/05	19:28:09.30	37.985	139.249	12.000	NA	EQ	5	JHD	CTBT98	Japan	13
1997/07/05	20:18:10.80	37.988	139.246	12.400	NA	EQ	5	JHD	CTBT98	Japan	13
1997/07/05	22:09:24.00	37.987	139.252	13.600	NA	EQ	5	JHD	CTBT98	Japan	13
1997/10/21	10:55:25.50	35.110	138.232	33.100	NA	EQ	5	JHD	CTBT98	Japan	13
1997/11/01	11:37:06.60	35.250	139.118	15.100	NA	EQ	5	JHD	CTBT98	Japan	13
1997/11/07	17:46:59.20	36.374	137.601	6.800	NA	EQ	5	JHD	CTBT98	Japan	13
1977/02/14	00:24:15.18	33.147	73.750	0.000	5.2	EQ	10	other	LDEO	Nilore, Pakistan	14
1977/02/14	00:25:55.97	33.937	71.434	0.000	5.2	EQ	10	other	LDEO	Nilore, Pakistan	14
1977/02/14	00:27:35.90	34.150	71.400	0.000	5.2	EQ	10	other	LDEO	Nilore, Pakistan	14
1977/02/14	00:29:15.42	31.550	74.333	0.000	5.2	EQ	10	other	LDEO	Nilore, Pakistan	14
1977/02/14	00:30:55.05	31.417	76.417	0.000	5.2	EQ	10	other	LDEO	Nilore, Pakistan	14
1977/02/14	00:34:15.46	37.900	69.780	0.000	5.2	EQ	10	other	LDEO	Nilore, Pakistan	14
1977/02/14	00:35:55.04	30.323	78.056	0.000	5.2	EQ	10	other	LDEO	Nilore, Pakistan	14
1977/02/14	00:37:35.32	39.000	70.317	0.000	5.2	EQ	10	other	LDEO	Nilore, Pakistan	14

1977/02/14	00:39:15.26	28.683	77.217	0.000	5.2	EQ	10	other	LDEO	Nilore, Pakistan	14
1977/02/14	00:40:55.48	38.558	68.775	0.000	5.2	EQ	10	other	LDEO	Nilore, Pakistan	14
1977/02/14	00:42:35.10	40.755	72.360	0.000	5.2	EQ	10	other	LDEO	Nilore, Pakistan	14
1977/02/14	00:44:15.52	39.673	66.990	0.000	5.2	EQ	10	other	LDEO	Nilore, Pakistan	14
1977/02/14	00:45:54.86	41.433	76.000	0.000	5.2	EQ	10	other	LDEO	Nilore, Pakistan	14
1977/02/14	00:47:35.30	41.325	69.295	0.000	5.2	EQ	10	other	LDEO	Nilore, Pakistan	14
1977/02/14	00:49:14.96	42.833	74.617	0.000	5.2	EQ	10	other	LDEO	Nilore, Pakistan	14
1977/02/14	00:50:54.79	42.483	78.400	0.000	5.2	EQ	10	other	LDEO	Nilore, Pakistan	14
1977/02/14	00:52:36.04	24.933	67.143	0.000	5.2	EQ	10	other	LDEO	Nilore, Pakistan	14
1977/02/14	00:54:14.84	43.267	77.383	0.000	5.2	EQ	10	other	LDEO	Nilore, Pakistan	14
1977/02/14	00:55:55.93	36.308	59.472	0.000	5.2	EQ	10	other	LDEO	Nilore, Pakistan	14
1977/02/14	00:57:36.06	32.963	59.193	0.000	5.2	EQ	10	other	LDEO	Nilore, Pakistan	14
1977/02/14	01:00:55.86	37.950	58.350	0.000	5.2	EQ	10	other	LDEO	Nilore, Pakistan	14
1977/02/14	01:02:35.86	37.948	58.108	0.000	5.2	EQ	10	other	LDEO	Nilore, Pakistan	14
1977/02/14	01:05:55.83	39.028	56.270	0.000	5.2	EQ	10	other	LDEO	Nilore, Pakistan	14
1977/02/14	01:07:35.70	18.529	73.849	0.000	5.2	EQ	10	other	LDEO	Nilore, Pakistan	14
1977/02/14	01:09:15.94	36.433	54.942	0.000	5.2	EQ	10	other	LDEO	Nilore, Pakistan	14
1977/02/14	01:12:34.86	25.567	91.883	0.000	5.2	EQ	10	other	LDEO	Nilore, Pakistan	14
1977/02/14	01:14:16.10	29.644	52.526	0.000	5.2	EQ	10	other	LDEO	Nilore, Pakistan	14
1977/02/14	01:15:55.97	35.738	51.386	0.000	5.2	EQ	10	other	LDEO	Nilore, Pakistan	14
1977/02/14	01:19:15.97	35.703	50.609	0.000	5.2	EQ	10	other	LDEO	Nilore, Pakistan	14
1977/02/14	01:20:55.94	36.758	49.383	0.000	5.2	EQ	10	other	LDEO	Nilore, Pakistan	14
1977/02/14	01:22:35.57	13.604	77.436	0.000	5.2	EQ	10	other	LDEO	Nilore, Pakistan	14
1977/02/14	01:24:15.48	13.000	80.183	0.000	5.2	EQ	10	other	LDEO	Nilore, Pakistan	14
1977/02/14	01:25:56.00	34.352	47.106	0.000	5.2	EQ	10	other	LDEO	Nilore, Pakistan	14
1977/02/14	01:27:34.80	53.253	86.277	0.000	5.2	EQ	10	other	LDEO	Nilore, Pakistan	14
1977/02/14	01:29:15.91	38.068	46.327	0.000	5.2	EQ	10	other	LDEO	Nilore, Pakistan	14
1977/02/14	01:30:55.87	39.500	46.333	0.000	5.2	EQ	10	other	LDEO	Nilore, Pakistan	14
1977/02/14	01:32:34.86	54.840	83.235	0.000	5.2	EQ	10	other	LDEO	Nilore, Pakistan	14
1977/02/14	01:34:15.84	40.647	46.319	0.000	5.2	EQ	10	other	LDEO	Nilore, Pakistan	14
1977/02/14	01:35:55.60	10.233	77.467	0.000	5.2	EQ	10	other	LDEO	Nilore, Pakistan	14
1977/02/14	01:37:35.24	56.827	60.637	0.000	5.2	EQ	10	other	LDEO	Nilore, Pakistan	14
1977/02/14	01:39:15.82	41.733	43.517	0.000	5.2	EQ	10	other	LDEO	Nilore, Pakistan	14
1977/02/14	01:40:54.67	51.683	100.983	0.000	5.2	EQ	10	other	LDEO	Nilore, Pakistan	14
1977/02/14	01:42:34.65	50.383	103.283	0.000	5.2	EQ	10	other	LDEO	Nilore, Pakistan	14
1977/02/14	01:44:14.66	52.272	104.310	0.000	5.2	EQ	10	other	LDEO	Nilore, Pakistan	14
1967/01/30	01:20:27.89	41.149	44.392	5.500	5.0	EQ	10	HDC	ERE	Spitak, Armenia	15
1967/12/10	22:51:21.52	17.398	73.828	10.700	5.9	EQ	5	HDC	ERE	Koyna, India	15
1967/12/11	20:49:48.84	17.189	73.723	8.000	5.0	EQ	5	HDC	ERE	Koyna, India	15
1967/12/12	06:18:35.05	17.256	73.739	8.000	5.0	EQ	5	HDC	ERE	Koyna, India	15
1967/12/12	15:48:53.32	17.208	73.754	8.000	5.0	EQ	5	HDC	ERE	Koyna, India	15
1967/12/24	23:49:51.64	17.242	73.800	8.000	4.8	EQ	5	HDC	ERE	Koyna, India	15
1968/01/05	06:42:47.55	30.523	79.182	12.000	5.0	EQ	5	HDC	ERE	Chamoli, India	15
1968/10/29	10:00:03.62	17.427	73.759	8.000	4.7	EQ	5	HDC	ERE	Koyna, India	15
1969/06/22	01:33:23.79	30.561	79.329	12.000	5.3	EQ	5	HDC	ERE	Chamoli, India	15
1971/01/30	20:15:36.79	30.537	79.154	12.000	4.7	EQ	5	HDC	ERE	Chamoli, India	15
1974/07/07	20:56:48.30	30.756	78.812	12.000	4.7	EQ	5	HDC	ERE	Chamoli, India	15
1974/07/29	23:17:27.05	17.265	73.767	8.000	4.6	EQ	5	HDC	ERE	Koyna, India	15
1975/06/09	18:36:44.66	38.850	70.270	3.600	5.1	EQ	5	HDC	ERE	Garm, Tajikistan	15
1975/08/10	03:31:52.80	38.933	70.807	7.500	4.8	EQ	5	HDC	ERE	Garm, Tajikistan	15
1976/01/23	11:54:00.27	38.601	70.526	7.500	4.6	EQ	5	HDC	ERE	Garm, Tajikistan	15
1976/09/03	21:52:42.14	38.970	70.580	9.900	5.1	EQ	5	HDC	ERE	Garm, Tajikistan	15
1976/09/03	22:20:27.48	38.939	70.608	7.500	4.7	EQ	5	HDC	ERE	Garm, Tajikistan	15
1977/04/20	04:21:08.27	30.602	79.290	12.000	4.9	EQ	5	HDC	ERE	Chamoli, India	15

1977/12/25	16:18:51.36	38.967	70.601	2.900	5.3	EQ	5	HDC	ERE	Garm, Tajikistan	15
1978/01/07	07:23:19.15	30.592	79.345	12.000	4.6	EQ	5	HDC	ERE	Chamoli, India	15
1978/09/16	15:35:53.77	33.350	57.349	15.000	6.4	EQ	10	HDC	ERE	Tabas, Iran	15
1978/09/16	19:50:18.59	33.688	57.015	15.000	4.7	EQ	10	HDC	ERE	Tabas, Iran	15
1978/09/17	07:35:47.31	33.159	56.929	15.000	4.6	EQ	10	HDC	ERE	Tabas, Iran	15
1978/09/17	08:17:22.21	33.619	56.973	15.000	4.9	EQ	10	HDC	ERE	Tabas, Iran	15
1978/09/18	04:50:00.36	33.587	57.259	15.000	4.7	EQ	10	HDC	ERE	Tabas, Iran	15
1978/09/18	17:35:05.75	33.664	56.862	15.000	4.9	EQ	10	HDC	ERE	Tabas, Iran	15
1978/09/22	18:53:04.36	33.286	56.793	15.000	4.4	EQ	10	HDC	ERE	Tabas, Iran	15
1978/09/24	18:16:01.64	33.592	57.077	15.000	4.4	EQ	10	HDC	ERE	Tabas, Iran	15
1978/09/26	19:21:46.58	38.994	70.689	7.500	4.8	EQ	5	HDC	ERE	Garm, Tajikistan	15
1978/10/09	16:04:38.20	33.340	57.283	8.000	4.6	EQ	10	HDC	ERE	Tabas, Iran	15
1978/10/12	15:01:39.42	33.362	57.334	8.000	4.9	EQ	10	HDC	ERE	Tabas, Iran	15
1978/11/06	16:49:54.78	33.331	57.391	15.000	4.5	EQ	10	HDC	ERE	Tabas, Iran	15
1978/11/17	12:59:31.20	38.566	70.453	7.500	4.9	EQ	5	HDC	ERE	Garm, Tajikistan	15
1978/12/06	17:18:12.10	33.344	57.061	15.000	5.3	EQ	10	HDC	ERE	Tabas, Iran	15
1978/12/06	20:38:07.73	33.319	57.025	15.000	4.7	EQ	10	HDC	ERE	Tabas, Iran	15
1978/12/30	05:06:54.41	38.499	70.545	7.500	4.9	EQ	5	HDC	ERE	Garm, Tajikistan	15
1979/01/17	03:29:47.17	33.737	56.997	15.000	5.1	EQ	10	HDC	ERE	Tabas, Iran	15
1979/02/13	10:36:14.03	33.321	57.388	15.000	5.4	EQ	10	HDC	ERE	Tabas, Iran	15
1979/05/27	06:43:16.28	33.253	57.264	15.000	4.6	EQ	10	HDC	ERE	Tabas, Iran	15
1979/06/03	17:38:46.19	33.467	57.265	15.000	4.5	EQ	10	HDC	ERE	Tabas, Iran	15
1979/07/05	04:46:09.45	33.620	57.021	15.000	4.5	EQ	10	HDC	ERE	Tabas, Iran	15
1979/09/05	09:26:50.88	33.859	56.922	15.000	4.9	EQ	10	HDC	ERE	Tabas, Iran	15
1979/10/20	19:40:39.30	38.940	70.590	13.400	4.7	EQ	5	HDC	ERE	Garm, Tajikistan	15
1979/12/02	06:10:46.83	33.660	57.037	15.000	4.7	EQ	10	HDC	ERE	Tabas, Iran	15
1980/01/12	15:31:39.40	33.589	57.150	15.000	5.3	EQ	10	HDC	ERE	Tabas, Iran	15
1980/05/16	09:46:36.48	33.536	56.983	15.000	4.4	EQ	10	HDC	ERE	Tabas, Iran	15
1980/09/02	16:39:12.46	17.245	73.731	8.000	4.7	EQ	5	HDC	ERE	Koyna, India	15
1980/09/20	07:28:55.96	17.243	73.818	8.000	4.8	EQ	5	HDC	ERE	Koyna, India	15
1980/09/20	10:45:29.50	17.257	73.706	8.000	5.2	EQ	5	HDC	ERE	Koyna, India	15
1981/03/19	09:59:44.78	38.852	70.235	7.500	4.6	EQ	5	HDC	ERE	Garm, Tajikistan	15
1981/04/30	09:39:27.89	33.201	57.167	15.000	4.4	EQ	10	HDC	ERE	Tabas, Iran	15
1981/04/30	10:21:24.98	33.278	57.238	15.000	4.7	EQ	10	HDC	ERE	Tabas, Iran	15
1981/06/19	10:41:39.75	30.609	79.206	12.000	4.5	EQ	5	HDC	ERE	Chamoli, India	15
1981/11/30	04:15:33.45	38.723	70.809	7.500	4.6	EQ	5	HDC	ERE	Garm, Tajikistan	15
1982/10/16	02:22:51.86	30.519	79.176	12.000	4.6	EQ	5	HDC	ERE	Chamoli, India	15
1983/02/26	20:07:44.79	38.978	70.621	7.500	5.3	EQ	5	HDC	ERE	Garm, Tajikistan	15
1983/04/04	00:45:04.45	38.531	70.411	7.500	4.6	EQ	5	HDC	ERE	Garm, Tajikistan	15
1983/05/03	13:30:23.74	33.321	57.402	15.000	4.7	EQ	10	HDC	ERE	Tabas, Iran	15
1983/10/01	07:15:15.28	38.845	70.451	7.500	4.8	EQ	5	HDC	ERE	Garm, Tajikistan	15
1984/05/03	13:17:57.82	30.910	78.640	12.000	4.5	EQ	5	HDC	ERE	Chamoli, India	15
1984/11/14	11:58:19.08	17.216	73.784	8.000	4.5	EQ	5	HDC	ERE	Koyna, India	15
1984/11/26	03:35:36.69	30.547	79.131	12.000	4.4	EQ	5	HDC	ERE	Chamoli, India	15
1987/02/23	00:21:17.87	38.960	70.568	7.500	5.0	EQ	5	HDC	ERE	Garm, Tajikistan	15
1987/06/06	03:14:22.80	30.481	79.136	12.000	4.6	EQ	5	HDC	ERE	Chamoli, India	15
1987/06/06	11:02:39.24	30.520	79.114	12.000	4.9	EQ	5	HDC	ERE	Chamoli, India	15
1987/07/17	17:23:24.32	38.909	70.677	7.500	4.8	EQ	5	HDC	ERE	Garm, Tajikistan	15
1987/07/20	16:47:45.43	33.815	56.957	15.000	5.0	EQ	10	HDC	ERE	Tabas, Iran	15
1987/08/30	05:57:50.70	33.440	57.086	15.000	4.7	EQ	10	HDC	ERE	Tabas, Iran	15
1987/12/21	04:28:22.76	38.811	70.687	7.500	4.9	EQ	5	HDC	ERE	Garm, Tajikistan	15
1988/02/20	01:51:04.16	38.624	70.572	7.500	4.8	EQ	5	HDC	ERE	Garm, Tajikistan	15
1988/06/09	12:11:49.15	30.554	79.125	12.000	4.7	EQ	5	HDC	ERE	Chamoli, India	15
1988/10/03	00:24:46.78	38.744	70.715	7.500	4.8	EQ	5	HDC	ERE	Garm, Tajikistan	15

1988/12/07	07:41:24.09	40.923	44.208	5.500	6.0	EQ	10	HDC	ERE	Spitak, Armenia	15
1988/12/07	07:45:45.04	41.058	44.226	5.500	5.8	EQ	10	HDC	ERE	Spitak, Armenia	15
1988/12/07	08:06:27.79	40.939	44.303	4.800	4.7	EQ	10	HDC	ERE	Spitak, Armenia	15
1988/12/07	09:34:33.49	40.972	44.139	5.500	5.0	EQ	10	HDC	ERE	Spitak, Armenia	15
1988/12/08	07:46:00.04	40.775	44.410	6.300	4.8	EQ	10	HDC	ERE	Spitak, Armenia	15
1988/12/08	20:32:05.80	40.890	44.197	6.300	4.8	EQ	10	HDC	ERE	Spitak, Armenia	15
1988/12/31	04:07:09.95	40.944	43.991	5.500	4.7	EQ	10	HDC	ERE	Spitak, Armenia	15
1989/01/04	07:29:40.85	40.987	44.314	5.500	4.9	EQ	10	HDC	ERE	Spitak, Armenia	15
1989/01/27	11:03:31.46	30.739	78.618	12.000	3.9	EQ	5	HDC	ERE	Chamoli, India	15
1989/03/30	16:36:23.16	40.992	43.903	5.500	4.5	EQ	10	HDC	ERE	Spitak, Armenia	15
1989/04/20	22:59:54.89	57.124	122.209	32.100	5.9	EQ	5	H71	EDR	Siberia, Russia	15
1989/04/21	19:08:37.16	57.106	122.365	33.000	4.8	EQ	5	H71	EDR	Siberia, Russia	15
1989/04/24	01:33:59.68	57.124	122.272	24.900	4.8	EQ	5	H71	EDR	Siberia, Russia	15
1989/04/29	06:25:39.71	57.127	122.312	33.000	5.3	EQ	5	H71	EDR	Siberia, Russia	15
1989/05/03	19:59:16.28	39.034	70.648	7.500	4.7	EQ	5	H71	ERE	Garm, Tajikistan	15
1989/05/07	16:28:06.20	57.041	122.264	33.000	5.0	EQ	5	H71	EDR	Siberia, Russia	15
1989/05/17	05:04:35.84	57.056	122.237	30.700	5.6	EQ	5	H71	EDR	Siberia, Russia	15
1989/05/17	15:55:22.84	57.063	122.241	32.100	4.5	EQ	5	H71	EDR	Siberia, Russia	15
1989/07/09	20:07:46.33	57.098	122.309	33.000	4.8	EQ	5	H71	EDR	Siberia, Russia	15
1990/03/25	00:01:07.60	33.714	56.982	15.000	4.8	EQ	10	HDC	ERE	Tabas, Iran	15
1990/05/27	18:27:57.11	40.904	44.284	5.500	4.9	EQ	10	HDC	ERE	Spitak, Armenia	15
1990/09/30	21:22:57.95	38.950	70.847	7.500	5.0	EQ	5	HDC	ERE	Garm, Tajikistan	15
1990/10/15	19:06:50.14	33.739	56.818	15.000	4.9	EQ	10	HDC	ERE	Tabas, Iran	15
1990/12/18	02:40:50.86	30.509	79.196	12.000	4.8	EQ	5	HDC	ERE	Chamoli, India	15
1991/04/26	22:24:00.45	38.990	70.886	7.500	5.3	EQ	5	HDC	ERE	Garm, Tajikistan	15
1991/04/29	09:12:46.40	42.422	43.695	7.000	6.2	EQ	5	HDC	ERE	Racha, Georgia	15
1991/04/29	09:37:37.20	42.480	43.858	7.000	4.8	EQ	5	HDC	ERE	Racha, Georgia	15
1991/04/29	09:59:24.06	42.487	43.397	7.000	4.8	EQ	5	HDC	ERE	Racha, Georgia	15
1991/04/29	10:52:41.68	42.487	43.948	7.000	4.6	EQ	5	HDC	ERE	Racha, Georgia	15
1991/04/29	11:04:29.36	42.457	43.908	7.000	4.3	EQ	5	HDC	ERE	Racha, Georgia	15
1991/04/29	11:10:12.21	42.503	43.915	7.000	4.9	EQ	5	HDC	ERE	Racha, Georgia	15
1991/04/29	11:51:10.25	42.454	43.822	7.000	5.0	EQ	5	HDC	ERE	Racha, Georgia	15
1991/04/29	11:59:54.61	42.434	43.955	7.000	4.7	EQ	5	HDC	ERE	Racha, Georgia	15
1991/04/29	13:49:58.96	42.500	43.366	7.000	4.4	EQ	5	HDC	ERE	Racha, Georgia	15
1991/04/29	14:43:06.41	42.433	43.915	7.000	5.4	EQ	5	HDC	ERE	Racha, Georgia	15
1991/04/29	17:54:59.83	42.528	43.953	7.000	4.4	EQ	5	HDC	ERE	Racha, Georgia	15
1991/04/29	18:23:15.25	42.478	43.768	7.000	5.5	EQ	5	HDC	ERE	Racha, Georgia	15
1991/04/29	18:30:41.10	42.456	43.905	13.200	5.8	EQ	5	HDC	ERE	Racha, Georgia	15
1991/04/29	19:07:03.75	42.411	43.697	7.000	4.5	EQ	5	HDC	ERE	Racha, Georgia	15
1991/04/29	19:19:55.40	42.474	43.920	7.000	4.3	EQ	5	HDC	ERE	Racha, Georgia	15
1991/04/29	19:44:54.38	42.486	43.929	7.000	4.5	EQ	5	HDC	ERE	Racha, Georgia	15
1991/04/29	20:24:42.79	42.368	43.822	7.000	4.8	EQ	5	HDC	ERE	Racha, Georgia	15
1991/04/29	20:32:54.27	42.463	43.325	7.000	5.4	EQ	5	HDC	ERE	Racha, Georgia	15
1991/04/29	21:24:09.76	42.516	43.739	7.000	4.5	EQ	5	HDC	ERE	Racha, Georgia	15
1991/04/29	22:28:22.66	42.474	43.780	7.000	4.8	EQ	5	HDC	ERE	Racha, Georgia	15
1991/04/29	23:32:28.84	42.409	43.907	7.000	4.5	EQ	5	HDC	ERE	Racha, Georgia	15
1991/05/01	05:13:35.87	42.587	43.544	7.000	4.6	EQ	5	HDC	ERE	Racha, Georgia	15
1991/05/02	01:25:29.65	42.437	44.013	7.000	5.1	EQ	5	HDC	ERE	Racha, Georgia	15
1991/05/02	09:44:42.24	42.544	43.601	7.000	4.5	EQ	5	HDC	ERE	Racha, Georgia	15
1991/05/03	20:19:39.60	42.584	43.246	7.700	5.4	EQ	5	HDC	ERE	Racha, Georgia	15
1991/05/03	23:41:01.93	42.568	43.317	7.000	5.2	EQ	5	HDC	ERE	Racha, Georgia	15
1991/05/06	01:35:27.29	42.540	43.240	7.000	4.3	EQ	5	HDC	ERE	Racha, Georgia	15
1991/05/10	01:25:16.29	42.538	43.272	7.000	4.5	EQ	5	HDC	ERE	Racha, Georgia	15
1991/05/10	20:52:27.23	42.392	43.980	7.000	4.8	EQ	5	HDC	ERE	Racha, Georgia	15

1991/05/14	09:36:25.11	42.593	43.530	4.500	3.9	EQ	5	HDC	ERE	Racha, Georgia	15
1991/05/15	14:28:50.20	42.493	43.385	4.300	5.0	EQ	5	HDC	ERE	Racha, Georgia	15
1991/06/15	00:59:20.10	42.431	44.023	7.000	5.9	EQ	5	HDC	ERE	Racha, Georgia	15
1991/06/17	03:04:45.60	42.359	44.193	7.000	4.4	EQ	5	HDC	ERE	Racha, Georgia	15
1991/06/30	20:09:19.31	42.473	43.772	7.000	4.7	EQ	5	HDC	ERE	Racha, Georgia	15
1991/07/04	06:26:30.44	42.351	44.155	7.000	5.1	EQ	5	HDC	ERE	Racha, Georgia	15
1991/07/14	05:51:22.98	33.293	57.256	15.000	4.5	EQ	10	HDC	ERE	Tabas, Iran	15
1991/08/20	05:06:26.00	30.635	79.582	12.000	4.2	EQ	5	HDC	ERE	Chamoli, India	15
1991/10/15	19:10:59.22	30.602	79.224	12.000	4.5	EQ	5	HDC	ERE	Chamoli, India	15
1991/10/19	21:23:15.54	30.763	78.733	12.000	6.4	EQ	5	HDC	ERE	Chamoli, India	15
1991/10/19	22:29:20.52	30.815	78.748	12.000	4.6	EQ	5	HDC	ERE	Chamoli, India	15
1991/10/19	22:41:16.07	30.748	78.665	12.000	4.8	EQ	5	HDC	ERE	Chamoli, India	15
1991/10/20	01:21:01.30	30.741	78.645	12.000	3.9	EQ	5	HDC	ERE	Chamoli, India	15
1991/10/20	04:20:27.41	30.841	78.671	12.000	4.4	EQ	5	HDC	ERE	Chamoli, India	15
1991/10/20	05:32:26.15	30.786	78.658	12.000	4.8	EQ	5	HDC	ERE	Chamoli, India	15
1991/10/23	20:41:54.89	33.278	57.366	15.000	4.4	EQ	10	HDC	ERE	Tabas, Iran	15
1991/10/23	20:45:05.31	33.135	57.344	15.000	4.6	EQ	10	HDC	ERE	Tabas, Iran	15
1991/10/27	00:40:23.51	30.777	78.784	12.000	4.1	EQ	5	HDC	ERE	Chamoli, India	15
1992/01/11	20:09:17.50	38.837	70.534	7.500	4.7	EQ	5	HDC	ERE	Garm, Tajikistan	15
1992/03/14	12:40:25.05	30.706	78.781	12.000	4.7	EQ	5	HDC	ERE	Chamoli, India	15
1992/09/06	08:42:05.58	33.813	56.885	15.000	4.7	EQ	10	HDC	ERE	Tabas, Iran	15
1993/08/08	22:41:41.90	38.648	70.330	7.500	5.0	EQ	5	HDC	ERE	Garm, Tajikistan	15
1993/08/15	03:19:33.75	30.836	78.807	12.000	4.2	EQ	5	HDC	ERE	Chamoli, India	15
1993/08/28	04:26:25.71	17.229	73.758	6.700	4.8	EQ	5	HDC	ERE	Koyna, India	15
1993/09/03	23:01:35.11	17.240	73.788	6.900	4.6	EQ	5	HDC	ERE	Koyna, India	15
1993/12/08	01:42:17.36	17.207	73.761	8.400	4.9	EQ	5	HDC	ERE	Koyna, India	15
1994/05/04	10:40:12.29	38.850	70.249	7.500	5.0	EQ	5	HDC	ERE	Garm, Tajikistan	15
1995/11/27	21:44:00.48	30.719	79.135	12.000	4.5	EQ	5	HDC	ERE	Chamoli, India	15
1996/01/23	17:34:39.68	30.527	79.362	12.000	4.3	EQ	5	HDC	ERE	Chamoli, India	15
1996/03/26	08:30:22.32	30.686	79.074	12.000	4.6	EQ	5	HDC	ERE	Chamoli, India	15
1996/04/26	12:19:31.62	17.138	73.660	8.400	4.3	EQ	5	HDC	ERE	Koyna, India	15
1996/08/03	13:33:22.96	30.798	78.793	12.000	3.9	EQ	5	HDC	ERE	Chamoli, India	15
1997/01/21	01:47:12.81	39.623	76.966	17.000	4.8	EQ	10	HDC	ERE	Jiashi, China	15
1997/01/21	01:48:28.04	39.645	77.111	18.000	5.1	EQ	10	HDC	ERE	Jiashi, China	15
1997/01/22	09:59:02.47	39.774	77.026	23.000	3.7	EQ	10	HDC	ERE	Jiashi, China	15
1997/01/23	10:56:26.55	39.694	77.200	20.000	4.0	EQ	10	HDC	ERE	Jiashi, China	15
1997/01/24	01:36:10.51	39.627	76.908	20.000	3.9	EQ	10	HDC	ERE	Jiashi, China	15
1997/01/24	12:42:55.30	39.616	76.939	20.000	3.7	EQ	10	HDC	ERE	Jiashi, China	15
1997/01/24	23:58:42.48	39.687	77.013	20.000	3.8	EQ	10	HDC	ERE	Jiashi, China	15
1997/01/30	21:57:39.60	39.688	77.035	20.000	4.0	EQ	10	HDC	ERE	Jiashi, China	15
1997/02/11	20:20:59.18	39.599	77.008	27.000	4.6	EQ	10	HDC	ERE	Jiashi, China	15
1997/02/15	05:26:07.34	39.729	77.056	20.000	4.5	EQ	10	HDC	ERE	Jiashi, China	15
1997/02/17	18:00:07.92	39.592	76.925	20.000	4.1	EQ	10	HDC	ERE	Jiashi, China	15
1997/02/21	14:29:11.57	39.680	77.062	20.000	4.2	EQ	10	HDC	ERE	Jiashi, China	15
1997/02/26	15:09:07.62	39.711	77.043	12.900	3.9	EQ	10	HDC	ERE	Jiashi, China	15
1997/03/01	04:25:24.70	39.711	77.056	21.500	4.2	EQ	10	HDC	ERE	Jiashi, China	15
1997/03/01	06:04:13.10	39.581	76.948	20.000	5.0	EQ	10	HDC	ERE	Jiashi, China	15
1997/03/01	09:35:07.50	39.665	77.068	20.000	4.0	EQ	10	HDC	ERE	Jiashi, China	15
1997/03/01	17:52:04.91	39.622	77.037	20.000	3.8	EQ	10	HDC	ERE	Jiashi, China	15
1997/03/31	19:12:47.52	39.635	76.942	20.000	3.8	EQ	10	HDC	ERE	Jiashi, China	15
1997/04/02	18:42:04.86	39.582	76.935	20.000	4.2	EQ	10	HDC	ERE	Jiashi, China	15
1997/04/03	20:41:40.96	39.640	76.941	20.000	4.0	EQ	10	HDC	ERE	Jiashi, China	15
1997/04/05	23:46:18.00	39.644	76.993	29.000	5.3	EQ	10	HDC	ERE	Jiashi, China	15
1997/04/06	00:06:28.68	39.656	76.964	20.000	4.1	EQ	10	HDC	ERE	Jiashi, China	15

1997/04/06	02:20:26.40	39.611	76.942	20.000	4.1	EQ	10	HDC	ERE	Jiashi, China	15
1997/04/06	04:36:32.52	39.646	77.107	21.000	5.4	EQ	10	HDC	ERE	Jiashi, China	15
1997/04/06	05:09:27.02	39.613	76.921	20.000	4.2	EQ	10	HDC	ERE	Jiashi, China	15
1997/04/06	06:57:55.83	39.689	76.977	20.000	3.9	EQ	10	HDC	ERE	Jiashi, China	15
1997/04/06	11:01:55.19	39.620	76.962	20.000	4.1	EQ	10	HDC	ERE	Jiashi, China	15
1997/04/06	12:40:01.32	39.676	77.046	11.500	3.5	EQ	10	HDC	ERE	Jiashi, China	15
1997/04/06	12:58:15.09	39.667	77.072	16.000	5.0	EQ	10	HDC	ERE	Jiashi, China	15
1997/04/06	15:14:07.34	39.674	76.953	20.000	3.9	EQ	10	HDC	ERE	Jiashi, China	15
1997/04/06	16:19:32.85	39.675	77.012	20.000	3.6	EQ	10	HDC	ERE	Jiashi, China	15
1997/04/06	17:38:32.58	39.643	77.009	20.000	3.6	EQ	10	HDC	ERE	Jiashi, China	15
1997/04/07	04:43:21.02	39.689	77.168	20.000	3.7	EQ	10	HDC	ERE	Jiashi, China	15
1997/04/07	08:28:25.54	39.661	76.896	20.000	3.7	EQ	10	HDC	ERE	Jiashi, China	15
1997/04/07	21:22:52.17	39.679	76.956	20.000	3.9	EQ	10	HDC	ERE	Jiashi, China	15
1997/04/08	01:29:04.55	39.636	76.922	20.000	3.7	EQ	10	HDC	ERE	Jiashi, China	15
1997/04/08	03:34:17.19	39.685	77.048	20.000	4.0	EQ	10	HDC	ERE	Jiashi, China	15
1997/04/08	13:11:44.39	39.700	77.084	20.000	4.0	EQ	10	HDC	ERE	Jiashi, China	15
1997/04/09	04:02:41.51	39.635	76.930	20.000	4.2	EQ	10	HDC	ERE	Jiashi, China	15
1997/04/10	02:58:33.25	39.695	76.984	20.000	4.4	EQ	10	HDC	ERE	Jiashi, China	15
1997/04/10	03:01:46.98	39.725	77.001	12.300	4.2	EQ	10	HDC	ERE	Jiashi, China	15
1997/04/11	03:33:45.09	39.703	76.991	20.000	4.3	EQ	10	HDC	ERE	Jiashi, China	15
1997/04/11	04:29:09.89	39.706	76.954	20.000	4.4	EQ	10	HDC	ERE	Jiashi, China	15
1997/04/11	05:34:42.62	39.674	77.054	21.000	5.6	EQ	10	HDC	ERE	Jiashi, China	15
1997/04/11	07:50:03.93	39.703	76.820	20.000	3.6	EQ	10	HDC	ERE	Jiashi, China	15
1997/04/11	09:05:14.81	39.691	76.958	20.000	4.1	EQ	10	HDC	ERE	Jiashi, China	15
1997/04/11	11:25:31.93	39.621	77.027	20.000	3.8	EQ	10	HDC	ERE	Jiashi, China	15
1997/04/11	12:32:15.55	39.636	77.019	20.000	3.8	EQ	10	HDC	ERE	Jiashi, China	15
1997/04/11	12:42:15.71	39.696	76.976	20.000	3.6	EQ	10	HDC	ERE	Jiashi, China	15
1997/04/12	21:09:08.60	39.593	77.019	23.000	5.0	EQ	10	HDC	ERE	Jiashi, China	15
1997/04/12	21:41:22.41	39.609	76.954	20.000	3.7	EQ	10	HDC	ERE	Jiashi, China	15
1997/04/14	00:02:09.53	39.633	76.984	20.000	4.2	EQ	10	HDC	ERE	Jiashi, China	15
1997/04/15	04:12:19.45	39.645	77.043	19.300	3.9	EQ	10	HDC	ERE	Jiashi, China	15
1997/04/15	18:02:14.29	39.611	77.045	12.300	3.7	EQ	10	HDC	ERE	Jiashi, China	15
1997/04/15	18:19:08.25	39.710	77.086	18.000	5.4	EQ	10	HDC	ERE	Jiashi, China	15
1997/04/15	18:51:25.20	39.749	77.084	20.000	4.0	EQ	10	HDC	ERE	Jiashi, China	15
1997/04/15	18:55:39.02	39.787	77.133	20.000	4.0	EQ	10	HDC	ERE	Jiashi, China	15
1997/04/16	01:23:24.45	39.712	76.967	20.000	4.1	EQ	10	HDC	ERE	Jiashi, China	15
1997/04/22	14:15:35.02	39.679	77.061	13.600	3.9	EQ	10	HDC	ERE	Jiashi, China	15
1997/04/24	23:15:38.16	39.686	77.081	14.800	3.7	EQ	10	HDC	ERE	Jiashi, China	15
1997/04/26	04:54:59.73	39.568	77.014	20.000	3.8	EQ	10	HDC	ERE	Jiashi, China	15
1997/05/02	12:19:59.20	39.595	76.814	20.000	3.7	EQ	10	HDC	ERE	Jiashi, China	15
1997/05/06	06:39:03.05	39.586	76.769	20.000	3.7	EQ	10	HDC	ERE	Jiashi, China	15
1997/05/17	03:58:22.13	39.662	77.067	26.000	4.8	EQ	10	HDC	ERE	Jiashi, China	15
1997/05/27	10:16:03.93	39.703	76.980	13.000	3.8	EQ	10	HDC	ERE	Jiashi, China	15
1997/06/06	00:23:04.08	39.580	76.817	20.000	4.1	EQ	10	HDC	ERE	Jiashi, China	15
1997/06/24	09:24:45.30	39.650	77.000	19.000	4.7	EQ	10	HDC	ERE	Jiashi, China	15
1997/06/24	10:06:39.25	39.675	76.888	20.000	3.6	EQ	10	HDC	ERE	Jiashi, China	15
1997/10/17	17:35:13.16	39.523	76.890	22.000	4.6	EQ	10	HDC	ERE	Jiashi, China	15
1998/02/11	01:08:46.06	17.159	73.753	13.300	4.2	EQ	5	HDC	ERE	Koyna, India	15
1998/02/14	00:59:49.69	17.143	73.740	4.900	4.3	EQ	5	HDC	ERE	Koyna, India	15
1998/05/01	11:57:35.43	30.301	79.432	12.000	4.1	EQ	5	HDC	ERE	Chamoli, India	15
1998/11/19	12:41:57.32	30.597	79.215	12.000	3.8	EQ	5	HDC	ERE	Chamoli, India	15
1998/11/19	16:34:15.63	30.603	79.201	12.000	4.3	EQ	5	HDC	ERE	Chamoli, India	15
1999/02/25	11:13:53.16	30.758	78.856	12.000	3.8	EQ	5	HDC	ERE	Chamoli, India	15
1999/03/28	19:05:11.54	30.494	79.347	12.000	6.4	EQ	5	HDC	ERE	Chamoli, India	15

1999/03/28	19:36:07.50	30.429	79.355	12.000	5.2	EQ	5	HDC ERE	Chamoli, India	15
1999/03/28	19:47:06.80	30.458	79.318	12.000	4.7	EQ	5	HDC ERE	Chamoli, India	15
1999/03/28	20:10:10.98	30.438	79.278	12.000	4.0	EQ	5	HDC ERE	Chamoli, India	15
1999/03/28	20:11:15.13	30.455	79.328	12.000	4.3	EQ	5	HDC ERE	Chamoli, India	15
1999/03/28	21:42:50.30	30.498	79.335	12.000	3.7	EQ	5	HDC ERE	Chamoli, India	15
1999/03/28	21:57:10.65	30.486	79.378	12.000	NA	EQ	5	HDC ERE	Chamoli, India	15
1999/03/28	23:01:40.18	30.529	79.415	12.000	3.9	EQ	5	HDC ERE	Chamoli, India	15
1999/03/28	23:04:39.38	30.621	79.290	12.000	4.2	EQ	5	HDC ERE	Chamoli, India	15
1999/03/28	23:20:29.04	30.531	79.365	12.000	4.0	EQ	5	HDC ERE	Chamoli, India	15
1999/03/29	00:22:46.84	30.436	79.370	12.000	3.9	EQ	5	HDC ERE	Chamoli, India	15
1999/03/29	00:54:14.56	30.501	79.406	12.000	NA	EQ	5	HDC ERE	Chamoli, India	15
1999/03/29	07:07:36.84	30.366	79.213	12.000	NA	EQ	5	HDC ERE	Chamoli, India	15
1999/03/29	08:49:47.70	30.468	79.235	12.000	4.3	EQ	5	HDC ERE	Chamoli, India	15
1999/03/29	13:21:00.25	30.442	79.300	12.000	3.9	EQ	5	HDC ERE	Chamoli, India	15
1999/03/30	15:51:51.83	30.446	79.386	12.000	4.0	EQ	5	HDC ERE	Chamoli, India	15
1999/03/30	21:02:12.31	30.438	79.328	12.000	5.2	EQ	5	HDC ERE	Chamoli, India	15
1999/03/30	21:20:46.10	30.486	79.389	12.000	3.7	EQ	5	HDC ERE	Chamoli, India	15
1999/03/31	08:39:59.05	30.444	79.324	12.000	NA	EQ	5	HDC ERE	Chamoli, India	15
1999/03/31	15:52:35.84	30.437	79.379	12.000	3.5	EQ	5	HDC ERE	Chamoli, India	15
1999/04/01	02:48:53.40	30.528	79.349	12.000	4.0	EQ	5	HDC ERE	Chamoli, India	15
1999/04/06	19:37:27.16	30.456	79.316	5.300	5.1	EQ	5	HDC ERE	Chamoli, India	15
1999/04/06	20:46:42.29	30.453	79.320	15.000	4.6	EQ	5	HDC ERE	Chamoli, India	15
1999/04/07	15:49:14.59	30.489	79.334	17.000	4.8	EQ	5	HDC ERE	Chamoli, India	15
1999/04/07	16:23:29.12	30.471	79.323	16.100	4.4	EQ	5	HDC ERE	Chamoli, India	15
1999/04/14	17:24:30.87	30.400	79.354	12.800	4.8	EQ	5	HDC ERE	Chamoli, India	15
1999/04/18	17:16:39.23	30.442	79.361	13.800	4.8	EQ	5	HDC ERE	Chamoli, India	15
1999/04/25	09:52:15.88	30.417	79.359	9.600	3.6	EQ	5	HDC ERE	Chamoli, India	15
1999/05/07	17:12:04.26	30.373	79.377	16.200	4.0	EQ	5	HDC ERE	Chamoli, India	15
1999/05/14	08:31:02.99	30.442	79.307	12.000	3.9	EQ	5	HDC ERE	Chamoli, India	15
1999/06/13	13:40:04.99	30.835	78.627	12.000	3.7	EQ	5	HDC ERE	Chamoli, India	15
2000/03/12	18:03:54.99	17.173	73.719	5.100	4.9	EQ	5	HDC ERE	Koyna, India	15
2000/04/06	22:30:12.48	17.142	73.747	7.000	4.9	EQ	5	HDC ERE	Koyna, India	15
2000/09/05	00:32:44.36	17.182	73.753	10.000	4.7	EQ	5	HDC ERE	Koyna, India	15
2000/12/24	11:22:01.90	24.021	69.765	18.000	4.6	EQ	5	HDC ERE	Bhuj, India	15
2001/01/26	03:16:42.11	23.436	70.344	18.000	6.9	EQ	5	HDC ERE	Bhuj, India	15
2001/01/26	03:33:33.01	23.388	70.021	18.000	5.3	EQ	5	HDC ERE	Bhuj, India	15
2001/01/26	03:59:03.09	23.414	70.123	18.000	4.9	EQ	5	HDC ERE	Bhuj, India	15
2001/01/26	04:23:45.40	23.450	70.227	18.000	5.2	EQ	5	HDC ERE	Bhuj, India	15
2001/01/26	04:48:18.29	23.442	70.410	18.000	5.1	EQ	5	HDC ERE	Bhuj, India	15
2001/01/26	06:04:55.08	23.553	70.229	18.000	4.9	EQ	5	HDC ERE	Bhuj, India	15
2001/01/26	07:32:32.83	23.486	70.090	18.300	5.2	EQ	5	HDC ERE	Bhuj, India	15
2001/01/26	18:19:47.01	23.534	70.437	18.000	4.7	EQ	5	HDC ERE	Bhuj, India	15
2001/01/27	03:50:04.55	23.486	70.409	18.000	4.7	EQ	5	HDC ERE	Bhuj, India	15
2001/01/27	04:36:09.21	23.536	70.391	18.000	4.8	EQ	5	HDC ERE	Bhuj, India	15
2001/01/27	11:24:25.37	23.422	70.503	18.000	4.6	EQ	5	HDC ERE	Bhuj, India	15
2001/01/28	01:02:14.54	23.533	70.598	22.700	5.9	EQ	5	HDC ERE	Bhuj, India	15
2001/01/28	03:26:15.77	23.491	70.142	23.400	4.3	EQ	5	HDC ERE	Bhuj, India	15
2001/01/28	11:10:46.73	23.332	70.395	18.000	4.8	EQ	5	HDC ERE	Bhuj, India	15
2001/01/28	17:15:28.44	23.302	70.027	31.000	4.7	EQ	5	HDC ERE	Bhuj, India	15
2001/01/28	19:42:22.98	23.514	70.099	26.400	4.3	EQ	5	HDC ERE	Bhuj, India	15
2001/01/29	01:39:06.53	23.448	70.111	18.000	4.8	EQ	5	HDC ERE	Bhuj, India	15
2001/01/29	09:38:48.13	23.591	70.504	19.800	4.8	EQ	5	HDC ERE	Bhuj, India	15
2001/01/29	19:14:57.01	23.450	70.538	18.000	4.0	EQ	5	HDC ERE	Bhuj, India	15
2001/01/29	23:54:59.64	23.551	70.293	6.600	4.8	EQ	5	HDC ERE	Bhuj, India	15

2001/01/30	18:19:59.97	23.383	70.380	18.000	4.7	EQ	5	HDC	ERE	Bhuj, India	15
2001/01/31	01:56:10.14	23.511	70.023	18.000	4.4	EQ	5	HDC	ERE	Bhuj, India	15
2001/01/31	03:34:59.75	23.457	70.428	18.000	4.4	EQ	5	HDC	ERE	Bhuj, India	15
2001/01/31	07:32:36.51	23.534	70.224	18.000	4.4	EQ	5	HDC	ERE	Bhuj, India	15
2001/01/31	09:42:24.74	23.489	70.531	11.500	4.9	EQ	5	HDC	ERE	Bhuj, India	15
2001/01/31	23:36:14.45	23.384	70.216	18.000	4.4	EQ	5	HDC	ERE	Bhuj, India	15
2001/02/01	21:07:03.55	23.516	70.178	18.000	4.1	EQ	5	HDC	ERE	Bhuj, India	15
2001/02/01	22:29:38.06	23.556	70.145	18.000	4.6	EQ	5	HDC	ERE	Bhuj, India	15
2001/02/03	03:04:36.30	23.693	70.531	18.000	5.3	EQ	5	HDC	ERE	Bhuj, India	15
2001/02/03	10:06:41.52	23.414	70.165	25.900	4.5	EQ	5	HDC	ERE	Bhuj, India	15
2001/02/04	04:47:27.78	23.604	70.204	18.000	4.5	EQ	5	HDC	ERE	Bhuj, India	15
2001/02/04	04:50:38.56	23.346	70.158	25.900	4.1	EQ	5	HDC	ERE	Bhuj, India	15
2001/02/04	15:34:09.89	23.559	70.123	18.000	4.4	EQ	5	HDC	ERE	Bhuj, India	15
2001/02/04	17:23:17.06	23.397	70.341	18.000	4.4	EQ	5	HDC	ERE	Bhuj, India	15
2001/02/05	02:59:39.29	23.534	70.043	18.000	4.7	EQ	5	HDC	ERE	Bhuj, India	15
2001/02/08	03:25:57.00	23.384	70.378	17.000	4.4	EQ	5	HDC	ERE	Bhuj, India	15
2001/02/08	09:33:13.38	23.397	70.486	26.300	4.3	EQ	5	HDC	ERE	Bhuj, India	15
2001/02/08	16:54:45.60	23.706	70.488	28.000	4.9	EQ	5	HDC	ERE	Bhuj, India	15
2001/02/09	10:07:44.12	23.589	70.126	35.600	4.7	EQ	5	HDC	ERE	Bhuj, India	15
2001/02/09	12:37:04.96	23.416	70.420	16.200	4.8	EQ	5	HDC	ERE	Bhuj, India	15
2001/02/11	02:33:21.48	23.408	70.555	15.500	4.6	EQ	5	HDC	ERE	Bhuj, India	15
2001/02/11	15:29:43.84	23.351	70.325	29.800	4.5	EQ	5	HDC	ERE	Bhuj, India	15
2001/02/15	10:04:42.17	23.341	70.354	25.500	4.7	EQ	5	HDC	ERE	Bhuj, India	15
2001/02/17	08:27:27.76	23.414	70.489	8.200	4.8	EQ	5	HDC	ERE	Bhuj, India	15
2001/02/19	02:11:14.42	23.605	70.227	30.500	4.6	EQ	5	HDC	ERE	Bhuj, India	15
2001/02/19	08:24:21.05	23.596	70.158	8.600	5.2	EQ	5	HDC	ERE	Bhuj, India	15
2001/02/19	09:22:00.23	23.598	70.139	10.000	4.2	EQ	5	HDC	ERE	Bhuj, India	15
2001/02/22	02:13:04.96	23.405	70.427	24.200	4.7	EQ	5	HDC	ERE	Bhuj, India	15
2001/03/01	00:53:21.07	23.445	70.390	25.500	4.5	EQ	5	HDC	ERE	Bhuj, India	15
2001/03/02	21:56:51.12	23.412	70.301	18.000	4.4	EQ	5	HDC	ERE	Bhuj, India	15
2001/03/04	07:54:27.21	23.113	70.525	22.700	4.8	EQ	5	HDC	ERE	Bhuj, India	15
2001/03/12	11:34:17.17	30.618	79.093	12.000	4.5	EQ	5	HDC	ERE	Chamoli, India	15
2001/03/14	10:42:11.62	23.368	70.304	34.000	4.5	EQ	5	HDC	ERE	Bhuj, India	15
2001/03/19	20:06:52.23	23.478	70.214	20.000	4.8	EQ	5	HDC	ERE	Bhuj, India	15
2001/03/24	01:13:50.84	23.450	70.450	20.000	NA	EQ	5	HDC	ERE	Bhuj, India	15
2001/04/01	08:56:53.04	23.509	70.569	20.000	4.6	EQ	5	HDC	ERE	Bhuj, India	15
2001/04/12	17:24:34.13	23.665	70.568	36.700	4.1	EQ	5	HDC	ERE	Bhuj, India	15
2001/04/26	09:00:28.17	23.578	70.370	23.000	4.2	EQ	5	HDC	ERE	Bhuj, India	15
2001/05/06	07:42:34.30	23.386	70.251	18.000	4.7	EQ	5	HDC	ERE	Bhuj, India	15
2001/05/06	22:58:54.47	23.500	70.062	18.000	4.7	EQ	5	HDC	ERE	Bhuj, India	15
2001/05/07	16:44:08.35	23.101	69.952	18.000	3.7	EQ	5	HDC	ERE	Bhuj, India	15
2001/05/13	04:05:43.56	23.431	70.203	18.000	4.4	EQ	5	HDC	ERE	Bhuj, India	15
2001/06/17	16:02:30.59	23.756	70.148	18.000	4.2	EQ	5	HDC	ERE	Bhuj, India	15
2001/06/21	14:19:23.55	23.077	69.567	18.000	4.4	EQ	5	HDC	ERE	Bhuj, India	15
2001/06/30	20:19:51.81	23.370	70.181	18.000	4.5	EQ	5	HDC	ERE	Bhuj, India	15
2001/07/04	02:15:17.57	23.276	70.242	18.000	4.1	EQ	5	HDC	ERE	Bhuj, India	15
2001/07/11	22:37:34.48	23.669	70.396	18.000	3.7	EQ	5	HDC	ERE	Bhuj, India	15
2001/08/01	06:20:09.69	23.658	70.440	18.000	4.0	EQ	5	HDC	ERE	Bhuj, India	15
2001/08/03	04:24:24.26	23.590	70.076	18.000	4.4	EQ	5	HDC	ERE	Bhuj, India	15
2001/08/04	11:24:39.27	23.366	70.332	18.000	4.3	EQ	5	HDC	ERE	Bhuj, India	15
2001/09/20	13:34:33.04	23.560	70.395	18.000	4.7	EQ	5	HDC	ERE	Bhuj, India	15
2001/09/21	02:40:41.33	23.522	70.065	18.000	4.5	EQ	5	HDC	ERE	Bhuj, India	15
2001/10/03	00:48:06.45	23.320	70.107	18.000	3.9	EQ	5	HDC	ERE	Bhuj, India	15
2001/10/31	09:17:50.46	23.719	69.961	18.000	4.8	EQ	5	HDC	ERE	Bhuj, India	15

2001/11/24	02:42:43.25	23.624	70.486	18.000	4.6	EQ	5	HDC	ERE	Bhuj, India	15
2001/12/01	22:03:26.38	23.357	70.142	18.000	4.1	EQ	5	HDC	ERE	Bhuj, India	15
2001/12/12	15:00:21.71	23.665	70.266	18.000	NA	EQ	5	HDC	ERE	Bhuj, India	15
2002/01/09	23:52:45.25	23.539	70.350	18.000	4.8	EQ	5	HDC	ERE	Bhuj, India	15
2002/03/30	06:17:50.23	23.544	70.421	18.000	4.5	EQ	5	HDC	ERE	Bhuj, India	15

Abbreviations:

Ba98: Barker, B., M. Clark, P. Davis, M. Fisk, M. Hedlin, H. Israelsson, V. Khalturin, W.-Y. Kim, K. McLaughlin, C. Meade, J. Murphy, R. North, J. Orcutt, C. Powell, P.G. Richards, R. Stead, J. Stevens, F. Vernon, and T. Wallace, Monitoring Nuclear Tests, Science, 281, 1967-1968, 1998.

Bo89: Bocharov, V.S., S.A. Zelentsov and V.N. Mikhailov, Characteristics of 96 underground nuclear explosions at the Semipalatinsk Test Site, Atomaya Energia, (in Russian), Vol. 67, no. 3, 210-214, 1989.

CS: Controlled source, with local recording of location and origin time.

CTBT98: CTBT/PC/V/WGB/JP/4 (1998). Comparison of the REB of the IDC with the Seismological Bulletin of the JMA, Delegation of Japan, Working Group B of the CTBT Preparatory Commission, Vienna, Austria.

CYT: Chen Yun-Tai, personal communication.

DD: Double-difference method hypoDD (Waldhauser, F., HypoDD: A program to compute double-difference hypocenter locations, *U.S. Geol. Surv. open-file report*, 01-113, Menlo Park, California, 2001)

ERE: E.R. Engdahl, personal communication.

EQ: Earthquake

EX: Chemical explosion.

Fi02: Fisk, M. D., Accurate locations of nuclear explosions at the Lop Nor Test Site using alignment of seismograms and IKONOS satellite imagery, *Bull. Seism. Soc. Am.*, 92, 2911-2925, 2002.

GTn: Ground truth location, with n being the horizontal uncertainty in km.

HDC: Hypocentral Decomposition method for earthquake location (Jordan, H.T. and K.A. Sverdrup, Teleseismic location techniques and their application to earthquake clusters in the south-central Pacific, *Bull. Seism. Soc. Amer.*, 71, 1105-1130, 1981).

HI: Program HYPOINVERSE (Klein, F., User's guide to HYPOINVERSE-2000, a Fortran program to solve for earthquake locations and magnitudes, *U.S. Geol. Surv. open-file report*, 02-171, Menlo Park, California, 2002).

H71: Earthquake location program HYPO71.

IDG: Institute of the Dynamics of the Geosphere, Russian Academy of Sciences.

JHD: Joint Hypocenter Determination.

LDEO: Lamont-Doherty Earth Observatory

LS: Program LocSat (Bratt, S., and T. Bache, Locating events with a sparse network of regional arrays, *Bull. Seism. Soc. Amer.* 78, 780-798, 1988).

KFM: Kuo-Fong Ma, personal communication.

NNC: National Nuclear Center, Kazakhstan.
PNE: Peaceful Nuclear Explosion.
SMR99: Sultanov, D. D., J.R. Murphy and Kh.D. Rubinstein, A seismic source summary for Soviet peaceful nuclear explosions, *Bull. Seism. Soc. Amer.*, 89, 640-647, 1999.
UNE: Underground Nuclear Explosion.
FW: Francis Wu, personal communication.

Footnotes:

[1] Location uncertainties from Sultanov et al. (1999) are converted to GT levels as follows:
GT 0 = location accuracy, 0.2 - 1 km and origin time accuracy, 0.01s;
GT 5 = location accuracy, 5 - 10 km and origin time accuracy, 0.01s; or location accuracy, 0.2 - 1 km and origin time accuracy, 0.5s;
GT 10 = location accuracy, 5 - 10 km and origin time accuracy, 0.5s.

[2] See Section 'Reference Events in China Derived from Cluster Analysis and Fault Data' for a detailed description of data and method used.

[3] Location is carried out using the HYPOINVERSE program (Klein, 2002) with P and S arrivals at seven stations in the distance ranges 8 km to 50 km. The rms residual is only 0.03s with a maximum station gap of 113 degree. Accuracy of the origin time and location are estimated to be GT5 quality.

[4] This is selected GT events from a set of 10 chemical explosions carried out in Jilin Province, China. Dr. Francis Wu of SUNY, Binghamton, NY provided the location and origin time. These events produced fairly clear P and S arrivals at the GSN station MDJ in northeastern China, and hence the GT0 or GT2 are assigned based upon the signal strength (clarity of arrivals).

[5] Dr. A. Frolova of the Kyrgyz seismological center was given the Bob Engdahl criteria for GT5 earthquakes and asked to provide phase data for local events that best met these criteria and had magnitude greater than 4.2. Data for 32 events were received. Jennifer Eakins of Univ. of California, San Diego then provided additional phase arrivals of these events on the KNET stations. Arrivals at Kazakh stations near the border of Kyrgyzia were included. Data for the Geoscope station WUS were added from the ABCE bulletin or reading of original seismograms. The events were located with LocSat and travel times for Kyrgyzia from our regionalization of Eurasia. The local travel times are for surface focus only so the depth was constrained at zero. After removing events with large azimuthal gap or inconsistent arrivals the final 26 locations remained.

[6] These events were selected out of a cluster of 74 events obtained from Chen Yun-tai's double-difference locations using phase picks from local stations in China. All of the events are greater than M 4 and have more than 450 P-wave observations each (no S-wave observations were used in the location). Although error estimates were not supplied, based on the scatter of the hypocenters less than 1 km, the observed fault structure at this scale, comparison with some high resolution cross correlation Lg locations for a subset of the events, and the extrapolation of the strike and dip of the fault to an isolated surface trace a few km away, we judge these events to be accurate at the GT5 level.

[7] These are GT5 candidate events obtained from Kuo-Fong Ma via Paul Richards that are expected to have accurate locations derived from the local network in Taiwan. All the events satisfy the following GT5 criteria from http://g2calibration.cmr.gov/calibration/data.html#refevents except for the third due to the GAP. GT5 candidate criteria at 95% confidence 1) at least 10 stations within 250 km from the epicenter 2) maximum primary azimuthal gap <= 110 degrees at stations within 250 km 3) maximum secondary azimuthal gap <= 160 degrees at stations within 250 km 4) at least one station within 30 km.

[8] We used phase data from a local network of 193 stations in the Sichuan/Yunnan province (Yang Zhi-xian, pers. communication). The same procedure as described under [2] has been applied to the P- and S-phase data recorded

at this network, to find 17 clusters of 10 or more events, 2 of which indicate fault structure after relocation that can be correlated with nearby fault information. From the 2 clusters a total of 6 GT5 events were selected that were also recorded at ABCE stations; 4 events near Pingwu and 2 events near Qianning. The 2 events near Qianning however were not recorded at IMS stations. Relative errors for these events are generally less than 1 km in horizontal, and less than 2 km in vertical direction.
The results from the Sichuan local network indicate that these data are of high qualitity, and therefore a somewhat less thorough approach is used to collect GT10 events in the two biggest clusters; two clusters of 734 and 205 well constrained events near Chengdu and Yuexi, respectively. These events were relocated using the DD method and GT10 events were identified as those that were recorded at ABCE stations. No formal relative error estimation was performed, and correlation of the seismicity with fault information has been proven difficult due to the complexity of the fault systems in these areas. Nevertheless, 89 GT10 events were selected in the Chengdu cluster, and 24 GT10 events in the Yuexi cluster.

[9] GT event locations at Degelen Mt. are based on existing enterances to tunnels. Origin times are recorded locally and checked with nearby seismograph (portable seismograph with GPS).

[10] Locations are derived from waveform based relative explosion location and correlation with satellite imagery. See Fisk (2002) for details.

[11] GT locations of the 11 May 1998 and 28 May 1998 underground nuclear explosions in India and Pakistan, respectively, were determined by Barker et al. (1998) using SPOT satellite imagery. They assessed the uncertainty of the GT locations as less than 1 km.

[12] GT locations of underground nuclear explosions at the Semipalatinsk test site until the end of 1972 were taken from Bocharov et al. (1989). Locations and origin times after 1972 are from Kitov's IDG data set.

[13] The Japan Meteorological Agency (JMA) operates a national seismic network consisting of 180 stations, including 8 ocean bottom seismometers in 2 lines extending for about 150 km offshore into the Pacific Ocean (CTBT/PC/V/WGB/JP/4). This very dense network and locally calibrated travel times provide very accurate location estimates of events in and near Japan. Since the onset of GSETT-3, the Seismological Bulletin of the JMA (SBJ) has been provided to the CMR and parsed into a database. We selected events that occurred within the JMA network and have been classified with location accuracy of GT5 in the Reference Event Database at the CMR. We then restricted these events to those that were also recorded by KSAR, one of the stations that we are under contract to calibrate. This resulted in 9 GT5 events in or near Japan. The 9 japanese events are considered GT2 in the report by Xiaoping Y. and C. Romney, PIDC Ground Truth (GT) Database, CMR Technical Report CMR-99/15 May, 1999.

[14] The 14 Feb 1977 event was located with the combined data of Tarbela Dam and the Pakistan Atomic Energy Commission seismic networks. Arrival times were taken from the ISC bulletin. By the principle of reciprocity, the travel time from the recording station to the earthquake will be the same as that observed for this earthquake recorded at these stations. After the small corrections for the three dimensional distance from the hypocenter to the Nilore station, these are travel times from a surface focus earthquake to Nilore.

[15] These GT data from various regions were provided to W.-Y. Kim at LDEO by Bob Engdahl (U. of Colorado) in May 2002. We appreciate access to this GT information, obtained by the HDC method. We have not carried out additional analysis.

Appendix C Phase Data from Peaceful Nuclear Explosions in Northern Eurasia

This Appendix describes three different sets of phase picks associated with Peaceful Nuclear Explosions (PNEs) conducted in the Soviet era. First, we describe the data derived from temporary stations deployed as part of the Deep Seismic Sounding Program to obtain refraction profiles from 19 PNEs. Second, we describe the phase picks obtained from seismographic stations (many of them in the U.S.S.R.) from 83 PNEs. And third, we describe the waveforms and phase picks acquired at the Borovoye Observatory, Kazakhstan, and at stations operated by the Complex Seismological Expedition headquartered in Talgar, Kazakhstan.

1. Phase Data from Deep Seismic Sounding Profiles in the Former Soviet Union

Igor Morozov and Elena Morozova at the University of Wyoming compiled phase picks from the DSS (Deep Seismic Sounding) profiles in northern Eurasia (Figure 16). There are seven DSS profiles carried out by using 19 PNEs (Peaceful Nuclear Explosion) conducted between July 26, 1977 through September 6, 1988. The best known ground truth data for these PNEs are from Sultanov et al. (1999) who reported 117 PNEs as listed in Table C1.

There are 8,411 phase picks in the data set, of which 4,761 are *P* phases and 3,650 picks are *S* arrivals. *P, Pn* and *Pg* phases are picked at 3,141 stations, whereas *S*, *Sn* and *Lg* arrivals are picked at 2,570 stations (Figure 16).

There is some uncertainty regarding origin times and locations of the PNEs used to derive these travel time data. We found out that for about half of the PNEs, arrival times appears to be fairly well constrained with respect to the GT1 or GT2 quality event location given in Sultanov et al. (1999). These PNEs are marked as "A" in the Table 8. There are arrival time data from certain PNEs which suggest some constant time offsets of few seconds. These are marked as "B" and are believed to be due to poor reference time given by GEON Center in Moscow, Russia. There are a few PNEs whose event parameters are not well constrained. These are GT10 or worse quality according to Sultanov et al. (1999) and are marked by "C" in Table 8.

It is noted that several PNEs can be used as "reverse" profiles because several segments of the DSS profiles are recorded by shots at forward and reverse ends of the profiles. These profiles can be useful to constrain the poor reference times given by GEON.

These phase data in CSS 3.0 (Center for Seismic Studies) relational database format have been combined in a Unix tar file, DSS_PHASE_DATA.tar. List of tar files with phase data in CSS 3.0 database are listed in Table C2.

Table C1: Origin time and location of the PNEs from Sultanov et al. (1999)

Date mo/dy/year	Origin time (hh:mn:sec)	Lat (N)	Long (E)	Depth (m)	mb (P)	Evid	PNE name
07/26/1977	17:00:00.22	69.575	90.375	850	5.0	45	Meteorite-2
08/10/1977	22:00:00.10	50.955	110.983	494	5.0	46	Meteorite-5
08/20/1977	22:00:00.78	64.108	99.558	600	5.0	47	Meteorite-3
09/10/1977	16:00:00.18	57.251	106.551	550	4.8	48	Meteorite-4
08/09/1978	18:00:00.79	63.678	125.522	567	5.6	52	Craton-4
08/24/1978	18:00:00.35	65.925	112.338	577	5.1	53	Craton-3
09/21/1978	15:00:00.19	66.598	86.210	886	5.2	55	Craton-2
10/17/1978	14:00:00.16	63.185	63.432	593	5.5	58	Craton-1
08/12/1979	18:00:00.21	61.803	122.430	982	4.9	64	Kimberlite-4
09/06/1979	18:00:00.31	64.110	99.562	599	4.9	65	Kimberlite-3
10/04/1979	16:00:00.03	60.675	71.455	837	5.4	67	Kimberlite-1
07/30/1982	21:00:00.00	53.80	104.15	554	5.0	80	Rift-3
09/04/1982	18:00:00.06	69.20	81.65	960	5.3	81	Rift-1
09/25/1982	18:00:00.18	64.35	91.80	554	5.2	82	Rift-4
08/11/1984	19:00:00.20	65.05	55.10	759	5.3	100	Quartz-2
08/25/1984	19:00:00.33	61.90	72.10	726	5.3	101	Quartz-3
09/17/1984	21:00:00.03	55.834	87.526	557	5.0	105	Quartz-4
08/22/1988	16:20:00.07	66.280	78.491	829	5.3	116	Ruby-2
09/06/1988	16:19:59.94	61.361	48.092	820	4.8	117	Ruby-1

Table C2: List of Unix tar files for CSS3.0 relational database of arrival picks from DSS profiles

Nphase	DB tables	Nsta	DB tables	Tar file name
226	crat1.arrival	305	crat1.site	crat-1.tar
631	crat2.arrival	305	crat2.site	crat-2.tar
675	crat3.arrival	305	crat3.site	crat-3.tar
561	crat4.arrival	305	crat4.site	crat-4.tar
288	kimb1.arrival	287	kimb1.site	kimb-1.tar
621	kimb3.arrival	287	kimb3.site	kimb-3.tar
500	kimb4.arrival	287	kimb4.site	kimb-4.tar
401	meteor2.arrival	199	meteor2.site	meteor-2.tar
221	meteor3.arrival	199	meteor3.site	meteor-3.tar
268	meteor4.arrival	199	meteor4.site	meteor-4.tar
117	meteor5.arrival	199	meteor5.site	meteor-5.tar
679	quartz2.arrival	388	quartz2.site	quartz-2.tar
690	quartz3.arrival	388	quartz3.site	quartz-3.tar
474	quartz4.arrival	388	quartz4.site	quartz-4.tar
410	rift1.arrival	249	rift1.site	rift-1.tar
388	rift3.arrival	249	rift3.site	rift-3.tar
362	rift4.arrival	249	rift4.site	rift-4.tar
549	ruby1.arrival	250	ruby1.site	ruby-1.tar
350	ruby2.arrival	162	ruby2.site	ruby-2.tar
8411	total	5200	total	

2. Phase Data from PNEs in FSU during 1966–1988 at Regional Stations

In the spring of 2001, Jack Murphy (then at Maxwell Technologies) informed us of the availability of phase picks from the PNEs (Peaceful Nuclear Explosions) recorded at stations in the Former Soviet Union in northern Eurasia (Figure C1). Most of these PNEs are GT1 to GT5 quality (Sultanov et al., 1999) and hence the travel times from these PNEs are used to calibrate regional travel times in northern Eurasia. We downloaded these data from a Harvard website.

The original phase data were reported to as having come from 1044 stations (129 Soviet plus 915 derived from the International Seismological Centre), however many of these stations reported only a small number of PNEs. Phase data were checked by Kim and Khalturin at LDEO, in particular, many old station names and locations were checked and corrected as necessary, resulting in 7,362 phase picks from 83 PNEs recorded at 355 sites.

The original phase data were compiled by Dr. Ivan Kitov of the Institute for Dynamics of Geosphere (IDG), Moscow, Russia. Hence we refer to the (groomed) data set as the "Kitov dataset."

The reviewed and corrected phase data and site tables are given in a Unix tar file (IDG_PNE.tar) and its contents are listed in Table C3.

There are 7,362 phase picks from 83 PNEs recorded at 355 sites (Figure C2).

Table C3: Arrival picks from 83 PNEs at Regional Stations

Nphase	DB tables
7,362	idg-pne.arrival
7,347	idg-pne.assoc
1	idg-pne.lastid
83	idg-pne.origin
355	idg-pne.site

3. Phase Data from PNEs in FSU during 1966–1988 Recorded at Borovoye and Talgar CSE

We acquired waveform data recorded at Borovoye (BRV), northern Kazakhstan from about 80 PNEs. John Armbruster and W. Y. Kim at LDEO picked 149 arrivals from these waveform data recorded at BRV (see Table C4). Arrival times in CSS3.0 relational database format are in a Unix tar file (PNE-BRV-PICKS.tar).

We also acquired waveform data recorded at Talgar (TLG) in southern Kazakhstan from 37 PNEs. Staff at Talgar Complex Seismological Expedition (Talgar CSE) led by Dr. Yuri Kopnichev digitized the old analog records at the Talgar archive, supported by the International Science and Technology Center in recent years. Talgar CSE provided us with picked arrival times from 37 PNEs recorded at 26 stations for the current project to calibrate IMS stations for improved event location (Table C5). The unix tar file for this dataset is Talgar_CSE_PNE.tar.

The event-station paths of arrival times from both the Talgar CSE and Borovoye archives are shown in Figure C3.

Table C4: Arrival picks for PNEs recorded at Borovoye

Nphase	DB tables
149	Pne-new.arrival
147	Pne-new.assoc
80	Pne-new.origin
1	Pne-new.site

Table C5: Arrival picks for PNEs recorded at Talgar CSE

Nphase	DB tables
89	CSE_PNE.arrival
89	CSE_PNE.assoc
37	CSE_PNE.origin
26	CSE_PNE.site
75	CSE_PNE.sitechan

References

Sultanov, D. D., J.R. Murphy and Kh.D. Rubinstein, A seismic source summary for Soviet peaceful nuclear explosions, *Bulletin of the Seismological Society of America*, Vol. **89**, pp. 640-647, 1999.

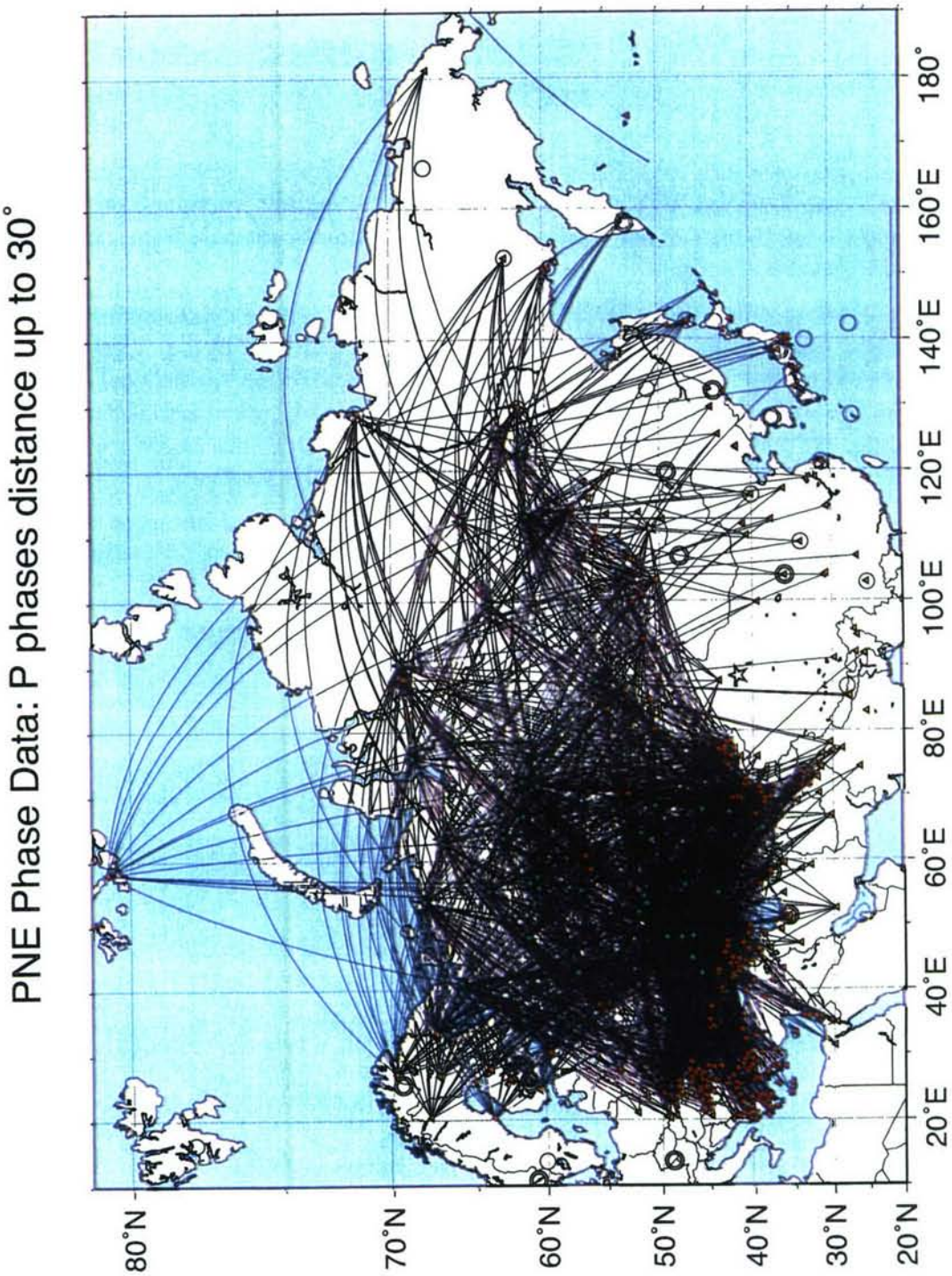


Figure C1: PNE shots (*green stars*) and seismographic stations (*red triangles*) of IDG phase data. The source-station pairs are plotted as great circles paths between them. IMS primary network stations (*double circles*) and auxiliary stations (*circles*) are indicated. 83 PNEs recorded at 355 stations are used.

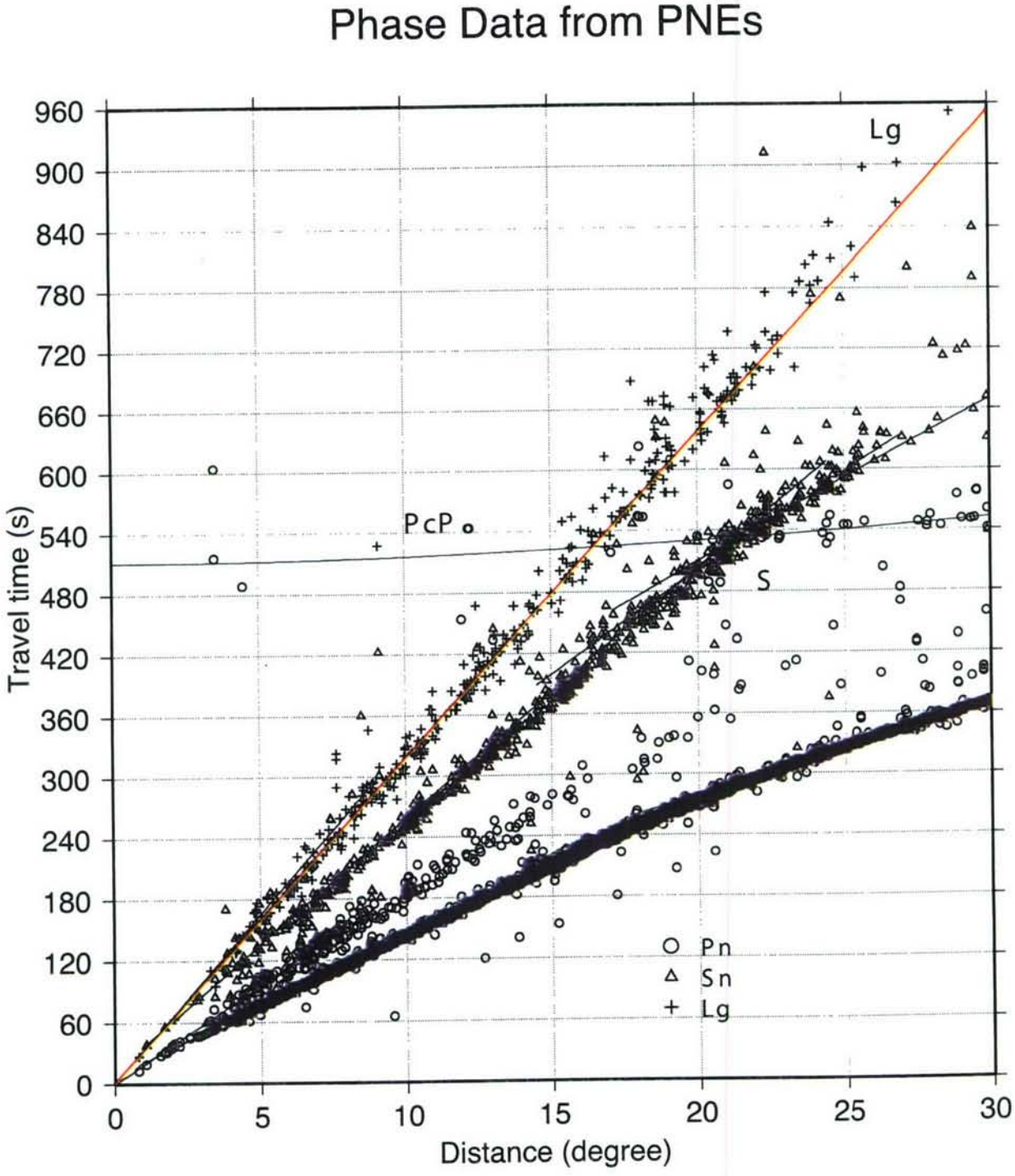


Figure C2: Travel times of Kitov dataset are plotted for up to 30 Calculated travel times of IASP91 Earth's model are indicated by solid lines for *Pn, P, Sn, S*, and *Lg* phases.

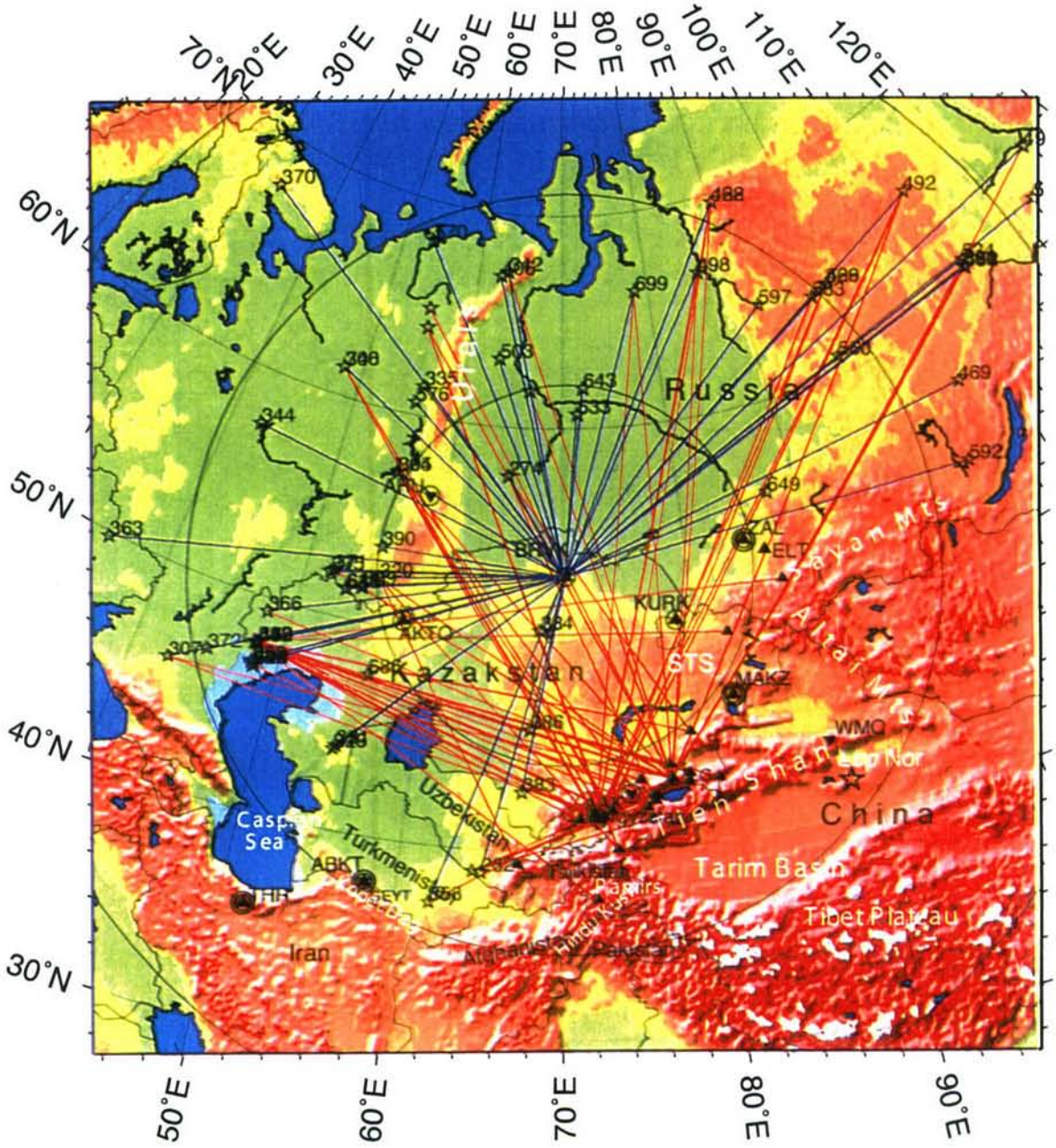


Figure C3: PNEs (*stars*) and seismographic stations (*solid triangles*) of the arrival times from the Borovoye archive (*blue lines*) and Talgar CSE (*red lines*) are plotted. Large circles indicate 10° and 20° epicentral distance from Borovoye. IMS primary and auxiliary network stations are indicated by circles.

Appendix D The Latitude/Longitude Points which Determine our Region Boundaries and the Final 1-D Velocity Models

R01		R02		R03	
LAT	LON	LAT	LON	LAT	LON
73	50	67.5	43.5	35.5	61
72.5763	49	66.3	41	36	60.5
72.6647	48	65	38	37	60
72.375	47	64	37.3	37.8	59
72.0095	46	62	37	38.8	57
72	44.9444	61	36	40	54.5
71.7848	44	60	33	41	52
71.8092	43	59.9	30	42	50
71.7569	42	59.8	25	43.5	47
71.3651	41	59.5	22	43.5	47
71	40.3611	58.5	20	45	41
70.2041	40	57	19	44.8557	38
70.2481	39	56	18	44.9116	37
70.7937	38	55	16	44.9082	36
71	37.2778	54.5	13	44.8246	35
71.0769	37	53	17	44.8832	34
71.1774	36	51	20	44.9418	33
71.2716	35	49	23	44.9244	32
71	34.3889	46	27	44.6847	31
70.4054	35	45	28.5	44	30.283
70	35.9375	43.8841	29	43.9304	30
69.9639	35	43.9304	30	43.8841	29
69.9977	34	44	30.283	43	28.1298
70	33.6667	44.6847	31	39.9843	25
70.0588	33	44.9244	32	39	25.9691
70.6216	32	44.9418	33	38	26.4764
70.0291	31	44.8832	34	37.3032	26

R01		R02		R03	
LAT	LON	LAT	LON	LAT	LON
70.3026	30	44.8246	35	37.4092	25
71	29.1758	44.9082	36	37	24.8171
71.1895	29	44.9116	37	36.8942	25
71.8093	28	44.8557	38	36.9216	26
71.1923	27	45	41	36.898	27
71.8333	26	43.5	47	36.5296	28
71.7375	25	44	50	36.6947	29
71.754	24	45	52.5	36.8995	30
71.3264	23	46	55	36.8857	31
71	22.5987	47	56	36.4828	32
70.669	22	49	57	36.1642	33
71	21.338	51	56	36.6964	34
71.2124	21	53.5	55	36.7698	35
71.2456	20	57	54.5	37	37
71.2315	19			37.3	38
71	18.4051			37.7	39
70.7698	18			37.9	40
70	16.9917			37.85	41
69.0647	16			37.3	42
69.0646	15			35.8	43
69	14.1872			35	44
68.6316	14			34	45
68.0976	13			31	47.5
68.0267	12			29	50
68	10.9708			27	53
67.6571	11			26	55
67.5069	12			25.4	55.8
67	12.9865			25	56.4265
66	11.9394			25.8584	57
65.8591	11			25.6278	58

R01		R02		R03	
LAT	LON	LAT	LON	LAT	LON
65	10.1043			25.5464	59
64.6087	9			25.5146	60
64	8.64331			25.271	61
63.6529	8			25.0048	62
63.6621	7			25.1367	63
63.3144	6			25.0019	64
63	5.18627			25.5393	65
62.9116	5			25	65.9565
62	4			24.4068	66
61	4.44606			24	66.1356
60	4.52222			24.4624	66.9809
59.211	5			24.4093	67.2397
59	5.10798			24.4638	67.4949
58.7473	5			24.4946	67.6662
58.5	6.5			24.5759	67.8934
57	7			24.7678	68.0086
56	8			25.0167	68.0957
55	10			25.2618	68.0361
54.5	13			25.3993	67.9240
55	16			25.5366	67.7526
56	18			25.6704	67.5217
57	19			25.7809	67.3817
58.5	20			26.0293	67.2940
59.5	22			26.3013	67.2099
59.8	25			26.6306	67.2095
59.9	30			26.8220	67.1499
60	33			27.0133	67.0658
61	36			27.3156	67.0061
62	37			27.6986	66.9777
64	37.3			28.0548	66.9774

R01		R02		R03	
LAT	LON	LAT	LON	LAT	LON
65	38			28.5219	66.9769
66.3	41			28.9589	67.0045
67.5	43.5			29.3994	67.1194
68	47			30	66.5
68.5	50			31	66.2
69.5	53			31.3	66
70	52			32.2	63
72	50			32.8	62
73	50			33	61.8
				34	61.5
				35.5	61

R03		R05b		R05c	
LAT	LON	LAT	LON	LAT	LON
69.5	53	69.5	67	44	74
69	57	69.3	68	43.5	75.5
68.7	58	68.8	69	44	77
68	58.8	68.3	69.5	46	80
67	58.8	67.7	69	47	82
66	58	67	67.7	48	81
65	57	66	65.5	49.5	80
62	55	65	64	51	80
60	54.5	64	63	52	78
57	54.5	62	62.2	53	76
53.5	55	60	62.5	54	74
51	56	57	62.5	55	72
49	57	54	62	55.7	69
48.5	57.5	51	61	56	67
48.7	58.5	50	60.1	55	66
49	59	49	59	51	65

R03		R05b		R05c	
LAT	LON	LAT	LON	LAT	LON
50	60.1	48.7	58.5	48	64.2
51	61	48.5	57.5	47	65
54	62	48.5	57.5	45	70
57	62.5	48.5	59	44	74
60	62.5	48	62		
62	62.2	47	65		
64	63	47	65		
65	64	48	64.2		
66	65.5	51	65		
67	67.7	55	66		
67.7	69	56	67		
68.3	69.5	55.7	69		
68.8	69	55	72		
69.3	68	54	74		
69.5	67	53	76		
70	65	52	78		
70.5	62	51	80		
71.2	60	51	80		
72	59	52	81		
73	60	53	81.7		
74	62	56	83		
75	65	56.7	88		
75.5933	69	56.5	91		
76	68.3796	57	92.8		
77	68.8514	58.5	93		
77.3913	68	60	93		
77.3993	67	61.5	92		
77.4041	66	64	91		
77.441	65	71	91		
77.4951	64	72	96		

R03		R05b		R05c	
LAT	LON	LAT	LON	LAT	LON
77.5123	63	73.8	112		
77.2828	62	74	115		
77	61.4058	75	117		
76.9717	61	76	117		
77	60.0345	77.3059	115		
77.0556	59	77.8601	114		
78	58	77.7757	113		
78	58	77.4142	112		
78	58	77.4894	111		
77.9831	57	78	110.225		
78	56.6667	78.0688	110		
78.1667	56	78.2987	109		
78	55.8333	79	108.183		
77.8387	55	79.0835	107		
77	53.9639	77.3059	115		
76.4118	53	77.8601	114		
76.0867	52	77.7757	113		
76	51.7833	77.4142	112		
75.254	51	77.4894	111		
75.0274	50	78	110.225		
75	49.8667	78.0688	110		
74.3158	49	78.2987	109		
74	48.8947	79	108.183		
73.8929	49	79.0835	107		
73	50	79.0953	106		
72.9889	50	79.2194	105		
72	50	79.2599	104		
		79.6352	103		
		80	101.901		
		80.0802	101		

R03		R05b		R05c	
LAT	LON	LAT	LON	LAT	LON
		80.1767	100		
		80.4059	99		
		80.2312	98		
		81	96.9668		
		81.1425	96		
		81.2024	95		
		81.2795	94		
		81.2593	93		
		81.2636	92		
		81.1888	91		
		81.044	90		
		81.0572	89		
		81	88.3288		
		80.3846	88		
		80	87.4		
		79.6296	87		
		79.5549	86		
		80	85.0759		
		80.08	85		
		81	84.4		
		81.0516	84		
		81.056	83		
		81.022	82		
		81.0174	81		
		81.0811	80		
		81.1386	79		
		81.1555	78		
		81.061	77		
		81	76.5633		
		80.2937	76		

R03		R05b		R05c	
LAT	LON	LAT	LON	LAT	LON
		80	75.7811		
		79	75.9652		
		78.3023	77		
		78	77.4727		
		77.3953	77		
		77.1538	76		
		77.2517	75		
		77	74.0513		
		76.8684	73		
		76.2878	72		
		76	70.8125		
		75.915	70		
		75.5933	69		
		75	65		
		74	62		
		73	60		
		72	59		
		71.2	60		
		70.5	62		
		70	65		
		69.5	67		

R05d		R06		R07	
LAT	LON	LAT	LON	LAT	LON
49	57	58.5	93	46.8	85
47	56	57	92.8	46.9	84
46	55	56.5	91	47	82
45	52.5	56.7	88	46	80
44	50	56	83	44	77
43.5	47	53	81.7	43.5	75.5

R05d		R06		R07	
LAT	LON	LAT	LON	LAT	LON
42	50	52	81	44	74
41	52	51	80	42.5	70
40	54.5	49.5	80	41	68
38.8	57	48	81	39	67
37.8	59	47	82	37	65.5
37	60	46.9	84	36	64
36	60.5	46.8	85	35.3	63
35.5	61	47	88	35	64
35.3	62	47	90.5	34.7	66
35.3	63	48	96	35	68
36	64	49	98	35.2	69
37	65.5	51	100	36	70
39	67	52	100	38	71
41	68	55	99.5	39.3	72
42.5	70	55.5	98	39.8	74.3
44	74	57	95.5	41	78
45	70			41.5	80
47	65			42	82.5
48	62			43	83.5
48.5	59			43.5	84
48.5	57.5			44	84.4
49	57			45	84.7
				46	84.5
				46.8	85

R08		R09		R10	
LAT	LON	LAT	LON	LAT	LON
41.3	92	38	71	31	96
41.5	90	36	70	32	95.7
42	87	35.2	69	33.5	95

R08		R09		R10	
LAT	LON	LAT	LON	LAT	LON
42	82.5	35	68	34.7	94
41.5	80	34.7	66	35.5	93
41	78	35	64	36.7	91.5
39.8	74.3	35.3	63	36.5	89.5
39	75	35.3	62	36	86
38	76	35.5	61	35.5	80.5
37	76.5	35.5	61	35.8	79
36	77.5	34	61.5	35.1094	79.0124
35.8	79	33	61.8	34.8912	79.1001
35.5	80.5	32.8	62	34.7000	79.2436
36	86	32.2	63	34.4517	79.3557
36.5	89.5	31.3	66	34.2605	79.4713
36.7	91.5	31	66.2	34.0425	79.6428
37	94	30	66.5	33.8514	79.7864
37.5	97	29.3994	67.1194	33.7142	79.9858
38	99.5	29.5915	67.2906	33.6341	80.1852
38.7	101	29.6759	67.4338	33.4969	80.3846
39	100	29.7033	67.6051	33.3865	80.5561
39.9	97.5	29.6199	67.8325	33.2493	80.7835
40.5	97	29.4018	67.9481	33.1154	80.9549
40.9	95	29.1265	68.0323	32.9512	81.1264
41.3	92	28.8816	68.1759	32.7300	81.3259
		28.6634	68.2635	32.5388	81.4415
		28.4993	68.4630	32.3207	81.5851
		28.4158	68.6623	32.1296	81.7286
		28.3898	68.9456	31.9084	81.9282
		28.5014	69.2042	31.7174	82.1276
		28.6935	69.4033	31.5534	82.3551
		28.8856	69.5745	31.4466	82.6139
		29.0773	69.6302	31.3634	82.9252

R08		R09		R10	
LAT	LON	LAT	LON	LAT	LON
		29.3262	69.7174	31.2837	83.2400
		29.4878	69.8291	31.2578	83.5826
		29.6263	70.0598	31.2017	83.9533
		29.7914	70.2309	31.1759	84.3240
		30.0673	70.3425	31.0961	84.6108
		30.4505	70.3701	31.0397	84.8661
		30.8637	70.3138	30.9867	85.1528
		31.1359	70.3135	30.8767	85.4676
		31.4650	70.2293	30.7429	85.6950
		31.8211	70.1975	30.6328	85.9504
		32.1772	70.1691	30.4956	86.1533
		32.3993	70.2563	30.3315	86.3807
		32.6448	70.3120	30.2213	86.6081
		32.8634	70.3992	30.1145	86.8670
		33.0286	70.5704	30.1692	87.1781
		33.0560	70.7417	30.2539	87.4368
		33.0026	70.8816	30.3892	87.7513
		32.8920	70.9971	30.4741	88.0345
		32.8925	71.1684	30.5554	88.2616
		32.9771	71.3677	30.6669	88.4923
		32.8937	71.5670	30.6139	88.7476
		32.8405	71.7944	30.5880	89.0903
		32.8682	72.0811	30.4779	89.3771
		32.8959	72.3398	30.4521	89.7757
		32.9268	72.5670	30.3961	90.1464
		33.0080	72.7662	30.3972	90.5450
		33.1462	72.9095	30.3983	90.9156
		33.2844	73.0807	30.3724	91.2583
		33.4495	73.2238	30.3196	91.6010
		33.5576	73.4230	30.3206	91.9717

R08		R09		R10	
LAT	LON	LAT	LON	LAT	LON
		33.6960	73.6222	30.2679	92.3458
		33.7800	73.6221	30.2690	92.7165
		34.0252	73.5659	30.2969	93.0591
		34.3005	73.4783	30.3517	93.4297
		34.5456	73.3941	30.4366	93.7408
		34.7097	73.1946	30.5720	94.0833
		34.8201	73.0232	30.6839	94.4538
		34.9573	72.8238	30.8226	94.7684
		35.1753	72.6802	30.8770	94.9676
		35.3664	72.5367	31	96
		35.6117	72.5084		
		38	71		

R11a		R11b		R12a	
LAT	LON	LAT	LON	LAT	LON
53.5	123.5	53.5	123.5	55	99.5
53	119.5	52	123.2	52	100
52	116	50	122.5	51	100
50	113	48	122	49	98
49	111	46	121.2	48	96
48	109	44	120.3	47	90.5
47	106	42.05	119.5	46	92
46	102	42.5	123	45.5	94
45.5	100	43	127	45.3	97
45.3	97	42.7915	131	45.5	100
45.5	94	42.9584	132	46	102
46	92	42.8072	133	47	106
47	90.5	42.8972	134	48	109
47	90.5	43	134.155	49	111
47	88	43.7141	135	50	113

R11a		R11b		R12a	
LAT	LON	LAT	LON	LAT	LON
46.8	85	44	135.819	56	108
46.8	85	44.1606	136	54.5	107
46	84.5	45	137.052	53.5	106
45	84.7	46	138.075	53	104.5
44	84.4	47	139.061	53.5	103
43.5	84	48	140.15	55	99.5
43	83.5	48.9266	141		
42	82.5	51	141		
42	87	52.5	141.5		
41.5	90	54	141.2		
41.3	92	54.3	139.5		
40.9	95	54.5	138		
40.5	97	54.9	136.2		
39.9	97.5	54.9	136.2		
39	100	54.5	134		
38.7	101	54	128		
38	103	53.5	123.5		
36.5	105				
36	106				
35.5	107				
35.3	108.5				
37	108.8				
38	109				
39.2	110				
40.3	111				
41	112				
41.5	115				
42	119				
42.05	119.5				
44	120.3				

R11a		R11b		R12a	
LAT	LON	LAT	LON	LAT	LON
46	121.2				
48	122				
50	122.5				
52	123.2				
53.5	123.5				

R12b		R13a		R13b	
LAT	LON	LAT	LON	LAT	LON
50	113	21.3	104	35.3	108.5
52	116	20	105	32	105
53	119.5	18.7	106.2	30	103
54	128	18	107	26.5	100
54.5	134	17	109.092	25	101
54.9	136.2	18	110.08	23	102.5
56	137.5	18.9236	111	21.3	104
56.5	137	19	112.074	23	105
57.3	135	19.782	113	24	105.8
57.8	132.5	20	113.608	26	107
57.8	130	20.32	114	28	108.3
59	126	20.7921	115	30	109.5
59.7	123	21	115.991	32	110.5
60	120	21.5683	117	34.5	111
60	117	22	117.368	35	109.5
59	112	22.5337	118	35.3	108.5
58	109.5	22.8809	119		
56	108	22.9142	120		
50	113	22.3714	121		
		23	121.235		
		24	121.485		
		25	121.391		

R12b		R13a		R13b	
LAT	LON	LAT	LON	LAT	LON
		25.8049	122		
		25.9823	123		
		26	124.014		
		27	125.063		
		28	126.077		
		29	126.979		
		30	127.256		
		31	127.99		
		32	128.189		
		32.6382	129		
		34	129		
		34	127		
		34	125		
		34	123		
		34	121		
		34	119		
		34	117		
		34	115		
		34	113		
		34.5	111		
		32	110.5		
		30	109.5		
		28	108.3		
		26	107		
		24	105.8		
		23	105		
		21.3	104		

R13c		R14		R15a	
LAT	LON	LAT	LON	LAT	LON
34	129	56	141.172	73.8	112
35	129	54	141.2	72	96
36	129.307	52.5	141.5	71	91
37	129.4	51	141	64	91
37.5963	129	48.9266	141	61.5	92
38	128.582	48	141.771	60	93
39	128.084	47	141.855	58.5	93
40	128.191	46	141.627	57	95.5
40.4985	129	45.1962	141	55.5	98
41	129.331	45	140.515	55	99.5
42	130.038	44	141.035	53.5	103
42.7915	131	43	140.503	53	104.5
43	127	42	140.353	53.5	106
42.5	123	41	140.36	54.5	107
42	119	40.7365	140	56	108
41.5	115	40	139.858	58	109.5
41	112	39	139.314	59	112
40.3	111	38.3118	139	60	117
39.2	110	38	138.905	60	120
38	109	37.5154	138	59.7	123
37	108.8	37.526	137	59	126
35.3	108.5	37	136.696	58	129
35	109.5	36.4454	136	57.8	130
34.5	111	36	135.438	57.8	132.5
34	113	35.6542	135	58.3	134
34	115	35.699	134	59	135.2
34	117	36	133.509	61	135.5
34	119	36.4852	133	63	135.5
34	121	36	132.83	63.5	135
34	123	35.1245	132	64	130

R13c		R14		R15a	
LAT	LON	LAT	LON	LAT	LON
34	125	35.0731	131	64.5	128
34	127	35.0796	130	65	127
34	129	36	129.307	66	126
		35	129	68.5	126
		32.6382	129	70	128
		32	129.702	71.5	128.5
		31	129.997	77.1006	129
		31	131.11	77.0308	128
		32	131.357	77	127.409
		32.8082	132	76.7473	127
		32.8783	133	76.2737	126
		33	133.242	76.817	125
		33.4063	134	76.4924	124
		33.8408	135	76.8303	123
		33.8671	136	77	122.876
		34	136.342	77.0907	122
		34.7889	137	77.0861	121
		34.7575	138	77.0911	120
		34.332	139	77.0571	119
		35	140.072	77.0936	118
		36	140.978	77.2039	117
		37	141.133	77.1458	116
		38	141.401	77.3059	115
		39	141.99	76	117
		40	142.143	75	117
		40.1967	142	74	115
		41	141.194	73.8	112
		42	141.161		
		42.5568	142		
		42	142.804		

R13c		R14		R15a	
LAT	LON	LAT	LON	LAT	LON
		41.8802	143		
		42	143.206		
		42.7643	144		
		43	145.104		
		43.8699	146		
		44.0636	146		
		44.2442	145		
		44.9634	144		
		45	143.857		
		46	143.13		
		47	143.194		
		47.8425	144		
		48	145.101		
		49	145.031		
		50	144.644		
		51	144.224		
		52	144.113		
		53	144.003		
		53.0112	144		
		54	143.338		
		55	143.064		
		55.4261	142		
		56	141.172		

R15b		R16a		R16b	
LAT	LON	LAT	LON	LAT	LON
74	115	70	128	71.5	128.5
72.5	115	68.5	126	70	128
66	113.5	66	126	67	140
59	112	65	127	65	150

R15b		R16a		R16b	
LAT	LON	LAT	LON	LAT	LON
60	117	64.5	128	68	160
60	120	64	130	70	172
59.7	123	63.5	135	76.0517	172
59	126	63	135.5	76.0187	171
58	129	61	135.5	77	170.327
57.8	130	59	135.2	77.0769	170
57.8	132.5	58.3	134	77.3507	169
58.3	134	57.8	132.5	77.5815	168
59	135.2	57.3	135	78	167.058
61	135.5	56.5	137	78.0402	166
63	135.5	56	137.5	78	165
63.5	135	54.9	136.2	77.4579	164
64	130	54.5	138	77.6281	163
64.5	128	54.3	139.5	78	162.439
65	127	54	141.2	78.0348	162
66	126	56	141.172	78.1195	161
68.5	126	55.4261	142	78.2915	160
70	128	55.2606	143	78.6471	159
71.5	128.5	55	143.064	78.7371	158
77.1006	129	54	143.338	78.7863	157
77.0308	128	53.0112	144	78.655	156
77	127.409	53	144.003	78.655	155
76.7473	127	52	144.113	79	154.068
76.2737	126	51	144.224	79.1241	153
76.817	125	50	144.644	79.1299	152
76.4924	124	49.1743	145	79.133	151
76.8303	123	49	145.031	79.157	150
77	122.876	48	145.101	79.1889	149
77.0907	122	50	150	79.1618	148
77.0861	121	50.5	152	79.12	147

R15b		R16a		R16b	
LAT	LON	LAT	LON	LAT	LON
77.0911	120	50.7	155	79.1077	146
77.0571	119	51	156.531	79.1143	145
77.0936	118	51.5621	156	79.1093	144
77.2039	117	52	155.14	79.0954	143
77.1458	116	52.2424	155	79.054	142
77.3059	115	53	154.693	79	140.848
76	117	54	154.666	78.3425	140
75	117	55	154.735	78.119	139
74	115	56	154.794	78.0721	138
		57	154.912	78.0642	137
		57.1304	155	78.062	136
		58	155.997	78.068	135
		59	158.2	78.056	134
		60	160	78.03	133
		62	166	78	132.576
		63	170	77.5546	132
		64	175	77.153	131
		65	180	77.107	130
		65	182	77.1006	129
		64.3	184.5	71.5	128.5
		64.5	188.5		
		65	189.5		
		66	190		
		74.3503	190		
		74.8158	189		
		74.2871	188		
		74.248	187		
		74.2714	186		
		74.2472	185		
		74.3552	184		

R15b		R16a		R16b	
LAT	LON	LAT	LON	LAT	LON
		74.4254	183		
		74.4129	182		
		74.4479	181		
		74.8347	180		
		74.9111	179		
		75	178.647		
		75.0719	178		
		75.1978	177		
		75.3383	176		
		75.0635	175		
		75.6515	174		
		75.9515	173		
		76	172.706		
		76.0517	172		
		70	172		
		68	160		
		65	150		
		67	140		
		70	128		

R17		R18		R19a	
LAT	LON	LAT	LON	LAT	LON
64.3	184.5	25.4	55.8	17	72.024
65	182	26	55	16	72.9395
65	180	27	53	15	73.0386
64	175	29	50	14	73.9117
63	170	31	47.5	13	73.9883
62	166	34	45	12	74.8988
60	160	35	44	11.7687	75
59	158.2	35.8	43	11	75.639

R17		R18		R19a	
LAT	LON	LAT	LON	LAT	LON
58	155.997	37.3	42	10	75.9309
57.1304	155	37.85	41	9	75.9782
57	154.912	37.9	40	8	76.9273
56	154.794	37.7	39	8	78.0284
55	154.735	37.3	38	8.9843	79
54	154.666	37	37	8	79.872
53	154.693	36.7698	35	7	79.8771
52.2424	155	36	35.4462	6.5824	80
52	155.14	35	35.6464	6.48088	81
51.5621	156	34	35.5482	7	81.3693
51	156.531	33	34.9677	8	81.0821
50.8895	157	32	34.5506	9	81.0521
51	157.656	28	35	10	80.0683
51.2521	158	27.8181	35	11	80.0502
52	158.101	27	35.6308	12	80.0431
52.9427	159	26.6152	36	13	80.0784
53	160.035	26	36.5108	14	80.0635
54	160.178	24.885	37	15	80.0798
54.5292	161	24	37.8163	15.9164	81
55	162.048	23.7731	38	16	81.2037
56	163.046	23	38.6125	16.7844	82
57	162.991	22	38.8079	16.9372	81.9708
58	163.053	21.0155	39	17.0744	81.7713
58.8182	164	21	39.0024	17.2655	81.5998
59	164.309	20	40.085	17.4565	81.4003
59.7885	165	19.4706	40	17.6743	81.2008
59.8458	166	19	39.9271	17.9225	81.0013
59.9678	167	18	40.8863	18.1405	80.8577
60	167.906	17.566	41	18.3046	80.6583
60	168.2	17	41.4926	18.5495	80.5147

R17		R18		R19a	
LAT	LON	LAT	LON	LAT	LON
59.9856	169	16	41.5106	18.7708	80.3431
59.8095	170	13	43	18.9888	80.1995
60	170.222	12	43.329	19.2068	80.0280
60.4735	171	12.5802	44	19.3709	79.8565
60.8866	172	12.7998	45	19.5619	79.6570
60.9668	173	13	45.1695	19.6991	79.4576
61	174.07	13.4932	46	19.8095	79.2582
61.8614	175	13.6749	47	19.9467	79.0587
61.9252	176	14	48.1034	20.0536	78.8279
61.9596	177	14.4636	49	20.1638	78.6005
61.958	178	14.8618	50	20.1632	78.3732
61.9341	179	15	51.0883	20.1893	78.1144
61.5526	180	15.6869	52	20.2155	77.8592
61	180.897	16	52.1705	20.2148	77.6319
60	182.028	16.6159	53	20.2140	77.3452
59	181.986	16.9268	54	20.2402	77.0899
58.9873	182	17	54.3333	20.2127	76.8872
58.986	183	17.3889	55	20.1581	76.6040
58.9848	184	17.9321	56	20.1574	76.3453
58.99	185	18	57.0347	20.1298	76.0900
58.8193	186	19	57.875	20.1291	75.8628
58	186.837	19.1795	58	20.0981	75.6040
57	186.973	20	58.0634	20.0705	75.3488
56.9779	188	21	59.0679	20.0966	75.0621
56.9552	189	22	59.2144	20.0690	74.8348
56.4758	190	23	59.1852	20.0417	74.6635
66	190	23.1768	59	20.0678	74.4048
65	189.5	23.5658	58	20.1513	74.2369
64.5	188.5	24	57.1818	20.2315	74.0655
64.3	184.5	24.2186	57	20.3957	73.8940

R17		R18		R19a	
LAT	LON	LAT	LON	LAT	LON
		25	56.4265	20.4527	73.8624
		25.4	55.8	20.2607	73.6913
				20.0955	73.5201
				19.9304	73.3490
				19.7350	73.1778
				19.6000	72.9787
				19.4616	72.7515
				17	72.024

R19b		R19c		R19d	
LAT	LON	LAT	LON	LAT	LON
16.7844	82	20.4196	87	20	92.064
17	82.9307	20.8459	88	19.757	93
18	84.0558	20.9049	89	19	93.757
19	85.0706	20.8638	90	18	93.9582
19.881	86	20.8205	91	17	94.7763
20	86.6039	20	92.064	16	93.9496
20.4196	87	22.0094	91.7805	15	93.9485
21.2036	87.3023	22.2577	91.6369	14.5657	95
21.3686	87.4455	22.4220	91.4934	14	96.037
21.5606	87.5886	22.6401	91.3813	13	96.9437
21.8063	87.7317	22.8583	91.3216	12.2222	97
22.0284	87.8434	23.0800	91.2655	15.3	97.7
22.2738	87.8432	23.3523	91.2932	20	97.2
22.5762	87.8429	23.5708	91.3209	23	98
22.8787	87.8706	23.7358	91.4362	24.5	97.7
23.1511	87.9297	23.9009	91.5793	24.5418	94.7745
23.4267	87.9295	24.0122	91.7226	24.5141	94.4878
23.7022	87.9012	24.0934	91.9218	24.5133	94.2326
23.9744	87.9010	24.2889	92.1209	24.5125	93.9459

R19b		R19c		R19d	
LAT	LON	LAT	LON	LAT	LON
24.2498	87.8412	24.4807	92.2361	24.4847	93.6312
24.4948	87.7571	24.4798	91.9214	24.4570	93.3480
24.6861	87.6415	24.5326	91.5787	24.4561	93.0054
24.8771	87.4700	24.5856	91.2920	24.4820	92.6627
24.9068	87.2707	24.6687	90.9772	24.4810	92.3200
24.8757	86.9840	24.6948	90.6940	24.4807	92.2361
24.7943	86.7288	24.6939	90.3793	24.2889	92.1209
24.7095	86.4422	24.7771	90.0925	24.0934	91.9218
24.6281	86.1870	24.8571	89.8651	24.0122	91.7226
24.5166	85.9599	25.0213	89.6936	23.9009	91.5793
24.4619	85.6452	25.2395	89.6095	23.7358	91.4362
24.4076	85.4460	25.5148	89.5498	23.5708	91.3209
24.3799	85.1593	25.7869	89.4936	23.3523	91.2932
24.3487	84.8167	26.0352	89.3780	23.0800	91.2655
24.3478	84.5335	26.2264	89.2379	22.8583	91.3216
24.3773	84.2467	26.3637	89.0664	22.6401	91.3813
24.4571	83.9599	26.4438	88.8950	22.4220	91.4934
24.5672	83.6766	26.5003	88.6642	22.2577	91.6369
24.5932	83.3619	26.5266	88.4369	22.0094	91.7805
24.6731	83.1066	26.5803	88.4369	20	92.064
24.6721	82.7639	26.5257	88.1257		
24.6711	82.4213	26.4977	87.7551		
24.6702	82.0786	26.4398	87.4685		
24.6691	81.7080	26.4388	87.1258		
24.6953	81.4492	26.4109	86.7832		
24.6943	81.1065	26.5209	86.4719		
24.7508	80.8792	26.6274	86.0977		
24.7767	80.5365	26.7642	85.7584		
24.8564	80.2218	26.8743	85.4715		
24.9397	79.9664	26.9811	85.2162		

R19b		R19c		R19d	
LAT	LON	LAT	LON	LAT	LON
25.0196	79.7076	27.0912	84.9294		
25.1567	79.4522	27.2551	84.6705		
25.2938	79.2248	27.3653	84.4151		
25.4309	78.9939	27.4720	84.1283		
25.5950	78.7945	27.5552	83.8450		
25.7322	78.5950	27.5814	83.5862		
25.8661	78.3956	27.6343	83.3030		
26.0604	78.1961	27.6906	83.0162		
26.1944	78.0247	27.7167	82.7295		
26.3852	77.7657	27.7966	82.4741		
26.5795	77.5662	27.8800	82.2468		
26.7974	77.3667	27.9599	81.9880		
26.9617	77.2547	28.0433	81.7606		
27.0687	77.0518	28.1233	81.5612		
27.2059	76.8523	28.2874	81.3338		
27.2893	76.6250	28.4513	81.0749		
27.4804	76.4814	28.5883	80.8195		
27.6713	76.2540	28.6985	80.5607		
27.8353	76.0265	28.7516	80.3333		
27.9994	75.8271	28.8316	80.1060		
28.0524	75.5403	28.9148	79.8192		
28.0516	75.2536	29.0249	79.5324		
27.9432	74.9705	29.1048	79.2771		
27.7779	74.7399	29.1578	78.9903		
27.5287	74.5688	29.3218	78.7629		
27.3099	74.4292	29.5126	78.5074		
27.0911	74.3140	29.6229	78.3080		
26.8992	74.1988	29.7601	78.0771		
26.6234	74.1151	29.9509	77.8217		
26.3744	74.0000	30.1150	77.6222		

R19b		R19c		R19d	
LAT	LON	LAT	LON	LAT	LON
26.2093	73.8568	30.3061	77.4787		
25.9907	73.8011	30.4971	77.2792		
25.7450	73.6580	30.4700	77.1918		
25.4422	73.5464	30.2781	77.0766		
25.2773	73.4311	30.0593	76.9649		
25.0854	73.3160	29.7833	76.7939		
24.8665	73.1763	29.5644	76.6228		
24.7015	73.0331	29.3153	76.4796		
24.5093	72.8340	29.0694	76.2806		
24.3711	72.6908	28.7666	76.1655		
24.2598	72.5475	28.5743	75.9104		
24.0948	72.4043	28.4090	75.6798		
23.9298	72.2926	28.2438	75.4807		
23.7113	72.2928	28.1320	75.1976		
23.4627	72.3210	27.9970	74.9669		
23.4357	72.2616	27.9432	74.9705		
23.2714	72.3772	28.0516	75.2536		
23.1644	72.5766	28.0524	75.5403		
23.1350	72.8913	27.9994	75.8271		
23.1358	73.1465	27.8353	76.0265		
23.1937	73.4332	27.6713	76.2540		
23.1944	73.6884	27.4804	76.4814		
23.2489	73.9157	27.2893	76.6250		
23.2226	74.1185	27.2059	76.8523		
23.0853	74.2899	27.0687	77.0518		
22.8941	74.4300	26.9617	77.2547		
22.5918	74.4897	26.7974	77.3667		
22.2895	74.5460	26.5795	77.5662		
21.9903	74.4903	26.3852	77.7657		
21.6340	74.4627	26.1944	78.0247		

R19b		R19c		R19d	
LAT	LON	LAT	LON	LAT	LON
21.3582	74.3755	26.0604	78.1961		
21.0823	74.2604	25.8661	78.3956		
20.8366	74.1208	25.7322	78.5950		
20.5875	73.9777	25.5950	78.7945		
20.4527	73.8624	25.4309	78.9939		
20.3957	73.8940	25.2938	79.2248		
20.2315	74.0655	25.1567	79.4522		
20.1513	74.2369	25.0196	79.7076		
20.0678	74.4048	24.9397	79.9664		
20.0417	74.6635	24.8564	80.2218		
20.0690	74.8348	24.7767	80.5365		
20.0966	75.0621	24.7508	80.8792		
20.0705	75.3488	24.6943	81.1065		
20.0981	75.6040	24.6953	81.4492		
20.1291	75.8628	24.6691	81.7080		
20.1298	76.0900	24.6702	82.0786		
20.1574	76.3453	24.6711	82.4213		
20.1581	76.6040	24.6721	82.7639		
20.2127	76.8872	24.6731	83.1066		
20.2402	77.0899	24.5932	83.3619		
20.2140	77.3452	24.5672	83.6766		
20.2148	77.6319	24.4571	83.9599		
20.2155	77.8592	24.3773	84.2467		
20.1893	78.1144	24.3478	84.5335		
20.1632	78.3732	24.3487	84.8167		
20.1638	78.6005	24.3799	85.1593		
20.0536	78.8279	24.4076	85.4460		
19.9467	79.0587	24.4619	85.6452		
19.8095	79.2582	24.5166	85.9599		
19.6991	79.4576	24.6281	86.1870		

R19b		R19c		R19d	
LAT	LON	LAT	LON	LAT	LON
19.5619	79.6570	24.7095	86.4422		
19.3709	79.8565	24.7943	86.7288		
19.2068	80.0280	24.8757	86.9840		
18.9888	80.1995	24.9068	87.2707		
18.7708	80.3431	24.8771	87.4700		
18.5495	80.5147	24.6861	87.6415		
18.3046	80.6583	24.4948	87.7571		
18.1405	80.8577	24.2498	87.8412		
17.9225	81.0013	23.9744	87.9010		
17.6743	81.2008	23.7022	87.9012		
17.4565	81.4003	23.4267	87.9295		
17.2655	81.5998	23.1511	87.9297		
17.0744	81.7713	22.8787	87.8706		
16.9372	81.9708	22.5762	87.8429		
16.7844	82	22.2738	87.8432		
		22.0284	87.8434		
		21.8063	87.7317		
		21.5606	87.5886		
		21.3686	87.4455		
		21.2036	87.3023		
		20.4196	87		

R19e		R19f		R19g	
LAT	LON	LAT	LON	LAT	LON
24.5	97.7	29	96.5	33.7800	73.6221
27	97	30	96.3	33.6960	73.6222
29	96.5	31	96	33.5576	73.4230
27.9162	94.9146	30.8770	94.9676	33.4495	73.2238
27.8584	94.6874	30.8226	94.7684	33.2844	73.0807
27.7771	94.4567	30.6839	94.4538	33.1462	72.9095

R19e		R19f		R19g	
LAT	LON	LAT	LON	LAT	LON
27.6387	94.2575	30.5720	94.0833	33.0080	72.7662
27.4735	94.0584	30.4366	93.7408	32.9268	72.5670
27.2813	93.8313	30.3517	93.4297	32.8959	72.3398
27.1429	93.6041	30.2969	93.0591	32.8682	72.0811
27.0347	93.4015	30.2690	92.7165	32.8405	71.7944
26.8961	93.0904	30.2679	92.3458	32.8937	71.5670
26.7575	92.8318	30.3206	91.9717	32.9771	71.3677
26.7028	92.4892	30.3196	91.6010	32.8925	71.1684
26.6449	92.2060	30.3724	91.2583	32.8920	70.9971
26.5903	91.9194	30.3983	90.9156	33.0026	70.8816
26.5892	91.5487	30.3972	90.5450	33.0560	70.7417
26.6151	91.2061	30.3961	90.1464	33.0286	70.5704
26.5873	90.8914	30.4521	89.7757	32.8634	70.3992
26.5866	90.6362	30.4779	89.3771	32.6448	70.3120
26.6397	90.4088	30.5880	89.0903	32.1772	70.1691
26.5586	90.2376	30.6139	88.7476	31.8211	70.1975
26.5310	89.9789	30.6669	88.4923	31.4650	70.2293
26.5301	89.6957	30.5554	88.2616	31.1359	70.3135
26.5292	89.3530	30.4741	88.0345	30.8637	70.3138
26.6090	89.0662	30.3892	87.7513	30.4505	70.3701
26.5812	88.7515	30.2539	87.4368	30.0673	70.3425
26.5803	88.4369	30.1692	87.1781	29.7914	70.2309
26.5266	88.4369	30.1145	86.8670	29.6263	70.0598
26.5003	88.6642	30.2213	86.6081	29.4878	69.8291
26.4438	88.8950	30.3315	86.3807	29.3262	69.7174
26.3637	89.0664	30.4956	86.1533	29.0773	69.6302
26.2264	89.2379	30.6328	85.9504	28.8856	69.5745
26.0352	89.3780	30.7429	85.6950	28.6935	69.4033
25.7869	89.4936	30.8767	85.4676	28.5014	69.2042
25.5148	89.5498	30.9867	85.1528	28.3898	68.9456

R19e		R19f		R19g	
LAT	LON	LAT	LON	LAT	LON
25.2395	89.6095	31.0397	84.8661	28.4158	68.6623
25.0213	89.6936	31.0961	84.6108	28.4993	68.4630
24.8571	89.8651	31.1759	84.3240	28.6634	68.2635
24.7771	90.0925	31.2017	83.9533	28.8816	68.1759
24.6939	90.3793	31.2578	83.5826	29.1265	68.0323
24.6948	90.6940	31.2837	83.2400	29.4018	67.9481
24.6687	90.9772	31.3634	82.9252	29.6199	67.8325
24.5856	91.2920	31.4466	82.6139	29.7033	67.6051
24.5326	91.5787	31.5534	82.3551	29.6759	67.4338
24.4798	91.9214	31.7174	82.1276	29.5915	67.2906
24.4807	92.2361	31.9084	81.9282	29.3994	67.1194
24.4810	92.3200	32.1296	81.7286	28.9589	67.0045
24.4820	92.6627	32.3207	81.5851	28.5219	66.9769
24.4561	93.0054	32.5388	81.4415	28.0548	66.9774
24.4570	93.3480	32.7300	81.3259	27.6986	66.9777
24.4847	93.6312	32.9512	81.1264	27.3156	67.0061
24.5125	93.9459	33.1154	80.9549	27.0133	67.0658
24.5133	94.2326	33.2493	80.7835	26.8220	67.1499
24.5141	94.4878	33.3865	80.5561	26.6306	67.2095
24.5418	94.7745	33.4969	80.3846	26.8491	67.2373
24.5	97.7	33.6341	80.1852	26.9874	67.4085
24.4570	93.3480	33.7142	79.9858	26.9881	67.6637
24.4847	93.6312	33.8514	79.7864	26.7970	67.8353
24.5125	93.9459	34.0425	79.6428	26.5789	67.9509
		34.2605	79.4713	26.3574	68.0350
		34.4517	79.3557	26.1394	68.2065
		34.7000	79.2436	25.9753	68.3780
		34.8912	79.1001	25.8685	68.6369
		35.1094	79.0124	25.7852	68.8922
		35.8	79	25.6748	69.0916

R19e		R19f		R19g	
LAT	LON	LAT	LON	LAT	LON
		36	77.5	25.4839	69.2911
		37	76.5	25.1852	69.4347
		38	76	24.8258	69.4945
		39	75	24.4998	69.4948
		39.8	74.3	24.1974	69.5231
		39.8	74.3	24.0333	69.7226
		39.3	72	24.0611	70.0372
		38	71	24.0889	70.3484
		35.6117	72.5084	24.1434	70.6071
		35.3664	72.5367	24.3086	70.7782
		35.1753	72.6802	24.4201	71.0054
		34.9573	72.8238	24.5585	71.2325
		34.8201	73.0232	24.6666	71.4317
		34.7097	73.1946	24.8049	71.6029
		34.5456	73.3941	24.8895	71.8057
		34.3005	73.4783	24.8631	71.9770
		34.0252	73.5659	24.6415	72.0332
		33.7800	73.6221	24.4231	72.0614
		33.5048	73.7378	24.1207	72.0616
		33.2867	73.8813	23.8755	72.1178
		33.0956	74.0214	23.6270	72.1775
		32.9585	74.2523	23.4357	72.2616
		32.8753	74.5356	23.4627	72.3210
		32.8763	74.9062	23.7113	72.2928
		32.8772	75.2209	23.9298	72.2926
		32.8511	75.4797	24.0948	72.4043
		32.7139	75.6791	24.2598	72.5475
		32.5227	75.8227	24.3711	72.6908
		32.2777	75.9348	24.5093	72.8340
		32.0025	76.0504	24.7015	73.0331

R19e		R19f		R19g	
LAT	LON	LAT	LON	LAT	LON
		31.7844	76.1625	24.8665	73.1763
		31.5663	76.2781	25.0854	73.3160
		31.3448	76.3937	25.2773	73.4311
		31.1806	76.5652	25.4422	73.5464
		31.0164	76.7087	25.7450	73.6580
		30.8253	76.8768	25.9907	73.8011
		30.6343	77.0797	26.2093	73.8568
		30.4971	77.2792	26.3744	74.0000
		30.3061	77.4787	26.6234	74.1151
		30.1150	77.6222	26.8992	74.1988
		29.9509	77.8217	27.0911	74.3140
		29.7601	78.0771	27.3099	74.4292
		29.6229	78.3080	27.5287	74.5688
		29.5126	78.5074	27.7779	74.7399
		29.3218	78.7629	27.9432	74.9705
		29.1578	78.9903	27.9970	74.9669
		29.1048	79.2771	28.1320	75.1976
		29.0249	79.5324	28.2438	75.4807
		28.9148	79.8192	28.4090	75.6798
		28.8316	80.1060	28.5743	75.9104
		28.7516	80.3333	28.7666	76.1655
		28.6985	80.5607	29.0694	76.2806
		28.5883	80.8195	29.3153	76.4796
		28.4513	81.0749	29.5644	76.6228
		28.2874	81.3338	29.7833	76.7939
		28.1233	81.5612	30.0593	76.9649
		28.0433	81.7606	30.2781	77.0766
		27.9599	81.9880	30.4700	77.1918
		27.8800	82.2468	30.4971	77.2792
		27.7966	82.4741	30.6343	77.0797

R19e		R19f		R19g	
LAT	LON	LAT	LON	LAT	LON
		27.7167	82.7295	30.8253	76.8768
		27.6906	83.0162	31.0164	76.7087
		27.6343	83.3030	31.1806	76.5652
		27.5814	83.5862	31.5663	76.2781
		27.5552	83.8450	31.7844	76.1625
		27.4720	84.1283	32.0025	76.0504
		27.3653	84.4151	32.2777	75.9348
		27.2551	84.6705	32.5227	75.8227
		27.0912	84.9294	32.7139	75.6791
		26.9811	85.2162	32.8511	75.4797
		26.8743	85.4715	32.8772	75.2209
		26.7642	85.7584	32.8763	74.9062
		26.6274	86.0977	32.8753	74.5356
		26.5209	86.4719	32.9585	74.2523
		26.4109	86.7832	33.0956	74.0214
		26.4388	87.1258	33.2867	73.8813
		26.4398	87.4685	33.5048	73.7378
		26.4977	87.7551	33.7800	73.6221
		26.5257	88.1257		
		26.5803	88.4369		
		26.5812	88.7515		
		26.6090	89.0662		
		26.5292	89.3530		
		26.5301	89.6957		
		26.5310	89.9789		
		26.5586	90.2376		
		26.6397	90.4088		
		26.5866	90.6362		
		26.5873	90.8914		
		26.6151	91.2061		

R19e		R19f		R19g	
LAT	LON	LAT	LON	LAT	LON
		26.5892	91.5487		
		26.5903	91.9194		
		26.6449	92.2060		
		26.7028	92.4892		
		26.7575	92.8318		
		26.8961	93.0904		
		27.0347	93.4015		
		27.1429	93.6041		
		27.2813	93.8313		
		27.4735	94.0584		
		27.6387	94.2575		
		27.7771	94.4567		
		27.8584	94.6874		
		27.9162	94.9146		
		29	96.5		

R19h		R20a		R20b	
LAT	LON	LAT	LON	LAT	LON
26.6306	67.2095	35.3	108.5	23	98
26.3013	67.2099	35.5	107	20	97.2
26.0293	67.2940	36	106	15.3	97.7
25.7809	67.3817	36.5	105	12.2222	97
25.6704	67.5217	38	103	12	97.1316
25.5366	67.7526	38.7	101	11	97.3721
25.3993	67.9240	38	99.5	10	97.1811
25.2618	68.0361	37.5	97	9	97.4615
25.0167	68.0957	37	94	8	97.7329
24.7678	68.0086	36.7	91.5	7.23214	98
24.5759	67.8934	35.5	93	6.70896	98
24.4946	67.6662	34.7	94	6	97.9184

R19h		R20a		R20b	
LAT	LON	LAT	LON	LAT	LON
24.4638	67.4949	33.5	95	6	109.282
24.4093	67.2397	32	95.7	6.81633	109
24.4624	66.9809	31	96	7.21687	109
24	66.1356	30	96.3	8.03385	109
23	67.1596	29	96.5	9	109.036
22	67.992	27	97	10	109.101
21.9946	68	24.5	97.7	11	109.32
21.8579	69	23	98	12	109.224
21	69.8545	25	99	13	109.2
20	69.9137	26.5	100	14	109.222
19	70.0865	30	103	15	109.393
18	70.948	32	105	16	109.128
17	72.024	35.3	108.5	17	109.092
19.4616	72.7515			18	107
19.6000	72.9787			18.7	106.2
19.7350	73.1778			20	105
19.9304	73.3490			23	102.5
20.0955	73.5201			25	101
20.2607	73.6913			26.5	100
20.4527	73.8624			25	99
20.5875	73.9777			23	98
20.8366	74.1208				
21.0823	74.2604				
21.3582	74.3755				
21.6340	74.4627				
21.9903	74.4903				
22.2895	74.5460				
22.5918	74.4897				
22.8941	74.4300				
23.0853	74.2899				

R19h		R20a		R20b	
LAT	LON	LAT	LON	LAT	LON
23.2226	74.1185				
23.2489	73.9157				
23.1944	73.6884				
23.1937	73.4332				
23.1358	73.1465				
23.1350	72.8913				
23.1644	72.5766				
23.2714	72.3772				
23.4357	72.2616				
23.6270	72.1775				
23.8755	72.1178				
24.1207	72.0616				
24.4231	72.0614				
24.6415	72.0332				
24.8631	71.9770				
24.8895	71.8057				
24.8049	71.6029				
24.6666	71.4317				
24.5585	71.2325				
24.4201	71.0054				
24.3086	70.7782				
24.1434	70.6071				
24.0889	70.3484				
24.0611	70.0372				
24.0333	69.7226				
24.1974	69.5231				
24.4998	69.4948				
24.8258	69.4945				
25.1852	69.4347				
25.4839	69.2911				

R19h		R20a		R20b	
LAT	LON	LAT	LON	LAT	LON
25.6748	69.0916				
25.7852	68.8922				
25.8685	68.6369				
25.9753	68.3780				
26.1394	68.2065				
26.3574	68.0350				
26.5789	67.9509				
26.7970	67.8353				
26.9881	67.6637				
26.9874	67.4085				
26.8491	67.2373				
26.6306	67.2095				

1-D Velocity Models

Depth (km)	V_P(km/s)	Depth (km)	V_P(km/s)	Depth (km)	V_P(km/s)
R01		R02		R03	
0	4.5	0	4.5	0	4.770
10	5.6	10	5.38814	10	5.51444
45	8.00	53	8.220	54	8.120
75	8.258	75	8.280	75	8.140
120	8.375	120	8.400	120	8.160
210	8.459	210	8.470	210	8.270
390	9.005	390	9.020	390	8.950
430	9.348	430	9.370	430	9.150
640	10.270	640	10.270	640	10.200
680	10.800	680	10.800	680	10.800
871	11.250	871	11.250	871	11.250

Depth (km)	V_P(km/s)	Depth (km)	V_P(km/s)	Depth (km)	V_P(km/s)
1271	11.870	1271	11.870	1271	11.870
R04		**R05b**		**R05c**	
0	4.7	0	4.5	0	4.728
10	5.8	10	5.6	10	5.5
48	8.194	46	8.0	44	8.054
75	8.236	75	8.2	75	8.150
120	8.255	120	8.419	120	8.239
210	8.419	210	8.552	210	8.431
390	9.091	390	9.218	390	9.090
430	9.439	430	9.5	430	9.416
640	10.270	640	10.280	640	10.269
680	10.800	680	10.800	680	10.800
871	11.250	871	11.250	871	11.250
1271	11.870	1271	11.870	1271	11.870
R05d		**R06**		**R07**	
0	4.6	0	4.2	0	4.6
10	5.6	10	5.4	10	5.6
44	8.101	44	8.00	55	8.0
75	8.2	75	8.083	75	8.1
120	8.3	120	8.2	120	8.2
210	8.4	210	8.3	210	8.36
390	8.9	390	9.0	390	9.0
430	9.4	430	9.210	430	9.225
640	10.2	640	10.268	640	10.249
680	10.800	680	10.800	680	10.800
871	11.250	871	11.250	871	11.250
1271	11.870	1271	11.870	1271	11.870
R08		**R09**		**R10**	

Depth (km)	V_P(km/s)	Depth (km)	V_P(km/s)	Depth (km)	V_P(km/s)
0	4.7	0	4.529	0	3.475
10	6.1	10	5.207	10	4.512
52	8.1	50	7.919	30	6.586
75	8.143	75	7.991	55	7.899
120	8.293	120	8.088	120	8.235
210	8.428	210	8.363	210	8.403
390	9.151	390	9.048	390	9.104
430	9.499	430	9.216	430	9.417
640	10.272	640	10.249	640	10.252
680	10.800	680	10.800	680	10.800
871	11.250	871	11.250	871	11.250
1271	11.870	1271	11.870	1271	11.870

R11a		R11b		R12a	
0	4.7	0	5.65	0	4.2
10	5.47045	17	6.25	10	5.4
44	7.95	33	7.79	54	8.0
75	8.05	75	7.81	75	8.10
120	8.1	120	8.1	120	8.150
210	8.2	210	8.2	210	8.200
390	9.0	390	9.0	390	8.880
430	9.514	430	9.514	430	9.130
640	10.273	640	10.273	640	10.240
680	10.800	680	10.800	680	10.800
871	11.250	871	11.250	871	11.250
1271	11.870	1271	11.870	1271	11.870

R12b		R13a		R13b	
0	4.3	0	5.56	0	5.25
10	5.6	21.4	6.44	16	6.2
36	8.10	32.4	7.97	50	8.19

Depth (km)	V_P(km/s)	Depth (km)	V_P(km/s)	Depth (km)	V_P(km/s)
75	8.150	75	7.99	75	8.21
120	8.170	120	8.10	120	8.29
210	8.6	210	8.290	210	8.30
390	9.2	390	8.960	390	8.960
430	9.475	430	9.210	430	9.210
640	10.240	640	10.260	640	10.260
680	10.800	680	10.800	680	10.800
871	11.250	871	11.250	871	11.250
1271	11.870	1271	11.870	1271	11.870

R13c		R14		R15a	
0	5.96	0	4.8	0	4.8
10	6.36	10	5.59024	10	5.7
32	7.9	41	8.040	51	8.029019
75	8.09	75	8.050	75	8.15
120	8.11	120	8.060	120	8.4
210	8.29	210	8.290	210	8.5
390	8.960	390	8.960	390	9.1
430	9.210	430	9.210	430	9.4
640	10.260	640	10.260	640	10.270
680	10.800	680	10.800	680	10.800
871	11.250	871	11.250	871	11.250
1271	11.870	1271	11.870	1271	11.870

R15b		R16a		R16b	
0	4.891499	0	4.0	0	4.8
10	5.979536	10	5.1	10	5.59024
51	8.136991	40	7.96	40	8.040
75	8.174137	75	8.050	75	8.050
120	8.421670	120	8.060	120	8.060
210	8.6	210	8.290	210	8.290

Depth (km)	V_P(km/s)	Depth (km)	V_P(km/s)	Depth (km)	V_P(km/s)
390	9.2	390	8.960	390	8.960
430	9.475	430	9.210	430	9.210
640	10.270	640	10.260	640	10.260
680	10.800	680	10.800	680	10.800
871	11.250	871	11.250	871	11.250
1271	11.870	1271	11.870	1271	11.870

R17		R18		R19a	
0	4.8	0	4.8	0	4.8
10	5.59024	10	5.59024	10	5.8
41	8.040	41	8.040	35	8.0
75	8.050	75	8.050	75	8.15
120	8.060	120	8.060	120	8.30
210	8.290	210	8.290	210	8.460
390	8.960	390	8.960	390	9.1
430	9.210	430	9.210	430	9.310
640	10.260	640	10.260	640	10.260
680	10.800	680	10.800	680	10.800
871	11.250	871	11.250	871	11.250
1271	11.870	1271	11.870	1271	11.870

R19b		R19c		R19d	
0	4.8	0	4.4	0	4.06
10	5.8	10	5.7	10	5.8
35	8.0	40	8.06	35	8.15
75	8.15	75	8.10	75	8.26
120	8.30	120	8.150	120	8.30
210	8.460	210	8.290	210	8.40
390	9.1	390	8.960	390	8.960
430	9.310	430	9.210	430	9.210
640	10.260	640	10.260	640	10.260

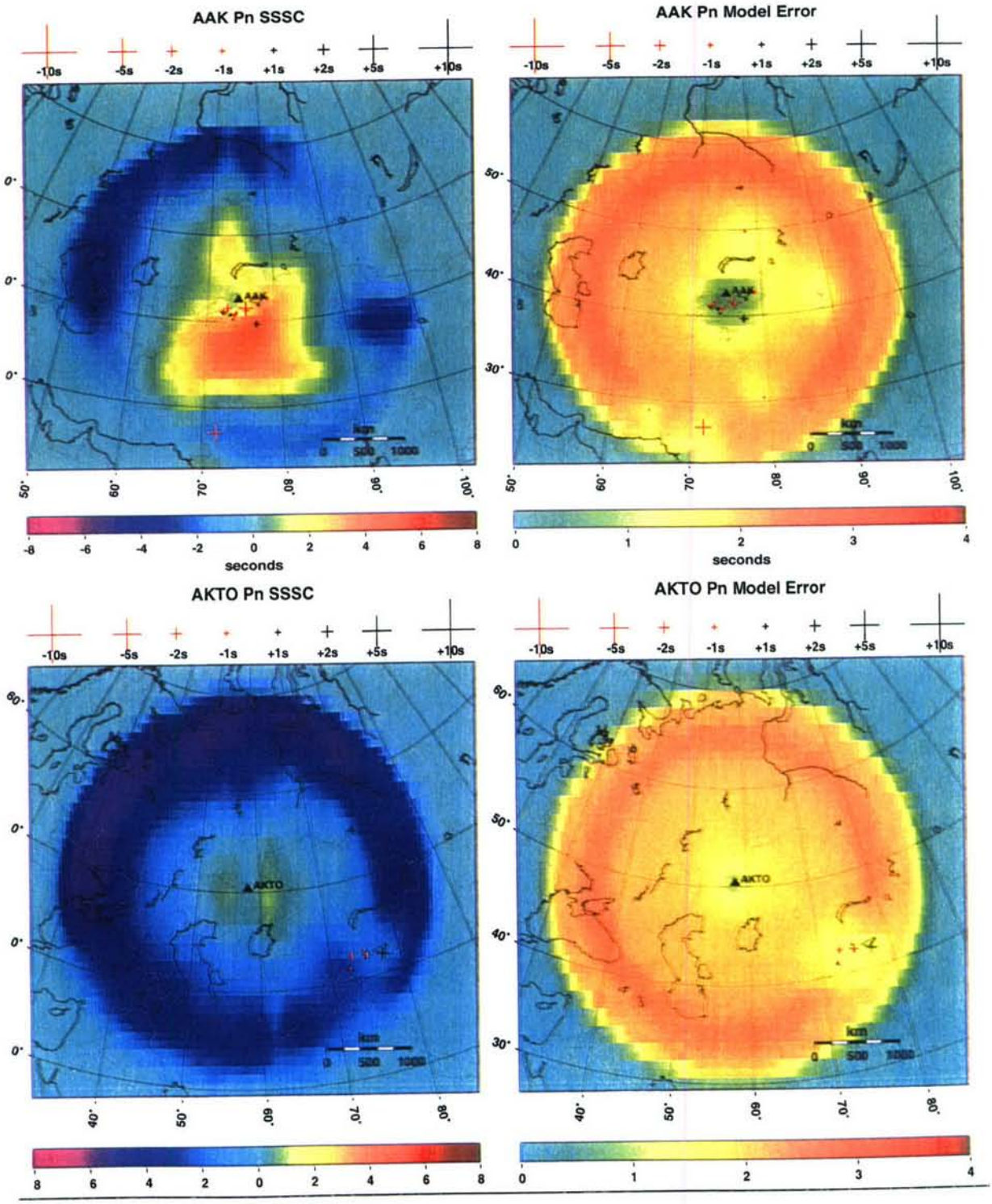
Depth (km)	V_P(km/s)	Depth (km)	V_P(km/s)	Depth (km)	V_P(km/s)
680	10.800	680	10.800	680	10.800
871	11.250	871	11.250	871	11.250
1271	11.870	1271	11.870	1271	11.870

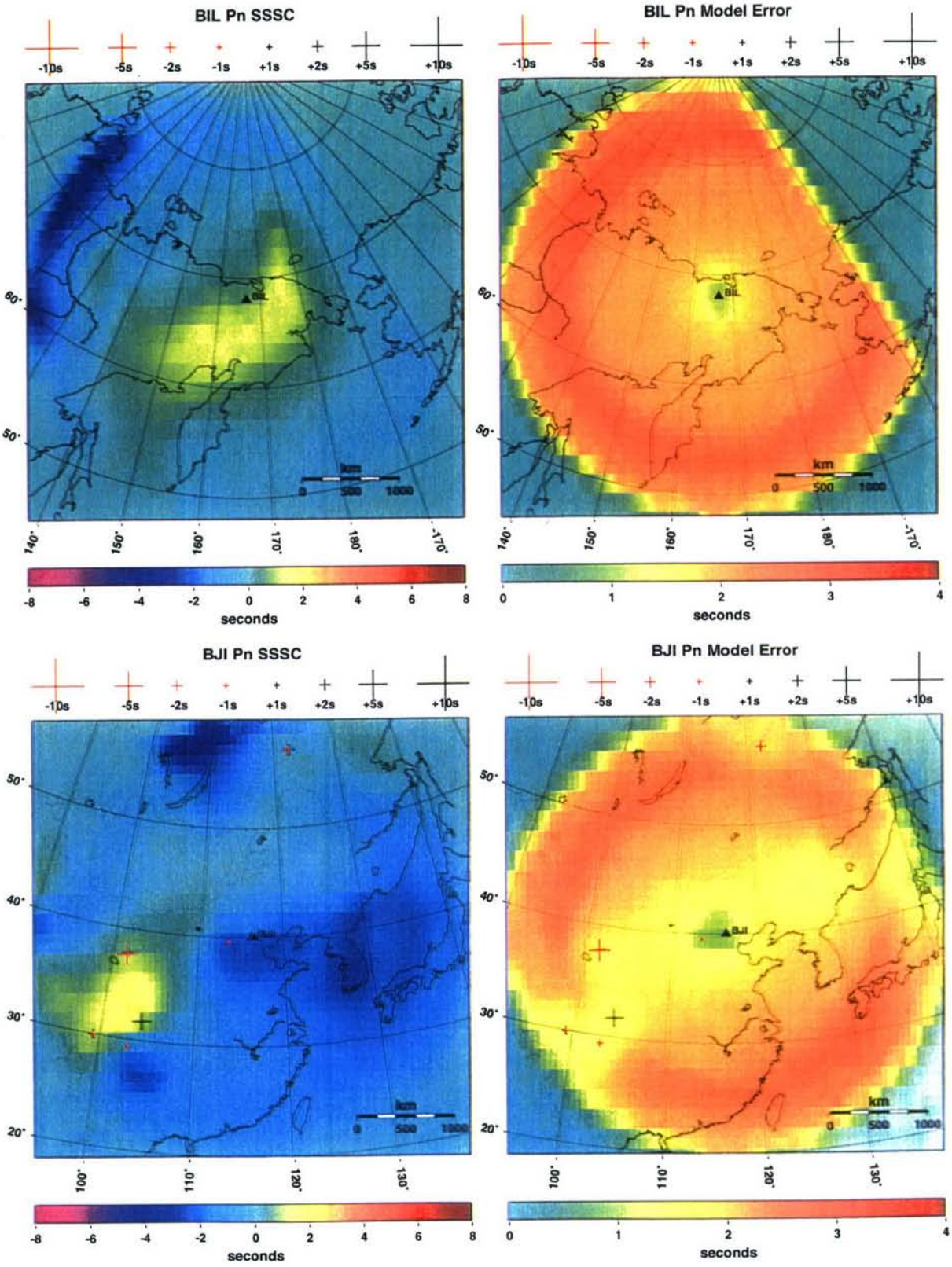
R19e		R19f		R19g	
0	4.06	0	4.4	0	4.1
10	5.8	10	5.7	10	5.9
35	8.15	30	6.586	40	8.0
75	8.26	55	7.899	75	8.08
120	8.30	120	8.235	120	8.15
210	8.40	210	8.403	210	8.290
390	8.960	390	9.104	390	8.960
430	9.210	430	9.417	430	9.210
640	10.260	640	10.252	640	10.260
680	10.800	680	10.800	680	10.800
871	11.250	871	11.250	871	11.250
1271	11.870	1271	11.870	1271	11.870

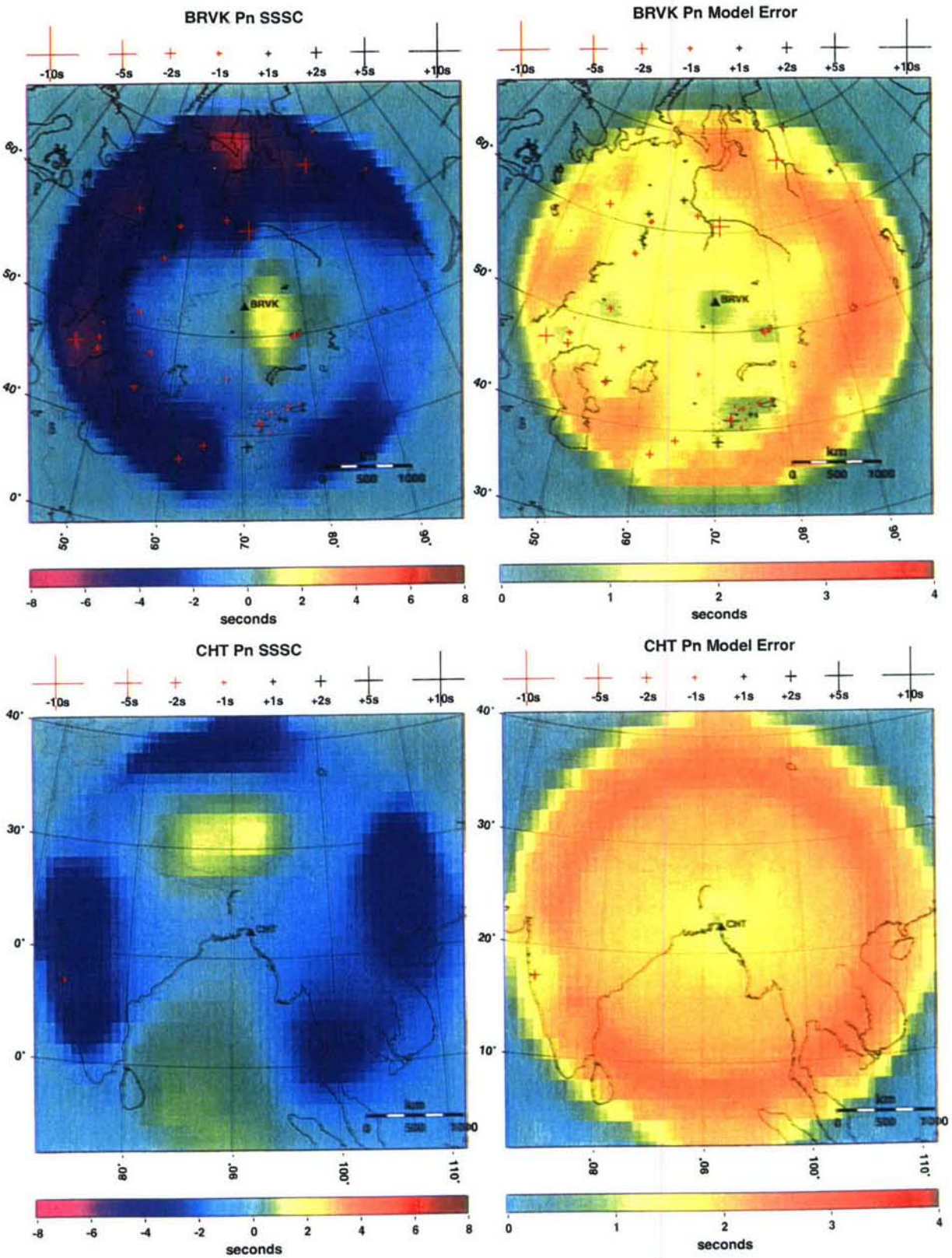
R19h		R20a		R20b	
0	3.2	0	4.7	0	4.800
10	5.95	10	5.6	10	5.59024
33	8.000	50	7.8	41	8.040
75	8.050	75	8.050	75	8.050
120	8.060	120	8.060	120	8.060
210	8.290	210	8.290	210	8.290
390	8.960	390	8.960	390	8.960
430	9.210	430	9.210	430	9.210
640	10.260	640	10.260	640	10.260
680	10.800	680	10.800	680	10.800
871	11.250	871	11.250	871	11.250
1271	11.870	1271	11.870	1271	11.870

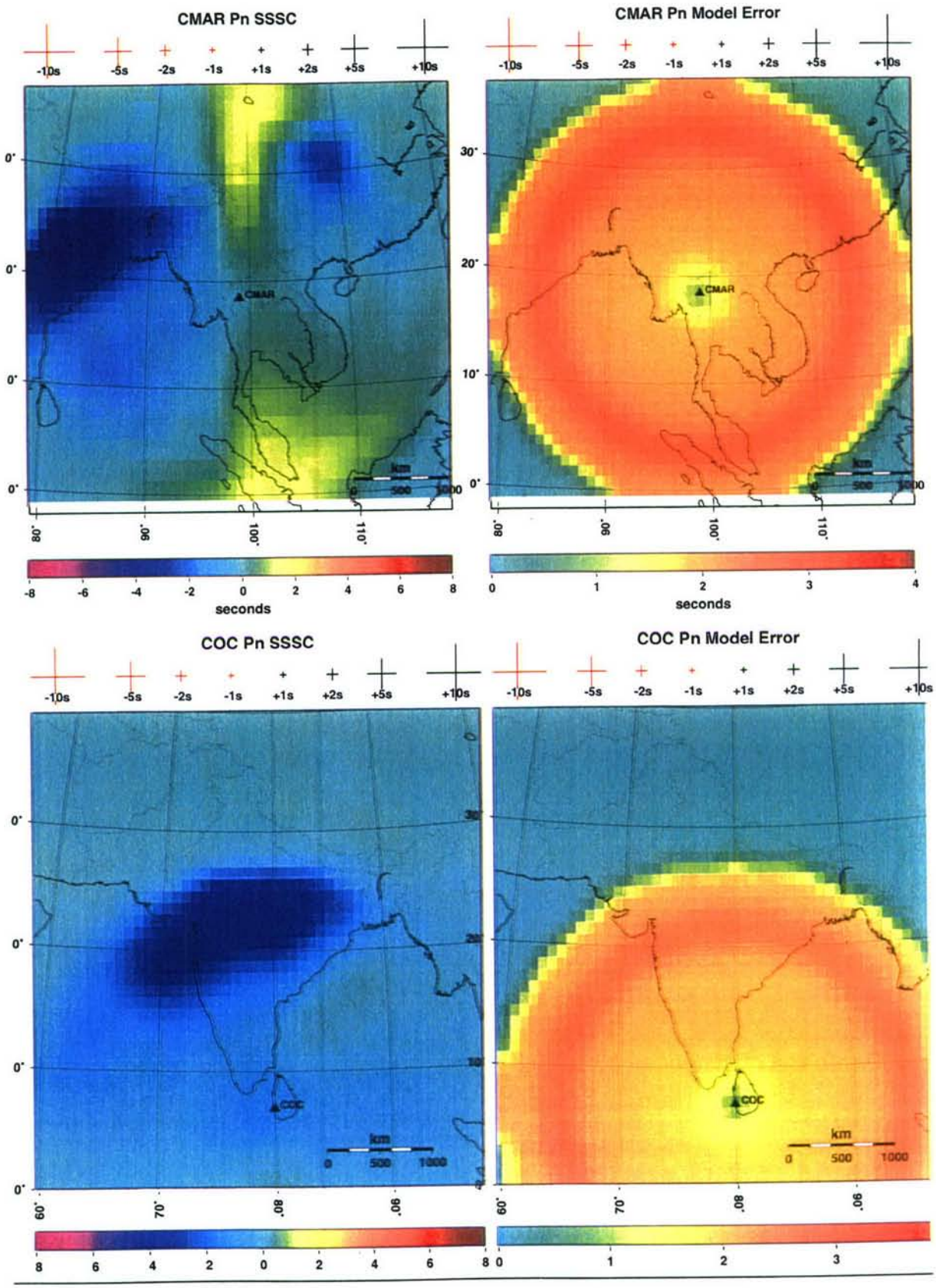
Appendix E Pn and Sn SSSCs and Modeling Errors

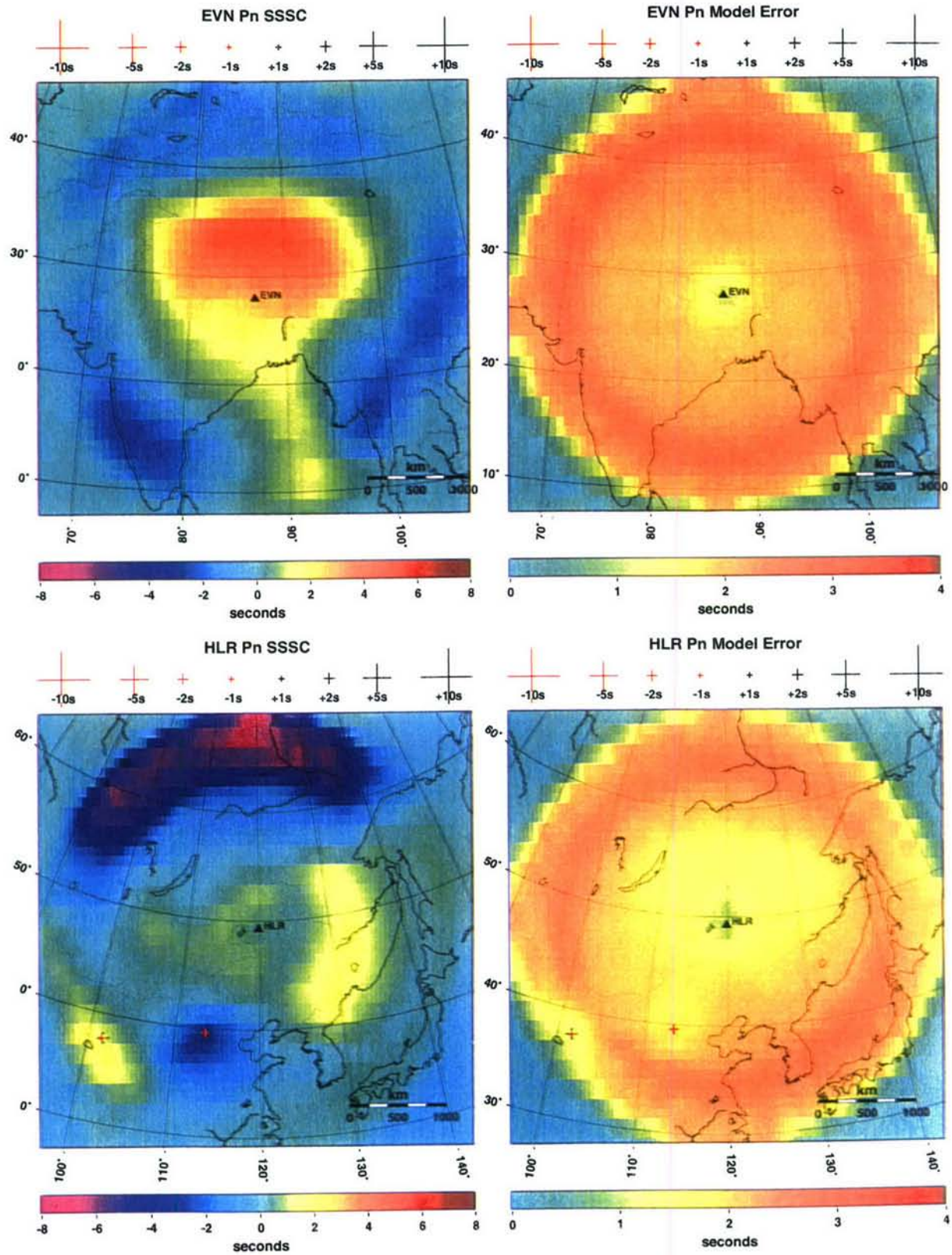
The following figures depict the Pn and Sn SSSCs and the corresponding modeling errors, computed with 3D ray tracing and refined by applying a kriging algorithm, for the 30 IMS stations (or sites of future IMS stations) listed in Table 1.

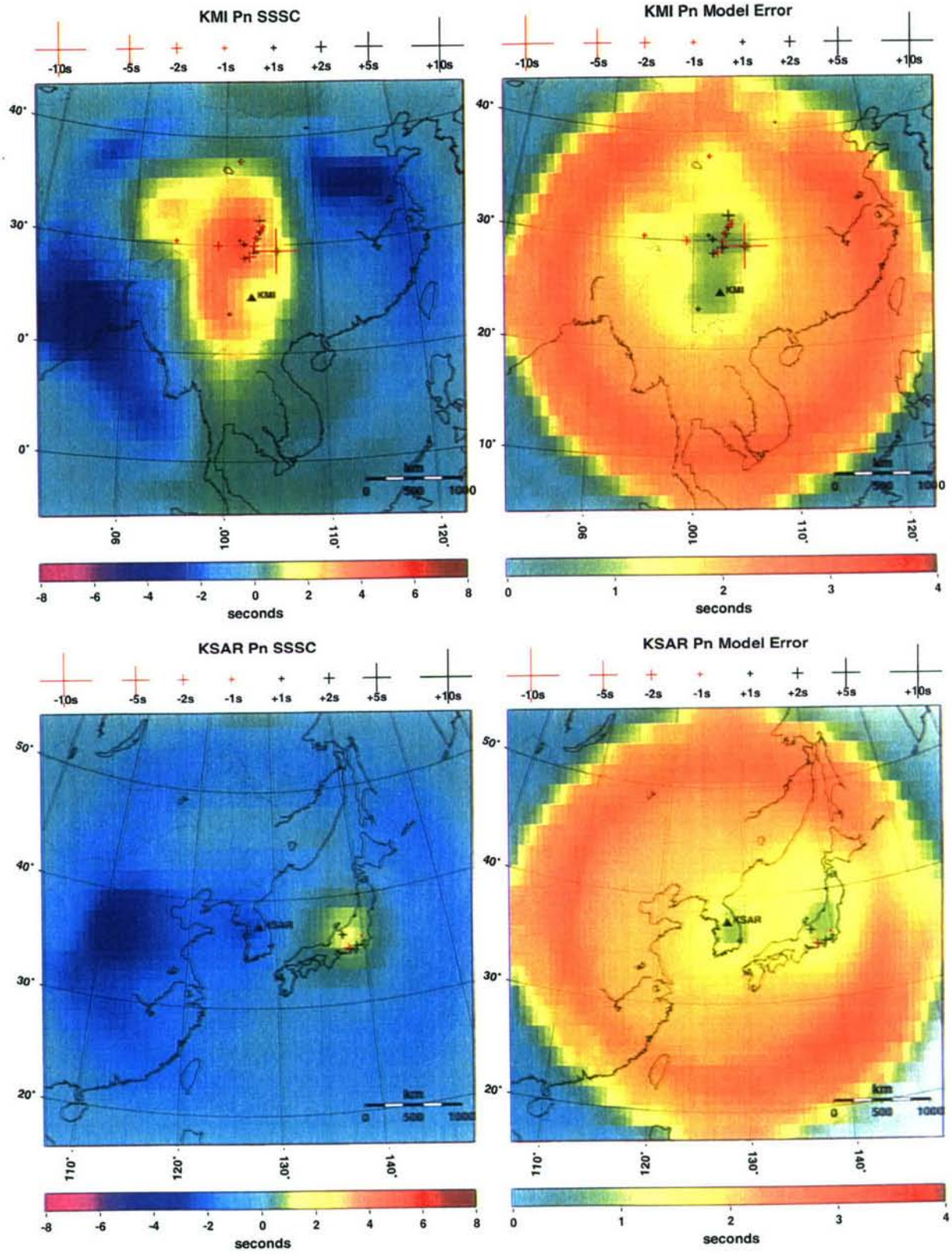


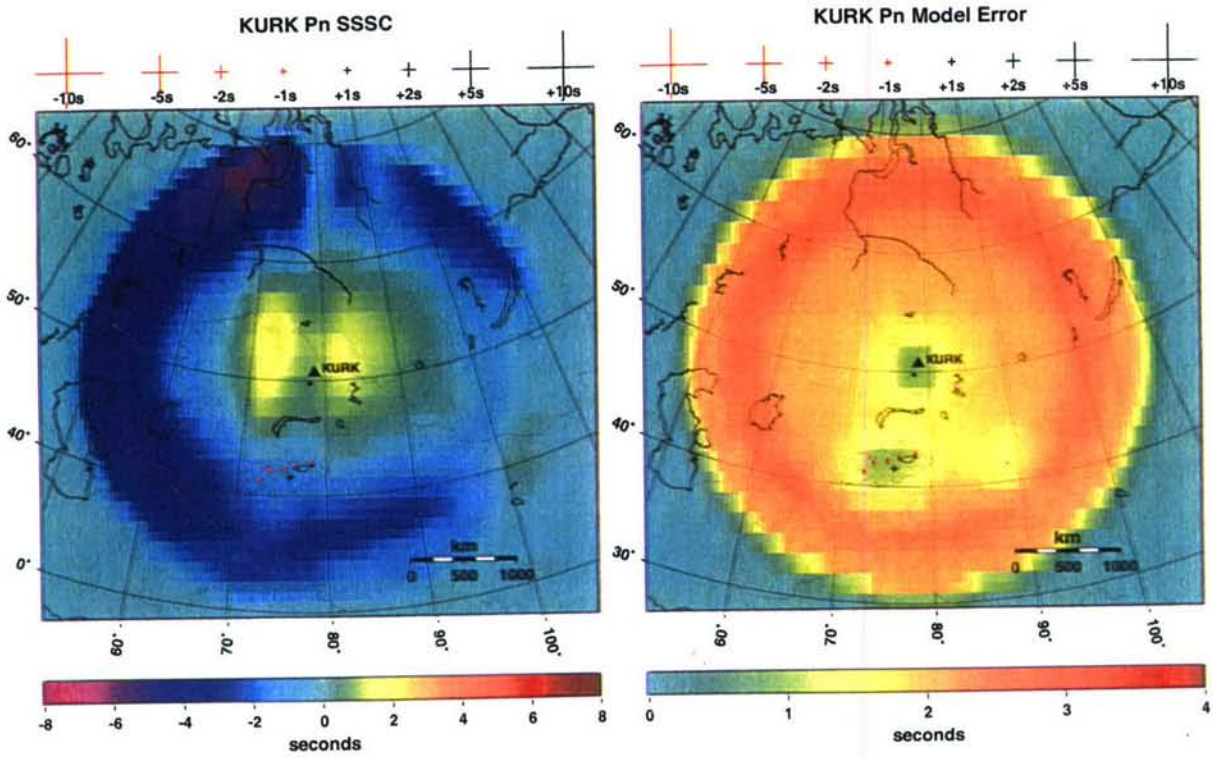

BIL Pn SSSC
-10s
-5s
-2s
-1s
+1s
+2s
+5s
+10s
BIL
km
0
500
1000
60°
50°
140°
150°
160°
170°
180°
-170°
-8
-6
-4
-2
0
2
4
6
8
seconds
BIL Pn Model Error
0
1
2
3
4
seconds
BJI Pn SSSC
40°
30°
20°
100°
110°
120°
130°
BJI Pn Model Error

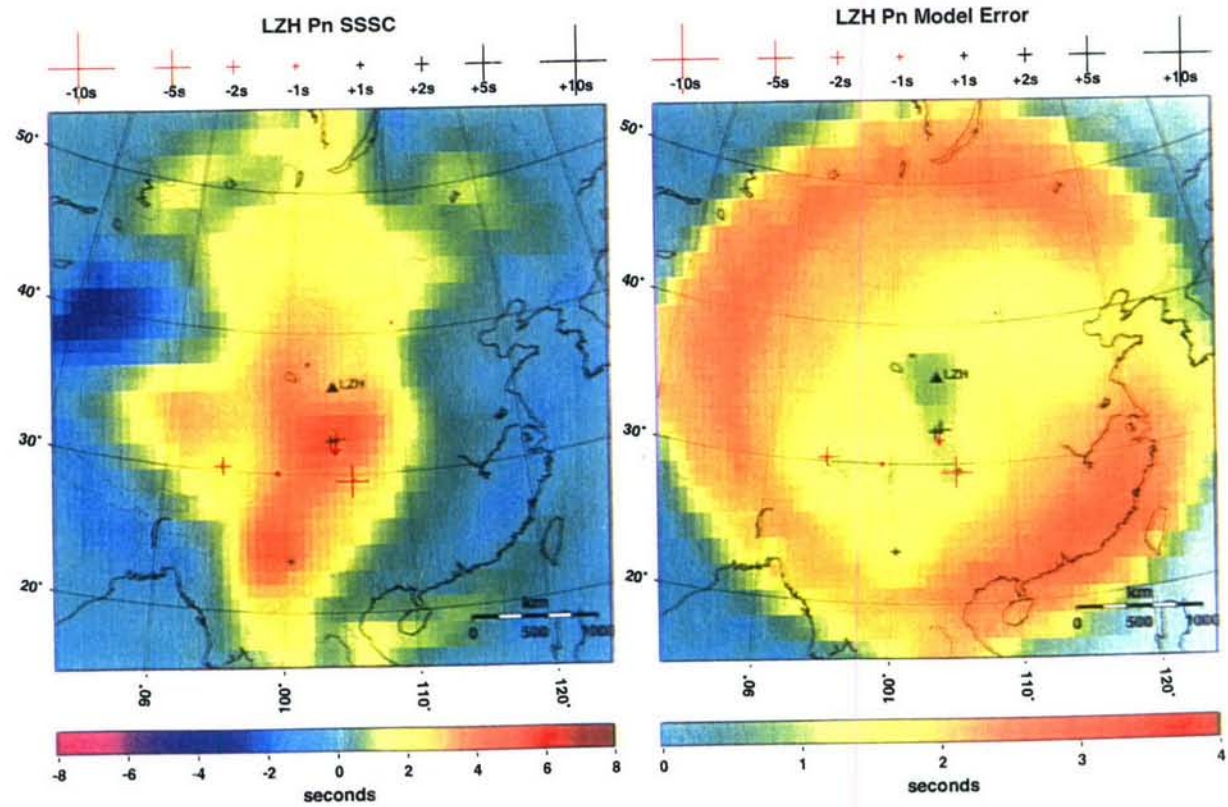

BRVK Pn SSSC
-10s
-5s
-2s
-1s
+1s
+2s
+5s
+10s
BRVK
seconds
BRVK Pn Model Error
CHT Pn SSSC
CHT
CHT Pn Model Error

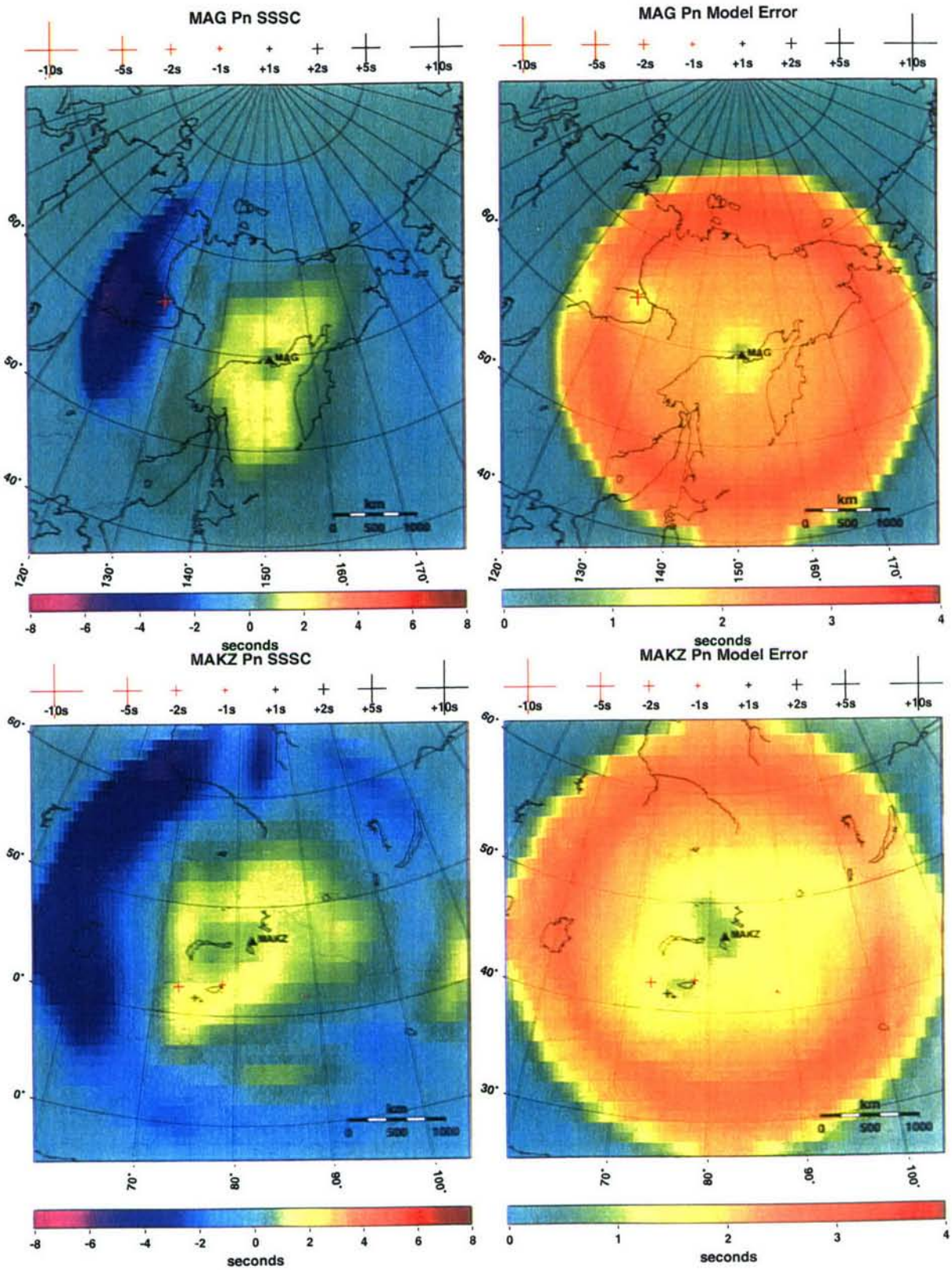

CMAR Pn SSSC
-10s
-5s
-2s
-1s
+1s
+2s
+5s
+10s
CMAR
km
0
500
1000
0°
0°
0°
80°
90°
100°
110°
-8
-6
-4
-2
0
2
4
6
8
seconds
CMAR Pn Model Error
30°
20°
10°
0°
0
1
2
3
4
seconds
COC Pn SSSC
COC
60°
70°
80°
90°
8
6
4
2
0
2
4
6
8
COC Pn Model Error
0
1
2
3

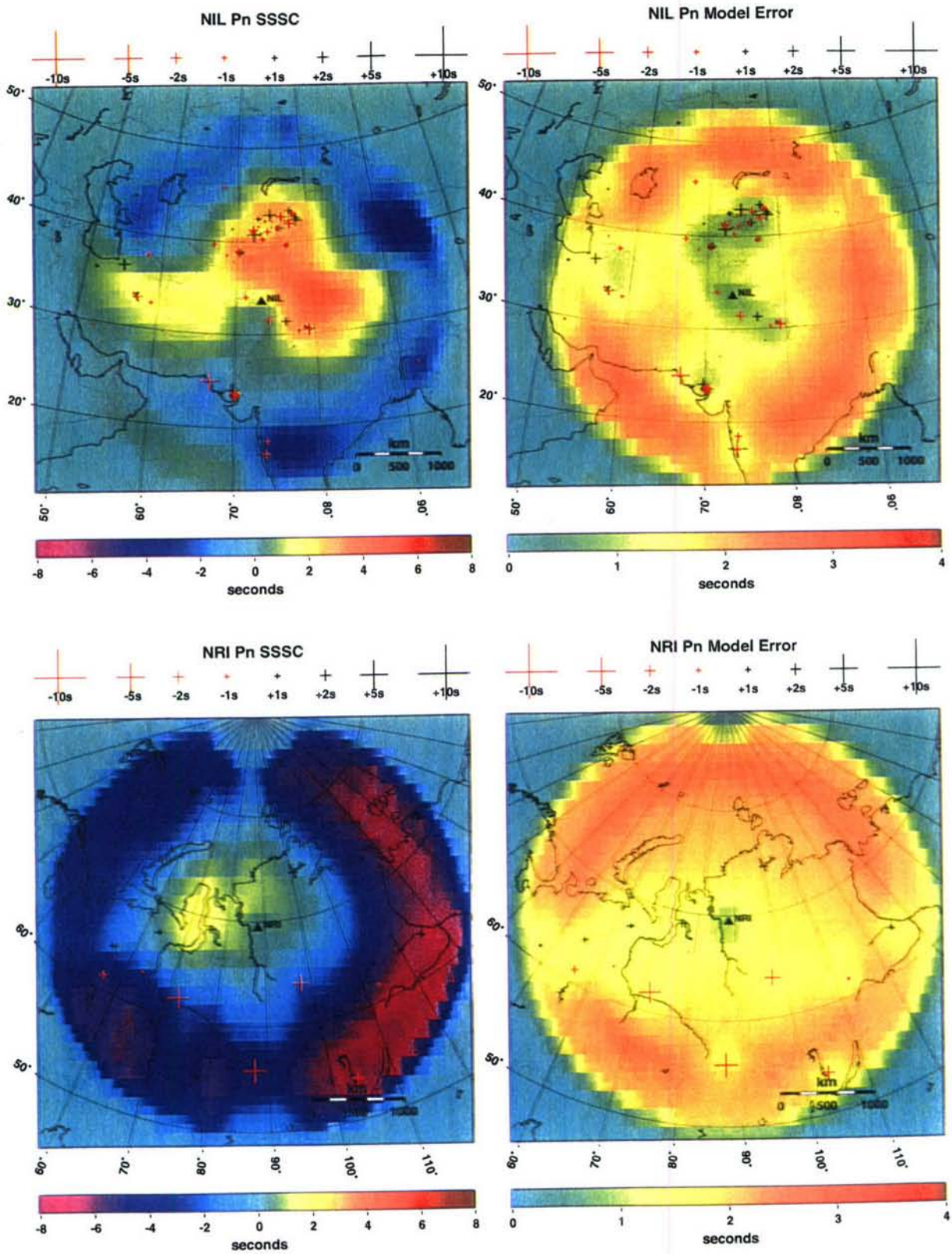

EVN Pn SSSC
-10s
-5s
-2s
-1s
+1s
+2s
+5s
+10s
EVN
km
0
500
1000
40°
30°
0°
0°
70°
80°
90°
100°
-8
-6
-4
-2
0
2
4
6
8
seconds
EVN Pn Model Error
-10s
-5s
-2s
-1s
+1s
+2s
+5s
+10s
EVN
km
0
500
1000
40°
30°
20°
10°
70°
80°
90°
100°
0
1
2
3
4
seconds
HLR Pn SSSC
-10s
-5s
-2s
-1s
+1s
+2s
+5s
+10s
HLR
km
0
500
1000
60°
50°
0°
0°
100°
110°
120°
130°
140°
-8
-6
-4
-2
0
2
4
6
8
seconds
HLR Pn Model Error
-10s
-5s
-2s
-1s
+1s
+2s
+5s
+10s
HLR
km
0
500
1000
60°
50°
40°
30°
100°
110°
120°
130°
140°
0
1
2
3
4
seconds

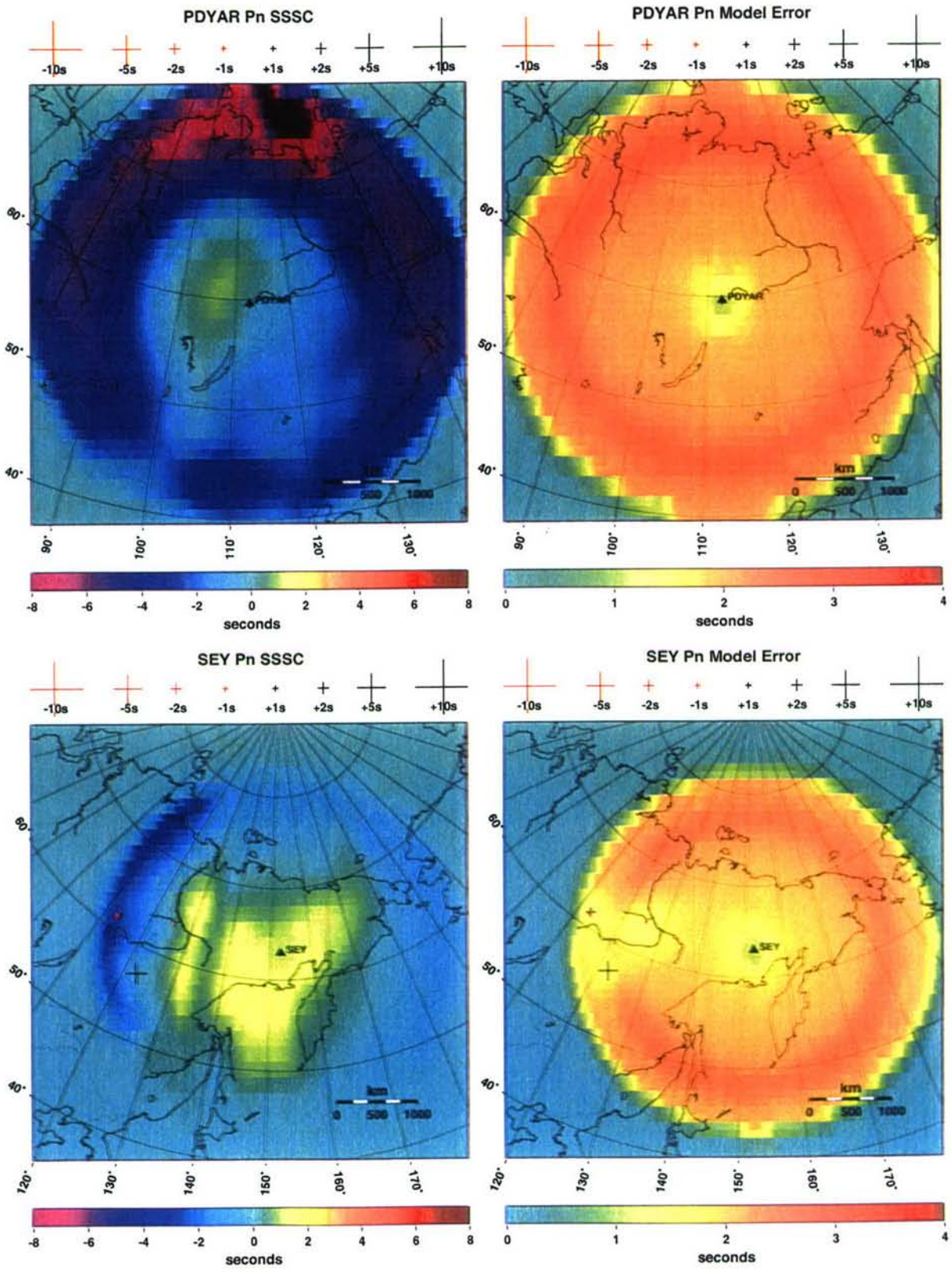

KMI Pn SSSC
-10s
-5s
-2s
-1s
+1s
+2s
+5s
+10s
40°
30°
0°
0°
KMI
km
0
500
1000
90°
100°
110°
120°
-8
-6
-4
-2
0
2
4
6
8
seconds
KMI Pn Model Error
-10s
-5s
-2s
-1s
+1s
+2s
+5s
+10s
40°
30°
20°
10°
KMI
km
0
500
1000
90°
100°
110°
120°
0
1
2
3
4
seconds
KSAR Pn SSSC
-10s
-5s
-2s
-1s
+1s
+2s
+5s
+10s
50°
40°
30°
20°
KSAR
km
0
500
1000
110°
120°
130°
140°
-8
-6
-4
-2
0
2
4
6
8
seconds
KSAR Pn Model Error
-10s
-5s
-2s
-1s
+1s
+2s
+5s
+10s
50°
40°
30°
20°
KSAR
km
0
500
1000
110°
120°
130°
140°
0
1
2
3
4
seconds

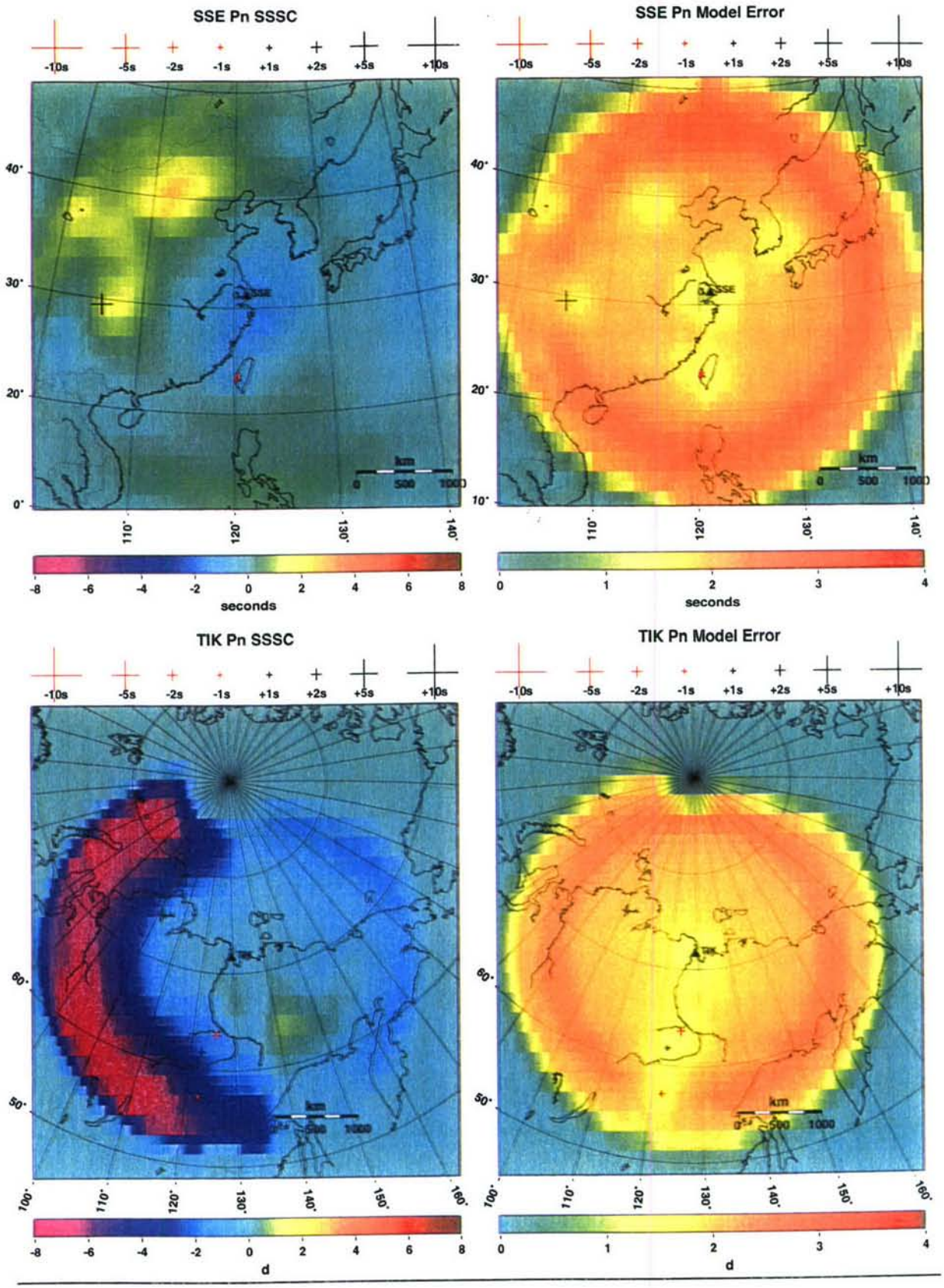

KURK Pn SSSC
KURK Pn Model Error
-10s
-5s
-2s
-1s
+1s
+2s
+5s
+10s
KURK
km
0
500
1000
60°
50°
40°
0°
30°
60°
70°
80°
90°
100°
-8
-6
-4
-2
0
2
4
6
8
seconds

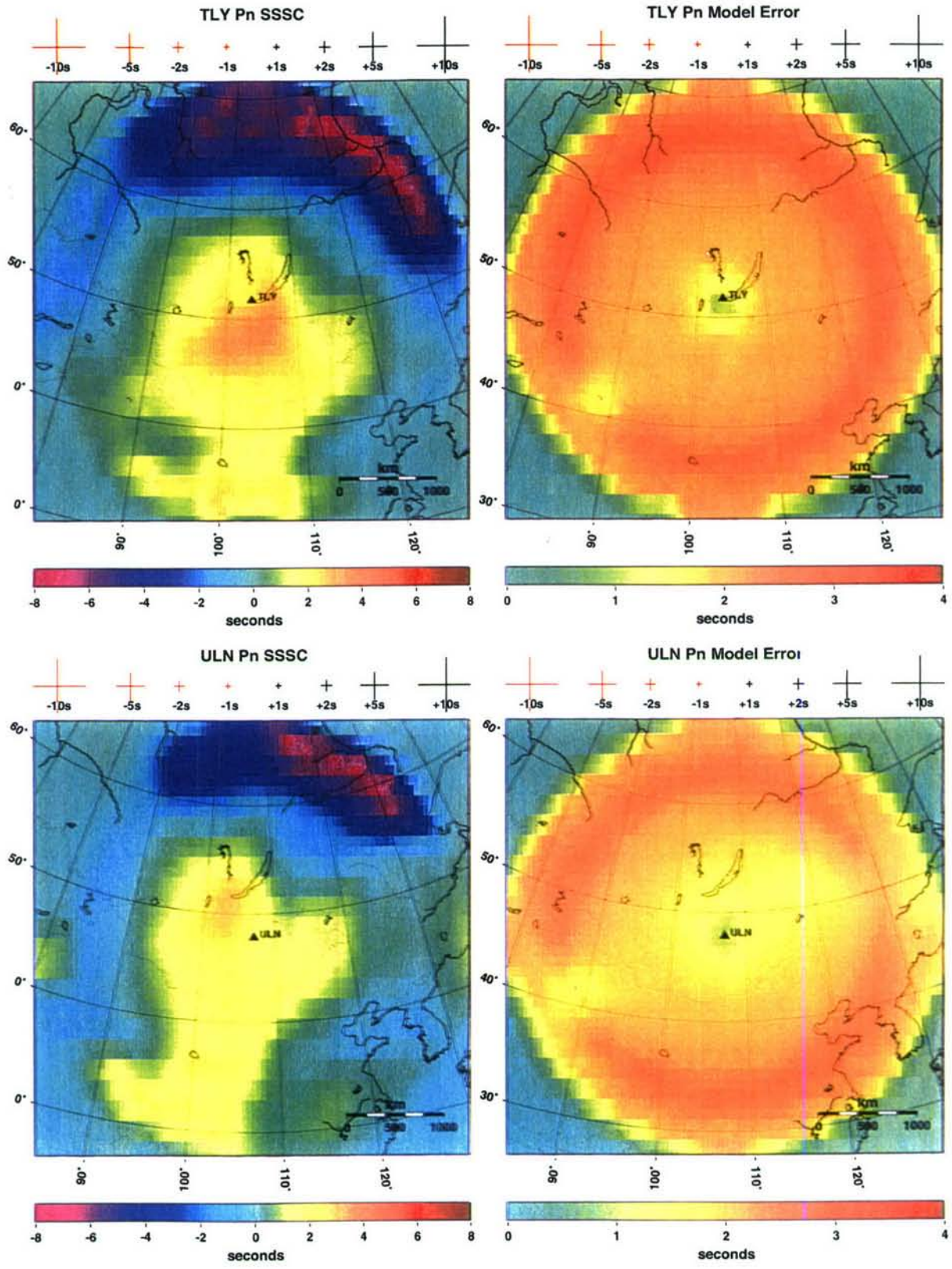

LZH Pn SSSC
LZH Pn Model Error
-10s
-5s
-2s
-1s
+1s
+2s
+5s
+10s
LZH
km
0
500
1000
50°
40°
30°
20°
60°
70°
80°
90°
100°
110°
120°
-8
-6
-4
-2
0
2
4
6
8
seconds

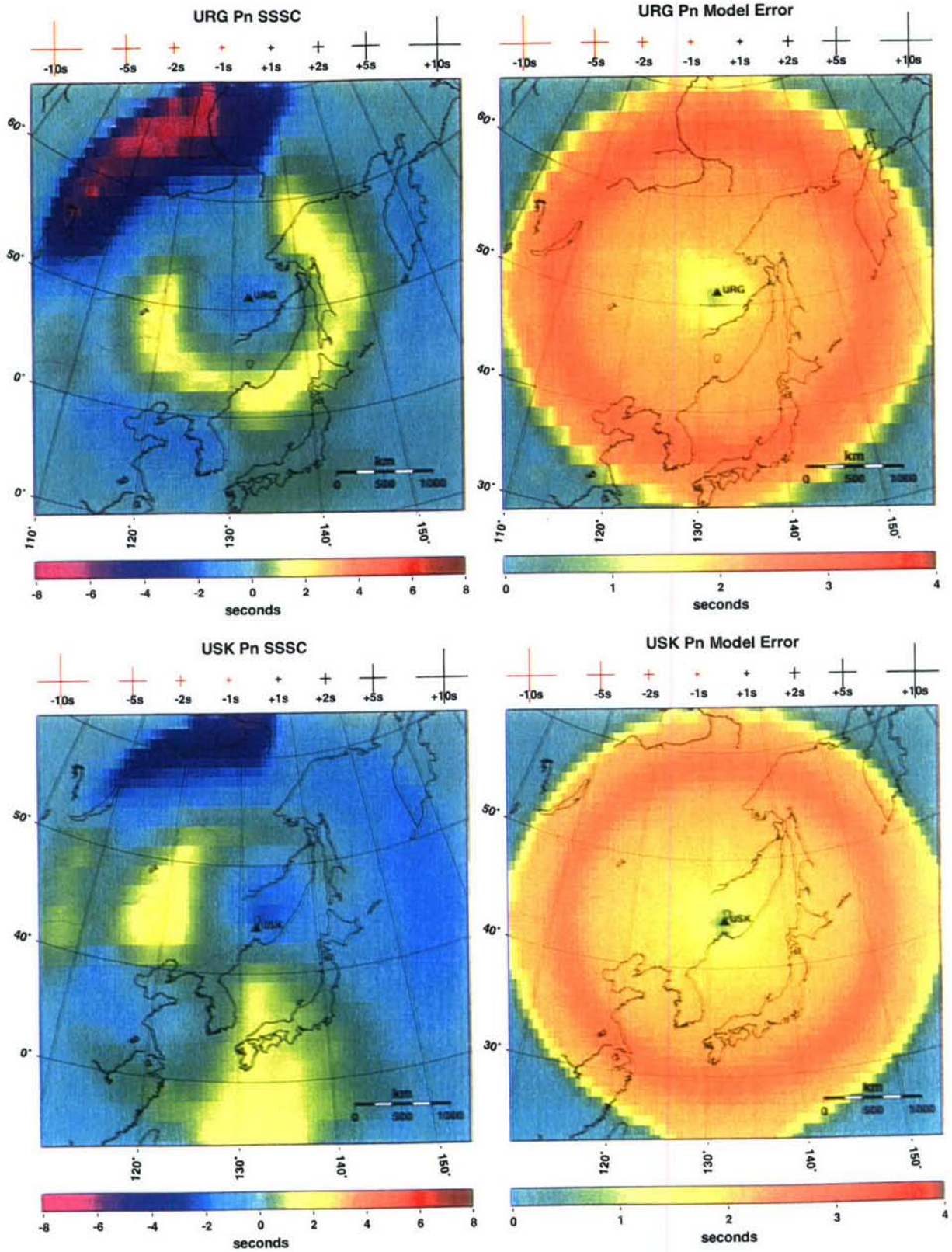

MAG Pn SSSC
MAG Pn Model Error
MAKZ Pn SSSC
MAKZ Pn Model Error
-10s
-5s
-2s
-1s
+1s
+2s
+5s
+10s
MAG
MAKZ
km
0
500
1000
seconds

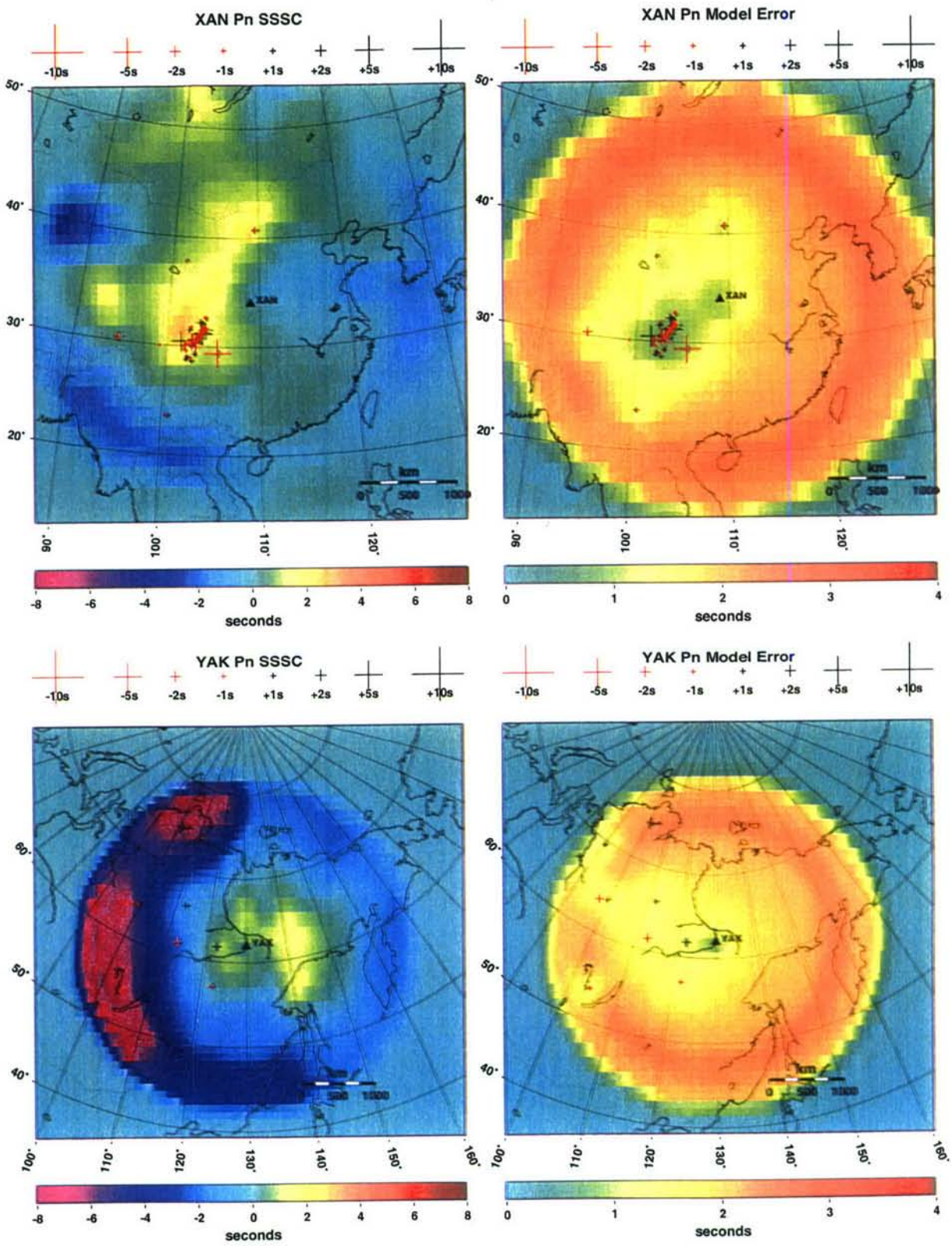

NIL Pn SSSC
-10s
-5s
-2s
-1s
+1s
+2s
+5s
+10s
50°
40°
30°
20°
NIL
km
0
500
1000
50°
60°
70°
80°
90°
-8
-6
-4
-2
0
2
4
6
8
seconds
NIL Pn Model Error
0
1
2
3
4
seconds
NRI Pn SSSC
60°
50°
NRI
100°
110°
NRI Pn Model Error

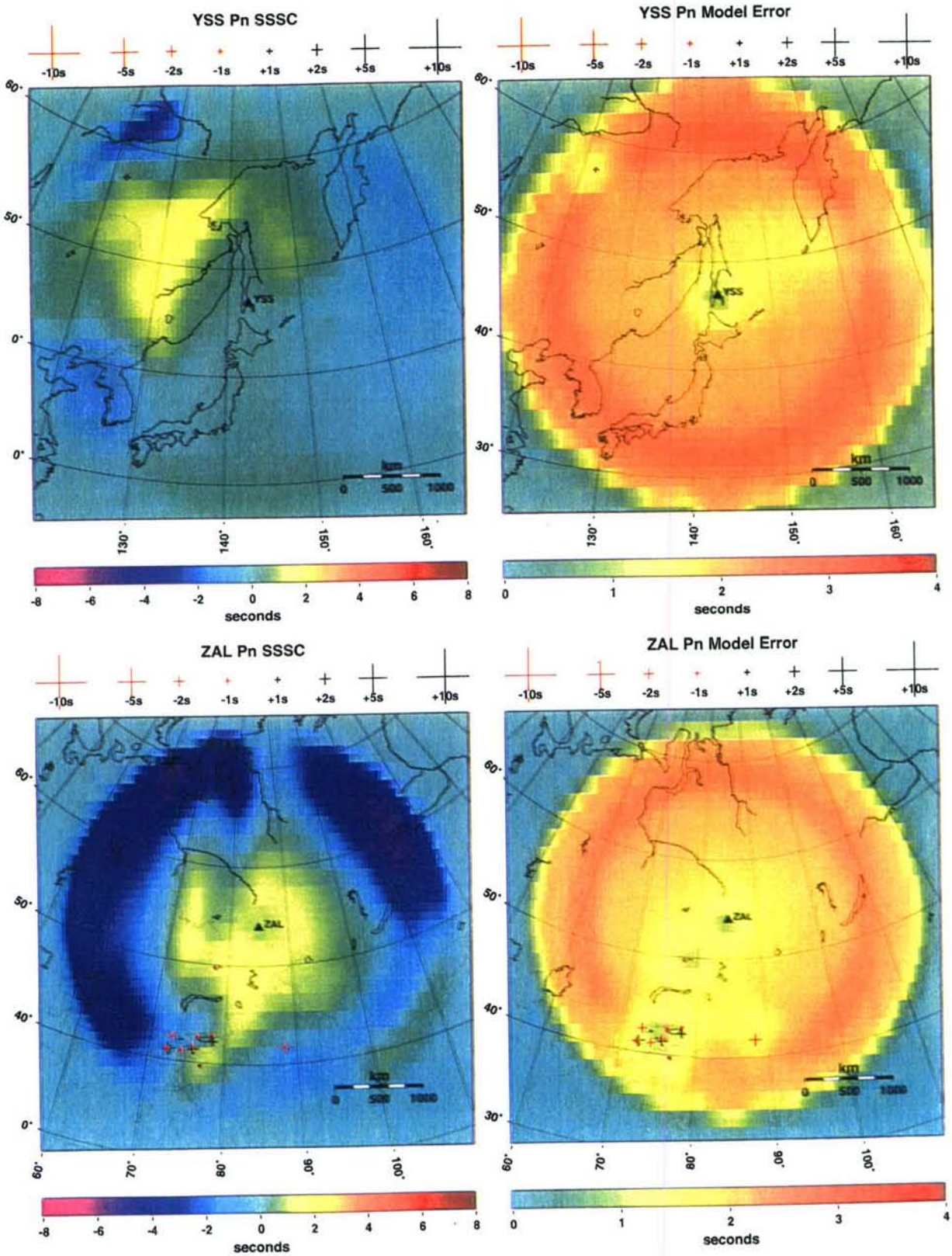

PDYAR Pn SSSC
-10s
-5s
-2s
-1s
+1s
+2s
+5s
+10s
PDYAR
km
0
500
1000
60°
50°
40°
90°
100°
110°
120°
130°
-8
-6
-4
-2
0
2
4
6
8
seconds
PDYAR Pn Model Error
-10s
-5s
-2s
-1s
+1s
+2s
+5s
+10s
PDYAR
km
0
500
1000
60°
50°
40°
90°
100°
110°
120°
130°
0
1
2
3
4
seconds
SEY Pn SSSC
-10s
-5s
-2s
-1s
+1s
+2s
+5s
+10s
SEY
km
0
500
1000
60°
50°
40°
120°
130°
140°
150°
160°
170°
-8
-6
-4
-2
0
2
4
6
8
seconds
SEY Pn Model Error
-10s
-5s
-2s
-1s
+1s
+2s
+5s
+10s
SEY
km
0
500
1000
60°
50°
40°
120°
130°
140°
150°
160°
170°
0
1
2
3
4
seconds

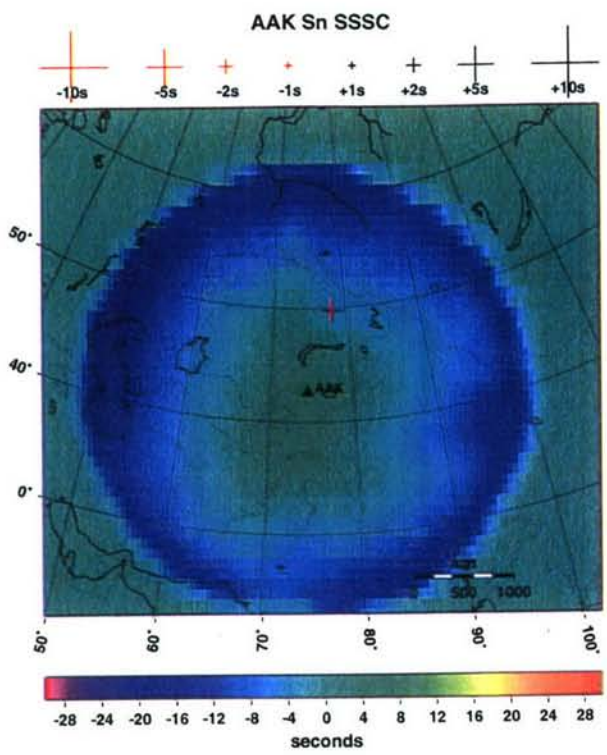

SSE Pn SSSC
-10s
-5s
-2s
-1s
+1s
+2s
+5s
+10s
40°
30°
20°
0°
110°
120°
130°
140°
km
0
500
1000
-8
-6
-4
-2
0
2
4
6
8
seconds
SSE Pn Model Error
10°
0
1
2
3
4
seconds
TIK Pn SSSC
60°
50°
100°
150°
160°
d
TIK Pn Model Error

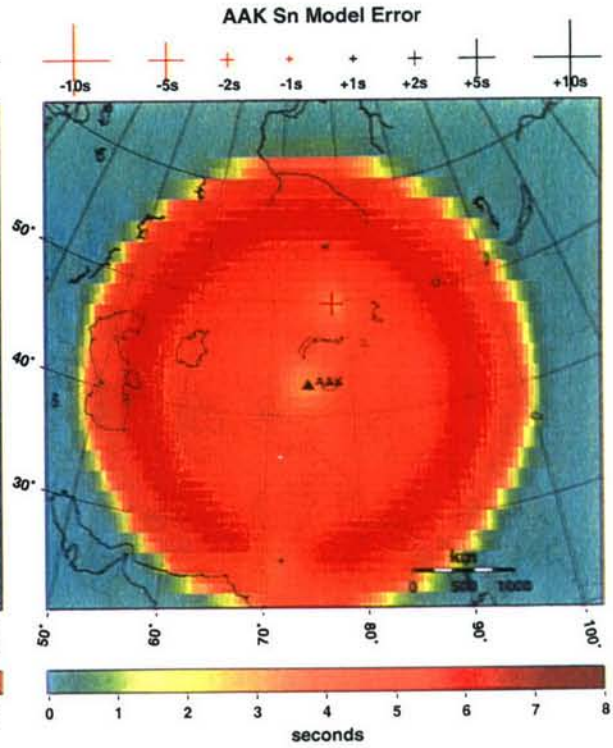

TLY Pn SSSC
TLY Pn Model Error
ULN Pn SSSC
ULN Pn Model Error
-10s
-5s
-2s
-1s
+1s
+2s
+5s
+10s
TLY
ULN
km
0
500
1000
60°
50°
0°
40°
30°
90°
100°
110°
120°
-8
-6
-4
-2
0
2
4
6
8
0
1
2
3
4
seconds

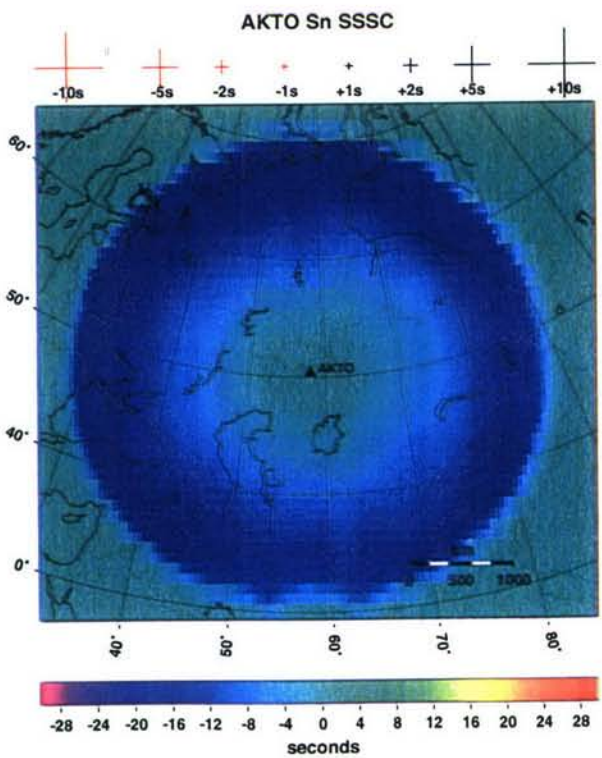

URG Pn SSSC
-10s
-5s
-2s
-1s
+1s
+2s
+5s
+10s
URG
km
0
500
1000
60°
50°
0°
110°
120°
130°
140°
150°
-8
-6
-4
-2
0
2
4
6
8
seconds
URG Pn Model Error
-10s
-5s
-2s
-1s
+1s
+2s
+5s
+10s
URG
km
0
500
1000
60°
50°
40°
30°
110°
120°
130°
140°
150°
0
1
2
3
4
seconds
USK Pn SSSC
-10s
-5s
-2s
-1s
+1s
+2s
+5s
+10s
USK
km
0
500
1000
50°
40°
0°
120°
130°
140°
150°
-8
-6
-4
-2
0
2
4
6
8
seconds
USK Pn Model Error
-10s
-5s
-2s
-1s
+1s
+2s
+5s
+10s
USK
km
0
500
1000
50°
40°
30°
120°
130°
140°
150°
0
1
2
3
4
seconds

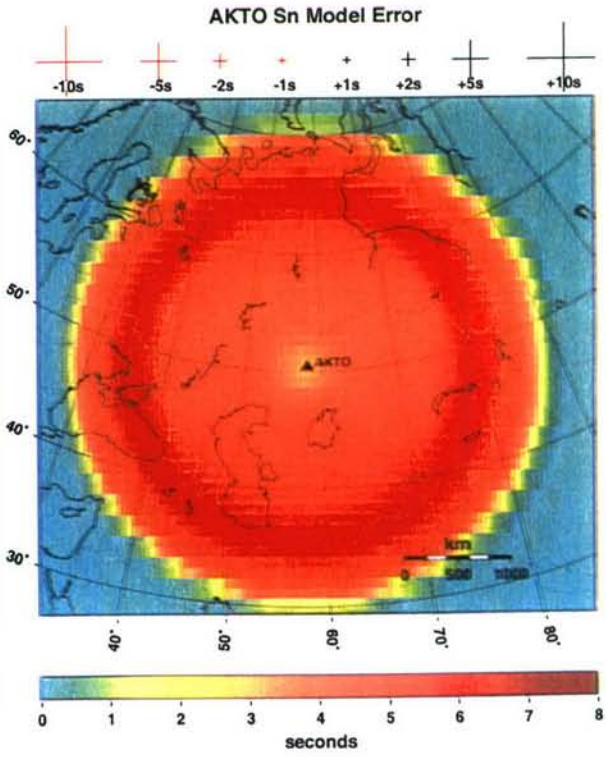

XAN Pn SSSC
XAN Pn Model Error
YAK Pn SSSC
YAK Pn Model Error
-10s
-5s
-2s
-1s
+1s
+2s
+5s
+10s
XAN
YAK
km
0
500
1000
seconds

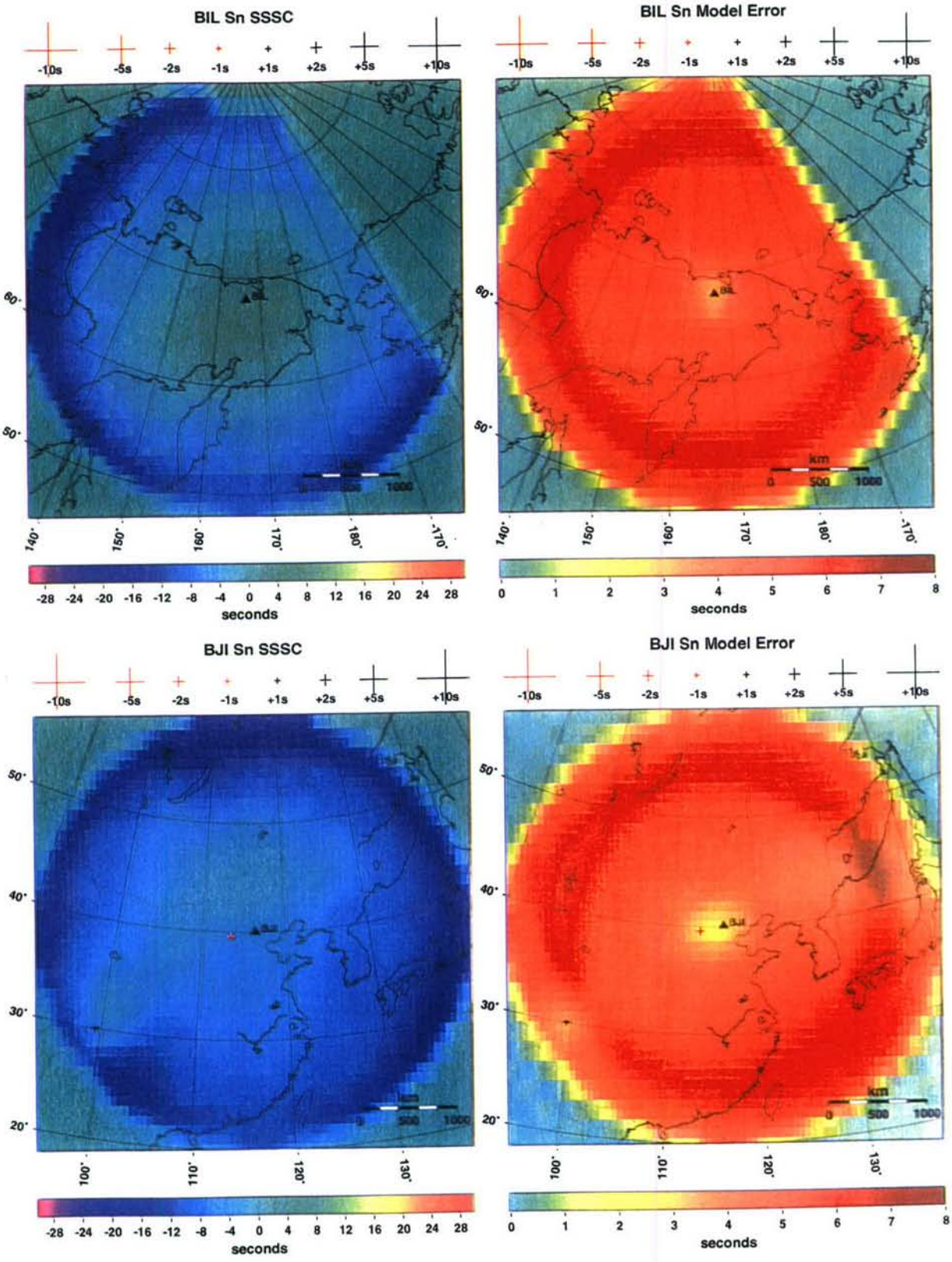

YSS Pn SSSC
-10s
-5s
-2s
-1s
+1s
+2s
+5s
+10s
60°
50°
0°
YSS
km
0
500
1000
130°
140°
150°
160°
-8
-6
-4
-2
0
2
4
6
8
seconds
YSS Pn Model Error
-10s
-5s
-2s
-1s
+1s
+2s
+5s
+10s
60°
50°
40°
30°
YSS
km
0
500
1000
130°
140°
150°
160°
0
1
2
3
4
seconds
ZAL Pn SSSC
-10s
-5s
-2s
-1s
+1s
+2s
+5s
+10s
60°
50°
40°
0°
ZAL
km
0
500
1000
60°
70°
80°
90°
100°
-8
-6
-4
-2
0
2
4
6
8
seconds
ZAL Pn Model Error
-10s
-5s
-2s
-1s
+1s
+2s
+5s
+10s
60°
50°
40°
30°
ZAL
km
0
500
1000
60°
70°
80°
90°
100°
0
1
2
3
4
seconds

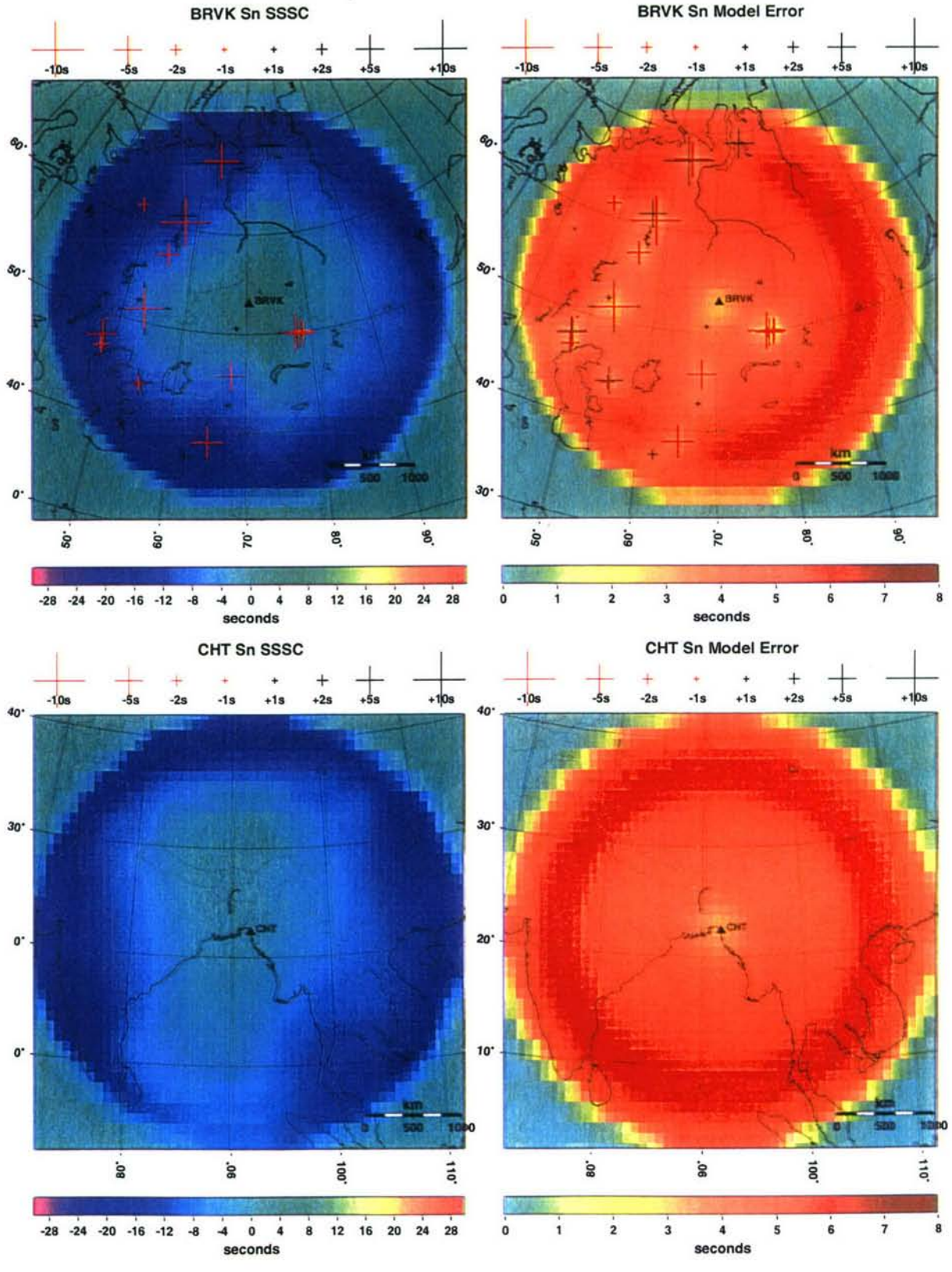

AAK Sn SSSC
-10s
-5s
-2s
-1s
+1s
+2s
+5s
+10s
50°
40°
0°
AAK
km
0
500
1000
50°
60°
70°
80°
90°
100°
-28 -24 -20 -16 -12 -8 -4 0 4 8 12 16 20 24 28
seconds

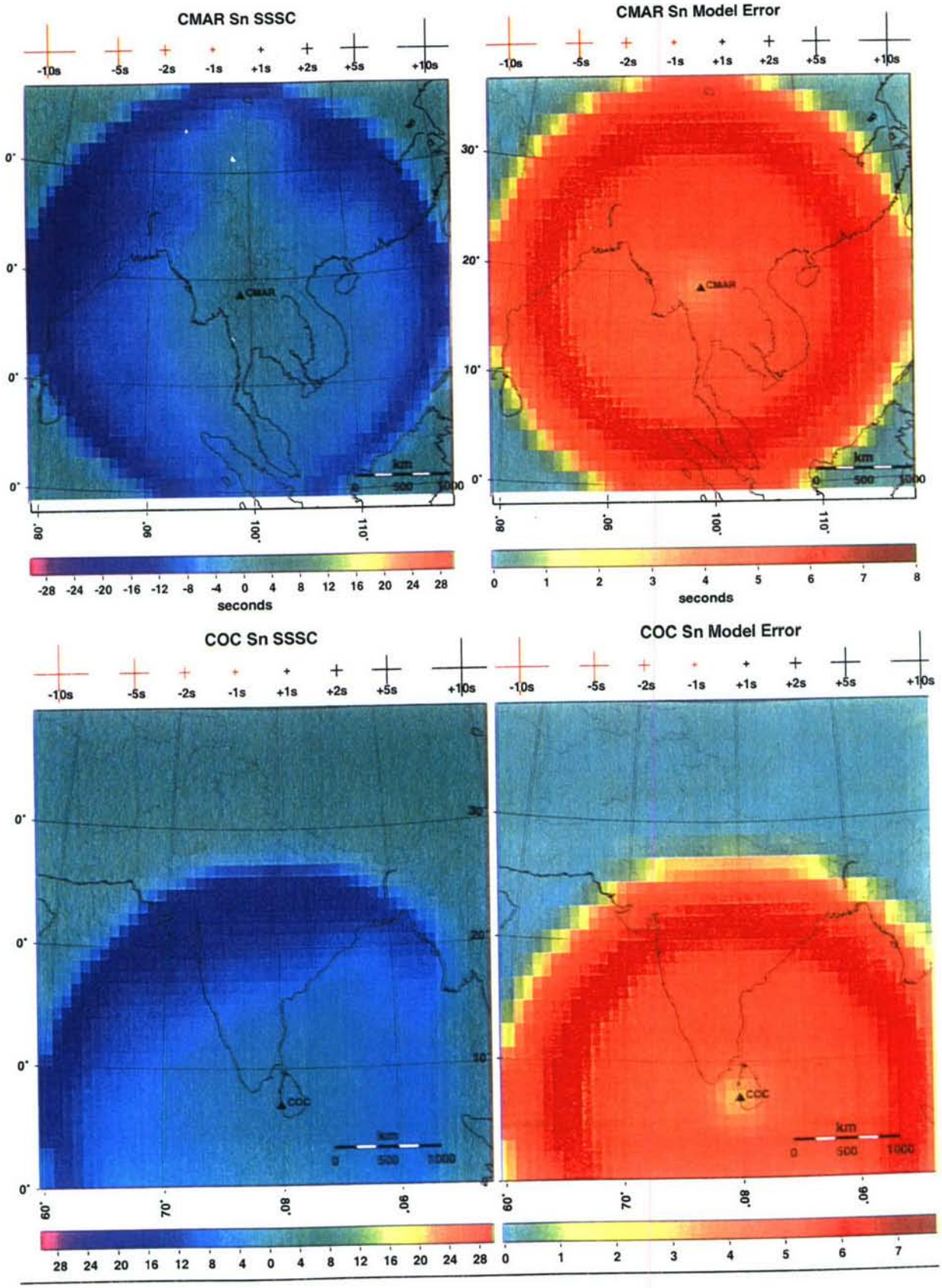

AAK Sn Model Error
-10s
-5s
-2s
-1s
+1s
+2s
+5s
+10s
50°
40°
30°
AAK
km
0
500
1000
50°
60°
70°
80°
90°
100°
0 1 2 3 4 5 6 7 8
seconds

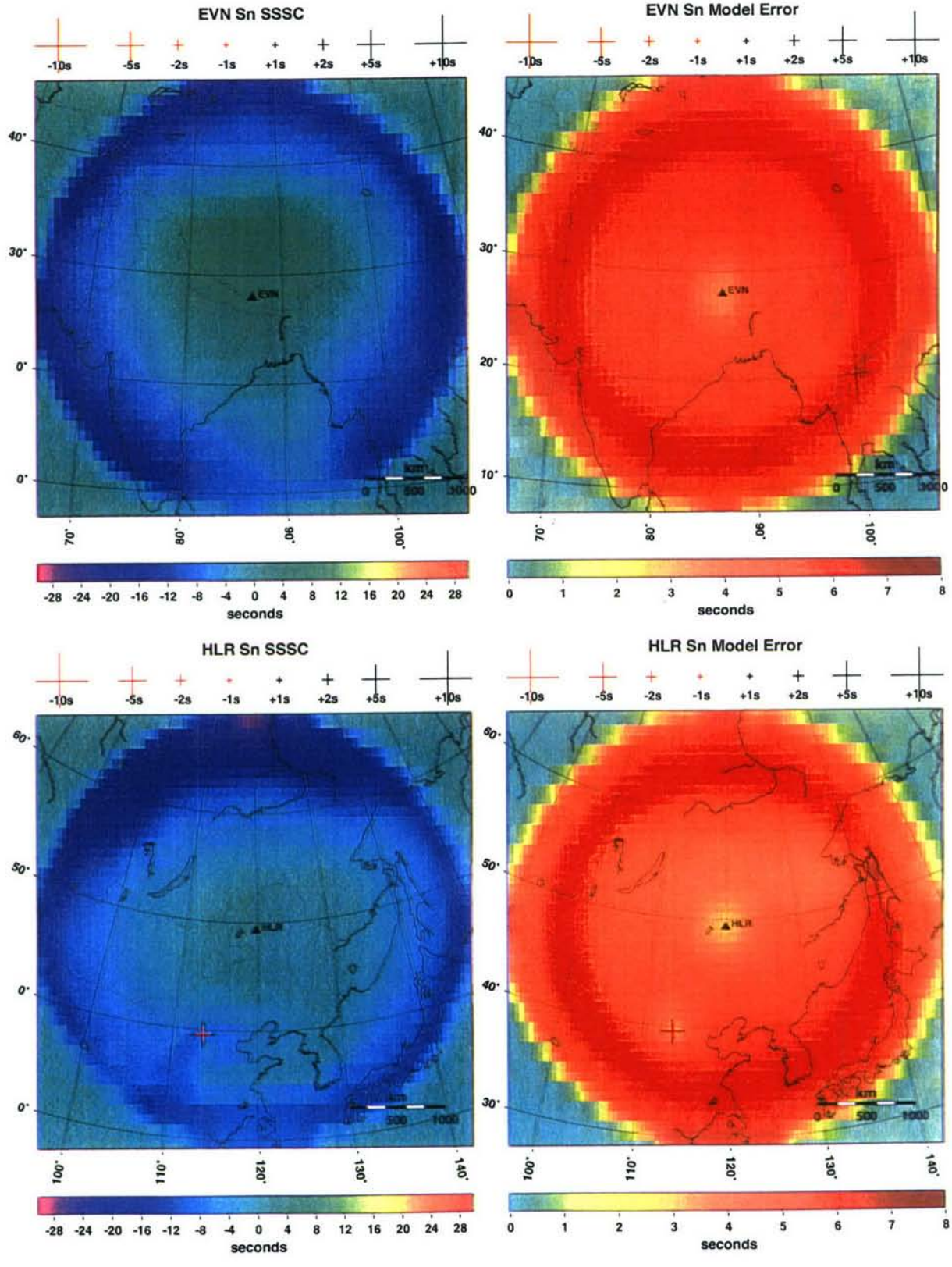

AKTO Sn SSSC
-10s
-5s
-2s
-1s
+1s
+2s
+5s
+10s
60°
50°
40°
0°
AKTO
km
0
500
1000
40°
50°
60°
70°
80°
-28 -24 -20 -16 -12 -8 -4 0 4 8 12 16 20 24 28
seconds

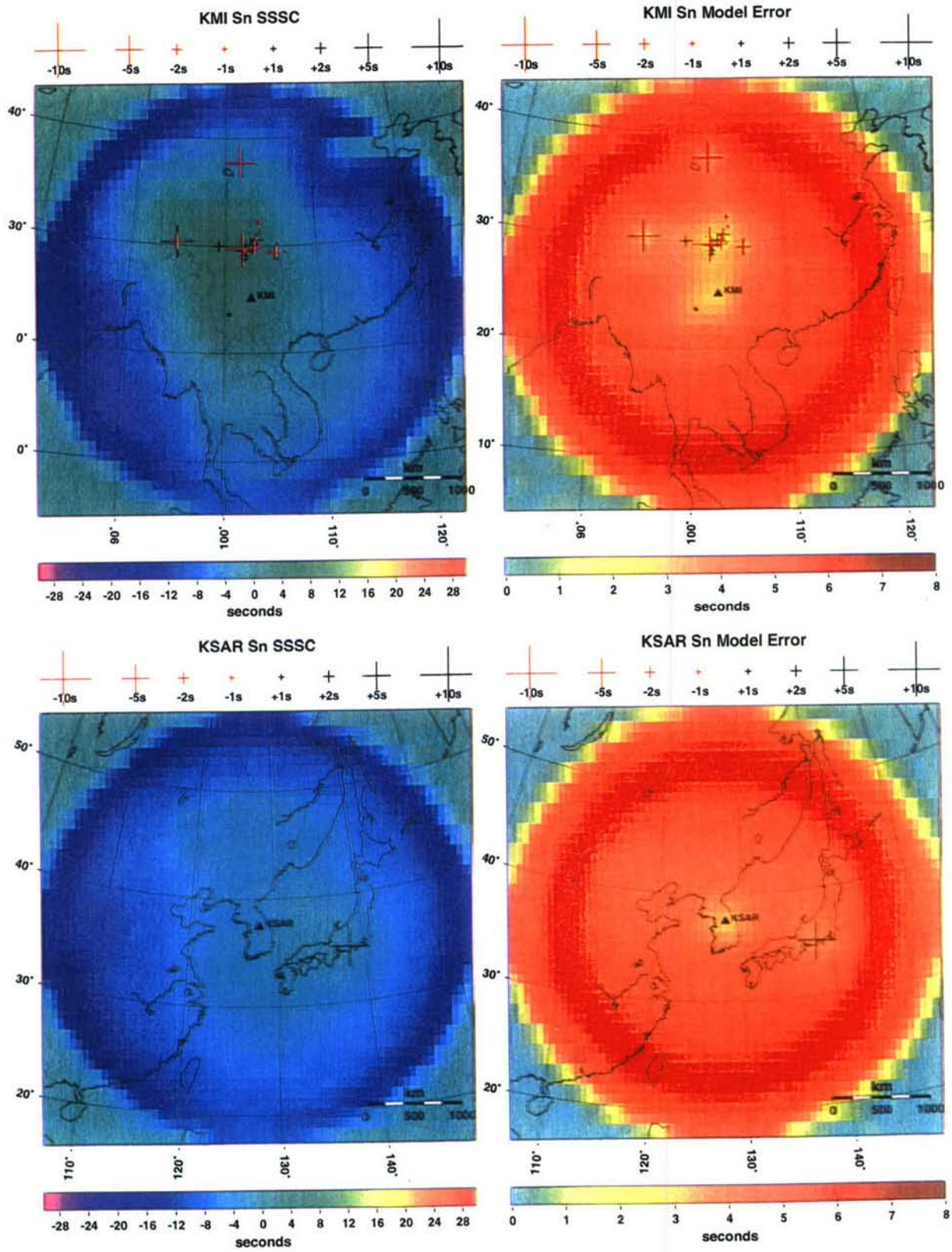

AKTO Sn Model Error
-10s
-5s
-2s
-1s
+1s
+2s
+5s
+10s
60°
50°
40°
30°
AKTO
km
0
500
1000
40°
50°
60°
70°
80°
0 1 2 3 4 5 6 7 8
seconds

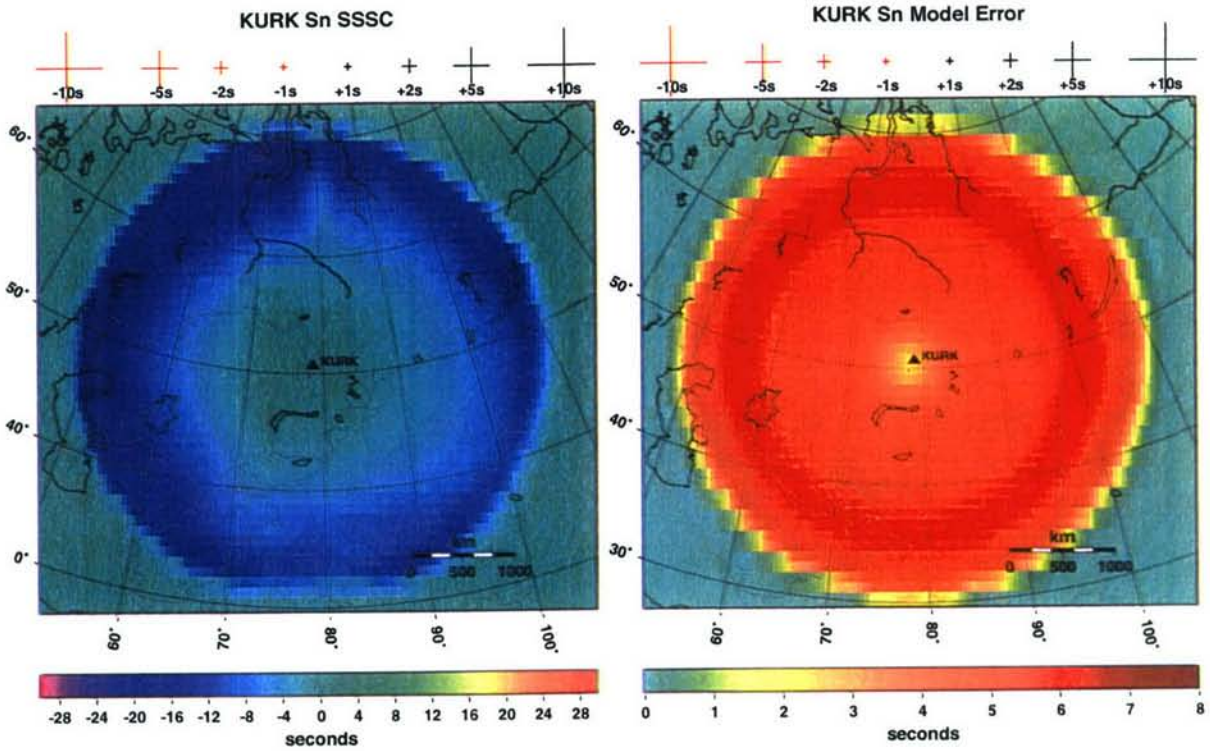

BIL Sn SSSC
-10s -5s -2s -1s +1s +2s +5s +10s
60°
50°
140° 150° 160° 170° 180° -170°
-28 -24 -20 -16 -12 -8 -4 0 4 8 12 16 20 24 28
seconds
BIL Sn Model Error
-10s -5s -2s -1s +1s +2s +5s +10s
km
0 500 1000
0 1 2 3 4 5 6 7 8
seconds
BJI Sn SSSC
-10s -5s -2s -1s +1s +2s +5s +10s
50°
40°
30°
20°
100° 110° 120° 130°
-28 -24 -20 -16 -12 -8 -4 0 4 8 12 16 20 24 28
seconds
BJI Sn Model Error
-10s -5s -2s -1s +1s +2s +5s +10s
km
0 500 1000
0 1 2 3 4 5 6 7 8
seconds

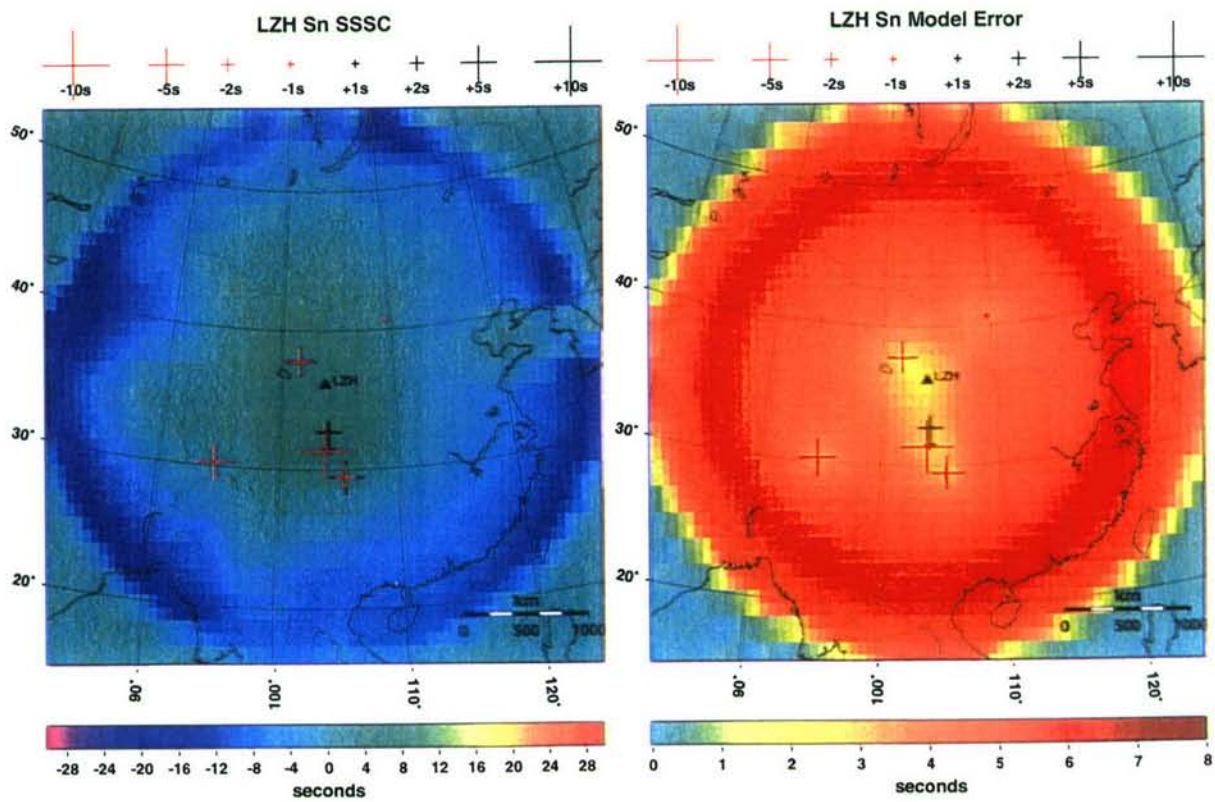

BRVK Sn SSSC
-10s -5s -2s -1s +1s +2s +5s +10s
BRVK
km
0 500 1000
-28 -24 -20 -16 -12 -8 -4 0 4 8 12 16 20 24 28
seconds
BRVK Sn Model Error
-10s -5s -2s -1s +1s +2s +5s +10s
BRVK
km
0 500 1000
0 1 2 3 4 5 6 7 8
seconds
CHT Sn SSSC
-10s -5s -2s -1s +1s +2s +5s +10s
CHT
km
0 500 1000
-28 -24 -20 -16 -12 -8 -4 0 4 8 12 16 20 24 28
seconds
CHT Sn Model Error
-10s -5s -2s -1s +1s +2s +5s +10s
CHT
km
0 500 1000
0 1 2 3 4 5 6 7 8
seconds

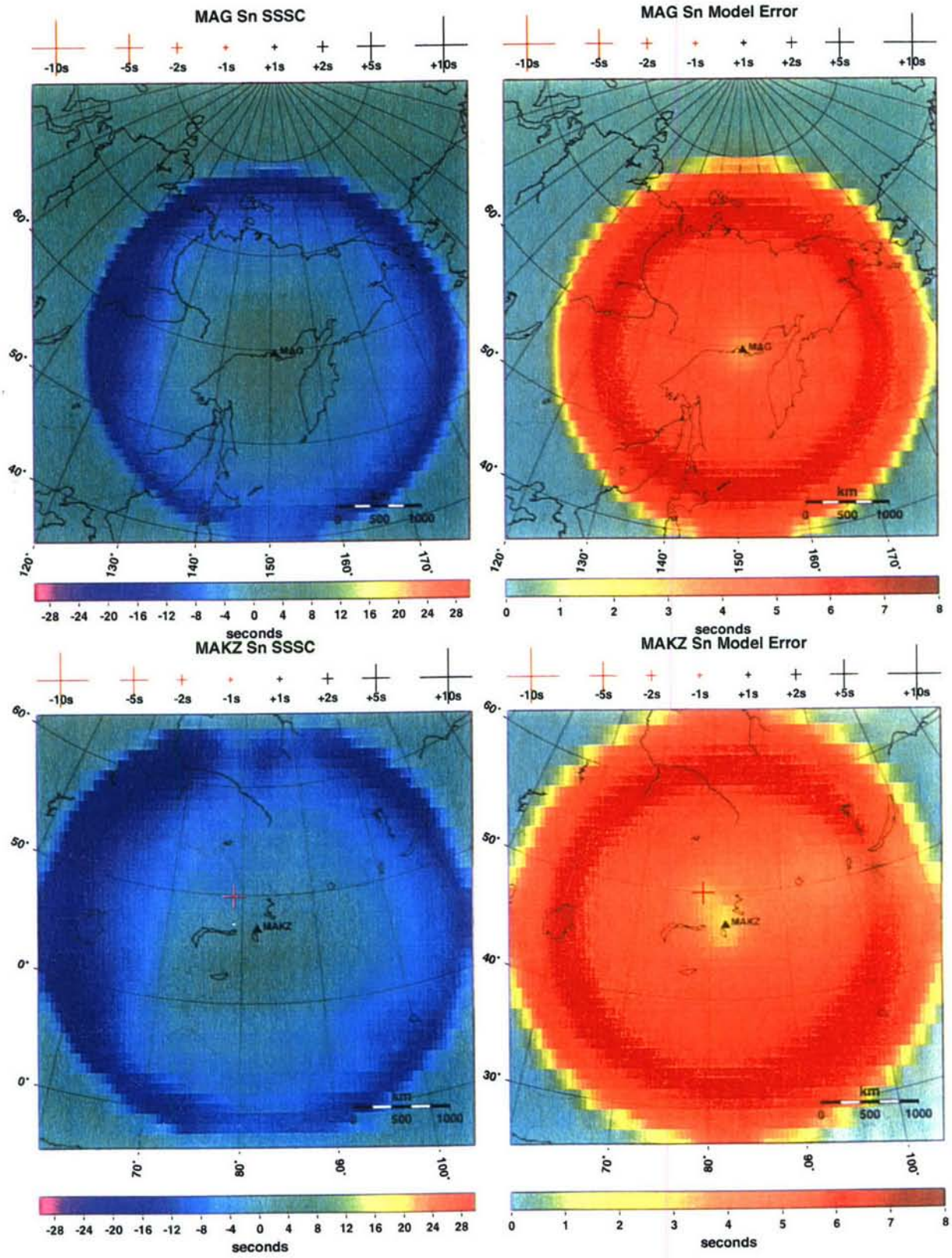

CMAR Sn SSSC
-10s -5s -2s -1s +1s +2s +5s +10s
CMAR
km
0 500 1000
-28 -24 -20 -16 -12 -8 -4 0 4 8 12 16 20 24 28
seconds
CMAR Sn Model Error
-10s -5s -2s -1s +1s +2s +5s +10s
CMAR
km
0 500 1000
0 1 2 3 4 5 6 7 8
seconds
COC Sn SSSC
-10s -5s -2s -1s +1s +2s +5s +10s
COC
km
0 500 1000
28 24 20 16 12 8 4 0 4 8 12 16 20 24 28
COC Sn Model Error
-10s -5s -2s -1s +1s +2s +5s +10s
COC
km
0 500 1000
0 1 2 3 4 5 6 7

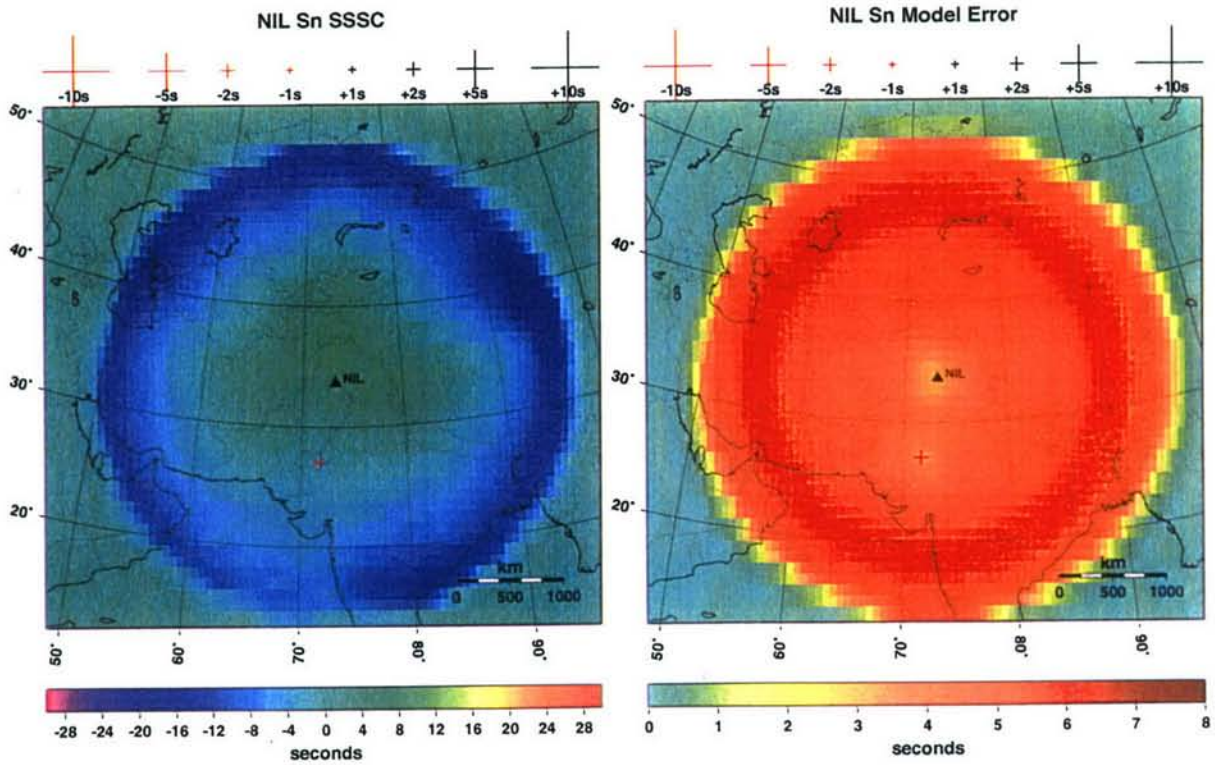

EVN Sn SSSC
-10s -5s -2s -1s +1s +2s +5s +10s
EVN
km
0 500 1000
70° 80° 90° 100°
-28 -24 -20 -16 -12 -8 -4 0 4 8 12 16 20 24 28
seconds
EVN Sn Model Error
-10s -5s -2s -1s +1s +2s +5s +10s
EVN
km
0 500 1000
70° 80° 90° 100°
0 1 2 3 4 5 6 7 8
seconds
HLR Sn SSSC
-10s -5s -2s -1s +1s +2s +5s +10s
HLR
km
0 500 1000
100° 110° 120° 130° 140°
-28 -24 -20 -16 -12 -8 -4 0 4 8 12 16 20 24 28
seconds
HLR Sn Model Error
-10s -5s -2s -1s +1s +2s +5s +10s
HLR
km
0 500 1000
100° 110° 120° 130° 140°
0 1 2 3 4 5 6 7 8
seconds

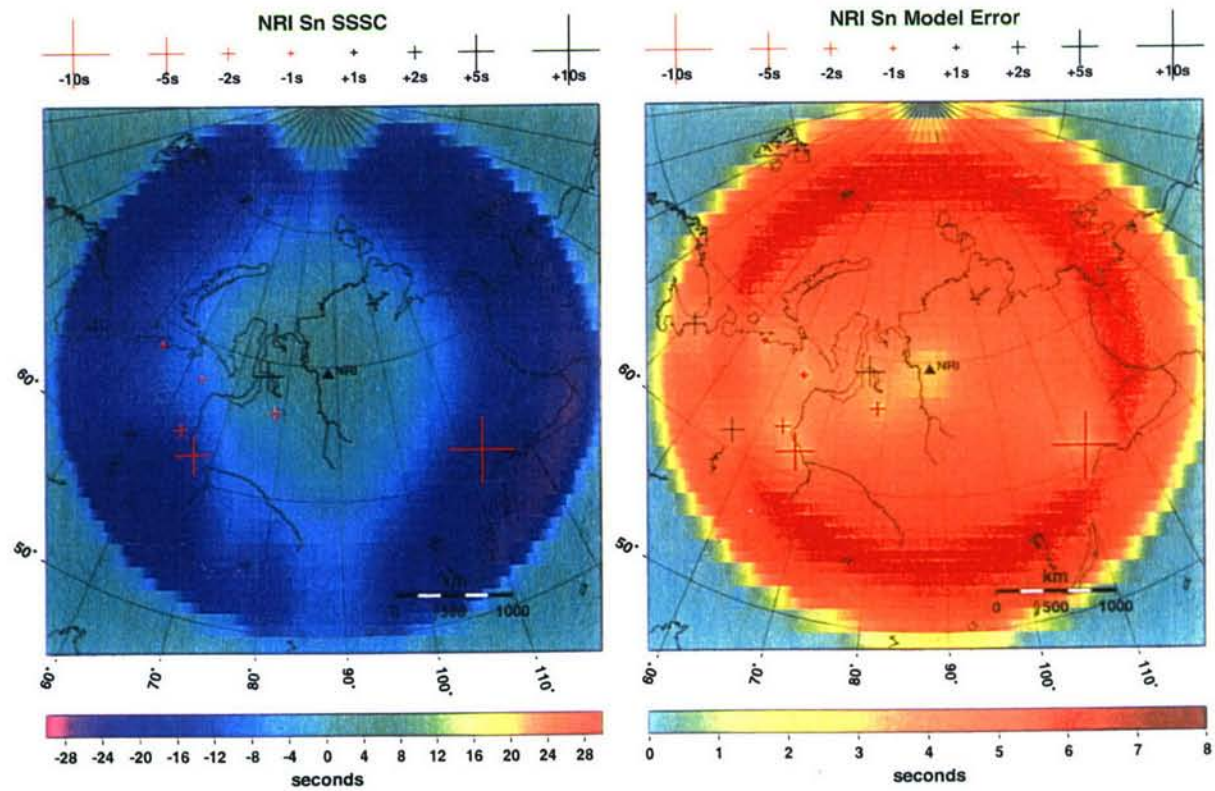

KMI Sn SSSC
-10s -5s -2s -1s +1s +2s +5s +10s
40°
30°
0°
0°
KMI
0 500 1000
90° 100° 110° 120°
-28 -24 -20 -16 -12 -8 -4 0 4 8 12 16 20 24 28
seconds
KMI Sn Model Error
-10s -5s -2s -1s +1s +2s +5s +10s
40°
30°
20°
10°
KMI
0 500 1000
90° 100° 110° 120°
0 1 2 3 4 5 6 7 8
seconds
KSAR Sn SSSC
-10s -5s -2s -1s +1s +2s +5s +10s
50°
40°
30°
20°
KSAR
0 500 1000
110° 120° 130° 140°
-28 -24 -20 -16 -12 -8 -4 0 4 8 12 16 20 24 28
seconds
KSAR Sn Model Error
-10s -5s -2s -1s +1s +2s +5s +10s
50°
40°
30°
20°
KSAR
0 500 1000
110° 120° 130° 140°
0 1 2 3 4 5 6 7 8
seconds

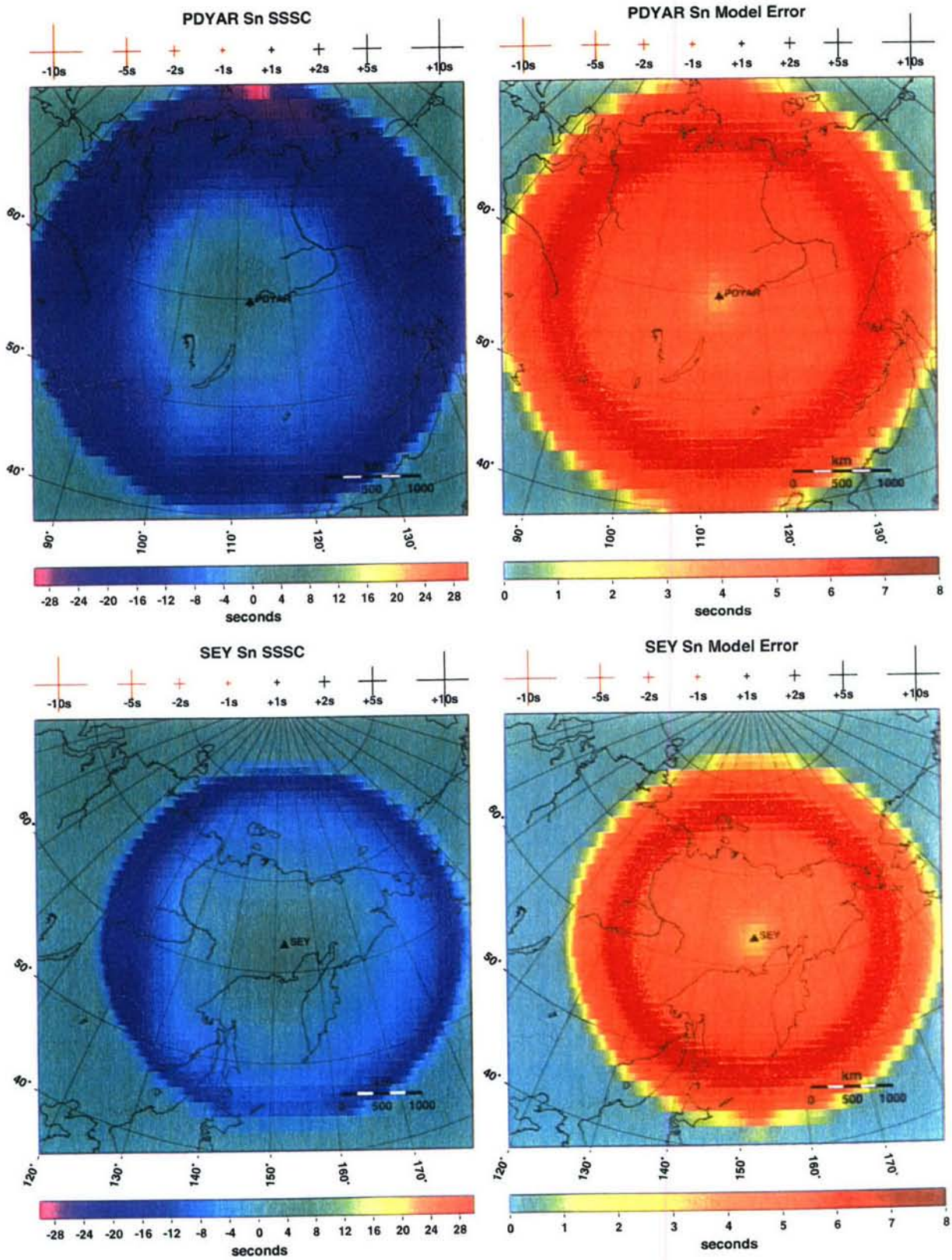

KURK Sn SSSC
KURK Sn Model Error
-10s
-5s
-2s
-1s
+1s
+2s
+5s
+10s
KURK
km
0
500
1000
60°
50°
40°
0°
30°
60°
70°
80°
90°
100°
-28 -24 -20 -16 -12 -8 -4 0 4 8 12 16 20 24 28
0 1 2 3 4 5 6 7 8
seconds

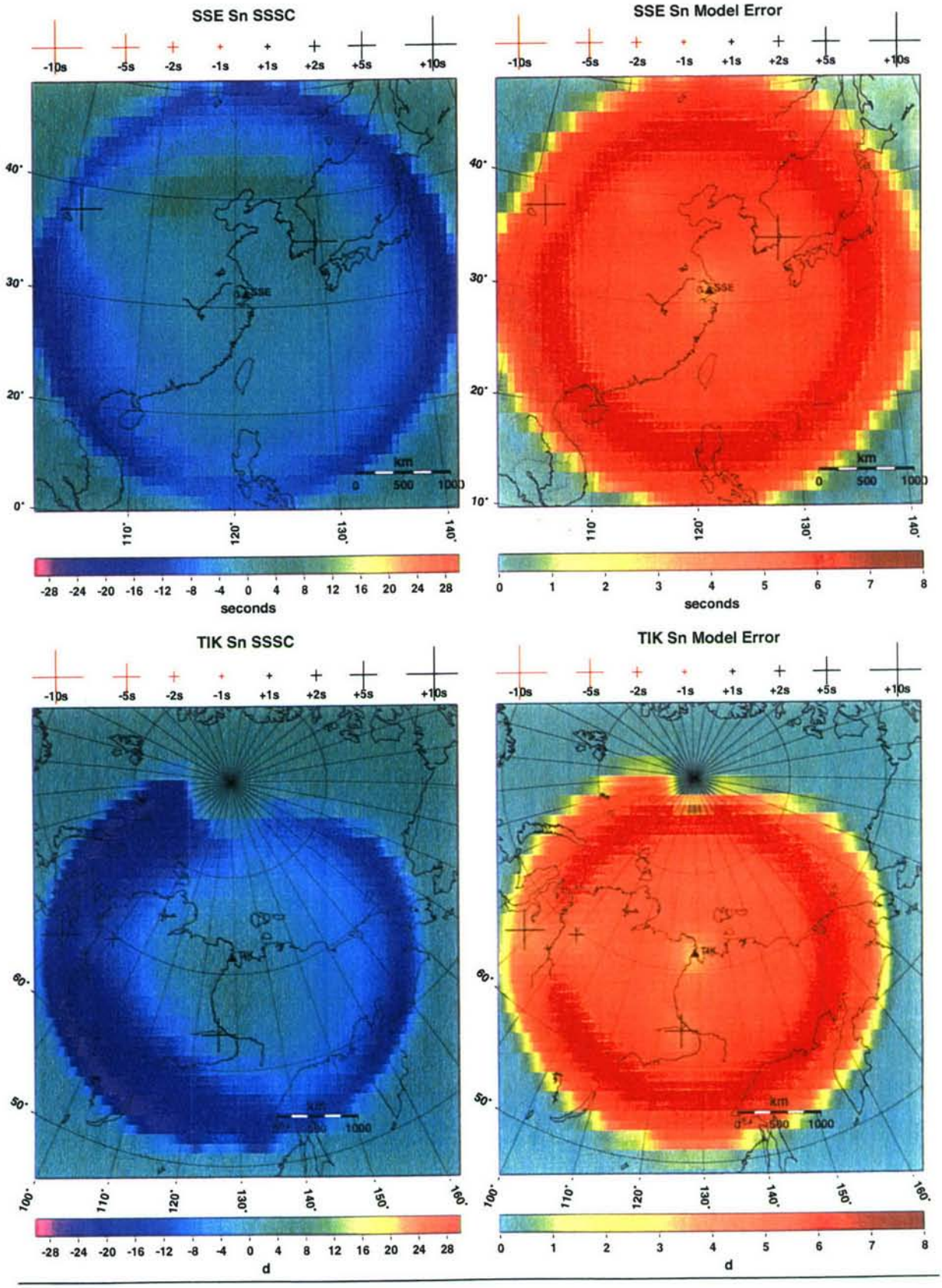

LZH Sn SSSC
LZH Sn Model Error
-10s
-5s
-2s
-1s
+1s
+2s
+5s
+10s
LZH
km
0
500
1000
50°
40°
30°
20°
60°
70°
80°
90°
100°
110°
120°
-28 -24 -20 -16 -12 -8 -4 0 4 8 12 16 20 24 28
0 1 2 3 4 5 6 7 8
seconds

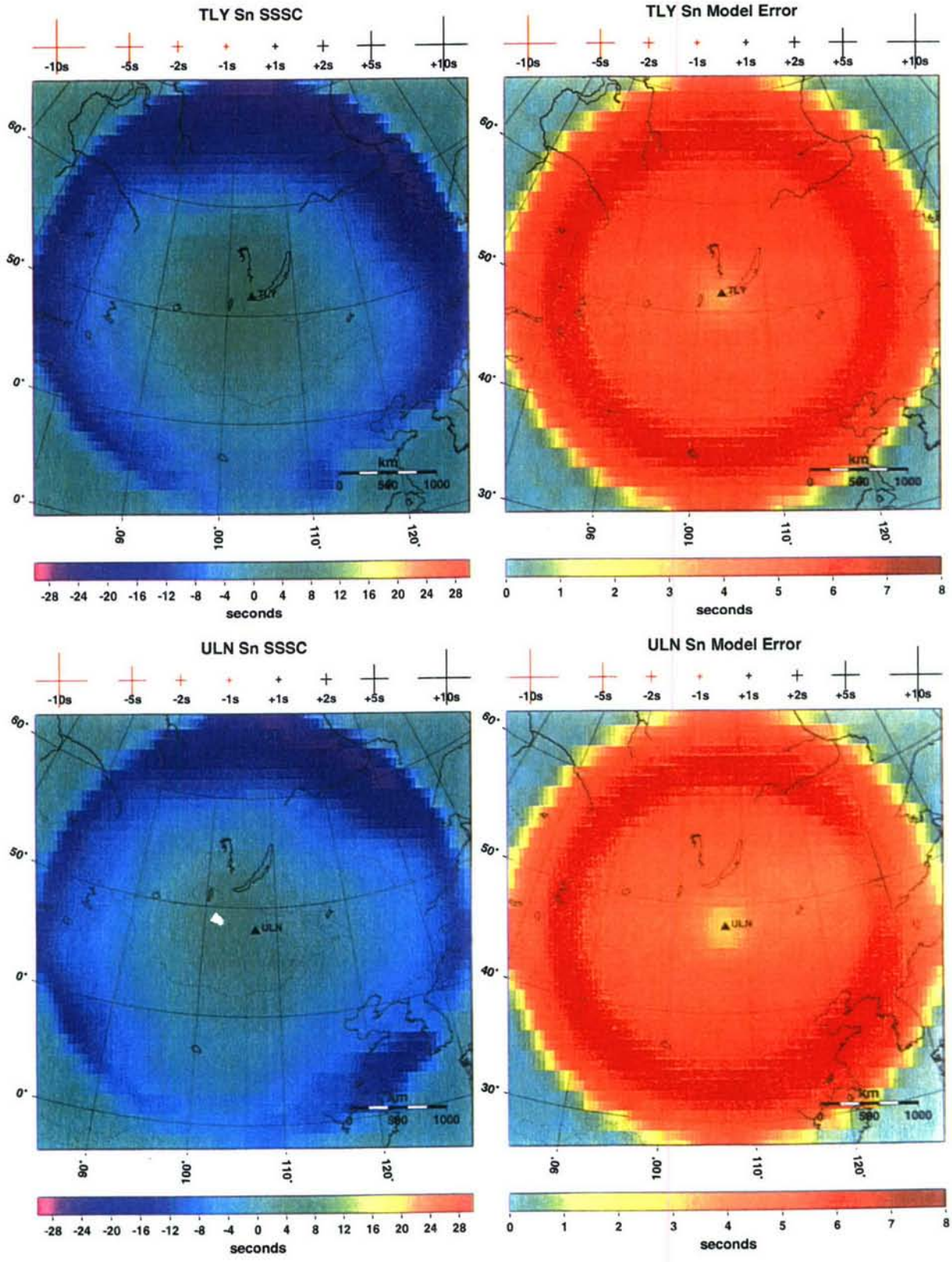

MAG Sn SSSC
-10s -5s -2s -1s +1s +2s +5s +10s
MAG
km
0 500 1000
60° 50° 40°
120° 130° 140° 150° 160° 170°
-28 -24 -20 -16 -12 -8 -4 0 4 8 12 16 20 24 28
seconds
MAG Sn Model Error
-10s -5s -2s -1s +1s +2s +5s +10s
MAG
km
0 500 1000
60° 50° 40°
120° 130° 140° 150° 160° 170°
0 1 2 3 4 5 6 7 8
seconds
MAKZ Sn SSSC
-10s -5s -2s -1s +1s +2s +5s +10s
MAKZ
km
0 500 1000
60° 50° 0° 0°
70° 80° 90° 100°
-28 -24 -20 -16 -12 -8 -4 0 4 8 12 16 20 24 28
seconds
MAKZ Sn Model Error
-10s -5s -2s -1s +1s +2s +5s +10s
MAKZ
km
0 500 1000
60° 50° 40° 30°
70° 80° 90° 100°
0 1 2 3 4 5 6 7 8
seconds

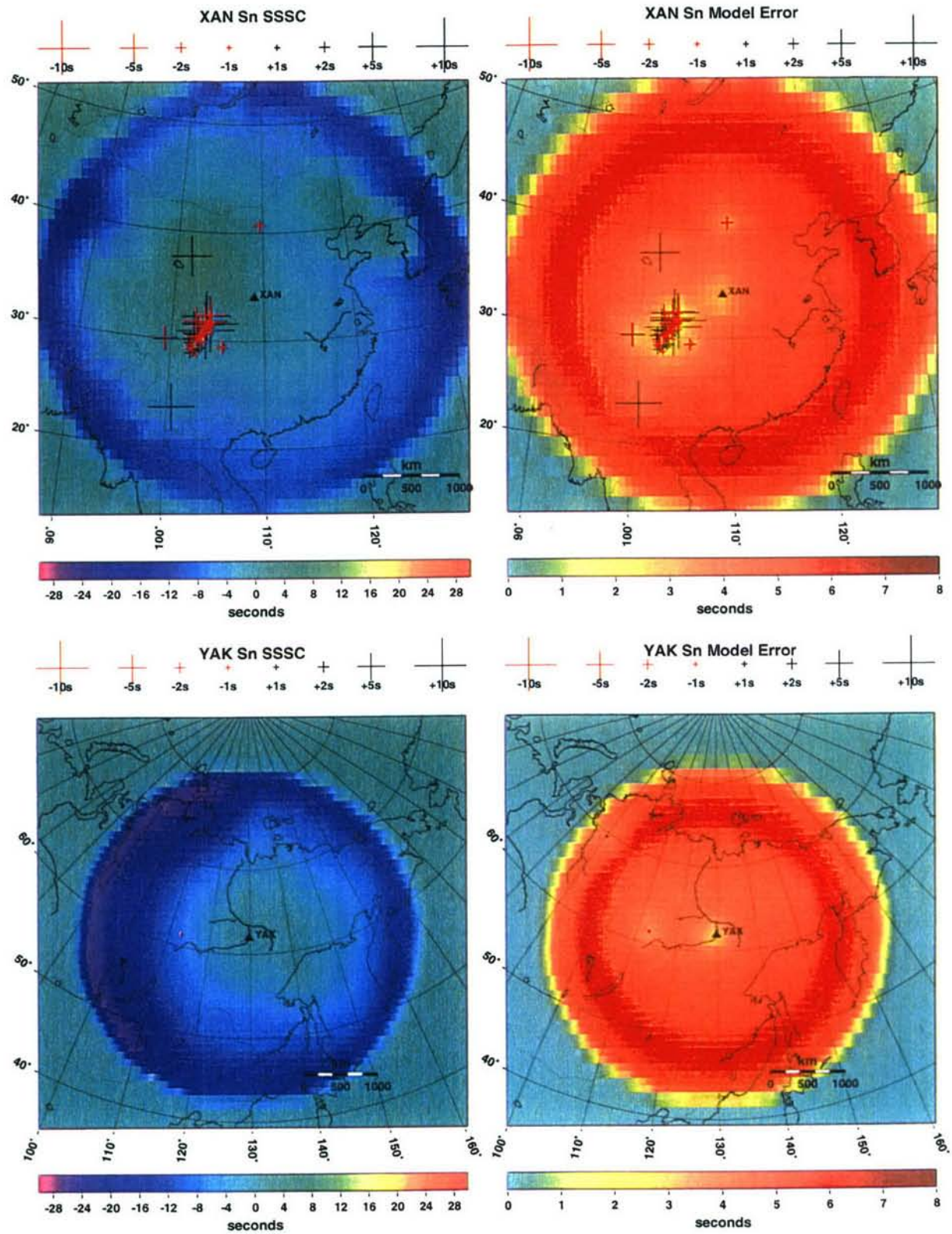

NIL Sn SSSC
NIL Sn Model Error
-10s -5s -2s -1s +1s +2s +5s +10s
NIL
km
0 500 1000
50° 60° 70° 80° 90°
20° 30° 40° 50°
-28 -24 -20 -16 -12 -8 -4 0 4 8 12 16 20 24 28
0 1 2 3 4 5 6 7 8
seconds

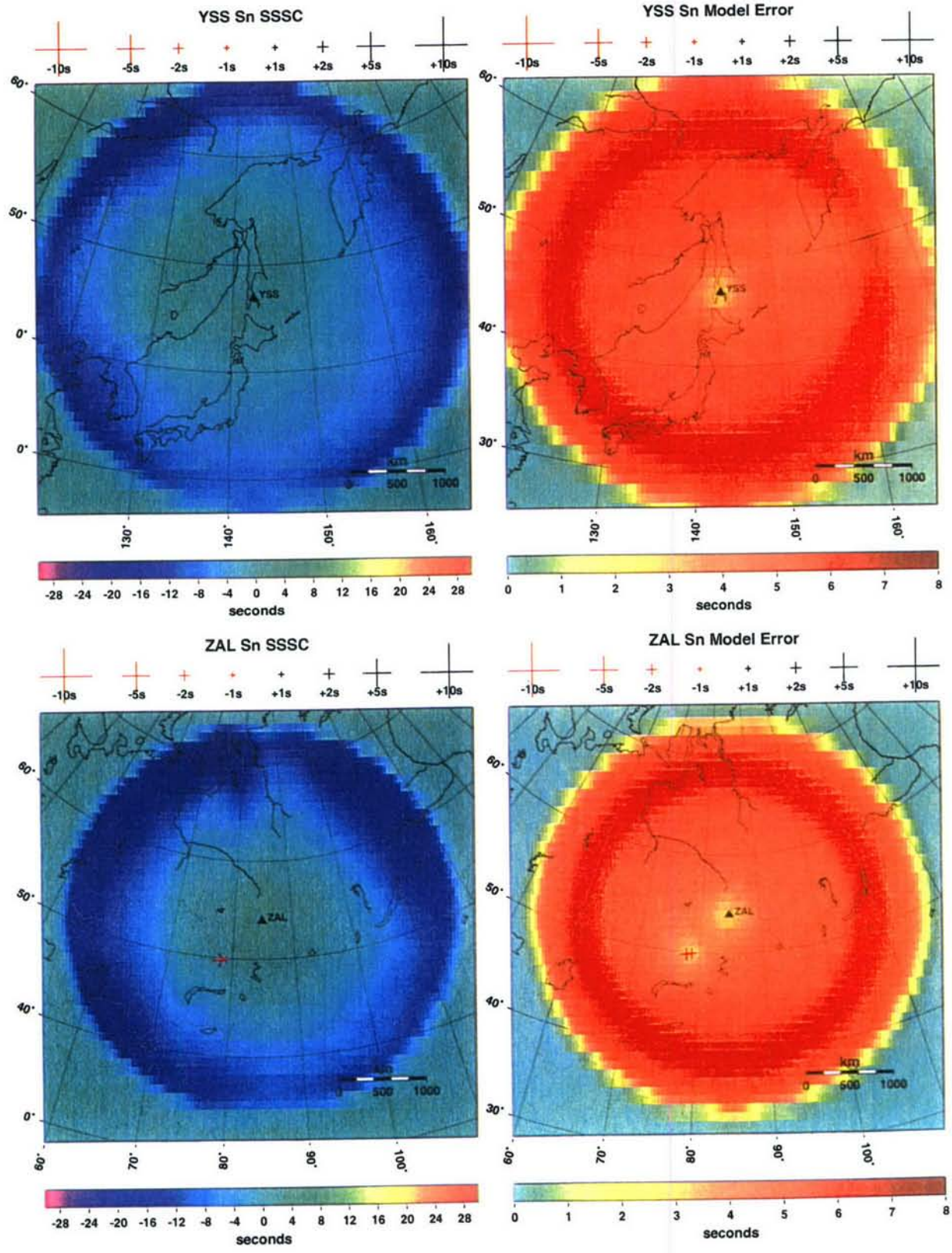

NRI Sn SSSC
NRI Sn Model Error
-10s -5s -2s -1s +1s +2s +5s +10s
NRI
km
0 500 1000
60° 70° 80° 90° 100° 110°
50° 60°
-28 -24 -20 -16 -12 -8 -4 0 4 8 12 16 20 24 28
0 1 2 3 4 5 6 7 8
seconds


PDYAR Sn SSSC
-10s -5s -2s -1s +1s +2s +5s +10s
PDYAR
60°
50°
40°
90° 100° 110° 120° 130°
km
0 500 1000
-28 -24 -20 -16 -12 -8 -4 0 4 8 12 16 20 24 28
seconds
PDYAR Sn Model Error
-10s -5s -2s -1s +1s +2s +5s +10s
PDYAR
60°
50°
40°
90° 100° 110° 120° 130°
km
0 500 1000
0 1 2 3 4 5 6 7 8
seconds
SEY Sn SSSC
-10s -5s -2s -1s +1s +2s +5s +10s
SEY
60°
50°
40°
120° 130° 140° 150° 160° 170°
km
0 500 1000
-28 -24 -20 -16 -12 -8 -4 0 4 8 12 16 20 24 28
seconds
SEY Sn Model Error
-10s -5s -2s -1s +1s +2s +5s +10s
SEY
60°
50°
40°
120° 130° 140° 150° 160° 170°
km
0 500 1000
0 1 2 3 4 5 6 7 8
seconds


SSE Sn SSSC
-10s -5s -2s -1s +1s +2s +5s +10s
40° 30° 20° 0°
SSE
km
0 500 1000
110° 120° 130° 140°
-28 -24 -20 -16 -12 -8 -4 0 4 8 12 16 20 24 28
seconds
SSE Sn Model Error
-10s -5s -2s -1s +1s +2s +5s +10s
40° 30° 20° 10°
SSE
km
0 500 1000
110° 120° 130° 140°
0 1 2 3 4 5 6 7 8
seconds
TIK Sn SSSC
-10s -5s -2s -1s +1s +2s +5s +10s
60° 50°
TIK
km
0 500 1000
100° 110° 120° 130° 140° 150° 160°
-28 -24 -20 -16 -12 -8 -4 0 4 8 12 16 20 24 28
d
TIK Sn Model Error
-10s -5s -2s -1s +1s +2s +5s +10s
60° 50°
TIK
km
0 500 1000
100° 110° 120° 130° 140° 150° 160°
0 1 2 3 4 5 6 7 8
d


TLY Sn SSSC
-10s -5s -2s -1s +1s +2s +5s +10s
60°
50°
0°
0°
TLY
km
0 500 1000
80° 100° 110° 120°
-28 -24 -20 -16 -12 -8 -4 0 4 8 12 16 20 24 28
seconds
TLY Sn Model Error
-10s -5s -2s -1s +1s +2s +5s +10s
60°
50°
40°
30°
TLY
km
0 500 1000
80° 100° 110° 120°
0 1 2 3 4 5 6 7 8
seconds
ULN Sn SSSC
-10s -5s -2s -1s +1s +2s +5s +10s
60°
50°
0°
0°
ULN
km
0 500 1000
80° 100° 110° 120°
-28 -24 -20 -16 -12 -8 -4 0 4 8 12 16 20 24 28
seconds
ULN Sn Model Error
-10s -5s -2s -1s +1s +2s +5s +10s
60°
50°
40°
30°
ULN
km
0 500 1000
80° 100° 110° 120°
0 1 2 3 4 5 6 7 8
seconds


XAN Sn SSSC
-10s
-5s
-2s
-1s
+1s
+2s
+5s
+10s
50°
40°
30°
20°
XAN
km
0
500
1000
90°
100°
110°
120°
-28 -24 -20 -16 -12 -8 -4 0 4 8 12 16 20 24 28
seconds
XAN Sn Model Error
0 1 2 3 4 5 6 7 8
seconds
YAK Sn SSSC
60°
50°
40°
YAK
100°
110°
120°
130°
140°
150°
160°
seconds
YAK Sn Model Error


YSS Sn SSSC
-10s -5s -2s -1s +1s +2s +5s +10s
60° 50° 0°
YSS
km 0 500 1000
130° 140° 150° 160°
-28 -24 -20 -16 -12 -8 -4 0 4 8 12 16 20 24 28
seconds
YSS Sn Model Error
-10s -5s -2s -1s +1s +2s +5s +10s
60° 50° 40° 30°
YSS
km 0 500 1000
130° 140° 150° 160°
0 1 2 3 4 5 6 7 8
seconds
ZAL Sn SSSC
-10s -5s -2s -1s +1s +2s +5s +10s
60° 50° 40° 0°
ZAL
km 0 500 1000
60° 70° 80° 90° 100°
-28 -24 -20 -16 -12 -8 -4 0 4 8 12 16 20 24 28
seconds
ZAL Sn Model Error
-10s -5s -2s -1s +1s +2s +5s +10s
60° 50° 40° 30°
ZAL
km 0 500 1000
60° 70° 80° 90° 100°
0 1 2 3 4 5 6 7 8
seconds

Appendix F Validation Test Report

```
**************************************************************************
                RDSS Validation Test Report June 4, 2003
**************************************************************************

TITLE:          Off-line Testing of G1 (Richards) Consortium Source-Specific
                Station Corrections (SSSCs) for Asia
RECEIVED:               May 12, 2003
TESTED:                 May 13 - May 22, 2003
CONDUCTED BY:           Istvan Bondar
FINAL STATE:            Successfully passed testing criteria with some notes


OBJECTIVES:
===========
To conduct two validation tests (off-line tests) on the SSSCs for Asia as
delivered by the G1 (Richards) Consortium. These tests are those that are
recommended in the "Validation Test Plan: Off-line Testing of Source-Specific
Stations Corrections for Asia" that was included in the delivery.


DELIVERY:
=========
The Group 1 Consortium delivery consists of the following:

    Database:
    - Database dump of
        * Kitov's dataset, Dataset-1, consisting of 156 events.
        * LopNor, India, Pakistan and Kazakhstan dataset, event clusters
          from LDEO and Engdahl, JMA events, Dataset-2.
        * Database tables needed for validation test run.
    - Script to import database tables.

        Reports:
        - Validation test plan used to conduct this validation test.
        - Validation test report of the G1 consortium testing.

        Executable, scripts and configuration data files (CDFs):
        - Scripts and CDFs to run Evloc with and without SSSCs.
```

- An executable to run kriging.
- Scripts and CDFs to run kriging executable.
- Script to convert SSSCs to PIDC format.
- Scripts and CDFs to compute metrics.

SSSCs:
- SSSCs in PIDC format for Dataset-1.
- SSSCs in PIDC format for Dataset-2.
- SSSCs corrected by kriging.
- SSSCs for 158 stations based on 3D ray tracing.

Others:
- List of orids in Dataset-1 and Dataset-2.
- List of stations in Dataset-1 and and Dataset-2.
- Arrivals from different events for 140 stations.
- ars.defs file containing list of stations with SSSCs

TEST REQUIREMENTS:
==========

- Test environment needed access to the /cmss tree in order to run Evloc.
- Disk space was needed for installation.
- A Database account was needed for testing.
- Scripts and logs provided by the G1 Consortium for conducting the test.

TESTS CONDUCTED:
==========

Two off-line validation tests were conducted. These tests follow the procedures outlined in the Validation Test Plan included as part of the delivery. These tests required use of Evloc for relocating GT event with and without SSSCs. Evaluation matrics were obtained using a script provided as part of the delivery.

The two tests, in the order of their execution, are:

- Test 1: Relocation of GT events using model based SSSCs.
  - Test 1A: Relocation of the GT events without SSSCs, using IASPEI91 travel-times only
  - Test 1B: Relocation of the GT events with the Pn SSSCs calculated with model-based method

- Test 2: Relocation of GT events of Test 1 with the SSSCs corrected by kriging. Kriged correction surfaces are calculated by the leave-one-out approach.

TEST RESULTS

==========

Total of 158 (PN, Sn) SSSCs are included in the delivery. In each test events were relocated and metrics were collected using scripts included as part of the delivery. The passing criteria used for these tests were to replicate the G1 test results using the scripts provided. In the following paragraphs tests are judged based on these criteria.

Test 1: Relocation of GT events using model-based SSSCs .

The first test was to reproduce the relocation results with and without model-based SSSCs. After creating the necessary database tables and making changes in the parfiles (DB account, pathnames, and some environment variables, all described in the Test Plan), I relocated the delivered reference events with and without calibrated travel-times using /cmss/local/bin/EvLoc in the testbed, and then ran the provided script for generating relocation metrics.

I found that the metrics are slightly different from the baseline metrics provided by Group1 (see the results in the directory radish:/home/rdtst/PROJECTS/G1/2/run/metrics). The differences in the various metrics are typically observed in the second or third decimal digits. The reason for the differences is due to a known bug in EvLoc. The bug is found in sssc.c and is related to the interpolation of travel-times and model errors from the SSSC grid. Although Division 206 was informed about this bug, I am not aware of any official EvLoc releases that would have addressed the defect. The testbed version (/cmss/local/bin/EvLoc) still suffers from this bug. The Group1 baseline results were generated using an informal

copy of EvLoc where the bug was fixed. When using this EvLoc version (/home/rdtst/PROJECTS/G1/2/run/EvLoc_relu) I was able to reproduce the baseline metrics.

Test 2: Relocation of GT events of Test 1 with the SSSCs corrected by kriging.

The second test was to reproduce the relocation results with and without kriged SSSC surfaces. The relocation exercise followed a leave-one-out approach, where the SSSCs for each station were recalculated using all observations but those from the particular event to be located. This approach turned out to be painfully slow, being able to locate three events in an hour on a Sparc20.

Unfortunately, after running the process for more than a week, my machine got rebooted, effectively killing all running processes. The reboot was unrelated to the test. However, 492 events out of 518 were successfully located using kriged SSSCs. I reckoned that the statistical sample was large enough to provide robust metrics and the results could be accepted if they are within a tolerance limit, that is, if the differences are found in the second or higher decimal digits. It should be noted that since I ran the second and first tests simultaneously, the second test also used the bugbitten testbed EvLoc version. The results are found again in radish:/home/rdtst/PROJECTS/G1/2/run/metrics, and the comparison of metrics_wk_group1.res.All and
metrics_wk_group1.res.All_trust (baseline)
files indeed confirms that the metrics are within the tolerance limits. Therefore we can expect that repeating the ~10 day run with the correct version of EvLoc would reproduce the baseline results.

TEST ARCHIVE
============

Tests were conducted through user "rdtst" on radish. Delivery was installed under /home/rdtst/PROJECTS/G1/2. All the test results, logs, test report are archived under /home/rdtst/PROJECTS/G1/2.

DISTRIBUTION LIST
DTRA – TR – 05 – 21

DEPARTMENT OF DEFENSE

DEFENSE TECHNICAL INFORMATION CENTER
8725 JOHN J. KINGMAN ROAD, SUITE 0944
FT. BELVOIR, VA 22060-6201
2 CYS ATTN: DTIC/OCA

DEFENSE THREAT REDUCTION AGENCY
8725 JOHN J. KINGMAN ROAD STOP 6201
FT. BELVOIR, VA 22060-6218
2 CYS ATTN: RD-NTX/E.STOKES

DEPARTMENT OF DEFENSE CONTRACTORS

ITT INDUSTRIES
ITT SYSTEMS CORPORATION
1680 TEXAS STREET, SE
KIRTLAND AFB, NM 87117-5669
2 CYS ATTN: DTRIAC
ATTN: DARE

LAMONT-DOHERTY EARTH OBSERVATORY
COLUMBIA UNIVERSITY
661 ROUTE 9 W
PALISADES, NEW YORK 10964
ATTN: P. RICHARDS